THE UNIVERSITY
OF BIRMINGHAM

STRUCTURE AND PROPERTY RELATIONSHIPS IN PET BLENDS

by

YI KONG

A thesis submitted to the School of Engineering of

The University of Birmingham

for the degree of

DOCTOR OF PHILOSOPHY

Department of Metallurgy and Materials
The School of Engineering
The University of Birmingham

May 2002

SYNOPSIS

Blends of poly(ethylene terephthalate) (PET) and polycarbonate (PC) have been prepared by twin-screw extruder with and without added a transesterification catalyst - lanthanum acetylacetonate hydrate. The blends without added catalyst are completely immiscible over the study range while the blends with added catalyst show partial miscibility. The mechanical properties are slightly improved in the latter blends.

Studies were made on the crystallization and melting behaviour of PET and both of blends. It has been found that the crystallisation was inhibited in the presence of PC, particularly in the blends with added catalyst for which the equilibrium m.pt. showed considerable depression greater than the other samples. Multiple melting endotherms are due to dual lamellar thickness distributions and recrystallisation during heating.

Miscibility, melting and crystallisation were also studied by MTDSC which proved to be a powerful tool separating reversing and non-reversing events.

The crystallinities of PET and blends were measured using the First Law method and consistent with those measured by density and WAXD procedures.

Both blends annealed at higher temperature the thermal properties, phase structure and transesterification have been investigated as a function of time. Kinetics parameters were also determined.

谨献给:

立华 及 令思

To Lihua, for her constant support and encouragement

and to our lovely daughter, Lingsi

ACKNOWLEDGEMENT

I would like to express my sincere thanks to my supervisor, Dr. J. N. Hay, without whose invaluable guidance and constant encouragement this work would not have been possible. My sincere thanks are also due to my supervisor Dr. S. N. Kukureka for his regular advice and help.

I am deeply indebted to Mr. F. Biddlestone for his advice and technical support throughout this study. I would also like to thank Mrs. S. Dipple and Miss C. Hardy for technique support on SEM and WAXD in this school, and to Mrs. L. Tomkins and Mr. P. Whittle for the use of the cryo-microtome in the Electron Microscopy Centre.

I am also grateful to all my colleagues in the Polymer group for helpful discussion and support as well as their multiple cultures that make the life so enjoyable.

Finally, the scholarship from Overseas Research Students Awards Scheme and the financial support from the School of Metallurgy and Materials in the University of Birmingham are gratefully acknowledged.

Contents

Chapter one

Introduction

1.1 Polymer Blends [1-3]

A polymer blend may be defined as an intimate mixture of two kinds of polymers, with no covalent bonds between them. Polymer blends can be produced by: mechanical mixing, dissolution in co-solvents then film cast, latex blending and fine powder mixing etc. The first two are more successful methods especially that of mechanical blending, not only for economic reason but also since the blends formed from mechanical mixing do not contain residual solvent. Mechanical blending is accomplished by using various mechanical means such as internal mixers, two-roll mills, single-screw and twin-screw extruders and other methods, mixing the polymer components in the molten state. Today blending of polymers constitute over 30% of polymer consumption, and with an annual growth rate of 9% (constant for the last 12 years) their role can only increase further.

There are many reasons for blending. Sometimes it is to modify a resin to produce a specific type of behaviour, such as improvement in impact strength and fracture toughness. Blending is also used to gain direct economy by diluting expensive engineering resins with cheaper ones or to improve the processability of some high temperature resistance engineering resins. Generally blending aims at securing a different set of specific properties required for particularly applications by blending materials which do not have these properties.

1.2 Miscible Blends [4-5]

The term compatibility is often used synonymously with miscibility of the components. However, after Olabisi[4] the term *miscible* is used to describe completely mutual soluble blends that are homogeneous at the molecular level, as defined by thermodynamics and phase diagrams. The term *compatible* is used to describe mechanically processable blends which resist gross phase segregation and/or give desirable properties. A compatible blend may consist of two or more phases. The term *immiscible* refers to combinations of two or more polymer that do not dissolve. Partial miscibility results in shifting or broadening of the glass transitions of the two parent polymers. According to the above definitions polymer blends can obviously be divided into three groups: miscible, partially miscible and immiscible blends. The immiscible group far more outnumbers those of the other two.

1.3 Thermodynamics of Blend Miscibility [6,7]

In classical thermodynamics for a two-polymers blend system, the free energy change on mixing can be written as:

$$\Delta G_{mix} = \Delta H_{mix} - T\Delta S_{mix} \quad (1.1)$$

where ΔG_{mix} is Gibbs free energy of mixing, ΔH_{mix} is enthalpy of mixing, ΔS_{mix} is entropy of mixing and T is the temperature. Negative values of ΔG_{mix} indicate that mixing will occur spontaneously and lead to miscible blends. The term $T\Delta S_{mix}$ is always positive because there is an increase in the entropy on mixing but for the mixing of two polymers it is very small, therefore, the sign of ΔG_{mix} depends on ΔH_{mix}. If ΔG_{mix} is positive the mixture phase spontaneously separates. The individual components are thermodynamically more stable even if the kinetics of phase separation is very slow.

From the solution theory of Flory and Huggins[8,9] the free energy change of mixing polymer 1 and 2 is:

$$\Delta G_{mix} = \frac{RTV}{V_r}\left(\frac{\Phi_1}{m_1}\ln\Phi_1 + \frac{\Phi_2}{m_2}\ln\Phi_2 + \chi_{12}\Phi_1\Phi_2\right) \quad (1.2)$$

where ϕ_i is the volume fraction of component i, m_i is the degree of polymerisation of component i, V is the total volume of mixing of the polymers, Vr is the reference volume, χ_{12} is the interaction parameter between polymer 1 and 2, and R is the gas constant. The first two terms are negative and appear as a result of the combinatorial entropy of the system. The last term is the enthalpic contribution to the free energy of mixing. As both m_1 and m_2 are very large, the entropy of mixing is very small. Since χ_{12}

is positive for the interaction between most polymer molecules (at least for non-polar molecule), most polymer pairs do not dissolve in one another except in the circumstances where there are very strong interactions between blend components such as dipole-dipole, hydrogen bonding, covalent bonding or co-crystallisation, where χ_{12} can be negative. If χ_{12} is negative, miscibility can occur. This solution theory has its own shortcoming in that it is based on random mixing and assumed no volume change on mixing. The enthalpy changes on mixing are also assumed to be independent of the entropy.

Several new "equation of state" theories have been developed by Flory and his collaborators[10-14] and others[15-18]. In these theories each component is characterised by three parameters, V*, T*, P*, corresponding to density, thermal expansion coefficient, and thermal pressure coefficient respectively. In addition two interaction terms, χ_{12} and Q_{12}, associated with enthalpy and entropy of mixing were introduced in order to calculate the thermodynamics of mixing. These theories can be used to predict phase separation and both upper critical solution temperature (UCST) and lower critical solution temperature (LCST). They also provide a better understanding of the physical nature of phase separation.

1.4 Methods for Determining Miscibility [4,5]

The (im)miscibility of blends is usually characterised by investigating blend morphology, optical properties, glass transition temperatures and crystalline melting

behaviour of the blends. The glass transition temperature, T_g, which marks the characteristic transition of the amorphous region of a polymer or blend from a glass to a rubber state is the most convenient and popular way of investigating miscibility of two polymers. The presence of a single T_g indicates that the blend is miscible and of two T_gs closer to that of the T_gs of the components indicates partially miscibility. The T_g normally can be measured by differential scanning calorimetry (DSC), dilatometry, dynamic mechanical thermal analysis (DMTA) and dielectric relaxation methods.

When miscibility is observed, the single T_g of the blend appears between the two T_gs of the original components. The T_g will vary with composition and can be predicted by the widely used empirical equation due to Fox[19]:

$$\frac{1}{T_g} = \frac{W_1}{T_{g1}} + \frac{W_2}{T_{g2}} \tag{1.3}$$

where W_i is the weight fraction of component i and T_{gi} is the T_g of component i. There are other quantitative expressions for T_g such as the Gordon-Taylor eqution[20], which accounts for differences in density and volume expansion coefficients, and also that of Couchman[21] that considers enthalpic changes. A simple additivity rule is contrary to the criterion of molecular interactions producing miscibility.

The measurement of T_g to determine miscibility has its limitation, for example, when both components have the same or very close T_gs or when a small quantity of one polymer is present in the mixture some difficulty will be experienced in measuring T_gs. Furthermore the T_g is associated with a domain size of at least 10 nm. It may not be observed phase separation by Tg measurement if the domain size of below this value

In amorphous/crystalline blends, the melting point (T_m) and fractional crystallinity of the crystalline phase is depressed. Under thermodynamic equilibrium, depression of T_m can be expressed as[22]:

$$\frac{1}{T_m} - \frac{1}{T_m^o} = -\frac{RV_2}{\Delta HV_1}\left[\frac{\ln \Phi_2}{m_2} + (\frac{1}{m_2} - \frac{1}{m_1})(1-\Phi_2) + \chi_{12}(1-\Phi_2)^2\right] \quad (1.4)$$

where the subscript 1 is identified with the amorphous polymer and 2 with the crystalline polymer. Φ represents the volume fraction, V is the molar volume of the repeat units, m is essentially the degree of polymerisation, T_m is the melting point of the polymer of the excess component, T^o_m is the thermodynamic melting point of the perfect polymer crystal, R is the gas constant, ΔH is the heat of fusion per mole of crystalline monomer and χ_{12} is the interaction parameter. In polymer blends, both m_1 and m_2 are very large compared to unity. Therefore, equation 2.2 reduces to[23,24]:

$$\frac{1}{T_m} - \frac{1}{T_m^o} = -\frac{RV_2}{\Delta HV_1}\chi_{12}(1-\Phi_2)^2 \quad (1.5)$$

With this equation, the interaction parameter χ_{12} can be obtained. This expression has been applied to transitions in polyesters and to blends where both components may be crystallisable yet still share a miscible amorphous phase[25].

1.5 Methods of Enhancing Miscibility [26]

Immiscible blends of several polymers may possess some desirable properties, but miscible blends are generally preferred for many aspects. To improve the miscibility, several strategies have been proposed:

1. modification of polymer structure of one or both components via the introduction of the specific interactions between the individual polymer chains;
2. addition of a small quantity of a third component or a copolymer that is miscible with both phases;
3. compounding blends in the presence of chemical reactants that lead to modification of at least one macromolecular species, resulting in the generation of an in-situ compatibilizer;
4. mechanical-chemical blending that may lead to chain fragmentation and recombination, thus generating block copolymers.

These different strategies lead to blends with a different set of properties. For example, addition of a small amount of copolymer mainly affects the interfacial tension, and the di-block copolymer seems to be more efficient in reducing the interfacial tension, but the tri-block was found to be better in improving mechanical behaviour[27]. Reactive blending was found to engender a thicker interphase boundary that results in excellent stability under high stress and strain. It has been reported[28] that reactive blending has a thicker and more rigid interphase than blends with added copolymer. The interphase thickness increases with time then attains a plateau, whose value depends on the temperature and net concentration of the reactive sites.

1.6 Introduction to PET and PC

1.6.1 Polyethylene terephthalate[29]

Poly(ethylene terephthalate) (PET) is a well-established engineering polymer. It was produced by Whinfield and Dickson[30] in 1941 and licensed to ICI. PET is a semicrystalline polymer with T_g about 70°C and T_m 265°C. It can be obtained as a glassy or amorphous transparent solid by quenching the melt below T_g. Amorphous PET is of little commercial significance because it has bad mechanical properties, high gas permeation rates, low dimensional stability and high extensibility. When PET is heated above its T_g it crystallises, forming an opaque material with a spherulitic superstructure. Crystalline PET has high strength and stiffness, good dimensional stability, slip and wear properties, low creep, good electrical characteristics and high chemical resistance. These properties make it widely used in the production of fibres, films and for blow moulding bottles particularly those for pressurised carbonated beverages.

PET is produced by two polymerisation processes. In the first step terephthalic acid and ethylene glycol are reacted to produce bis-β-hydroxyethyl-terephthalate. In the next step, the bis-β-hydroxyethyl-terephthalate is reacted by raising the temperature and reducing the pressure to allow condensation by ester exchange, eliminating ethylene glycol units, to forms higher molecular weight polymer. The PET molecular repeat unit is shown in Fig. 1.

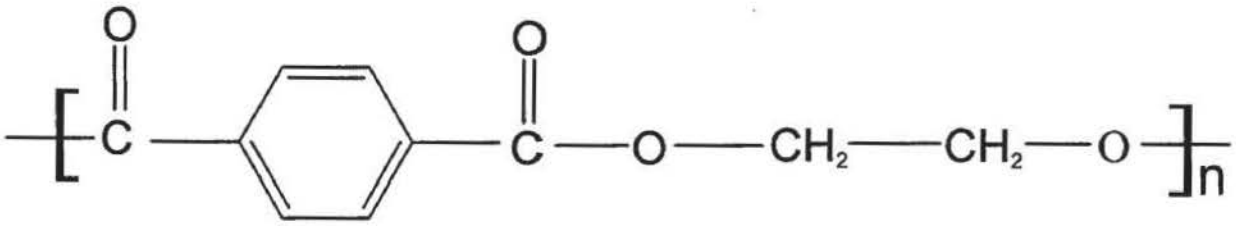

Fig. 1.1 The monomer repeat unit of PET

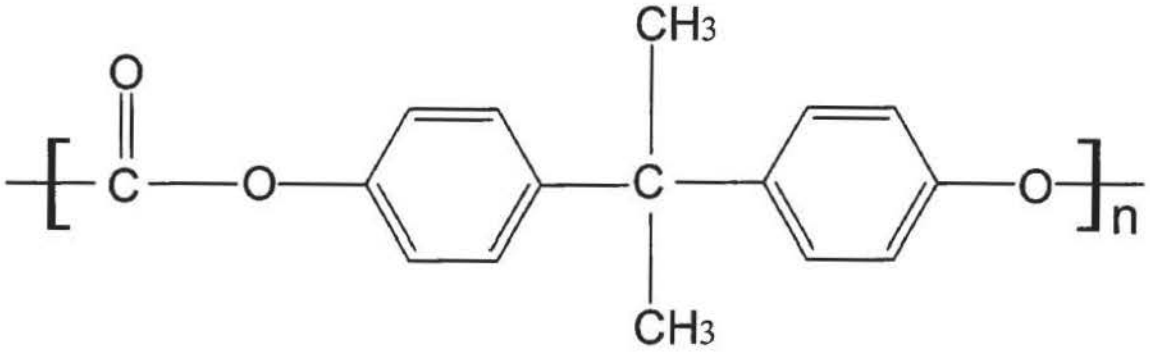

Fig. 1.2 The monomer repeat unit of PC

1.6.2 Polycarbonate [31, 32]

The term polycarbonate (PC) refers to a class of polyhydric phenols linked through carbonate groups but, in general usage, polycarbonate refers to the PC derived from bisphenol-A (BPA) since over 99% of the world commercial polycarbonates are based on BPA. PC was first commercially produced by General Electric and Farbenfabriken Bayer simultaneously in 1958. PC is characterised by a unique combination of useful properties, such as good mechanical characteristics over a wide temperature range (particularly impact strength), resistance to long-term exposure to high temperature, good electrical properties, dimensional stability, transparency, low flammability and good resistant to salts and oxidation. The main disadvantages of PC are its susceptibility to abrasion, stress-cracking and attack by solvents, acids and alkali. Another deficiency of PC is its sensitivity to specimen thickness in notched impact strength. PC is one of the principal engineering polymers with a broad range of application in safety equipment and structural materials, in transportation and electricity.

Commercial PC grades can be produced by interfacial polymerisation which gives a higher thermal stability and a better molecular weight distribution (MWD), compared to these prepared via transesterification. Interfacial polymerisation involves reaction at a boundary between two immiscible solvents, one protic and the other aprotic. The transeterification process is carried out in the molten state and in this case the carbonyl group is provided by an aromatic carbonate. All industrial processes lead to polymer that contains hardly any hydroxyl terminal groups, which, if present, are deleterious to the thermal stability of PC[33]. The molecular repeat unit of PC is presented in Fig. 2.

1.6.3 PET/PC Blends

As mentioned above, the relatively low T_g is a potential disadvantage for PET. This may result in a significant decrease in modulus at temperatures between T_g and T_m, which limits its use in some applications. On the other hand PC has a higher T_g, 145°C, and its solvent resistance is improved by mixing with PET. Therefore, there has been considerable scientific and industrial interest in the blending of PET/PC. Even though a great deal of research by different authors has been performed no consistency has been achieved[34-45].

From thermal analysis and dynamic mechanical testing of the PET/PC blends, Paul *et al.*[34] reported that melt-mixing PET / PC blends formed a homogeneous amorphous phase if the PET content is above 60~70 wt % and an inhomogeneous amorphous phase is produced if the PET content is below this range. Later[35], they reported that the extent of interchange reactions between PC and PET was not very great and did not lead to a random copolymer during melting-mixing in a Brabender blender at 563 – 573 K. They also found that the percent elongation at break of some blends was larger than expected but the reason for this was not clear.

However, Chen *et al.*[36] and Hannah *et al.*[37] have pointed out that over the entire composition range, the PET/PC blends were immiscible. Chen *et al.*[36] concluded from DSC, DMTA and infrared spectroscopic (IR) studies that extruder mixed blends showed a small extent of transesterfication but were inhomogeneous in the amorphous phase. Hanrahan *et al.*[37] demonstrated the immiscibility of PC and PET using DSC and

dielectric loss spectroscopy for the solvent-cast blends. Later Suzuki *et al.*[38] made a further study on both extruder-mixed and solvent-cast blends with the help of DSC, phase contrast microscopy and IR spectroscopy. They also concluded that PET/PC blends were immiscible over the whole composition, because the copolyester products of the reactions were not efficient enough as a homogenizer. The crystallisation of PET was strongly suppressed by the change of chemical structure and blending.

The contradictions in these conclusions can be attributed to the different methods of blend preparation, which lead to different degrees of transesterification.

1.7 The Objectives of the Current Study

PET/PC blends which have undergone no transesterification will exhibit phase separation. The objective of the current research was to prepare PET/PC blends in the presence of a transesterification catalyst to improve their compatibility. Immiscible blends produced in the absence of transesterification will also be prepared to compare with those in the presence of catalyst.

The microstructure and the glass transition temperature will be analysed to assess the degree of miscibility of the blends. Isothermal crystallisation kinetics, melting and degree of crystallinity will be studied as a function of composition.

Modulated temperature differential scanning calorimerty (MTDSC) is a relatively new technique in thermal analysis[46-48]. MTDSC is capable of separating reversing and non-reversing components of the specific heat which conventional DSC techniques cannot do as the reversing and non-reversing heat is measured simultaneously on heating. MTDSC will also be used to separate the glass transition of PC and crystallisation of PET. The quasi-isothermal crystallisation of PET will also be investigated.

The transesterification in PET/PC blends could occur in the molten state in the presence and absence of catalyst. The kinetics of this reaction will be studied at different temperatures. The thermal properties and structural changes will be analysed under different degrees of the transesterification.

Chapter Two

Materials, Apparatus and Experimental Procedures

2.1 Materials

The raw materials used in this project were obtained from commercial sources. The poly(ethylene terephthalate) (PET) was manufactured by DuPont, USA, as moulding pellets. It has a number average molecular weight of 19.6 kg mol^{-1} and weight average molecular weight of 36.4 kg mol^{-1}. The polycarbonate (PC) was supplied by ECP Enichem Polimeri, Italy, carrying the identification of Sinvet®. It has a number average molecular weight of about 20 kg mol^{-1}. Metallocene polyethylene (m-PE) was purchased from Exxon Chemical Co. France, as an Exact grade 3009. It is a copolymer of ethylene and hexene-1. The number and weight average molecular weight are 40 and 100 kg mol^{-1} respectively.

Lanthanum acetylacetonate hydrate ($La(acac)_3 \cdot xH_2O$), transesterification catalyst, was purchased from Aldrich Chemical Co. Ltd. and used as obtained. Diethylenetriamine (DETA), 99%, was also purchased from Aldrich Chemical Co. Ltd. and used as obtained

2.2 Apparatus and Experimental Procedures

2.2.1 Compounding and Sample Preparation

2.2.1.1 Twin Screw Compounder

Blending of PET and PC was carried out in an APV model MP2000 twin-screw compounder. The feed section picked up the predried granulated polymer mixture from a hopper and propelled it into the heated cylindrical barrel, which contained two counter rotating, inter-meshing screws, which blended the molten mixture. The blend was forced though a die containing two holes of diameter 5 mm. The strands produced were quenched in cold water and chopped into granules by a pelletizer.

The temperature of the barrel zones was set at 295°C and the die zones at 305°C, and a mixing blade speed of 100 to 150 rpm was used depending on the mixture to maintain a high torque (70% of full scale). This gave thorough mixing.

The barrel and the system were initially purged with PET. The first 200 to 300g of each blend was also discarded.

2.2.1.2 Blends in the Absence of Catalyst

The two polymers were dried in an oven at 135°C for at least 4 hrs prior to blending, and were premixed to ensure good distribution and a dispersed mixture. Initially, the PET/PC (50/50 by weight) blends were made as master batch, then, the other PET/PC blends were made in ratios of 90/10, 80/20 and 70/30 by weight respectively.

2.2.1.3 Blends in the Presence of Catalyst

The catalyst was initially dispersed on 100 g of the PC pellets by a solvent cast method. The PC was initially dried to remove the solvent in a fume cupboard and then moved into a vacuum oven at 60°C for 12 hrs. The rest of the PC and PET were dried in an oven at 135°C for at least 4 hrs prior to blending. These raw materials were premixed in a closed container. The concentration of catalyst was 0.075% by weight with respect to the final product. Three blends were prepared in the ratios of PET/PC 50/50, 70/30 and 90/10 respectively. The conditions for blending were the same as that used in preparing blends in the absence of catalyst.

2.2.1.4 Sample Preparation

A Moore 25-ton hydraulic press was used to prepare plaques from the blend granules. The granules were dried in a vacuum oven at 120°C for 12 hrs before moulding. The press was preheated to 280°C and 25 g granules were placed in 10 cm square mould in

between two polytetrafluoroethylene (PTFE) sheets. The granules were softened for 3 minutes before a pressure of 15 ton was applied on it for 2 minutes. The plate was removed from the press and quenched in ice-water to obtain an amorphous sheet. The m-PE was moulded at 433 K for 5 minutes under the same pressure. The plaques were either quenched directly in ice water or slow cooled in the hydraulic press to room temperature over 5 hrs. DSC samples were cut directly as discs from the plaques.

2.2.2 Differential Scanning Calorimetry (DSC)

A Perkin-Elmer differential scanning calorimeter, DSC-2, interfaced to a PC was used to study the thermal properties of the blends. In the DSC a reference and sample holder contained a platinum sensor to measure temperature and a platinum resistance heater. The temperature of the sample and reference were kept at the same value throughout isothermal and dynamic runs. This is carried out by two control loops. Figure 2.1 shows the diagram of the temperature and power control loops. The first loop allowed the average temperature of both sample and reference holders to vary according to programmed conditions and the second maintained the sample and reference at the same temperature by adjusting the voltage to the heaters. Usually, the programmed temperature is maintained in both the reference and sample holders and any deviation from the set programme is immediately rectified by adjusting the power to both heaters. The power difference supplied to each holder is recorded as a function of temperature and time, and energy differences associated with transitions in the sample can be determined directly.

At each point, the power difference associated with heating the sample through dT is

$$dH/dt = (dH/dT)*(dT/dt) = C_p*\beta \quad (2.1)$$

The power difference reflects heat flow, equals to heat capacity of the sample multiplied by the heating rate. As the heat capacity changes during phase transitions, such as glass transition, crystallisation and melting, heat flow can be readily measured by DSC. Figure 2.2 shows a DSC trace for amorphous PET on heating from room temperature to above the melting point. Thermal transitions such as glass transition, crystallisation and melting, are present in this trace.

The temperature of the DSC was calibrated by using the melting of ultra-purified materials: lead (600.65 K), tin (505.06 K), indium (429.78 K) and stearic acid (343.65 K). A calibration curve relating melting temperature and calorimeter temperature which was extrapolated to zero heating rate was found to be linear.

The heat flow of the calorimeter was calibrated by two methods. The first used the enthalpy of fusion of ultra-purified indium (28.45 J g^{-1}). The second used the specific heat of sapphire where the heat flow response was used for heat capacity calibration. In the latter case, empty aluminium pans matched in weight to within 0.02 mg were used for the sample and reference. Initially, the two empty pans were scanned to determine the calorimeter baseline and this was repeated with a sapphire standard sample to calibrate the thermal response of the calorimeter, finally was repeated with the sample. The calibration and sample traces were obtained by subtracted the calorimeter baseline.

The samples weigh 10 ± 0.1 mg in order to get comparable and reproducible results. For dynamic runs, the samples were heated or cooled at a constant rate between the interested temperature range under the range of 5.0 mcal s^{-1}. For isothermal crystallisation, the samples were heated from 320 to 550 K at a heating rate of 80 K min^{-1}, kept for 5 minutes to erase the previous thermal history and cooled to predetermined temperature T_c at a cooling rate of 160 K min^{-1} with the range set to 2 mcal s^{-1}. The isothermal crystallisation baseline was collected immediately after finishing the isothermal crystallisation by cooled to $(2T_c - 550)$ K under the same conditions. All the DSC experiments were operated under nitrogen flow of 20 cm^3min^{-1}.

2.2.3 Modulated Temperature Differential Scanning Calorimetry[49]

The modulated temperature adopted a sinusoidal temperature change superimposed on a linear heating ramp, i.e.

$$T = T_0 + B\,t + A_T \sin \omega\, t \qquad (2.2)$$

where T and T_0 are the temperature at time t and 0 respectively, B is a linear heating rate, ω the modulation frequency such that $\omega = 2\pi/p$ with p representing the time of one cycle, A_T is the amplitude of the sinusoidal frequency in temperature.

The Perkin-Elmer power compensation DSC-2 was modified into a MTDSC interfaced to a PC. A multifunctional card with several digital to analogue (D to A) and analogue to digital (A to D) converters was used to measure the temperature and heat flow *versus* time. The D to A port was used to generate a voltage following a predetermined time dependence. When a sinusoidal profile was chosen from D the similar sinusoidal

voltage was produced in A. After the voltage was applied to the zero calibration potentiometer of the calorimeter the voltage changed the sample and reference temperature. Thus sinusoidal temperature variation was generated.

MTDSC data deconvolution was performed according to the procedure proposed by Reading[50]. The heating rate, B, was calculated from the first derivative of the temperature *versus* time data. The period of the modulation, p, was determined by counting the successive minima or maxima in the temperature profile. The algorithm applied a linear least-squares fit to the heat flow *versus* heating rate data over one period. The reversing heat capacity, $C_{p,r}$, was obtained from the slope of dH/dt *versus* dT/dt over one modulation and non-reversing heat flow, dH_N/dt, from difference between the average heat flow and reversing heat flow. This is summarised as:

$$dH/dt = C_{p,r}*B + dH_N/dt \qquad (2.3)$$

The phase lag, δ , was determined by shifting the heat flow data with time on to the temperature profile until the best fit was achieved. Deconvolution software was provided by D. Price of Loughborough University initially. Latterly the software developed by J. Atkinson of Birmingham University was used.

2.2.4 Scanning Electron Microscopy (SEM)

A scanning electron microscopy, Jeol 5410 model, was used to examine the morphology of the PET and its blends. The microscope consisted of an electron beam accelerated through a 10-25kV p.d. scanning the surface of the sample with a resulting release of secondary electrons. These were detected by a scintillation counter and displayed on an x-ray cathode tube, which could be viewed directly[51]. The image was recorded as a digital file through **Orion™** software.

Fracture surfaces of the samples were prepared by cooling sample in liquid nitrogen and breaking sample at this temperature. Subsequently, the samples were etched with DETA for about 1 min at ambient temperature to remove the PC [52]. The etched samples were washed with distilled water and dried in air. After etching, samples were fixed on to an aluminium stub. Since polymer samples were electrical insulators, they were coated with gold to conduct the surface change generated by the electron beam. A silver paint adhesive was used to make good electrical contact between the base of the specimen and the metal holder.

2.2.5 Hot Stage Microscopy

The phase structure which had developed in the of PET/PC blends was investigated using a polarised light microscope, Leitz Dialux Pol 50, fitted with a Linkam hot stage, TH600, and a temperature controller, PR600. The microscope was used with a constant

wavelength light source from a sodium vapour lamp. The temperature range of the temperature controller was from ambient to 873 K and heating rates from 0.1 to 90 K min^{-1} could be used. The temperature of the hot stage unit was calibrated using the m.pt. of high purity materials: benzoic acid (395.52 K), ammonium dihydrogenphosphate (463.2 K) and tin (505.06 K). The calibration equation showed a very good linear relationship. The microscope was used in transmitted light mode and independently adjustable polarising filters were fitted above and below the sample chamber.

Samples were cut using a cryo-microtome to about 10 μm thick and pressed between two 16 mm diameter glass covers. They were melted in a hot plate. The cover slips were placed in the sample holder and inserted into the furnace of the hot stage. The temperature was raised from ambient to the desired one at a heating rate of 90 K min^{-1}. The field of view could be viewed through an eyepiece or a Nikon-100 digital camera which was used to take photographs.

2.2.6 Fourier Transform Infrared Spectroscopy (FTIR)

A Fourier Transform infrared spectrometer, Nicolet Magna-IR 760, with a Linkam hot stage 600 was used to collect spectra as a function of temperature and time. When the infrared beam passes through a sample, some of the frequencies are absorbed while the rest are transmitted. The infrared absorption bands are associated with the molecule structure and molecular vibration of the bands. Different bands presented in a spectrum have different vibration frequencies, from which it is possible to identify the molecular structure.

The hot stage was calibrated as above. Spectra were collected at room temperature and at various temperatures. To prevent sample oxidation at high temperature, nitrogen gas flowed across the sample and potassium bromide, KBr, windows were used to seal the sample chamber. Spectra recorded at 4 cm^{-1} resolution and 100 scans were accumulated for both sample and background unless specified.

2.2.7 Instron Tensile Tester

Tensile properties were measured on an Instron, model 5566 interfaced to a PC. The crosshead speed could be selected from 0.005 to 500 mm/min with an accuracy of ± 0.1%. Both load accuracy and strain accuracy were ± 0.1% of full scale, or ± 0.5% of the readings. Stress-strain data were collected as a function of time at default strain rate and extension, load, stress and % strain were calculated.

Standard dumbbell shaped specimens were cut directly from the moulded plaque. The specimens had a gauge length of 25 mm, width 4 mm and thickness 0.80 mm. For each experiment carried out on Instron, at least five samples were used. The final result was an average of them. The crosshead speed used was 2 mm min^{-1}, unless specified. All tests were carried out at constant temperature of 296 ± 1 K and constant relative humidity of 35 ± 1%.

2.2.8 Zwick Impact tester

Impact tests were used to measure the toughness of the materials under high strain rate. The impact test was carried out using a Zwick impact tester at a strain rate of 3.5 m s^{-1}. The tester consists of an anvil-shaped pendulum with weight of 2.4 kg.

The dumbbell shaped specimens used were identical to that used in the Instron tests. A specimen was clamped at one end and the pendulum was raised to a fixed height of 0.64 m and released to break the sample. The energy to failure was recorded from the return of the pendulum. The energy to failure was corrected for the resistance of the free moving pendulum alone. An average of at least eight specimens were used. The tests were carried out at constant temperature of 296 ± 1 K and constant relative humidity of 35 ± 1 %.

2.2.9 Wide Angle X-ray Diffraction (WAXD)

Wide angle X-ray diffraction experiments were carried out using a Philips X'Pert vertical diffractomter interfaced to a PC. The diffractometer operated with Copper Kα radiation and wavelength of 0.1542 nm at 40 keV and 50 mA. The diffraction intensities were recorded as a function of increasing scattering angle 2θ, which was in the range 5-80° with a step angle of 0.02° and the scan time of 1 s per step.

The volume crystallinity, $X_{c,v}$, was calculated from the ratio of the areas under the crystalline peak, A_c, to the total areas, A_t. As can be seen from Fig. 2.3, the A_c was calculated by using the partially crystalline intensity subtracting amorphous background, i.e. $A_c = A_t - A_a$,

$$X_{c,v} = A_c/A_t = A_c/(A_c + A_a) \tag{2.4}$$

2.2.10 Density Measurement

Densities were measured on moulded specimens by Archimedes' method: first by weighing in air and then in n-heptane at 296 K. A Perkin-Elmer Auto Balance, AD-2, was used to weigh the samples to an accuracy of ± 0.01 mg. An average of at least three specimens taken from the same sample were used. The density is given by

$$\rho = \frac{W_{air}}{(W_{air} - W_{hep})}\rho_{hep} \tag{2.5}$$

where ρ_{hep} is 0.683 g cm^{-3} for n-heptane.

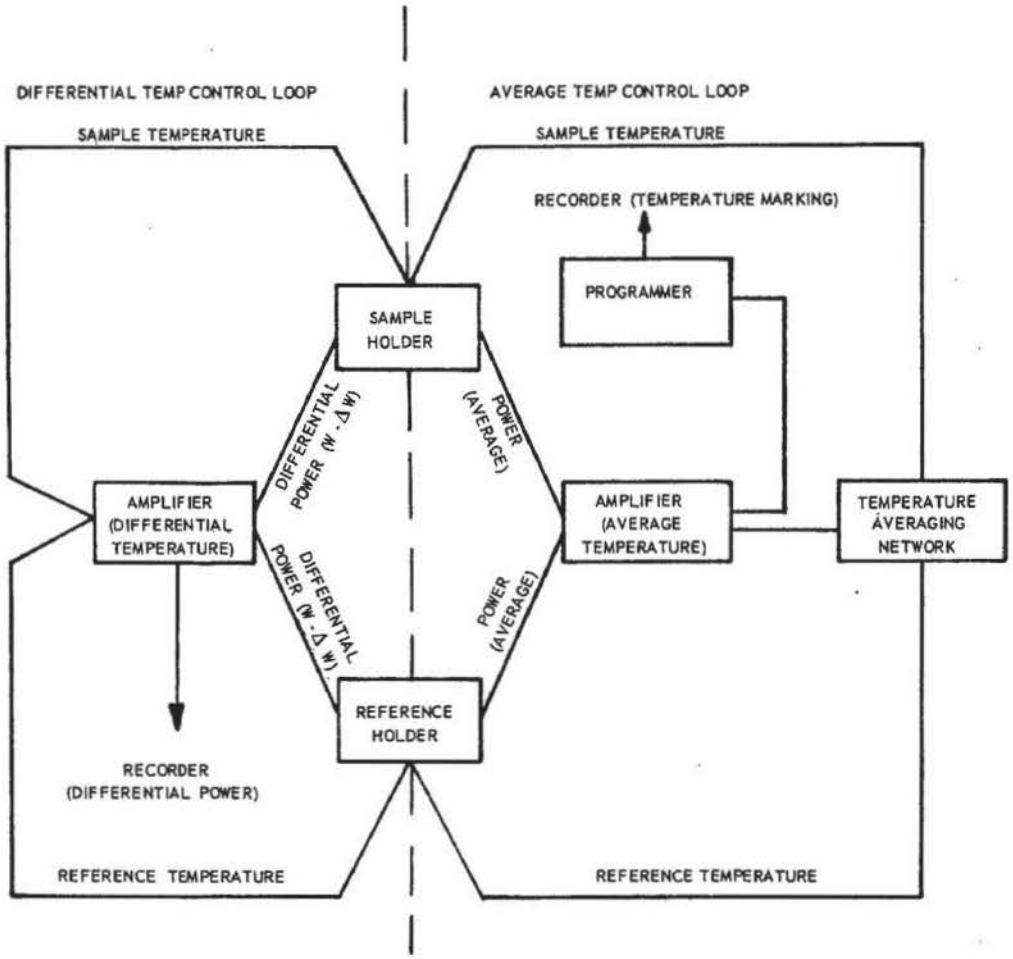

Fig. 2.1 Diagram of the two control loops of DSC-2

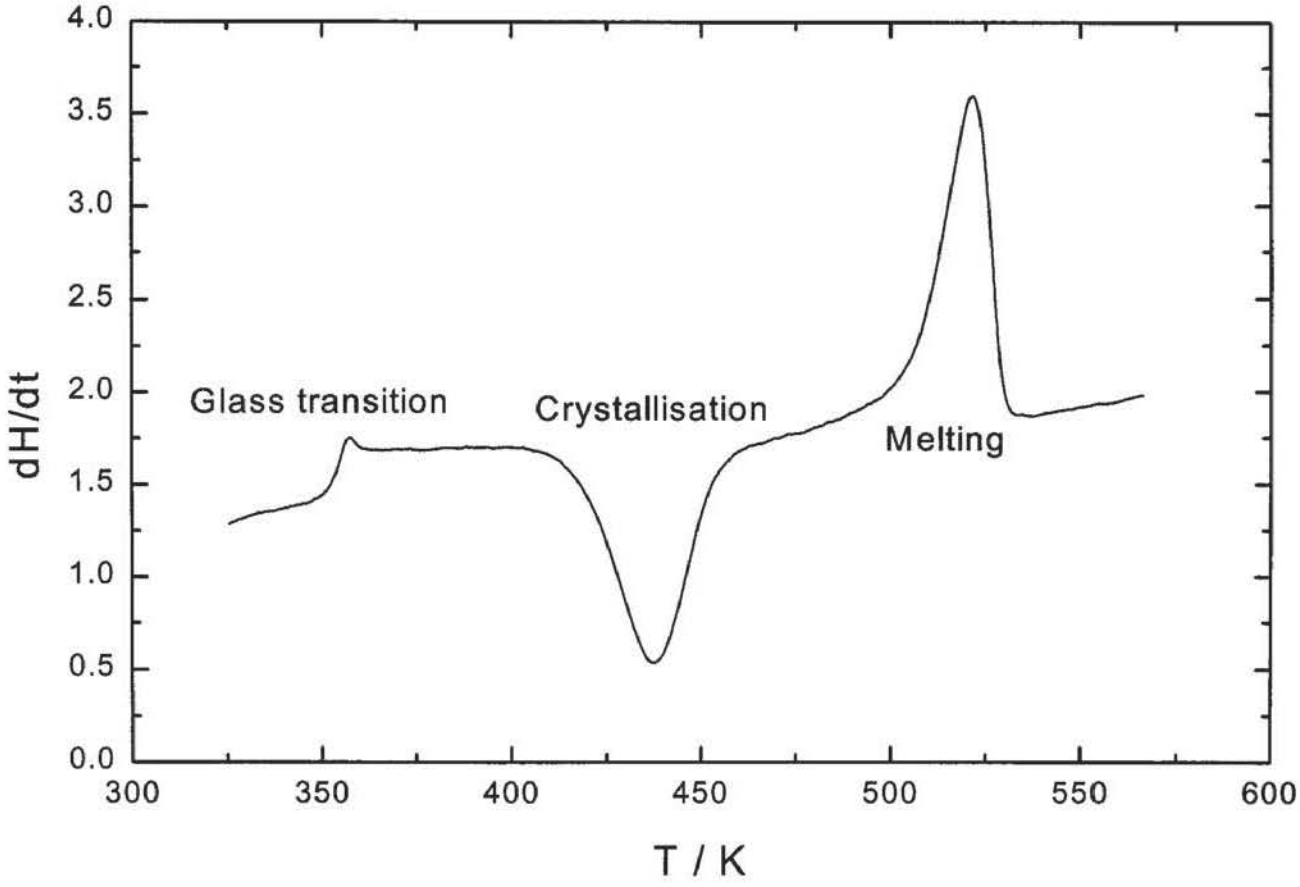

Fig. 2.2 DSC trace of amorphous PET on heating from room temperature to above melting point

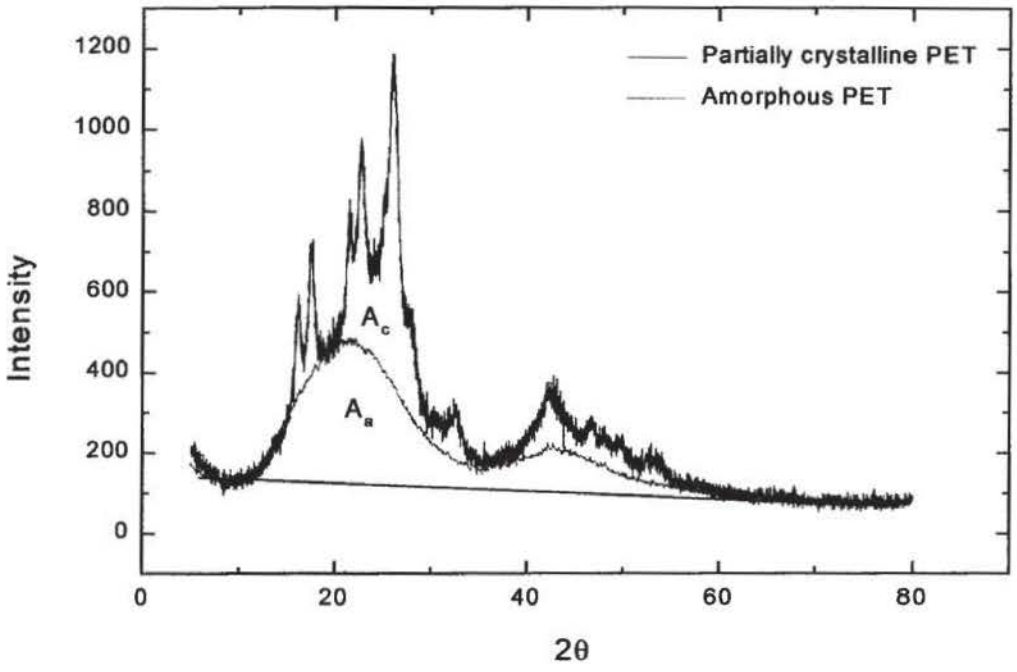

Fig. 2.3 WAXD diffractogram of PET

Chapter Three

Glass Transition and Miscibility of Polymer Blends

3.1 Introduction

The glass is a "solid" state and its molecular structure is very similar to that of the liquid state, such that there is only localised short range order up to few molecular diameters and no long range 3-dimensional order[53]. The glass state is also synonymous with the amorphous "solid" state.

When a material is cooled from the liquid state through the glass transition there is no discontinuous change in volume, enthalpy or entropy but a rigid "solid" is formed. In the glass transition region the properties of a polymer change dramatically with temperatures, for example, the elastic modulus changes by three orders of magnitude over this region.

The glass transition temperature, T_g, is the most important parameter of an amorphous thermoplastic material, since it determines its upper working limit. T_g is defined as the temperature corresponding to the onset of long-range consented segmental motions. Therefore any molecular change which alters the chain mobility will be reflected in a change in T_g, for example, the addition of plasticizer lowers the T_g while cross-linking increases it. In polymer blends, if there is some interaction between the two components there will be a change of T_g. Strong molecular interaction between the molecular chains leading to compatibility produces only one T_g and this is indicated of the blends being miscible; if there is less interaction and two T_gs are present displaced from the values of the components, and the blends are partially miscible; if there is little or no interaction between the two components, two T_gs independent of compositions are present and the blends are immiscible.

In this chapter, the miscibility of the PET/PC blends have been studied from the change in T_gs. Changes in morphology and in the FTIR spectra with composition have also been studied as well as changes in tensile properties.

3.2 Glass Transition

3.2.1 Free Volume Theory

Early attempts at explaining the glass transition involved the concept of free volume[54,55]. Free volume is defined as the empty space arising from imperfect packing of the molecules, i.e.

$$V_f = V - V_0 \quad (3.1)$$

where V_f is the free volume, V is the observed volume and V_0 the volume occupied by close-packed molecules in the crystalline state at 0 K. V_0 cannot be measured directly. f = V_f / V is called the fractional free volume. The free volume is a measure of the space available for the polymer to undergo segmental motions, by rotational and translational movement. For a liquid the free volume increases with temperature as molecular motions increase.

If the temperature of the liquid is decreased, the free volume decreases and eventually reaches a critical value at which there is insufficient freedom for large-scale segmental motion to take place. The glass transition is considered to occur at this temperature. Below T_g the free volume remains essentially constant as the temperature decreases further since molecule motion is frozen.

Using the concept of free volume Doolittle *et al.*[56, 57] proposed a relationship between viscosity and free volume for a liquid, i.e.,

$$\eta = \eta_0 \exp (C (V - V_f) / V_f) \quad (3.2)$$

where η_0 and C were adjustable parameters, C being of order unity and V and V_f are as defined above. It was found that the relationship was valid over the temperature range between crystallisation and boiling temperature, and V and V_f were linear with temperature in this range. Deviations occurred, however, at lower temperature when f > 0.25 for organic liquids.

Williams *et al.*[58] observed that with polymer f was typically from 0.13 to 0.25. Based on the assumption that free volume increased linearly with temperature above the T_g, they derived an important relationship between viscosity and temperature i.e. the Williams, Landel and Ferry equation,

$$\ln \alpha_T = \frac{\eta_T}{\eta_{T_g}} = \frac{-C_1(T - T_g)}{C_2 + (T - T_g)} \tag{3.3}$$

where α_T is the shift factor, η_T and η_{Tg} refer to the viscosity of the polymer at temperature T and T_g, C_1 and C_2 are universal constants. For a large number of polymers, $C_1 = 17.44$ and $C_2 = 51.6$ K. Early experiment suggested that C_1 and C_2 were universal constants and were the same for all polymers. Later experiments, however, indicated that this was not true[59, 60]. It was also found that a value of the fractional free volume of about 0.025 was required for most polymers at T_g.

3.2.2 Thermodynamic Model

In thermodynamic terms, the glass transition is considered to be a second-order transition and does not involve any order-disorder

It is measured experimentally by: (a) the change in slope of volume expansion or enthalpy, or (b) the discontinuity in the thermal expansion coefficient or heat capacity curves against temperature. As shown in fig. 3.1, the glass transition is well defined and is normally observed to be reversible.

changing the transitions. However, the main weakness of this theory are (a) that a chain of zero stiffness would have a T_g of 0 K and (b) that the Tg would be essentially independent of any molecular interaction[64].

Later, Adam and Gibbs[65] sought to bridge that gap between the equilibrium treatment of G-D theory and the free volume approach embodied in WLF equation, by relating the relaxation behaviour close to T_g with the static properties of the ideal glass at T_2. The resulting relationship derived similar in form to the WLF equation, i.e.

$$-\log \alpha_T = c_1 \frac{T - T_s}{c_2 + (T - T_s)} \tag{3.8}$$

in which

$$c_1 = 2.303 \frac{C}{\Delta C_p T_s \ln(T_s / T_2)}$$

and

$$c_2 = \frac{T_s \ln(T_s / T_2)}{\ln(T_s / T_2) + [1 + T_s / (T - T_s)] \ln(T / T_s)}$$

where α_T is the shift factor, T_s is a reference temperature, C is a constant related to the configuration entropy of the sample and ΔC_p is the difference in specific heat between the equilibrium melt and the glass at T_g. This provided an alternative interpretation for the change in material behaviour of polymers close to their glass transition temperatures.

3.2.3 Factors Affecting T_g

The T_g varies widely from polymer to polymer and it is largely dependent on the amount of thermal energy required to activate the segmental mobility and the rotational energy levels about the chain links. Factors which affect the values of T_g. include[31]:

1) *Chain flexibility.* This is a measure of the ability of a chain to rotate about the constituent chain bonds. Hence a flexible chain has a low T_g whereas a rigid chain has a high T_g.
2) *Molecular structure.* When polymer chains are asymmetric the bulky pendant and polar groups hinder rotation around the backbone and this leads to an increase in Tg, but flexible branches lower the T_g. Factors such as cross-linking, hydrogen bonding and the presence of crystalline regions all decrease chain mobility and raise T_g.
3) *Molar mass.* Tg also varies with the polymer chain length. With high molar masses the Tg is essentially constant, but it decreases as the molar mass is lowered in line with the following relationship, i.e.

$$T_g = T_{g,\infty} - K / M_n = T_{g,\infty} - (2\rho N_A \theta / \alpha_f M_n) \tag{3.9}$$

where $T_{g,\infty}$ is the glass temperature of a polymer with infinite molar mass, θ is the free volume contribution of a chain end and is 2θ for linear polymer, ρ the polymer density, N_A is Avogradro number, M_n is the number average molar mass, and α_f is the free volume expansivity defined as

$$\alpha_f = \alpha_l - \alpha_g \tag{3.10}$$

where α_l and α_g are thermal expansion coefficient for liquid and glass, respectively.

3.3 Results and Discussion

3.3.1 Glass Transition of PET and its Blends

In thermodynamics the glass transition is defined by equating the enthalpies of liquid and glass, i.e.

$$H_l^o + AT_g + \frac{B}{2}T_g^2 = H_g^o + aT_g + \frac{b}{2}T_g^2 \qquad (3.11)$$

where H_l^o and H_g^o are the enthalpies of liquid and glass at a standard temperature and A, B, a and b define the temperature dependence of the specific heat of the liquid and glass respectively, as a consequence the shaded areas in Fig.3.3 are equal at T_g as indicated by Richardson *et al.*[66]

Since the measured glass transition temperature, T_g, depends on the rate of cooling during which the glass was formed, a standard quench rate was adopted for all the samples to produce a standard glass. Thermal lag corrections were also made in measuring T_gs. This involved linear extrapolation of the T_g to zero heating rate at constant sample weight. Using this method, the T_gs of PET and PC were measured as 349 and 413 K respectively. Both values are in good agreement with literature values[67].

On heating the amorphous blend sample prepared without added transesterification catalyst only one glass transition close to that of PET was observed in the first DSC scan. This can be seen in Fig. 3.4a. The glass transition was followed by an exotherm due to the crystallisation of PET, the size of the exotherm varying with PET content. No

transition could be observed in the glass transition region of PC since it was masked by the crystallization exotherm of PET. The second glass transition, close to that of PC, was detected during the second scan of the blend sample once the PET crystallization was complete as shown in Fig. 3.4b. The two T_gs did not vary substantially with blend composition.

Differences were observed in the thermal response of blends prepared in the presence of the transesterification catalyst. As can be seen in Fig.3.5, two T_gs were observed, one close to that of PET which was attributed to a PET-rich phase and the other close to but lower than that of PC attributed to PC-rich phase, during the first heating scan above a heating rate of 10 K min^{-1}. The crystallization of the PET had been inhibited and occurred at a much higher temperature, 425 rather than 400 K. This took it out of the glass transition region of PC, thus enabling it to be observed.

The variation of the T_gs with composition is shown in Table 3.1 and listed in Fig. 3.6. The dashed line represents the variation of T_g with composition assuming miscibility and Fox equation[19] dependence. It can be seen that for the blends without added catalyst, both T_gs are independent of composition. For the blends prepared in the presence of catalyst, two T_gs could be observed in the 50/50 and 70/30 blends. The T_g of PET-rich phase is slightly higher than that of 100% PET and increases with increasing PC content while the T_g of PC-rich phase is somewhat lower than that of PC and also increases with PC content. The values of the T_gs suggest that there is only 0.5 – 0.7% PC in the PET-rich phase for 50/50 and 70/30 blends prepared without added catalyst while there is 8 – 10% PC in the PET-rich phase for corresponding blends added

catalyst. This clearly indicates that the blends prepared without added catalyst were completely immiscible, while those prepared in the presence of catalyst showed some partial miscibility. The T_g values confirmed that there was more PET in the PC-rich phase than PC in the PET-rich phase [39].

3.3.2 The Morphology of PET/PC Blends

The morphology of the blends was investigated by SEM from the appearance of the fracture surfaces after etching with diethylene triamine (DETA). DETA is highly selective in etching PC without attacking PET[52]. The SEM micrographs of the blends prepared without added catalyst are shown in Fig. 3.7. All the blends exhibited a binary structure. At 50/50 composition a co-continuous morphology was observed while at lower PC compositions, spherical PC particles were distributed uniformly throughout a continue PET matrix. The etched spherical cavities had sharp boundaries and there was no evidence of any interfacial layer between the matrix and the domains. The PC particles decreased in size from about 2-4 μm at 70/30 to 0.5-2 μm at 90/10 PET/PC blends.

In the blends prepared in the presence of catalyst it can be seen from Fig. 3.8 that the PET/PC 50/50 blend shows a co-continuous morphology and a similar trend with increasing PET composition from 70/30 to 90/10 of smaller PC particles embedded in a PET matrix. However the PC particles are significantly smaller than observed previously with the blends prepared without the catalyst. The particle sizes were about 1.0 micro in diameter at 70/30 and sub-micron at 90/10, consistent with their being

more dispersed. It is difficult to accept that 30 and 10% of the sample was present in the dispersed phase.

The SEM analysis was in good agreement with DSC result in that the PET/ PC blends prepared without added catalyst were completely immiscible and exhibiting a two phase structure, while the blends prepared in the presence of added catalyst show partially miscibility only and a more dispersed phase, which demonstrates that the components appeared to be more compatible as a result of the treatment with the transesterification catalyst.

3.3.3 FTIR Spectra of PET and the Blends

Samples were prepared by solvent-casting on to KBr discs. The solutions were made by directly dissolving the samples cut from moulded sheets without any further thermal treatment. Fig. 3.9 shows the FTIR spectra of PET, PC and the PET/PC blends collected from 4000 to 400 cm^{-1} for 400 scans at a resolution of 1 cm^{-1}. Characteristic absorption bands for the polymers are listed in Table 3.2 along with their group assignments[38,40,45]. From Fig. 3.9, it is clear that no new bands developed at 1740 and 1070 cm^{-1}, which could be attributed to transesterification of the blends during melting processing.

In order to perform a more detail study of the FTIR spectra, the spectrum of PC was subtracted from that of the blend, see Fig. 3.10. It was obvious that almost all the bands in the Fig. 3.10 were identical except for region the around 1780 cm^{-1}, suggesting that

there was some interaction between the two components. Transesterification did not produce obvious new bands.

3.3.4 Mechanical Properties of the Blends

3.3.4.1 Tensile Properties of the Blends

The tensile properties were measured at a constant strain rate of 2 mm min^{-1}. A typical stress-strain curve is shown in Fig. 3.11. Initially there was a linear increase in stress with the strain such that Hooke's Law was obeyed. The Young's modulus, E, was measured from this initial slope, i.e.,

$$E = \sigma/\varepsilon \tag{3.12}$$

in which σ is the nominal stress defined as

$$\sigma = F/A_0 \tag{3.13}$$

and ε is the nominal strain defined as

$$\varepsilon = (L-L_0)/L_0 = \Delta L/L_0 \tag{3.14}$$

where F is the stretching force, A_0 is the original cross-sectional area, L_0, L and ΔL are the original, instantaneous and increased gauge length of the sample respectively.

The yield point is defined as the point at which $d\sigma/d\varepsilon = 0$ as shown in Fig 3.11. For polymer materials deformation is reversible on unloading up to the yield point. Beyond this point the deformation is partially recoverable and permanent deformation is observed on unloading. However, if the deformed polymer is subsequently heated above its T_g, it will return to its original demensions[68].

After yielding, the stress drops to some extend which is due to geometric change. This localised decrease in cross-sectional area in a region of the gauge length is known as necking. During neck formation the average stress of the sample is almost constant. Eventually, when the whole specimen has necked, strain hardening occurs as the stress increases further up to fracture. The total area under the stress-strain curve measures the tensile fracture energy of the material under these experimental conditions.

The stress-strain curves of the blends compared to that of PET are shown in Fig. 3.12. All amorphous samples exhibited the typical stress-stain curves of ductile polymer materials as described above. The tensile modulus was measured from the initial slope of curve i.e. from 0.5 to 2.5% of strain. The yield stress, extension at yield, breaking strength, elongation at break and the energy to break were directly measured from the stress-strain response of each material.

The tensile characteristics of the amorphous PET/PC blends are listed against composition in Table 3.3 as well as shown in Fig.3.13. It can be seen that the blends are all ductile and form a neck on yielding. The modulus of PET/PC blends is shown in Fig. 3.13a. It can be seen the moduli of the blends prepared in the presence of catalyst were greater than those in the absence. Generally, the mechanical properties of the blend were between those of the two components, and the average values followed a simple addivity rule, i.e.

$$P = \sum_{i=1}^{n} w_i P_i \qquad (3.15)$$

where P refers to a property of the blends, and w_i and P_i are the weight fraction and property of the i^{th} component. It is quite clear that the modulus of a blend prepared in the absence of catalyst was close to the average of modulus of the components and decreased with increasing PC content. On the other hand the modulus of a blend prepared in the presence of a catalyst was higher than the average value and almost independent of compositions.

The yield stresses of the amorphous PET/PC blends are plotted against composition in Fig. 3.13b. The values for the 70/30 and 50/50 blends prepared in the presence of catalyst were higher than the average for the components, and also higher than the correspondent blends prepared without catalyst. The yield stresses of the blends prepared without catalyst decreased with increasing PC content.

The extensions at yield of the PET/PC blends are shown in Fig. 3.13c, both prepared with and without catalyst. These were lower than the average value for the components. Blends prepared without catalyst yielded at almost constant extension at yield independent of composition but the extensions were greater than those prepared in the presence of catalyst. In the blends prepared in the presence of a catalyst the extensions at yield increased slightly with increasing PC content.

The breaking strengths were quite varied. In the blends with lowest PC content the breaking strengths of the blends were higher than the average value but with the higher PC content the breaking strengths were lower than the average value. At each

composition the breaking strength of blends prepared in the presence catalyst was higher than that without especially at 70/30 composition.

The elongations at break of both blends show the same trend with changing composition. The elongation at break decreases with increasing PC content and both elongations at break were slightly above the average value. This can be seen in Fig. 3.13e.

The energies at break of PET/PC blends prepared in the presence and absence of catalyst are shown in Fig.3.13f. For both blends the energies at break exhibited a similar trend as the elongation at break - both decreasing with increasing PC content. The energies at break of the blends prepared with catalyst were higher than those prepared without catalyst.

Plots of the tensile properties *versus* composition can be used as a relative indication of blend homogeneity. Fried[69] has shown that such measurements are very sensitive to blend compatibility. It was observed that the blends prepared in the absence of catalyst showed tensile properties were similar or lower to the average values but also lower than those of blends prepared in the presence of catalyst. This was consistent with the blends prepared absence of catalyst being immiscible and the others partially miscible, consistent with previous conclusions.

3.3.4.2 Tensile Impact Property of the Blends

Tensile impact measures the toughness of polymer materials at high strain rate. The energies to break under tensile impact for PET, PC and their blends are shown in Fig. 3.14. It can be seen that there both sets of blends were much lower than the average value but increased to a limited extent with increasing PC content. The energies to break of the blends prepared with catalyst were almost identical to those blends prepared without catalyst at each composition within experiment error.

It is well known that high impact thermoplastics such as rubber filled materials require good interfacial adhesion between the matrix and the dispersed phase. Wetton *et al.*[70] have shown that the impact strength increased with particle size within a range between 0.1 and 0.4 μm. In study of the miscible blends of poly(3-hydroxybutyrate) and poly(vinyl acetate), Sharma[71] found that energy to break of the blends were somewhat lower than the average values over all the composition range. Therefore, the energy to break of PET/PC blends are much lower than the average value due to immiscible or partially miscible structure.

Table 3.1 Glass transition temperatures of PET, PC and their blends prepared with and without in the presence of a transesterification catalyst determined by DSC

Sample	$T_{g, pet}$ K	$T_{g, pc}$ K
PC	--	413 ± 1
PET/PC 50/50	349 ± 1	410 ± 1
PET/PC 70/30	349 ± 1	410 ± 1
PET/PC 80/20	349 ± 1	411 ± 1
PET/PC 9010	349 ± 1	--
PET	349 ± 1	--
In the presence of catalyst		
PET/PC 50/50	353 ± 1	396± 1
PET/PC 70/30	354 ± 1	394 ± 1
PET/PC 90/10	351 ± 1	--

Table 3.2 Assignment of FTIR bands in PET/PC blend

Wavenumber cm^{-1}	Assignment
727	Ring modes of a terephthalate unit
1070	Ring modes of an aromatic group
1724	Carbonyl stretching of aliphatic ester
1770	Carbonyl stretching of mixed aliphatic-aromatic carbonate
1768	Carbonyl stretching of aromatic carbonate (crystalline)
1775	Carbonyl stretching of aromatic carbonate (amorphous)

Table 3.3 Tensile properties of amorphous PET and PC and their blends

Sample	Young's modulus GPa	Yield stress MPa	Extension at yield %	Breaking strength MPa	Elongation at break %	Energy to break MJ m^{-3}
PC	1.10 ± 0.01	52.9 ± 0.6	8.8 ± 0.3	50.9 ± 3.0	91 ± 16	42 ± 8
PET50	1.18 ± 0.02	50.1 ± 0.6	6.0 ± 0.2	45.2 ± 1.5	164 ± 12	63 ± 8
PET70	1.19 ± 0.01	51.1 ± 0.2	5.8 ± 0.1	47.1 ± 3.0	288 ± 27	110 ± 13
PET80	1.21 ± 0.01	51.1 ± 0.7	5.6 ± 0.1	56.7 ± 3.1	440 ± 40	179 ± 23
PET90	1.23 ± 0.02	52.0 ± 0.4	5.5 ± 0.1	54.9 ± 4.3	460 ± 37	177 ± 20
PET	1.29 ± 0.02	52.1 ± 2.0	4.8 ± 0.2	54.0 ± 5.8	500 ± 50	180 ± 32
In the presence catalyst						
PET50	1.39 ± 0.01	53.3 ± 0.4	5.9 ± 0.2	46.4 ± 4.8	174 ± 53	74 ± 24.6
PET70	1.42 ± 0.01	53.3 ± 1.2	5.4 ± 0.3	59.4 ± 3.5	389 ± 24	172 ± 15.6
PET90	1.40 ± 0.02	50.5 ± 0.7	5.0 ± 0.2	57.6 ± 3.9	477 ± 32	189 ± 18.5

Note: Values given are the means of at least 5 samples and error limits are standard deviation.

Table 3.4 Tensile properties of crystallised PET /PC blends without added catalyst

Sample	Young's modulus GPa	Yield stress MPa	Extension at yield %	Breaking strength MPa	Elongation at break %	Energy to break MJ m^{-3}
PC	1.15 ± 0.01	59.2 ± 0.8	7.9 ± 0.3	56.0 ± 3.5	112 ± 15	54.3 ± 8.7
PET50	1.19 ± 0.04	55.3 ± 2.0	6.5 ± 0.1	45.8 ± 3.1	90 ± 50	39.6 ± 22
PET70	1.26 ± 0.02	56.9 ± 0.6	6.1 ± 0.1	44.3 ± 1.3	180 ± 42	76.8 ± 18
PET80	1.26 ± 0.01	57.0 ± 0.8	5.9 ± 0.2	47.1 ± 3.1	258 ± 66	112 ± 30
PET90	1.40 ± 0.03	63.5 ± 0.7	6.5 ± 0.1	45.9 ± 0.9	150 ± 80	68.8 ± 37
PET	1.35 ± 0.03	61.6 ± 2.0	6.7 ± 0.2	57.4 ± 4.7	481 ± 50	221 ± 27

Note: Values given are the means of at least 5 samples and error limits are standard deviation.

Samples crystallised at 383 K for 60 minutes

Table 3.5 Tensile properties of crystallised PET /PC blends without added catalyst

Sample	Young's modulus GPa	Yield stress MPa	Extension at yield %	Breaking strength MPa	Elongation at break %	Energy to break MJ m^{-3}
PC	1.13 ± 0.01	59.4 ± 1.1	8.3 ± 0.4	47.2 ± 0.9	40 ± 13	18.3 ± 6
PET50	1.30 ± 0.04	61.4 ± 1.5	7.1 ± 0.5	60.9 ± 1.4	7.4 ± 0.7	3.2 ± 0.6
PET70	1.37 ± 0.04	63.5 ± 0.9	6.2 ± 0.4	63.5 ± 0.9	6.2 ± 0.4	2.3 ± 0.2
PET80	1.39 ± 0.03	65.3 ± 0.2	7.1 ± 0.5	65.3 ± 0.2	7.1 ± 0.5	3.0 ± 0.3
PET90	1.46 ± 0.03	65.6 ± 0.7	7.0 ± 0.5	65.2 ± 1.2	7.5 ± 0.4	3.3 ± 0.3
PET	1.53 ± 0.05	65.3 ± 2.2	6.6 ± 0.4	50.2 ± 11	23 ± 14	9.8 ± 4

Note: Values given are the means of at least 5 samples and error limits are standard deviation

Samples crystallised at 160°C for 20 minutes

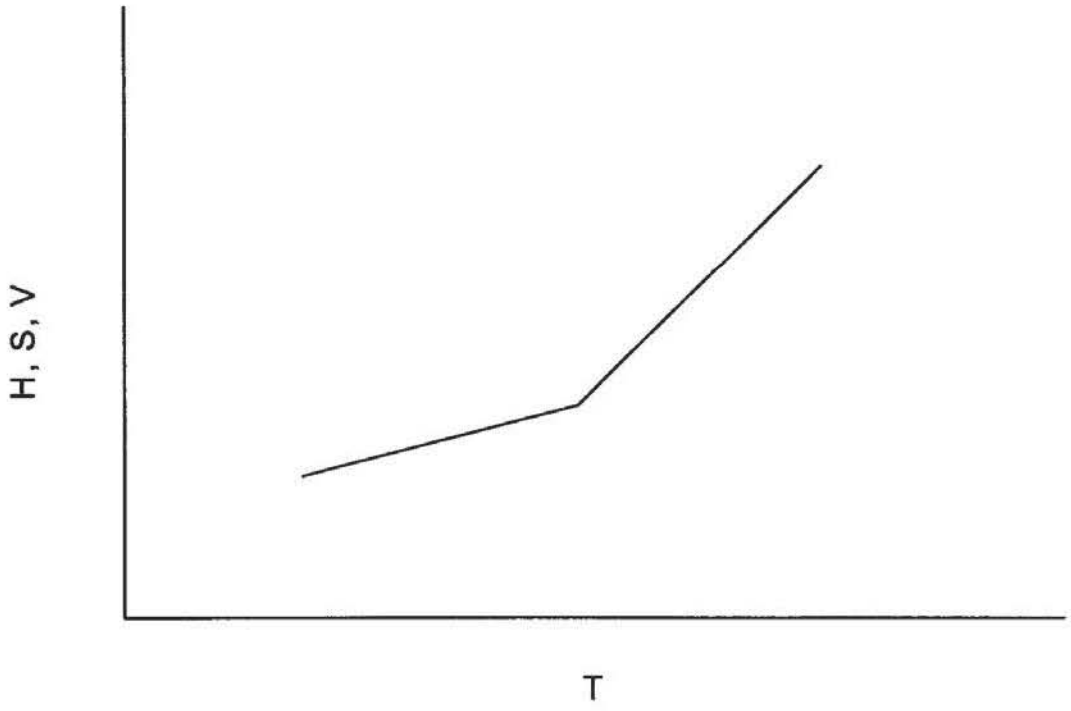

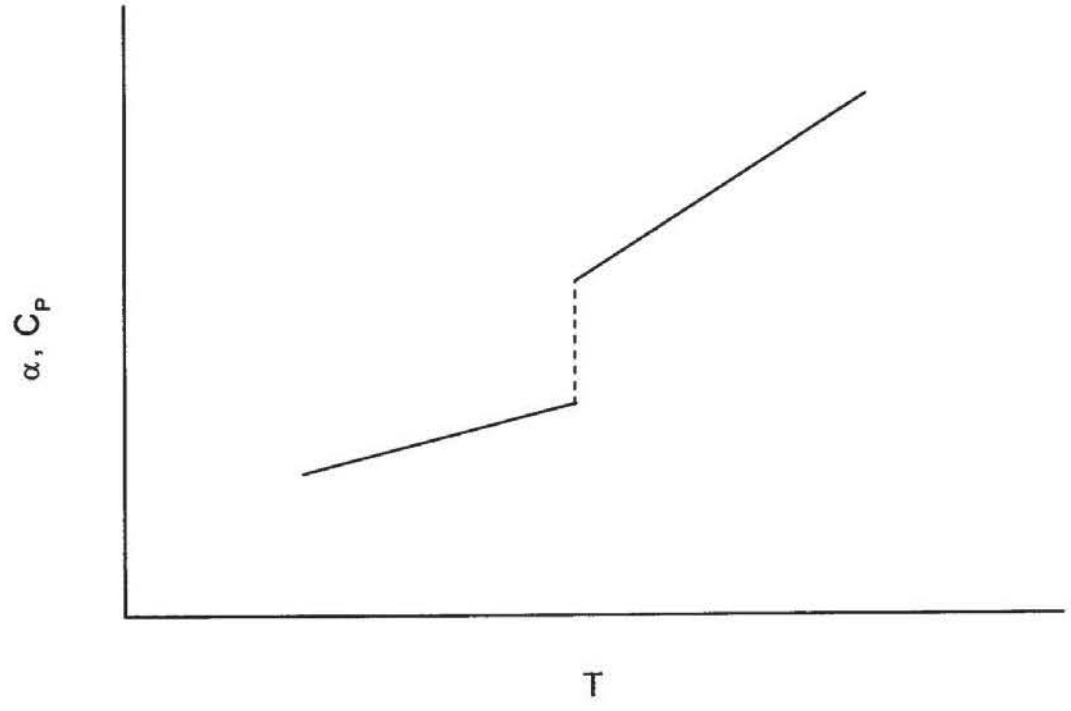

Fig. 3.1 Schematic representation of the glass transition

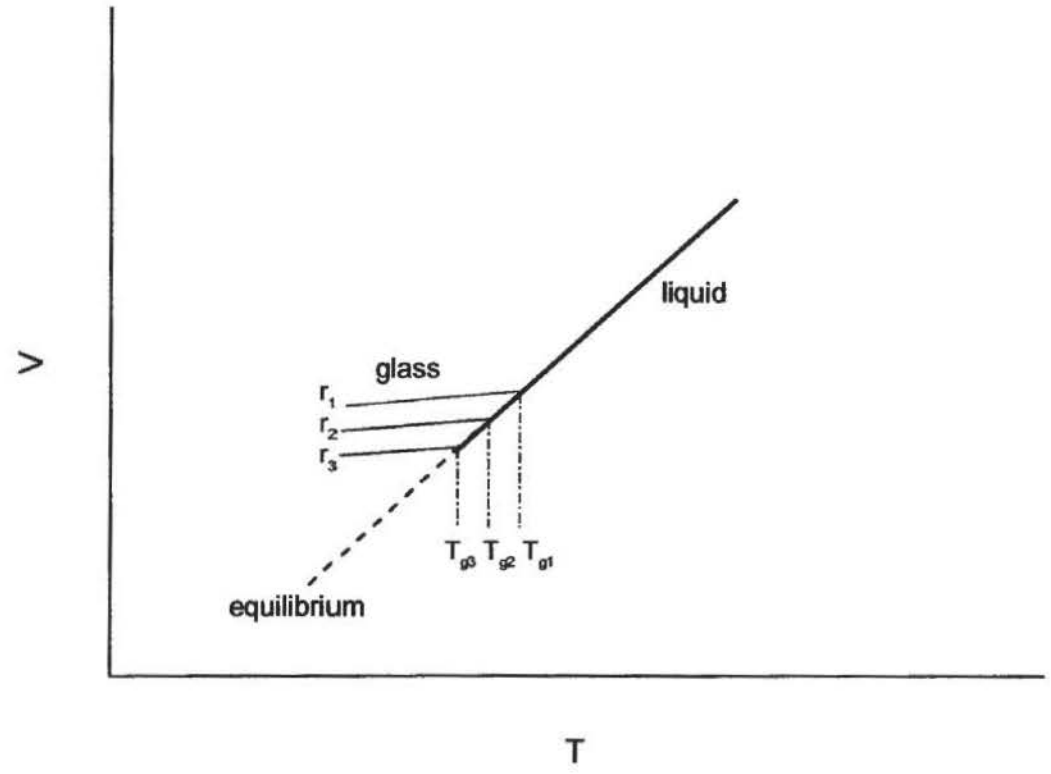

Fig. 3.2 Volume-temperature curve at different rates of cooling $r_1 > r_2 > r_3$

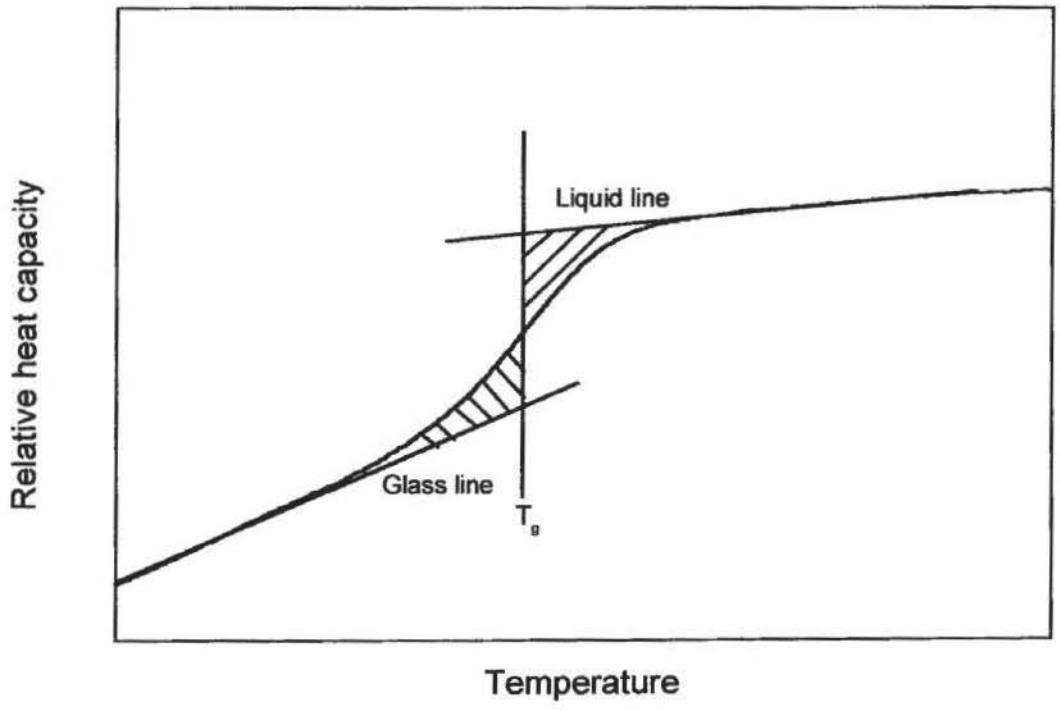

Fig. 3.3 Schematic Diagram of measuring T_g

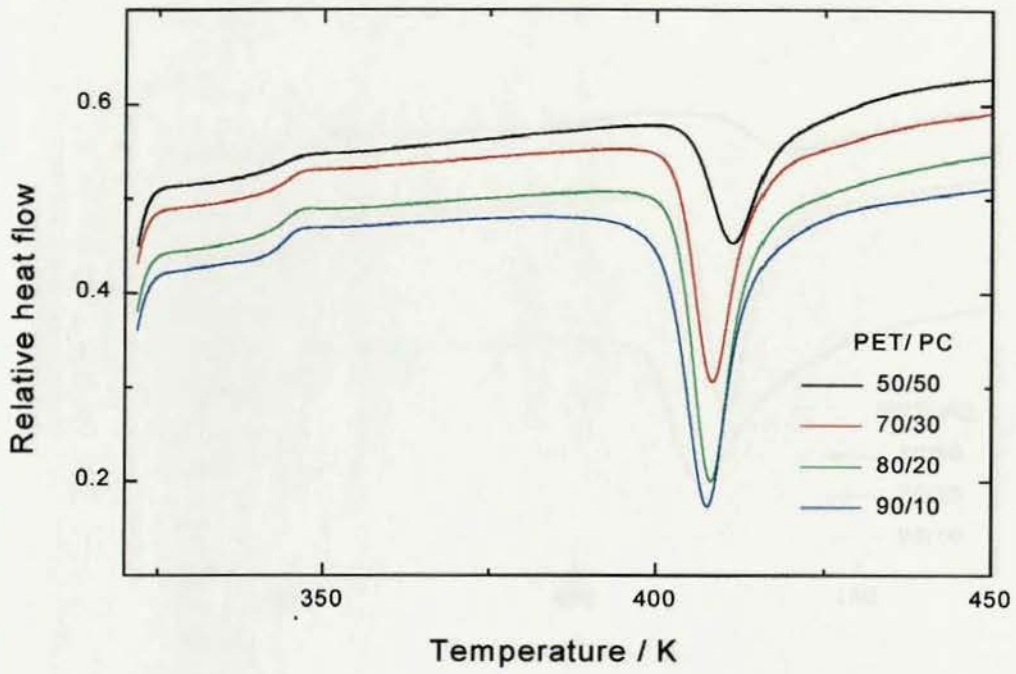

Fig. 3.4a DSC thermograms of amorphous PET/PC blends prepared without added catalyst. The first scan to 460 K at a heating rate of 10 $Kmin^{-1}$

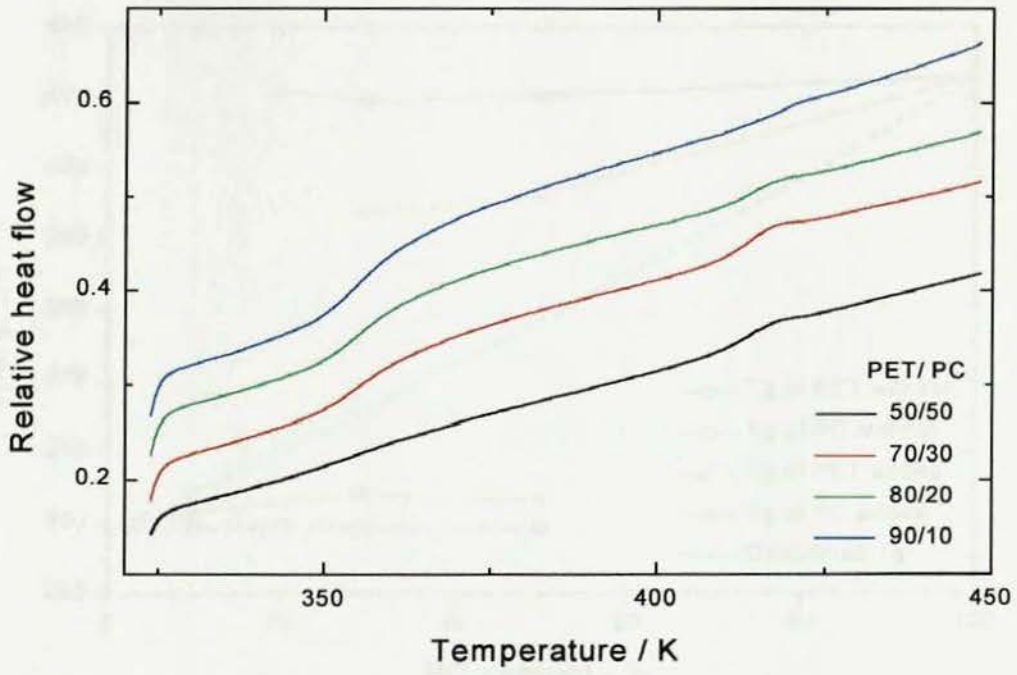

Fig. 3.4b DSC thermograms of crystalline PET/PC blends prepared without added catalyst. Second scan to 460 K at a heating rate of 10 $Kmin^{-1}$

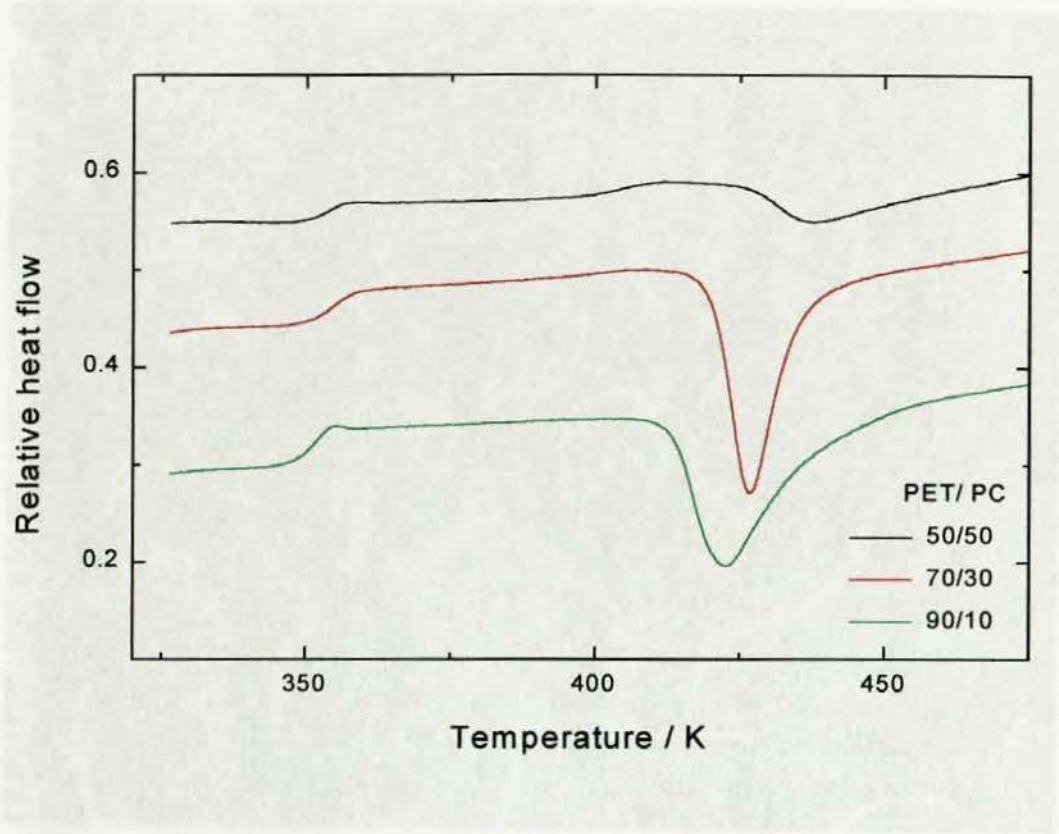

Fig. 3.5 DSC thermograms of amorphous PET/PC blends prepared in the presence of catalyst. The first scan at a heating rate of 10 $Kmin^{-1}$

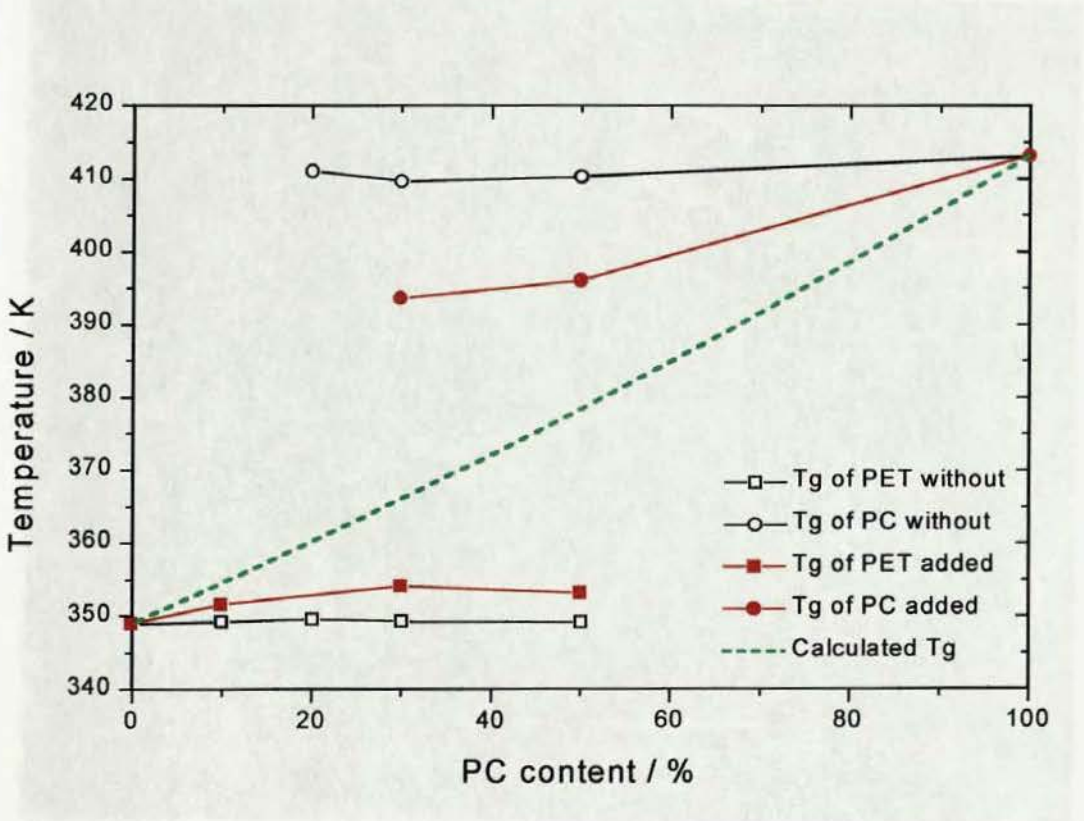

Fig. 3.6 The effect of PET/PC blend composition on T_gs, dash line is the T_g calculated by Fox equation

a

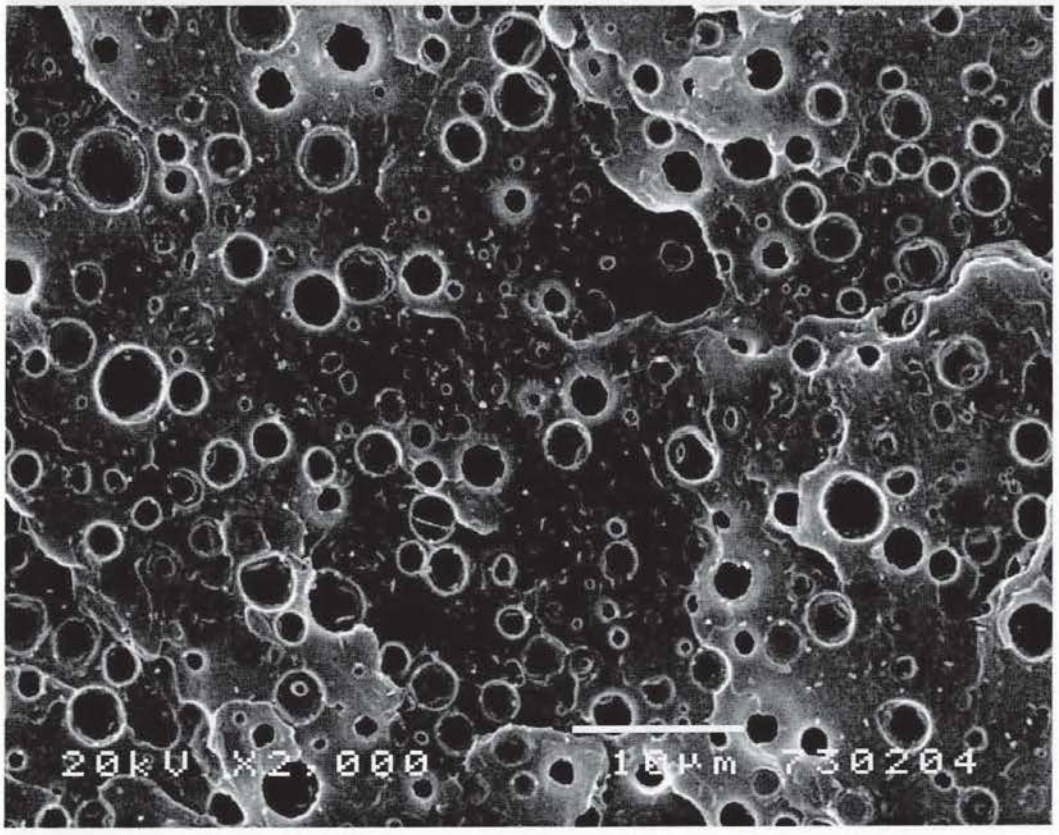

b

continued

a

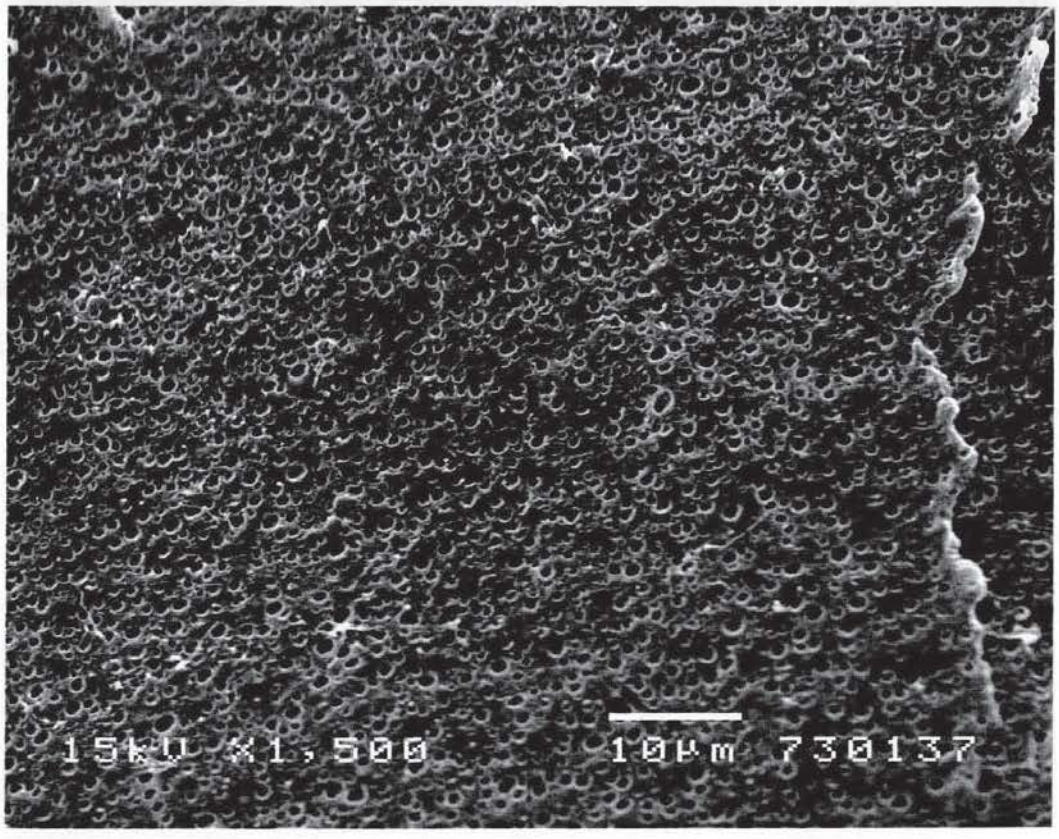

b

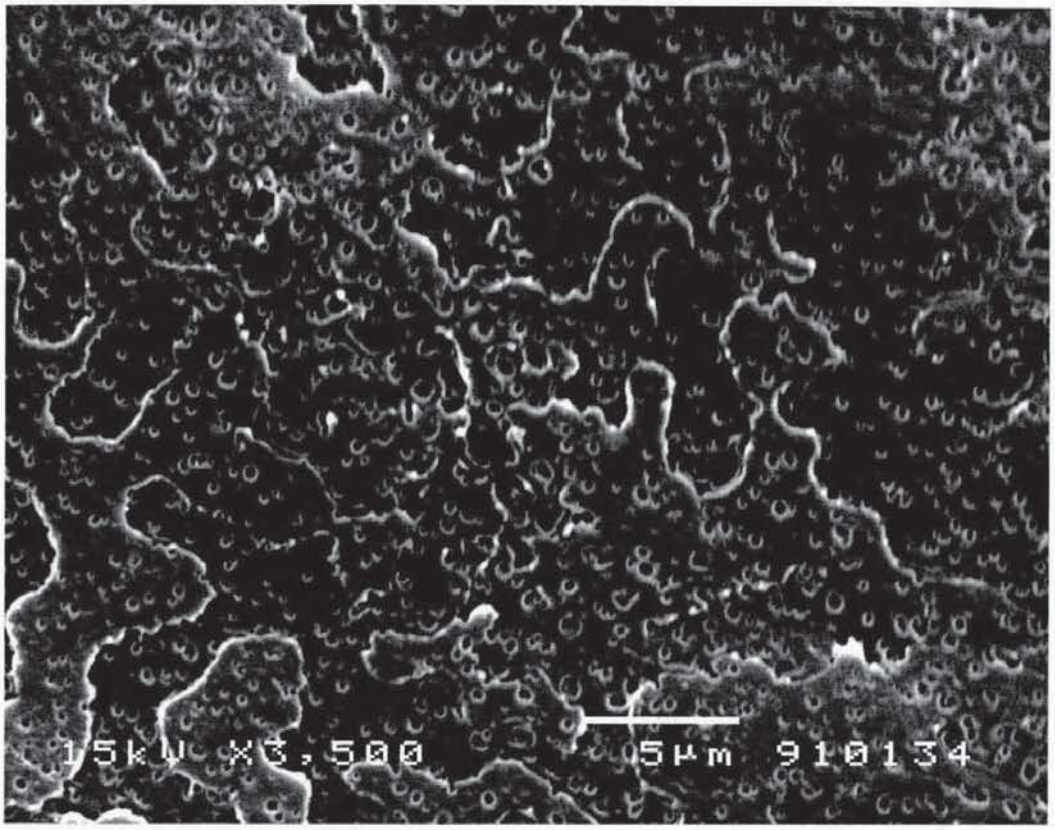

c

Fig. 3.8 SEM micrographs of the cryo-fracture surfaces of PET/PC blends prepared in the presence of a catalyst. Surfaces etched with DETA for 1 min:
a. PET50/PC50; b. PET70/PC30; and c. PET90/PC10

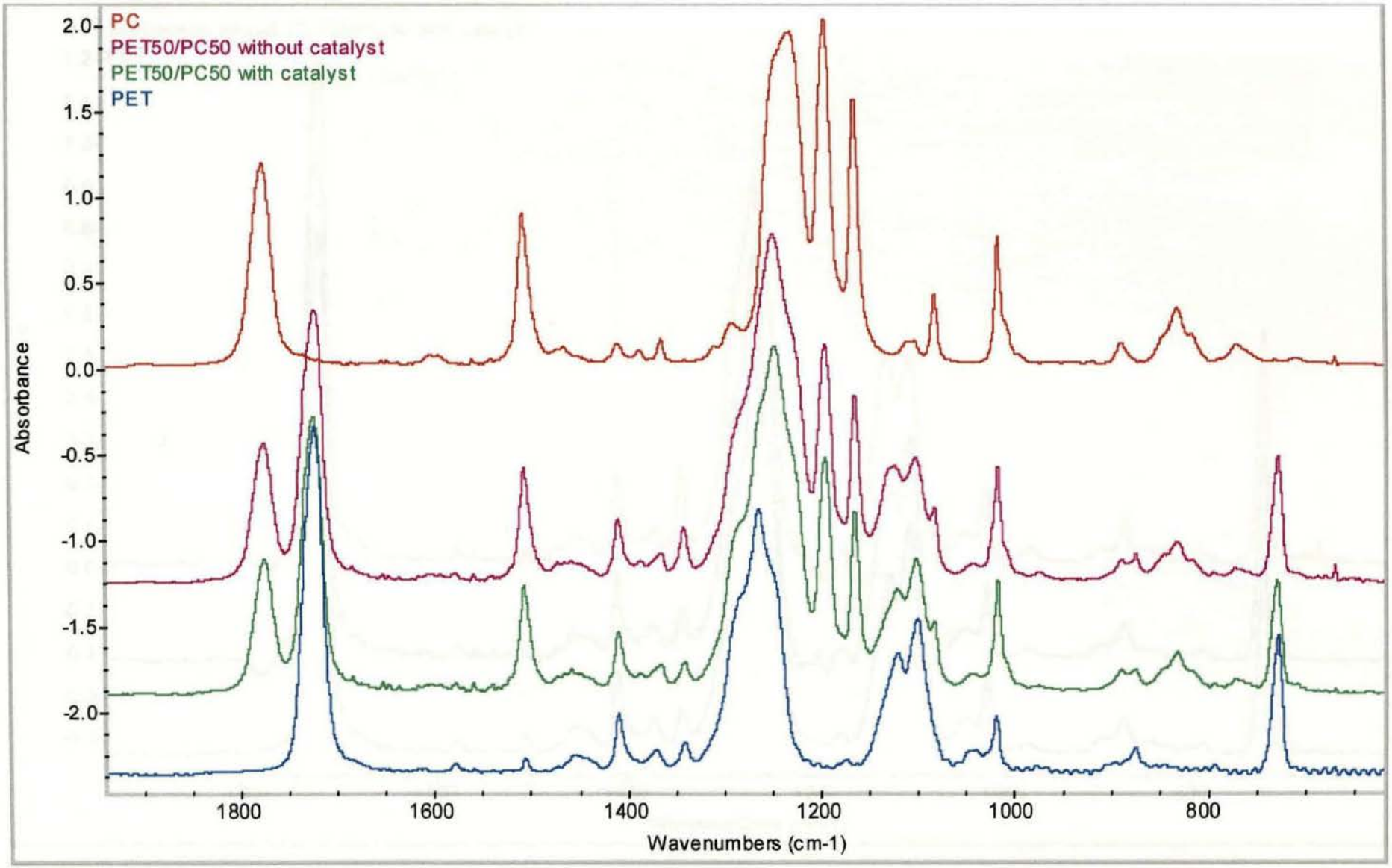

Fig. 3.9 FTIR spectra of PET, PC and their blends

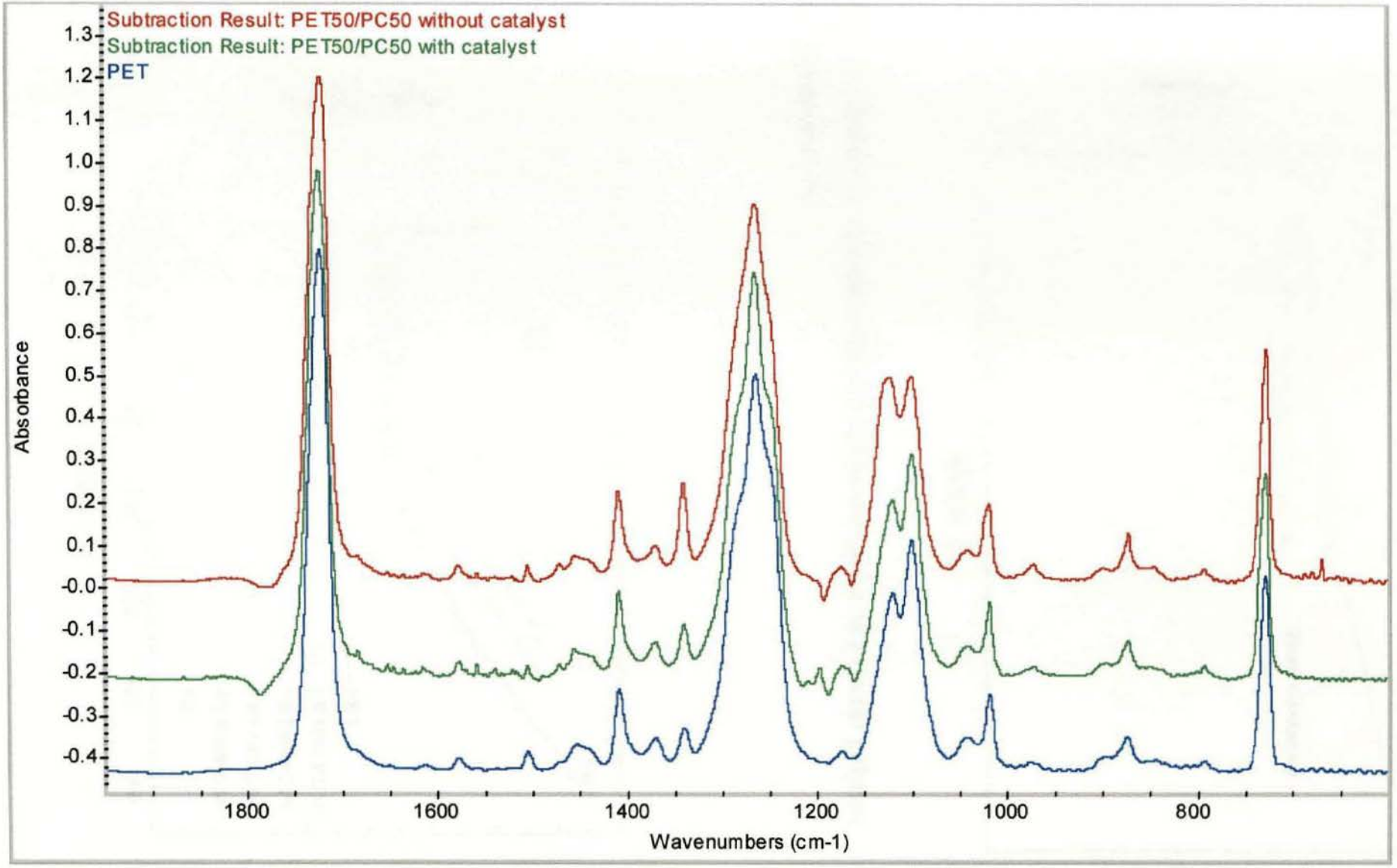

Fig. 3.10 FTIR spectra of PET and it blends after subtraction

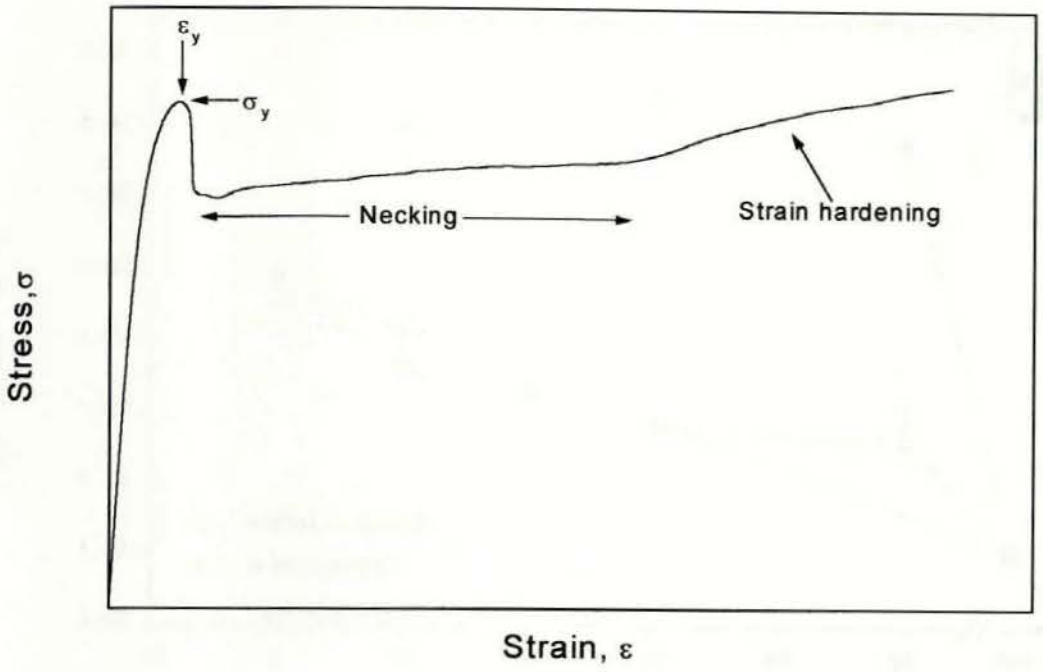

Fig 3.11 Schematic representation of a tensile behaviour of a ductile polymer. nominal tress-strain

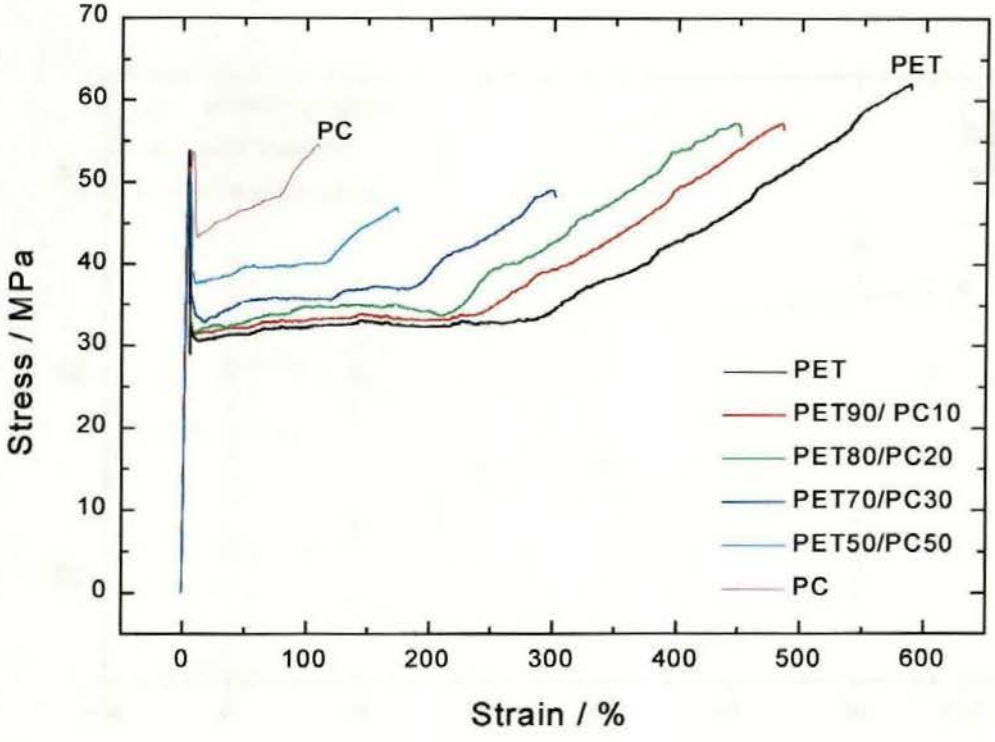

Fig. 3.12 Nominal stress – strain behaviours of amorphous PET/PC blends

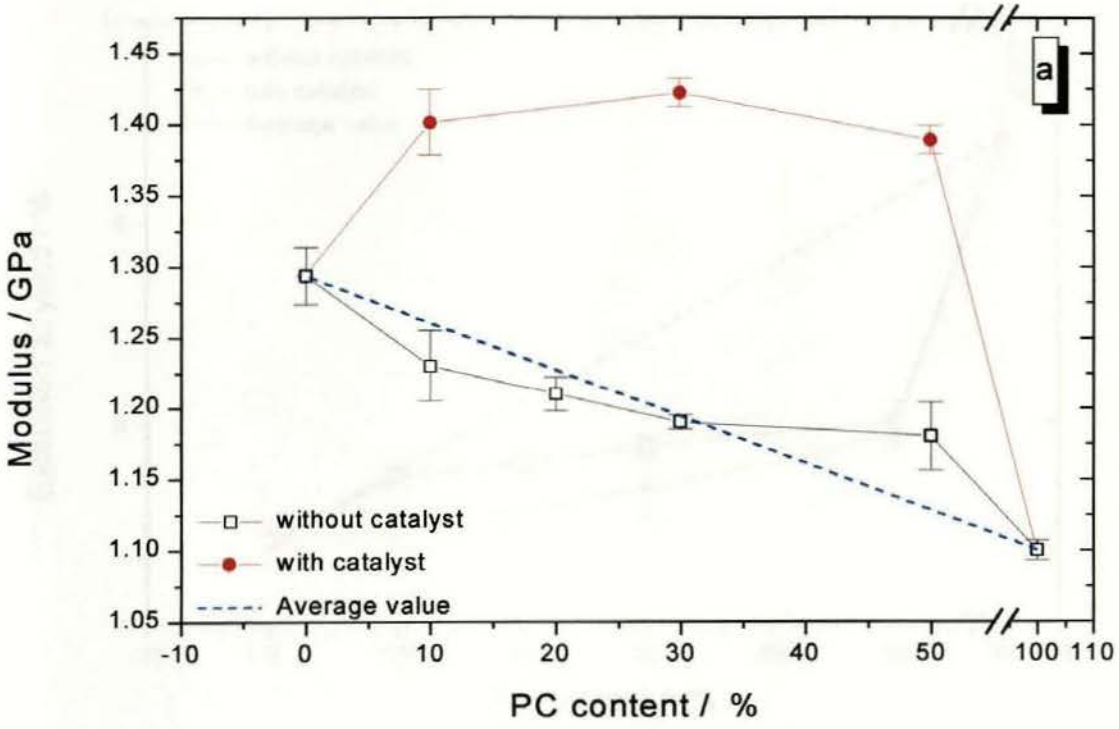
a
Modulus / GPa
1.45
1.40
1.35
1.30
1.25
1.20
1.15
1.10
1.05
without catalyst
with catalyst
Average value
-10
0
10
20
30
40
50
100
110
PC content / %

A

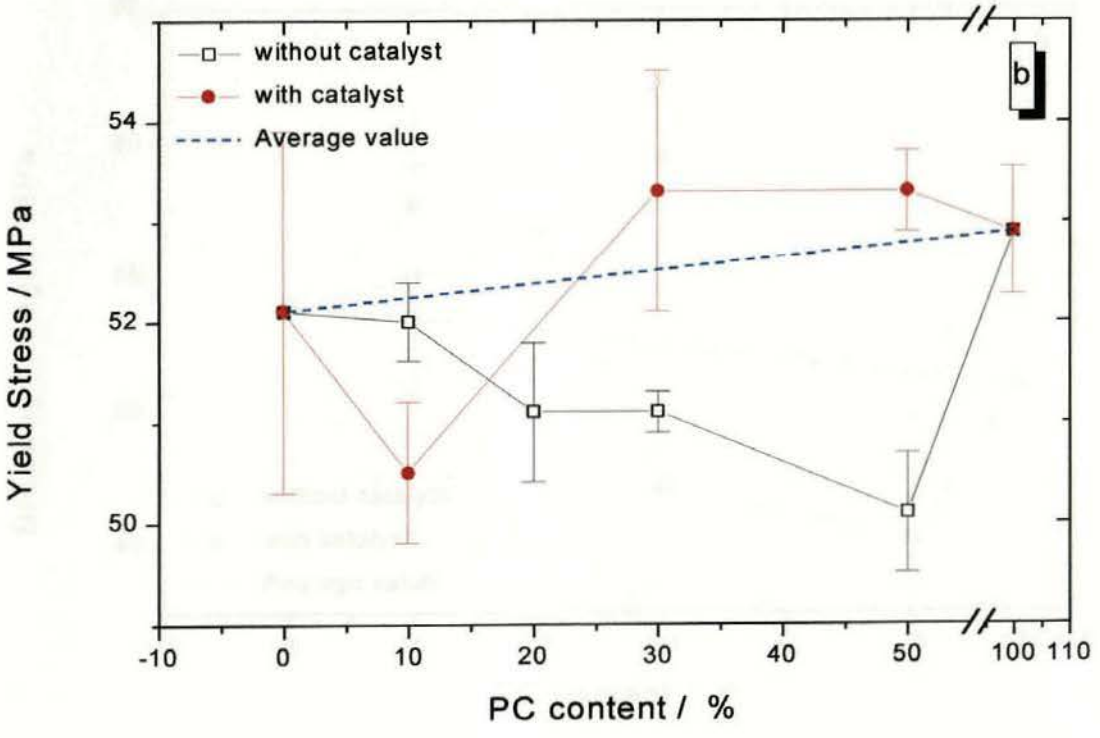
b
without catalyst
with catalyst
Average value
Yield Stress / MPa
54
52
50
-10
0
10
20
30
40
50
100
110
PC content / %

B

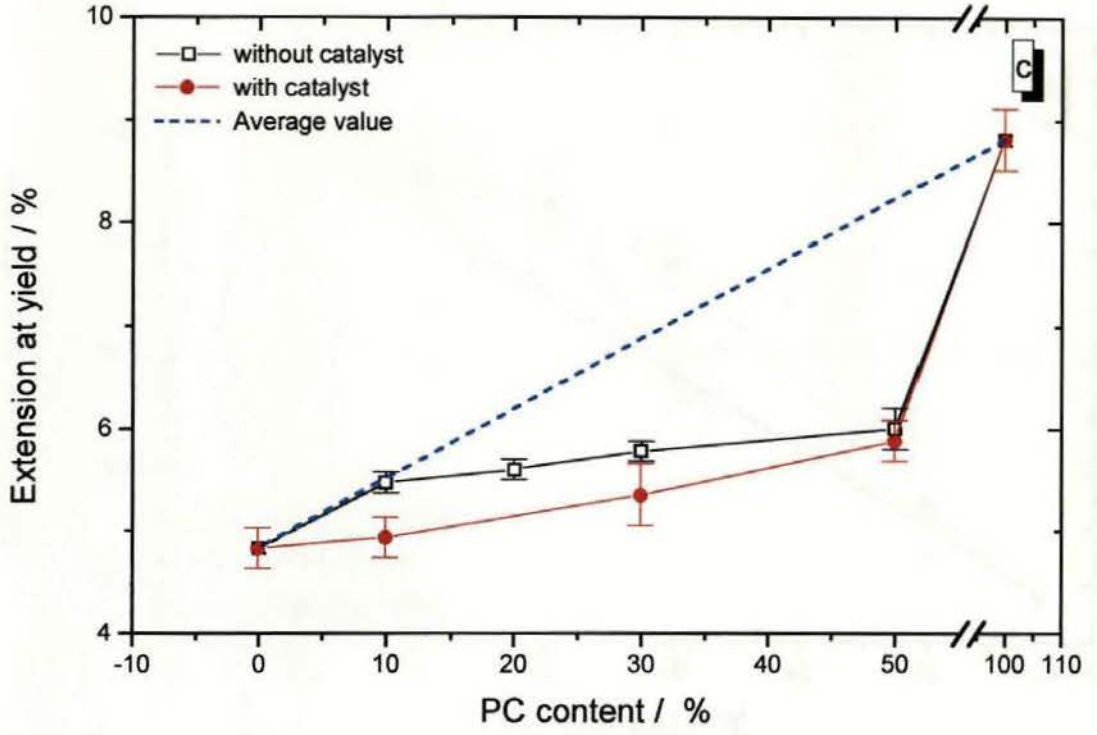
without catalyst
with catalyst
Average value
c
Extension at yield / %
PC content / %
10
8
6
4
-10
0
10
20
30
40
50
100
110

C

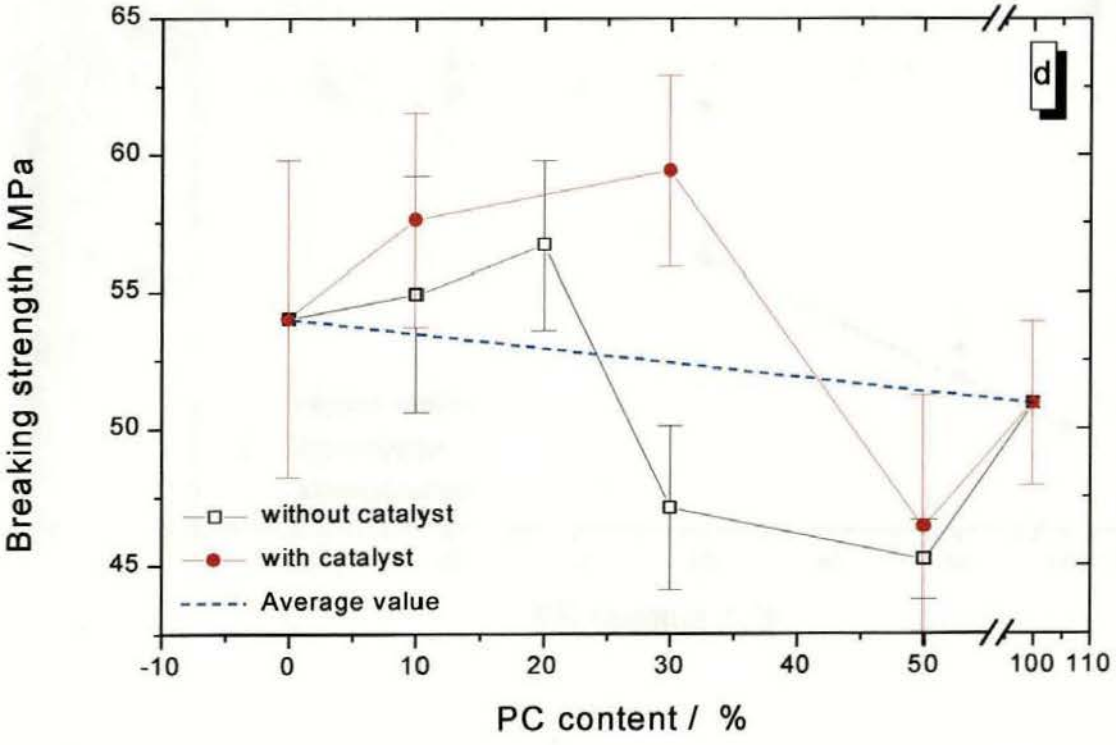
without catalyst
with catalyst
Average value
d
Breaking strength / MPa
PC content / %
65
60
55
50
45
-10
0
10
20
30
40
50
100
110

D

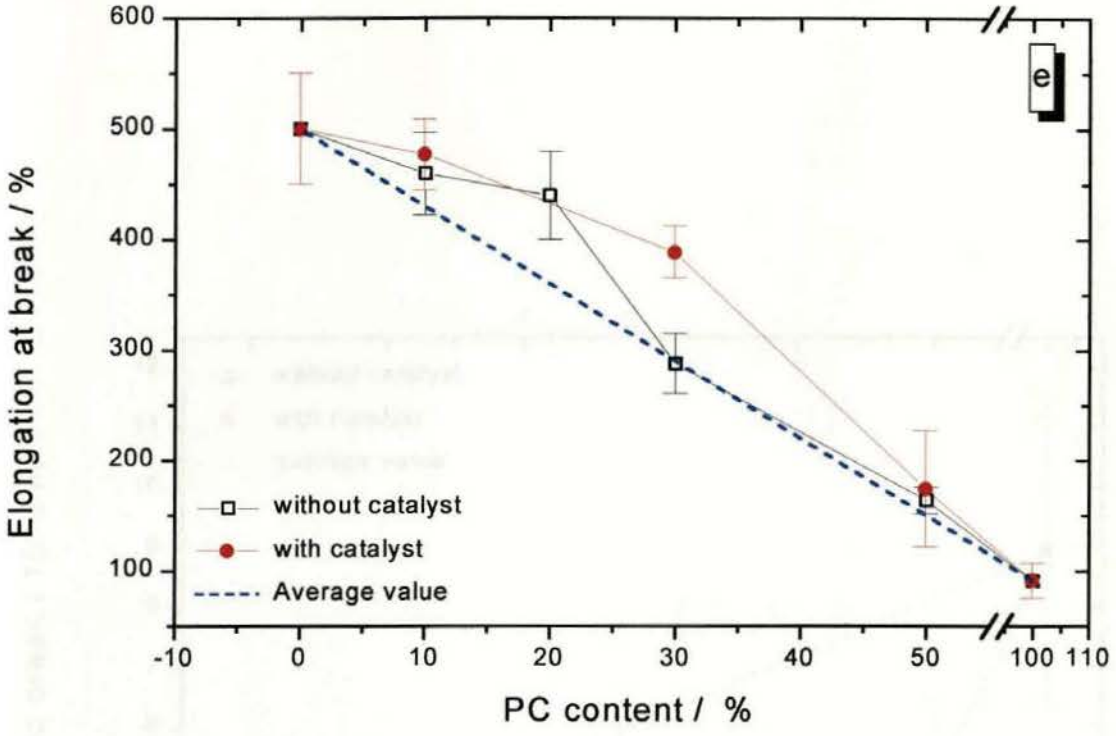

E

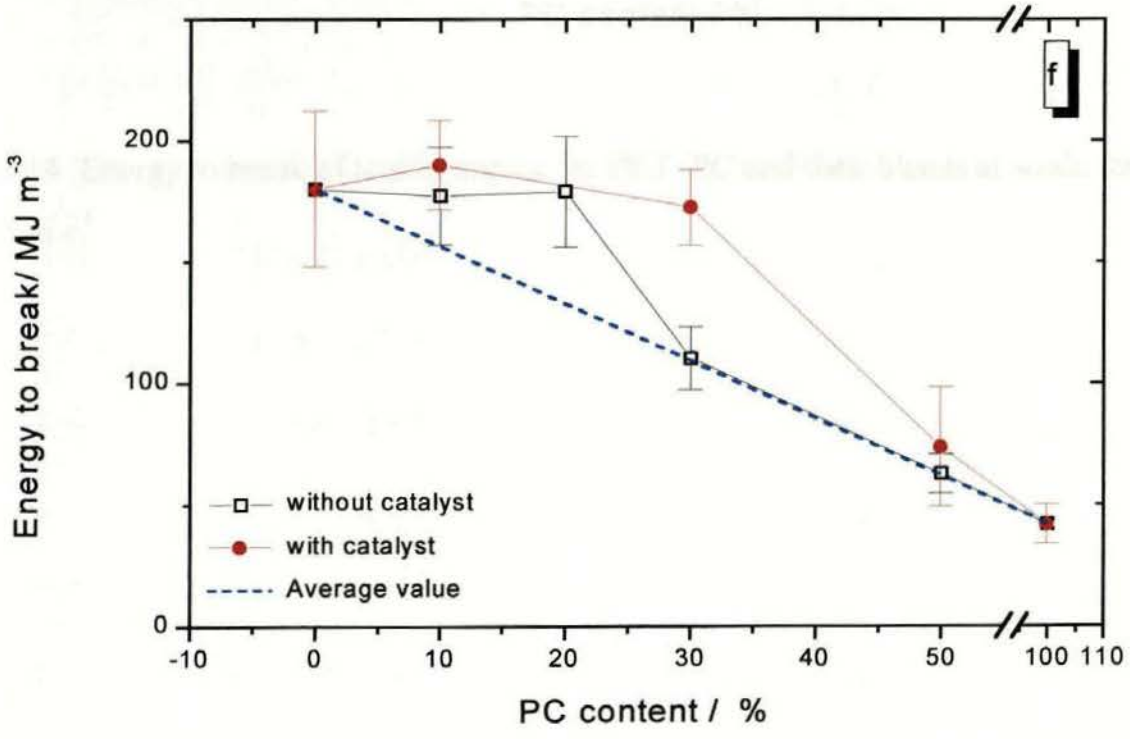

F

Fig. 3.13 Tensile properties of amorphous PET/PC blends at strain rate of 2 mm min^{-1}

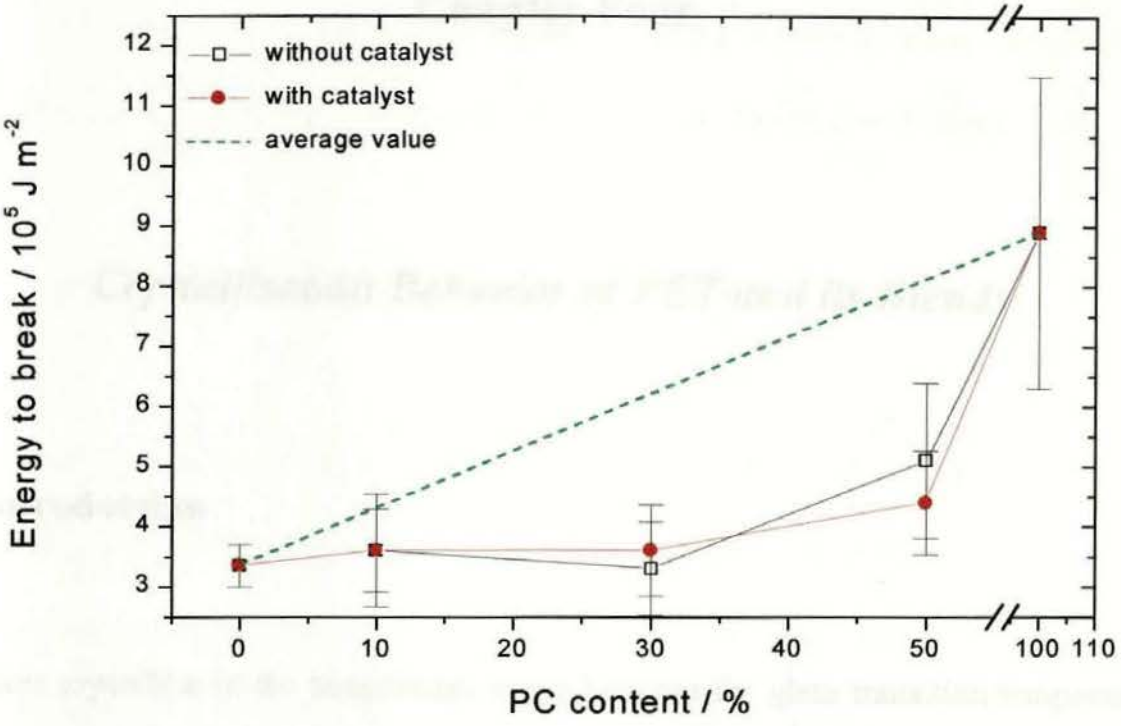

Fig. 3.14 Energy to break of tensile impact for PET, PC and their blends at strain rate of 3.5 m s^{-1}

Chapter Four

Crystallisation Behavior of PET and its Blends

4.1 Introduction

Polymers crystallise in the temperature range between the glass transition temperature, T_g and the melting point, T_m, where the chain segments are sufficiently mobile to rearrange and crystallise. The ability to crystallise is different from one polymer to another, the difference being due to microstructure, chain tacticity and the bulkiness and polarity of side groups as well as external factors such as the rate of cooling, the presence of orientation in the melt and nucleating agents. Generally, symmetry in the chains and polar interactions help crystallisation, while branching and high molar mass inhibit crystallisation. However, polymers crystallised from the melt are never totally crystalline as a consequence of their high viscosity, long-chain nature and chain entanglements.

4.2 Crystallisation Kinetics

4.2.1 Crystallisation Process

Polymer crystallisation is the process whereby an ordered solid structure forms from a disordered liquid. It involves two distinct processes, nucleation and crystal growth.

4.2.1.1 Nucleation[72]

When a polymer is cooled from the melting point there is a tendency for the randomly organised molecules in the melt to become aligned and form small ordered regions. This process is called nucleation and can be subdivided into primary, secondary and tertiary nucleation according to the mode of formation, as shown in Fig. 4.1.

Primary nucleation is the first step in the formation of a crystal from the liquid state. If there is no preformed nucleus or foreign surface to act as a nucleus then the primary nucleation is called homogeneous nucleation, otherwise it is called heterogeneous nucleation. Nucleation on an existing surface area decreases the free enthalpy barrier to nucleation. Consequently, heterogeneous nucleation always occurs at lower supercoolings than homogeneous.

On primary nucleation, further growth of the nucleus takes place on the crystal surface by the appearance of a secondary nucleus. This involves formation of a new layer of crystalline material on an already existing crystalline surface as shown in Fig. 4.1B.

Secondary nucleation also occurs with a lower free enthalpy barrier than primary since it has a lower surface to bulk free energy ratio. Crystal growth occurs by secondary nucleation and the rate of crystal growth is nucleation controlled at low degrees of supercooling.

Tertiary nucleation has an even lower surface to bulk free energy ratio and it determines rate at which a nucleated crystal surface is covered with fresh material.

The thermodynamics of nucleation involve balancing bulk free energy with surface free energy terms. The overall change in free energy on formation of a nucleus, ΔG_n, at a constant temperature is

$$\Delta G_n = \Delta G_v + \sum \sigma A \tag{4.1}$$

where ΔG_v is the bulk free enthalpy change between solid and liquid phase, σ is the specific surface free energy and A is the crystal surface area. For primary nucleus with a lamellar thickness l and width a, the overall free energy change is

$$\Delta G_n = -a^2 l \Delta G_v + 2a^2 \sigma_e + 4al\sigma \tag{4.2}$$

where σ and σ_e are the surface free energy for lateral and folding chain surfaces, respectively. By differentiation with respect to the dimension a and l

$$\frac{\partial \Delta G_n}{\partial a} = -2al\Delta G_v + 4a\sigma_e + 4l\sigma \tag{4.3}$$

$$\frac{\partial \Delta G_n}{\partial l} = -a^2 \Delta G_v + 4a\sigma \tag{4.4}$$

The critical nucleus dimensions, a^* and l^*, are obtained by setting equations 4.3 and 4.4 equal to zero

$$a^* = \frac{4\sigma}{\Delta G_v} \tag{4.5}$$

$$l^* = \frac{4\sigma_e}{\Delta G_v} \tag{4.6}$$

The bulk free energy change is

$$\Delta G_v = \Delta H_v - T\Delta S_v \tag{4.7}$$

where ΔH_v and ΔS_v are the enthalpy and entropy of crystallisation. At the equilibrium melting temperature T_m^o, ΔG_v is zero. Therefore,

$$\Delta S_v = \frac{\Delta H_v}{T_m^o} \tag{4.8}$$

As long as the degree of supercooling is not too large, ΔH_v and ΔS_v can be considered to be temperature independent such that

$$\Delta G_v = \Delta H_v - T\frac{\Delta H_v}{T_m^o} = \frac{\Delta T}{T_m^o}\Delta H_v \tag{4.9}$$

where $\Delta T = T^0_m - T_c$ and T_c is the crystallisation temperature. At high supercooling it is better to change the equation 4.9 to

$$\Delta G_v = (\frac{\Delta T}{T_m^o}\Delta H_v) f \tag{4.9a}$$

where $f = 2T_c/(T_m^o + T_c)$. On inserting equations 4.5, 4.6 and 4.9 into 4.2

$$\Delta G_n^* = \frac{32\sigma^2\sigma_e(T_m^o)^2}{(\Delta H_v \Delta T)^2} \tag{4.10}$$

It can be seen from equation 4.10 that, the free energy of formation of the critical nucleus is proportional to $(\Delta T)^{-2}$. This means that supercooling is required to form a stable nucleus. The maximum value in ΔG_n corresponds to a critical size nucleus, as shown in Fig. 4.2. Nuclei smaller than the critical size are called subcritical nuclei or embryos, nuclei larger than the critical size are called supercritical as long as their ΔG_n are still positive, and the supercritical nuclei will grow spontaneously as long as ΔG_n is negative.

4.2.1.2 Crystal Growth[73-75]

On formation of the critical size nucleus, crystals begin to grow on the surfaces present by a presence of secondary nucleation. This involves successive laying down of molecular strands on a smooth crystal surface followed by addition of further segments by chain folding process[74]. This process is illustrated schematically in Fig. 4.3.

It is assumed that the polymer lamella has a fold surface energy of σ_e, a lateral surface energy of σ and that the free energy change on crystallisation is ΔG_v per unit volume. By laying down n adjacent molecular strands of length l, with each strand having a cross-section area of (a×b), the surface energy is:

$$\Delta G_{n\ surface} = 2nab\sigma_e + 2bl\sigma \qquad (4.11)$$

There is a reduction in free energy with nucleation incorporation of n molecular strands in a crystal:

$$\Delta G_{n\ crystal} = -\ nabl\ \Delta G_v \tag{4.12}$$

The overall change in free energy when n strands are laid down is

$$\Delta G_n = \Delta G_{n\ surface} + \Delta G_{n\ crystal}$$

$$= 2nab\sigma_e + 2bl\sigma - nabl\ \Delta G_v \tag{4.13}$$

Inserting equation 4.9 into 4.13,

$$\Delta G_n = 2nab\sigma_e + 2bl\sigma - \frac{nabl\Delta H_v \Delta T}{T_m^0} \tag{4.14}$$

Normally n is very large and σ_e is 10 times bigger than σ, therefore the term $2bl\sigma$ is negligible. For a given value of n, ΔG_n decreases as l increases. Finally the critical length of strand, l^*, will be achieved and the secondary nucleus will be stable at this critical value when $\Delta G_n = 0$,

$$l^* = \frac{2\sigma_e T_m^0}{\Delta H_v \Delta T} \tag{4.15}$$

The reciprocal dependence of the lamellar thickness l^* on ΔT as predicted by the above equation is observed experimentally.

4.2.2 Theory of Growth Rate

Turnbull and Fisher[76] proposed that the temperature dependence of the growth rate, g, was described by the equation

$$g = g_0 \exp(-\frac{\Delta E}{RT}) \exp(-\frac{\Delta G_n^*}{RT}) \tag{4.16}$$

where, g is the steady state growth rate of a crystal, g_0 is a temperature independent constant which depended on molecular parameters, and crystal geometry. ΔE represents

the energy barriers for the transport of material across the crystal-liquid interface, ΔG_n^* is the free energy of formation of a critical size secondary nucleus and R is the gas constant. Accordingly, at temperatures close to T_g the diffusion is the controlling factor and the first term on the right hand side dominates, whereas at higher temperature close to T_m nucleation is the controlling factor and the second term dominates. Between these two extremes, the growth rate passes through a maximum where the two exponential terms contribute equally.

Hoffman et al[77,78] have defined three regimes of crystallisation growth kinetics from the melt, which differ according to the rate of chain deposited onto the crystal surface. It is assumed that growth occurs on pre-existing crystal surfaces and the growth rate is same at all crystal growth faces. It also assumed that the fold chain length is uniform and the reptation rate characteristics of the melt is fast enough to allow significant degree of adjacent re-entry.

In regime I, supercooling is quite small and the nucleation rate is lower than the molecular crystallisation rate. Only one surface nucleus causes the completion of the entire substrate length, as can be seen from Fig.4.4a. The absolute growth rate can be expressed as

$$G_1 = \left(\frac{C_1}{n}\right)\exp\left(-\frac{Q_d^*}{RT}\right)\exp\left(-\frac{K_{g(I)}}{T\Delta T}\right) \qquad (4.17)$$

in which $K_{g(I)} = 4b_o\sigma\sigma_e T_m^o / \Delta H_f k$

where, G_1 is the absolute growth rate for regime I

$\frac{C_1}{n}$ is the pre-exponential factor for regime I, n refers to the number unit in polymer chain. At a given supercooling the pre-exponent reduces the growth rate with increasing of molecular weight.

Q_d^* is the activation energy of the steady-state reptation process in the melt,

$K_{g(I)}$ is nucleation constant in regime I,

ΔH_f is heat of fusion per unit volume,

k is Boltzman constant,

and b_o, σ, σ_s, R, T_m^o and ΔT are as defined previously.

In regime II, larger supercooling is necessary and the rate of nucleation is larger than the rate of crystallisation of each molecule such that multiple surface nuclei occur on the same crystallising surface, as can be seen from Fig.4.4b. The absolute growth rate for regime II has a same form as in regime I except for the value of the pre-exponential factor, $\frac{C_2}{n}$, and nucleation constant $K_{g\,(II)}$.

$$K_{g(II)} = 2b_o\sigma_e\sigma T_m^o / \Delta H_f k \tag{4.18}$$

In regime III, supercooling is even larger and the crystallisation rate is very rapid. In this regime the chains do not undergo adjacent re-entry on to the lamellae as occur in the other regimes, but rather have only a few folds. They are free to re-enter the same lamella via a type of switchboard model or go on the next lamella, as can be seen from Fig.4.4c. The growth rate in regime III gives the same expression as in regime I except for the value of the pre-exponential factor $\frac{C_3}{n}$, and so

$$K_{g(III)} = K_{g(I)} = 2K_{g(II)} \tag{4.19}$$

As the temperature is lowered through regimes I, II and III, substrate completion rates per chain decrease. However, more chains are crystallising simultaneously.

At temperatures approaching Tg, crystallisation becomes severely limited by reduced chain mobility.

4.2.3 Crystallisation Kinetics

Avrami derived an equation to describing the overall kinetics of crystallisation[79] involving nucleation and growth. This derivation was later simplified by Evans[80] and applied to crystallisation and mechanisms using as a model the problem of expanding circular wave fronts caused by raindrops falling on the surface of a pond. He considered that the probability of a point P crossed by x fronts is described by a Poisson distribution, and

$$P_x = \frac{e^{-E}E^x}{x!} \tag{4.20}$$

where E is the number of fronts crossing over the point, P, calculated by averaging over all points. When P is not crossed by any of the fronts, then x = 0, and the probability, P_0, is,

$$P_0 = e^{-E} \tag{4.21}$$

The above equation can be applied to the crystallisation of polymers, where P_0 is equivalent to the amount of uncrystallised material, i.e.

$$P_0 = 1 - X_t \tag{4.22}$$

and so

$$1 - X_t = e^{-E} \tag{4.23}$$

where X_t is the volume fraction of converted material. For bulk crystallisation E can be replaced by V_t the volume of crystallised material

$$1 - X_t = e^{-V_t} \tag{4.24}$$

For growth of spherical particles in 3-dimensional space with radius r, increasing linearly with time and with a constant radial growth rate g, then at time t

$$r = gt \tag{4.25}$$

For heterogeneous nucleation and for L nuclei present, the volume increase in crystallinity in the time interval, dt, is,

$$dV_t = 4\pi r^2 L dr = 4\pi g^3 L t^2 dt \tag{4.26}$$

On integration

$$V_t = \frac{4}{3}\pi g^3 L t^3 \tag{4.27}$$

For homogeneous nucleation at rate of l, the spherical particles nucleated at time t_i produce a volume increase of

$$dV_t = 4\pi g^2 (t - t_i)^2 l t dt \tag{4.28}$$

On integration

$$V_t = \frac{2}{3}\pi g^3 l t^3 \tag{4.29}$$

Combining the equations 4.24, 27 and 29 gives a general form Avrami equation:

$$1 - X_t = \exp(-Zt^n) \tag{4.30}$$

where Z is a composite rate constant including nucleation and growth characteristics. The value of n reflects the crystallisation mechanism and the geometry of growth. The corresponding expressions for n and Z are listed in table 4.1.

In the above derivation besides assuming random nucleation in a supercooling melt, the following assumptions are also included[72,81]:

- the rates of nucleation and growth increase linearly with time
- only primary crystallisation processes and no secondary crystallisation occur
- volume constant during crystallisation
- crystal keeps its original shape in either one (rods), two (discs) or three (spheres) dimension until impingement takes place
- no induction time before crystallisation

Although the Avrami equation is successful in describing the kinetics of polymer crystallisation several limitations have been observed[82]. These restrictions are reflected in the repeated observation of non-constant and fractional n values with many polymers, which could not be explained by the assumption of a complex mode of crystallisation involving two or more processes each following its own Avrami equation[83]. Instead, the variations in crystalline density on moving outwards from the centre of the spherulite and branching of the internal spherulite structure have been attributed to the discrepancy of n value considerably less than 3 for spherulitic crystallisation.

4.3 Results and Discussion

4.3.1 Dynamic Crystallisation

Because of its structural regularity, PET readily crystallises in the temperature range 40 K above its T_g to 50 K below its T_m. Normally, the crystallisation occurring above T_g is called cold crystallisation and that close to T_m is called hot crystallisation. Fig. 4.5 shows DSC traces of cold crystallisation of PET and its blends prepared without catalyst. As can be seen the temperature corresponding to the onset of crystallisation, $T_{c,onset}$, was about 400 K for PET and about 415 K for PET/PC 50/50 blend. The values of $T_{c,onset}$ decreased with decreasing PC content. This was the opposite to what was observed during hot crystallisation, as can be seen in Fig. 4.6. The crystallisation exotherms increased with decreasing PC content as the crystalline materials content increase. This was all consistent with the PET in the blends alone crystallising.

The DSC traces of cold and hot crystallisations of the PET/PC blends prepared in the presence of catalyst are shown in Fig.s 4.7 and 8 respectively. They exhibited the same trends as those observed for the blends prepared without catalyst.

The temperature corresponding to the peak in the crystallisation exotherm, $T_{c,peak}$, and $T_{c,onset}$ for cold crystallisation of PET and its blends prepared with and without added catalyst are plotted in Fig. 4.9. It can be seen that the $T_{c,onset}$s and $T_{c,peak}$s showed the same trend in both blends. The values of $T_{c,onset}$s and $T_{c,peak}$s increased with decreasing PC content, and these values for blends prepared with catalyst were higher than those

prepared without catalyst. The same was also exhibited in hot crystallisation. These demonstrated that the PET crystallisation rate was reduced by the presence of PC but the effects were greater in blends prepared with catalyst than those without. This was consistent with the conclusion drawn in the previous chapter – the presence of PC in the partially miscible blends had more effect on the crystallisation of PET than the in completely miscible blends.

4.3.2 Isothermal Crystallisation

4.3.2.1 Avrami Analysis on Isothermal Crystallisation

DSC has been widely used in the study of the thermal properties of polymers, particularly in investigating isothermal crystallisation kinetics[83,84]. Isothermal crystallisation is usually measured as a function of time and temperature. In analysing the isotherm, the point at which the heat evolution returned to the isothermal baseline was taken to be the end of process (t_∞) [83]. This can be seen in Fig. 4.10.

A baseline correction[84] was made to define the onset of crystallisation, t_0, since on quenching (at 160 or 320 K min^{-1}), the thermal lag of the instrument could not be ignored and the initial DSC trace reflected both cooling of the instrument to the crystallisation temperature and the onset of crystallisation. To eliminate the effect of cooling, a cooling curve was collected on cooling the sample through the same temperature difference 60 – 80 K lower (equal to $\Delta T = T_m - T_c$) than the crystallisation

temperature immediately after finishing the isothermal crystallisation. This was then subtracted from the overall crystallisation exotherm. This enabled $t_0 = 0$ to be determined before analysis of the isothermal crystallisation. This procedure is shown in Fig. 4.10. The fractional crystallinity X_t which developed from $t_0 = 0$ to time t was defined from the ratio of the areas between the heat flow- time curve so determined, i.e.

$$X_t = \frac{\Delta H_t}{\Delta H_\infty} = \int_0^t \frac{dH}{dt} dt \Big/ \int_0^{t_\infty} \frac{dH}{dt} dt \tag{4.31}$$

The time dependence of the relative crystallinity was then analysed using the Avrami equation, equation 4.30, from

$$\log(-\ln(1 - X_t)) = \log Z + n \log t \tag{4.32}$$

The isothermal crystallisation of PET and the blends are shown in Fig. 4.11. All of them exhibit a similar temperature dependence. The isothermal crystallisation curves were initially analysed using equation 4.32. By plotting log[-ln(1-X_t)] *against* log(t), a linear relationship was obtained with a slope equal to the Avrami exponent n and intercept of log(Z) at log(t) = 0. However, it was found that for PET and the blends, this linear relationship was maintained only up to 70 - 80% conversion and thereafter the slope changed to much lower value, as can be seen in Fig. 4.12. This was attributed to the onset of secondary crystallisation a process involving either crystallisation of interlamellar amorphous region, lamellar thickening or crystal perfecting. However, the exact mechanism has not been precisely determined yet[72,84]. Primary and secondary crystallisations were considered to occur consequently[83,85] and the primary crystallisation could be analysed separately using a modified from of the Avrami equation to account for primary crystallisation finishing at $X_{p,\infty}$, i.e

$$1-\frac{X_t}{X_{p,\infty}}=\exp(-Zt^n) \tag{4.33}$$

$$\log[-\ln(1-\frac{X_t}{X_{p,\infty}})]=\log Z+n\log t \tag{4.34}$$

where $X_{p,\infty}$ refers to the relative crystallinity at the end of the primary crystallisation. $X_{p,\infty}$ was defined from the change in slope of the log[-ln(1-X_t)] *against* log(t) plot as can be seen in Fig 4.12.

Plots of log [-ln (1-$X_t/X_{p,\infty}$)] *versus* log (t) are shown in Fig.4.13. It is clear that they were linear, and thus the values of n and Z could be determined from the slopes and intercepts at log(t) = 0, respectively. The half-life of crystallisation $t_{1/2}$, i.e., the time at which 50% relative crystallinity has achieved during the primary crystallisation was also determined. The rate constant, Z, was also calculated from the half-life, $t_{1/2}$, and the average value of n

$$Z=\ln 2/t_{1/2}^n \tag{4.35}$$

Instantaneous values of the Avrami exponent, n, as a function of crystallinity were obtained from the differentiated form of equation 4.33, i.e.

$$n=-t\frac{d(X_t/X_{p,\infty})}{dt}/[(1-\frac{X_t}{X_{p,\infty}})\ln(1-\frac{X_t}{X_{p,\infty}})] \tag{4.36}$$

A constant value of n over most of the conversion range was obtained, see Fig. 4.14, which was consistent with that obtained from log-log plot in Fig. 4.13.

The rate parameters of the primary crystallisation of both PET and the blends were also determined as a function of crystallisation temperature. These were listed in Tables 4.2

and 4.3, from which it can be seen that n values were essentially constant at 3.0 (within experimental error). This was attributed to 3-dimensional growth of spheres from heterogeneous nucleation. Polarized light microscopy confirmed that PET crystallised by the growth of spherulites from heterogeneous nuclei. Micrographs of the spherulites present in PET and PET/PC 50/50 blend taken by polarized light microscopy are shown in Fig. 4.15. They exhibited the characteristic Maltese cross birefringence of spherulites and straight impingement boundary characteristic of heterogeneous nucleation.

Tables 4.2 and 4.3 list the values of $t_{1/2}$ and Z for each sample as a function of crystallisation temperature. PET crystallised at a faster rate than the blends at the same crystallisation temperature, indicating that PC inhibited the crystallisation of PET. Plots of the half-life vs. T_c, for both blends prepared with and without catalyst are shown in Fig. 4.16. The reduction in rate is more marked with the blends prepared with added catalyst than those without. Indeed the later blends crystallised over a similar temperature range to that of PET but with half-lives increased in proportion to the content of PET in the blend, see Table 4.2. Thus the 50/50 blends have half-lives which are approximately double those of PET, and similarly with the other blends. The reduction in crystallisation rate in these blends is considered to occur from a physical restriction of the growth by the PC domains.

Very different temperature dependences were observed in the crystallisation half lives of the blends prepared with added catalyst, see Fig. 4.16b, in that they crystallised at much lower temperatures and were displaced to lower crystallisation temperatures and

disproportionate to the amount of PC present. 10% PC in the blend had a greater effect proportionally than either 30% or 50%.

4.3.2.2 Temperature Dependence of Crystallisation Rates

The temperature dependence of the crystallisation rate can be described by the Turnbull –Fisher equation, equation 4.16. As the melt crystallisation temperature is well above the T_g secondary nucleation is the rate determining step and equation 4.16 can be simplified to:

$$g = g_0 \exp(-\frac{\Delta G_n^*}{RT}) \tag{4.37}$$

The bulk crystallisation rates of polymer at different temperatures were expressed in the form of reciprocal crystallisation half-life, $1/t_{1/2}$. Mandelkern *et al.*[86] have used the half-lives of isothermal crystallisation instead of g in equation 4.37, such that

$$\ln(1/t_{1/2}) = C - \frac{\Delta G_n^*}{RT_c}$$

$$= C - (\frac{4\sigma\sigma_e}{R\Delta H_f})\frac{T_m^o}{T_c(T_m^o - T_c)} \tag{4.38}$$

in which C is a constant, the rest of the parameters are as defined previously. In plots of $\ln (1/t_{1/2})$ *vs.* $T_m^o / T_c(T_m^o - T_c)$ the slopes are equal to $4\sigma\sigma_e/R\Delta H_f$ They are shown for PET and its blends in Fig. 4.17. Similar slopes were observed in that most of the lines were parallel to each other. By assuming[87] that $\sigma = 0.1\Delta H_f$, the values of σ_e were calculated and the results are listed in table 4.4.

It is clear that the σ_e values of PET/PC blends prepared without added catalyst were very similar to those of PET while those of PET/PC blends prepared with added catalyst were significantly less than that of PET. Normally, the surface free energy of the chain folding surface in polymer crystal is directly related to the chemical nature of the amorphous layer in the fold surface such that with increasing surface free energy crystallisation ability is reduced[72]. Therefore, PC inhibiting the PET crystallisation in PET/PC blends prepared with added catalyst cannot be due to the small changes in the fold surface free energy, which can only be due to presence of PC close to the fold surface.

It is apparent from equation 4.38 that $\ln(t_{1/2})$ was a function of the degree of super-cooling, $\Delta T = T_m^{\circ} - T_c$. Plots of $\ln(t_{1/2})$ against T_c, see Fig. 4.18, for each blend could be superimposed on the PET data by a lateral shift along the temperature axis equivalent to a ΔT value for each blend. These were 15, 19 and 20 K for the 90/10, 70/30 and 50/50 blends prepared with added catalyst. Indeed, the measured equilibrium melting points for the above blends are 16, 12, and 16 K lower than that of PET respectively. The presence of soluble impurities clearly decreases the crystallisation ability of PET. This is consistent with the blends prepared with added catalyst being partially miscible and consistent with the conclusion drawn in the last chapter.

4.4 Conclusion

The crystallisation kinetics of PET and its blends prepared with and without added catalyst have been studied. It was observed that the crystallisation of the PET crystal was inhibited by the presence PC, particularly in the blends prepared in the presence of catalyst. For blends without added catalyst the retardation was by PC domains acting as physical constraints to the development of the PET crystallisation while in the other blends there was also some limited solubility of PC in the PET which depressed the equilibrium melting points. This is consistent with the conclusion on the miscibility of the blends. The Avrami model was applied to analyse the crystallisation kinetics of PET and both sets of blends which indicated that crystallisation develops spherulites from the heterogeneous nucleation

Table 4.1 Avrami parameters

Crystallisation mechanism		n	Z
Spheres	sporadic	4	$2/3\pi g^3 l$
	predetermined	3	$4/3\pi g^3 L$
Discs	sporadic	3	$\pi/3 g^2 ld$
	predetermined	2	$\pi g^2 Ld$
Rods	sporadic	2	$\pi/4 glr^2$
	predetermined	1	$1/2\pi gLr^2$

* where g = crystal growth rate

l = nucleation rate

L = density of nuclei

d = constant thickness of the discs

r = constant radius of rods

Table 4.2 Avrami parameters for molten-crystallisation of PET and its blends prepared without added catalyst

Sample	Temperature K	$t_{1/2}$ min	n ±0.1	Z $min^{-n}.10^{-4}$
PET	483.4	4.6	3.0	71.2
	485.3	5.5	3.0	41.7
	487.2	6.9	3.1	17.4
	488.8	7.8	3.0	14.6
	491.2	9.5	3.0	8.11
	493.1	11.8	3.0	4.2
PET/PC 50/50	483.4	10.4	2.7	12.4
	485.4	11.9	2.7	5.2
	487.3	15.8	2.8	3.1
	489.3	19.6	2.8	1.7
	491.2	22.9	2.9	1.5
	493.2	26.1	2.7	1.0
PET/PC 70/30	483.4	7.1	3.1	15.7
	485.4	8.9	3.1	7.9
	487.3	11.1	3.0	5.1
	489.3	12.7	2.9	4.4
	491.2	16.2	2.9	2.2
	493.2	17.9	2.8	2.1
PET/PC 80/20	483.4	6	3.1	26.8
	485.4	7.8	3.2	9.7
	487.3	8.5	3.3	6.0
	489.3	10.7	3.0	5.6
	491.2	12.9	3.0	3.2
	493.2	19.1	3.0	1.0
PET/PC 90/10	483.4	4.5	3.1	65.4
	485.4	5.8	3.1	29.8
	487.3	7.2	3.3	10.3
	489.3	8.4	3.1	9.4
	491.2	10.0	3.2	4.4
	493.2	13.2	3.2	1.8

Table 4.3 Avrami parameters for molten-crystallisation PET/PC blends prepared in the presence of catalyst

Sample	Temperature K	$t_{1/2}$ min	n ±0.1	Z $min^{-n}.10^{-4}$
PET/PC 50/50	469.9	9.6	2.9	9.8
	471.8	11.7	3.0	4.3
	473.8	13.4	3.0	2.9
	475.3	15.3	2.9	2.5
	477.6	18.0	2.9	1.6
	479.5	20.2	3.0	0.84
PET/PC 70/30	471.8	12.0	3.0	4.0
	473.8	14.0	3.1	1.9
	475.7	16.0	3.2	0.97
	477.6	19.0	3.1	0.75
	479.5	21.6	3.0	0.65
	481.4	25.0	3.0	0.44
PET/PC 90/10	477.6	13.4	3.0	2.9
	479.5	15.3	3.1	1.5
	481.4	17.7	3.0	1.2
	483.1	21.6	3.0	0.69
	483.3	22.6	3.0	0.60
	485.3	29.8	3.0	0.26
	487.2	34.8	3.0	0.16

Table 4.4 The fold surface free energy of PET and blends

Sample	Slope	T_m^o K	σ_e kJ mol^{-1}
PET	-506.0	561	10.5 ± 0.5
Without catalyst			
PET90	-567.5	561	11.8 ± 0.5
PET80	-525.8	558	10.9 ± 0.5
PET70	-465.0	557	9.7 ± 0.5
PET50	-448.3	555	9.3 ± 0.5
With catalyst			
PET90	-413.5	545	8.6 ± 0.5
PET70	-408.7	549	8.5 ± 0.5
PET50	-384.8	545	8.0 ± 0.5

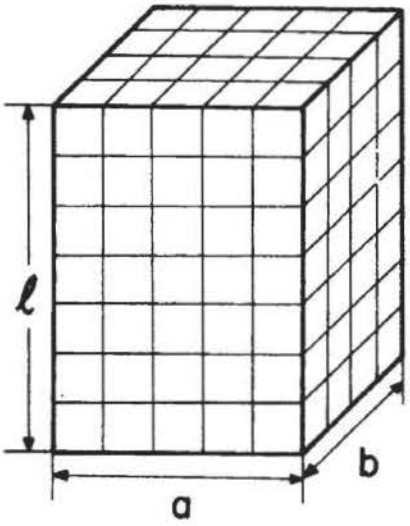

A

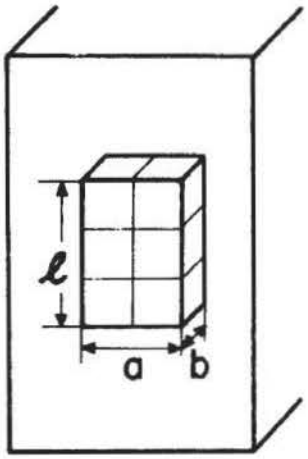

B

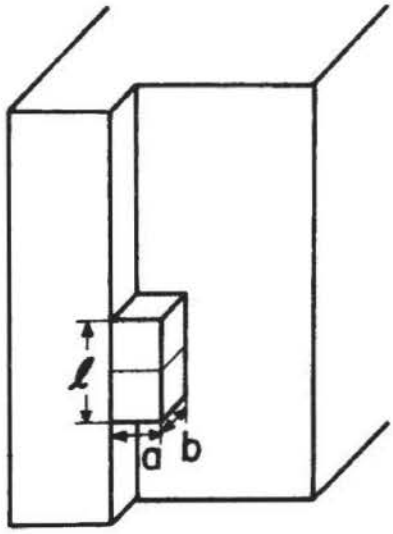

C

Fig. 4.1 Types of crystal nucleation. l refers to lamellar thickness, a and b are nucleus length and width, respectively. A. Primary, B. Secondary and C. Tertiary nucleation[72]

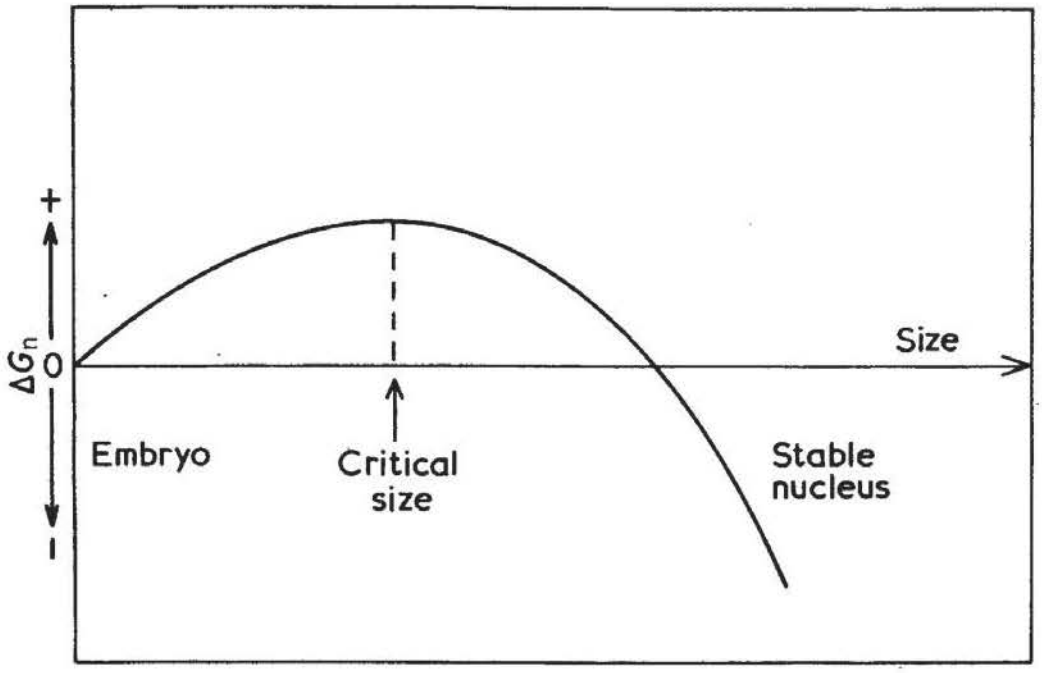

Fig. 4.2 Schematic representation of change in free energy for the nucleation process during polymer crystallisation[72]

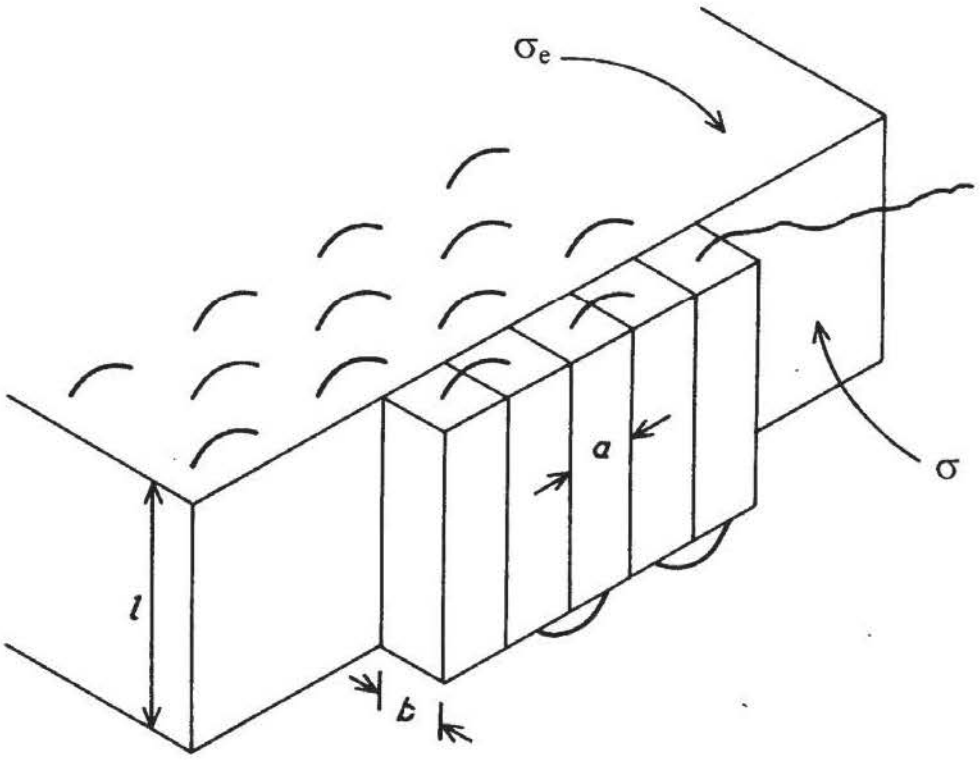

Fig.4.3 Model of the growth of a lamellar polymer crystal through the successive laying down of adjacent molecular strands[74]

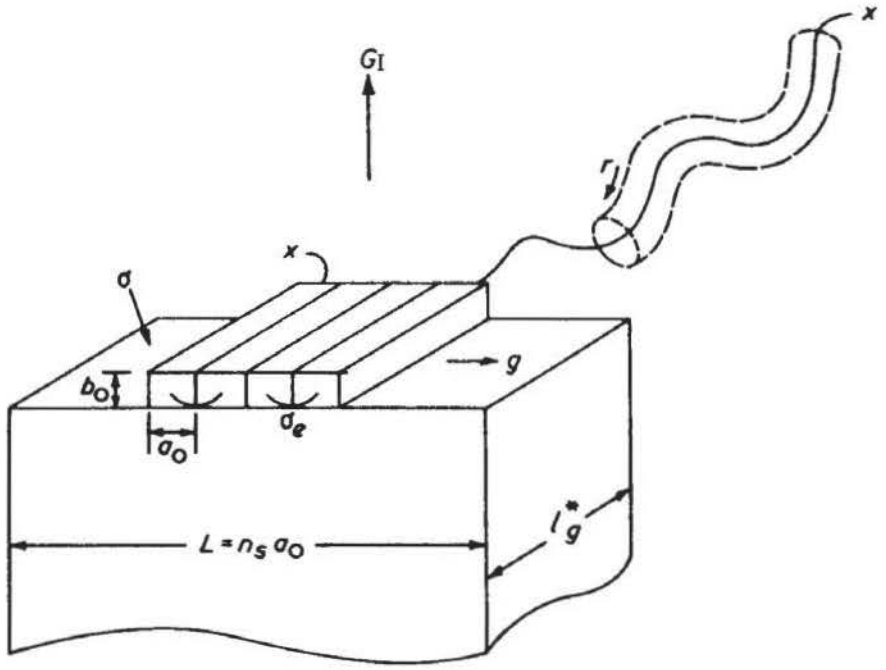

A

Regime I

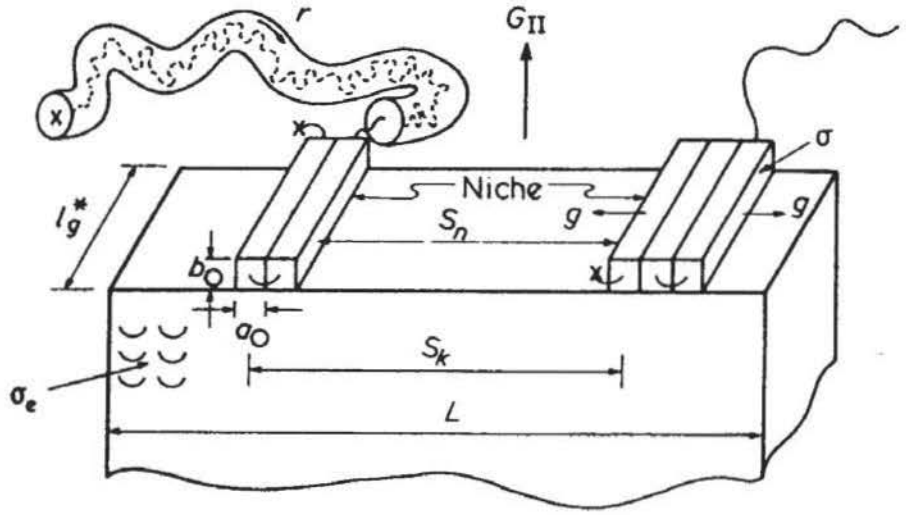

B

Regime II

continued

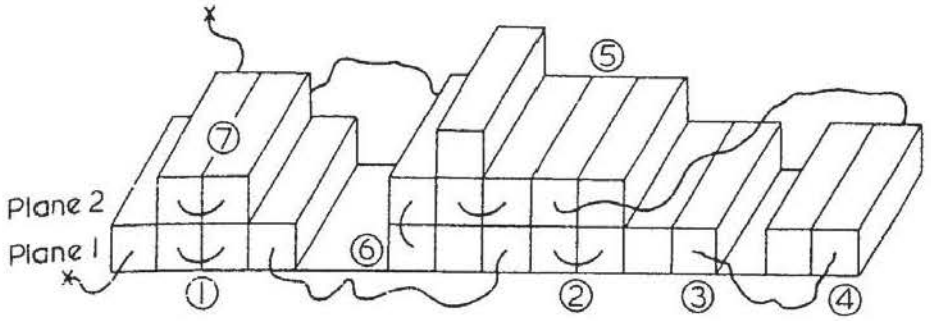

C
Regime III

Fig. 4.4 Schematic represents of three regimes model. G is the overall growth rate, g is the substrate completion rate associated with the reptation rate
$r = (l_g^*/a_o)\ g$ for case of adjacent reentry, a_o and b_o refer to molecule width and layer thickness, σ_e and σ_s are the surface energy of the fold surface and the lateral surface, l_g^* refers to the initial fold thickness of lamellar. A. Regime I where one surface nucleus grown completion of substrate of length L. B. Regime II where multiple surface nuclei occur and lead to completion of substrate of length of L; the quantity S_k represents the mean separation between the nuclei, and S_n denotes the mean distance between the associated niches. C. Regime III where molecule in variable cluster conformation[78]

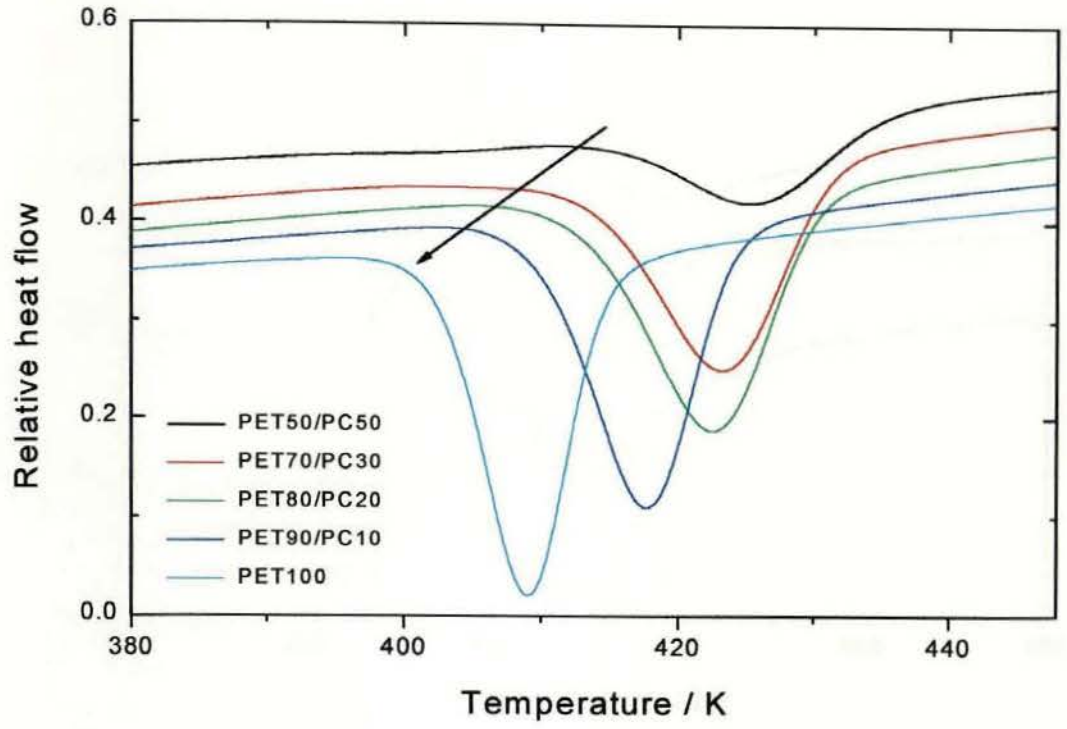

Fig. 4. 5. DSC traces of cold crystallisation of PET/PC blends produced in the absence of catalyst. The sample weight is 10 mg and a heating rate is 10 K/min

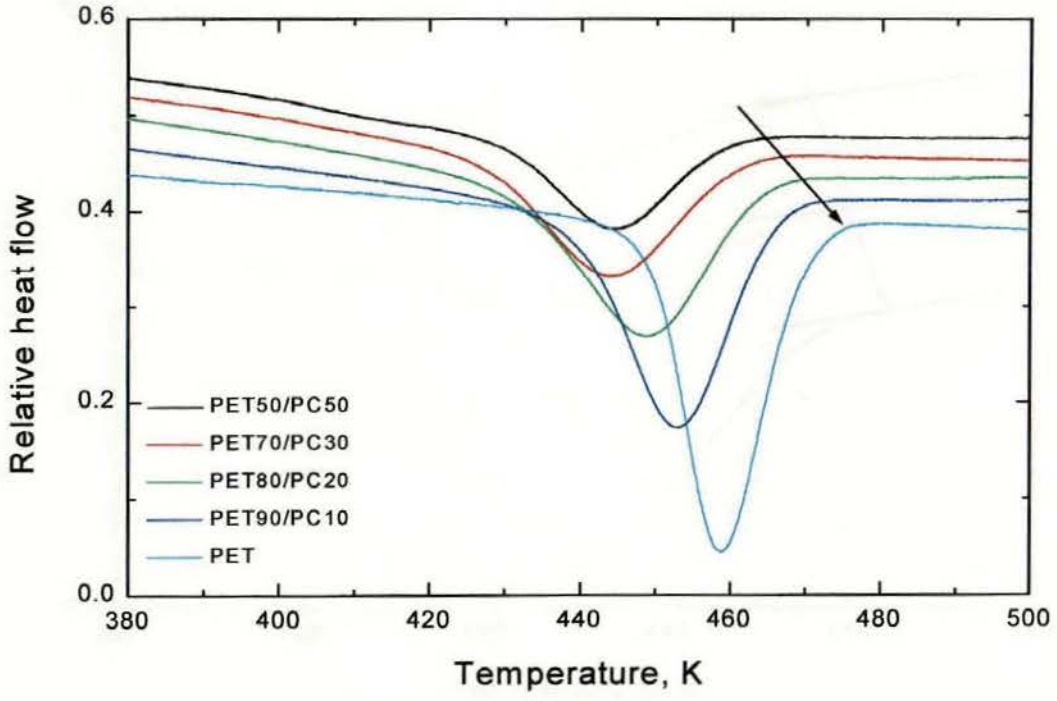

Fig. 4. 6. DSC traces of melt crystallisation of PET/PC blends produced in the absence of catalyst. The sample weight is 10 mg and a cooling rate is 10 K/min

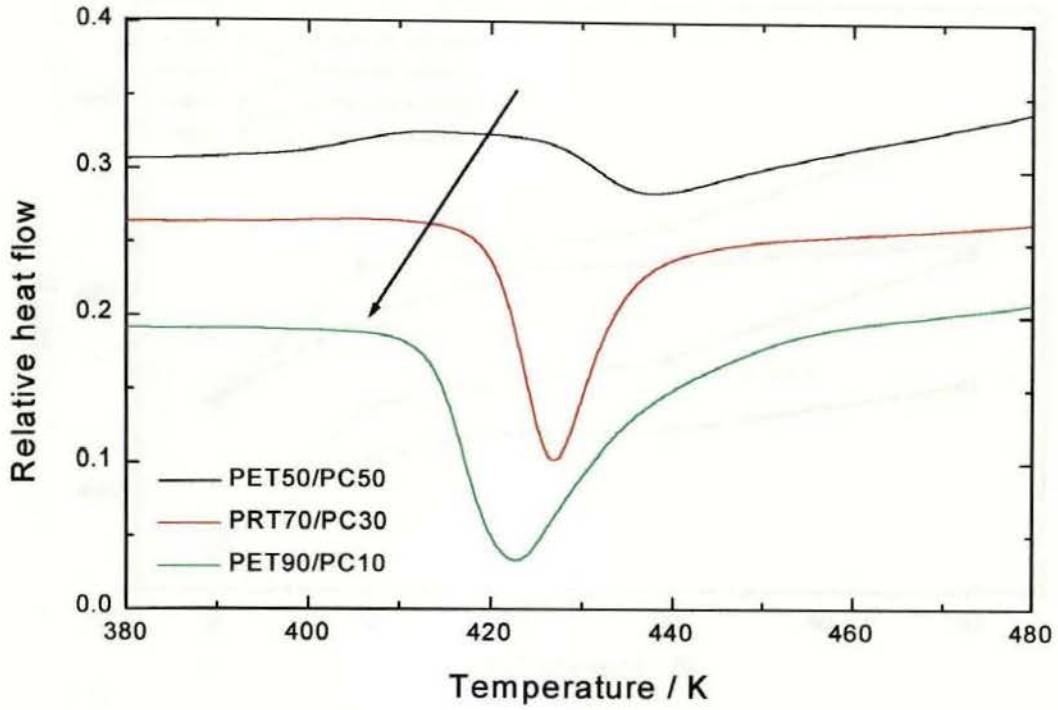

Fig. 4. 7. DSC traces of cold crystallisation of PET/PC blends produced in the presence of a catalyst. The sample weight is 10 mg and a heating rate is 10 K/min

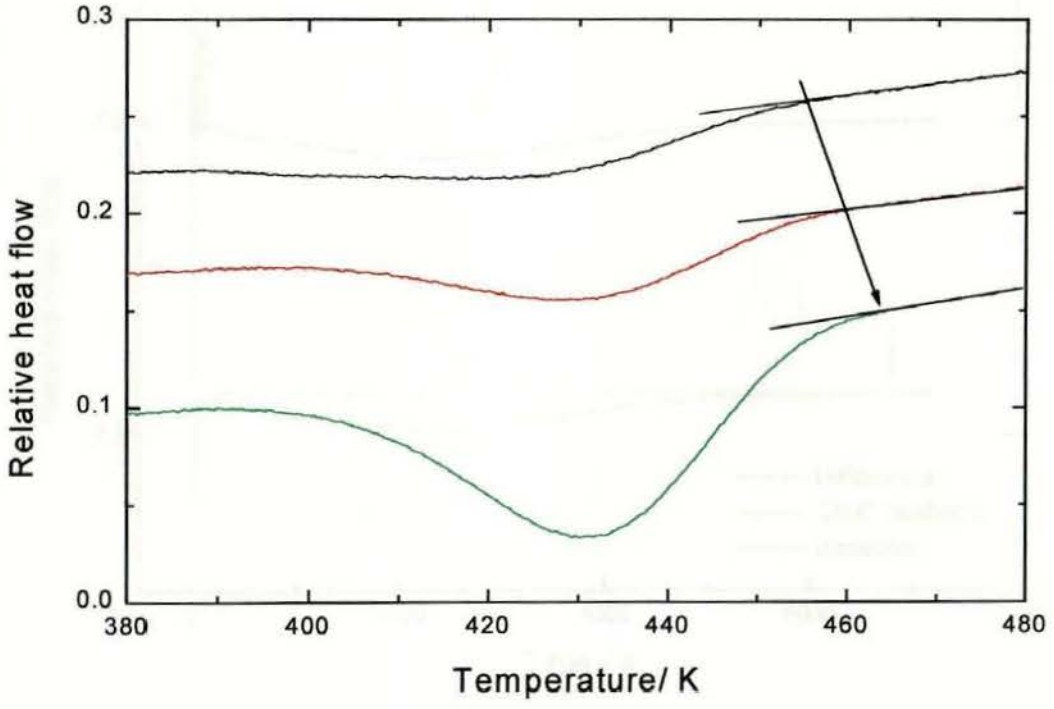

Fig. 4.8. DSC traces of hot crystallisation of PET/PC blends produced in the presence of a catalyst. The sample weight is 10 mg and a cooling rate is 10 K/min

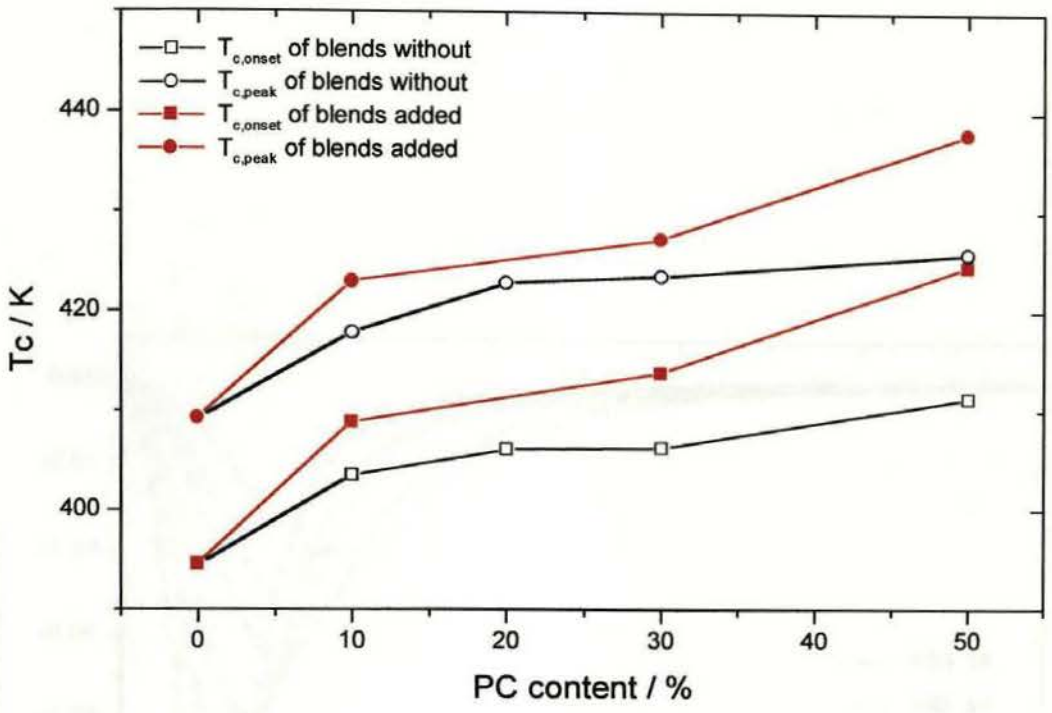

Fig.4.9 The crystallisation temperature of $T_{c,onset}$ and $T_{c,peak}$ for cold crystallisation for PET and blends change with composition

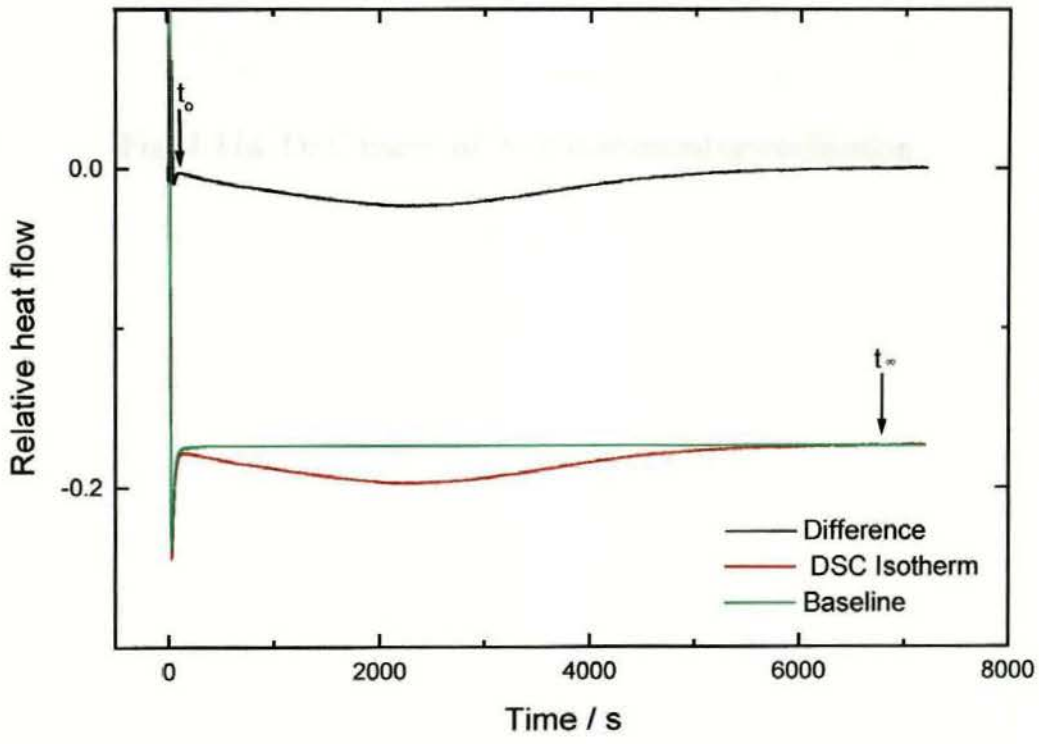

Fig. 4.10 PET isothermal crystallisation measured by DSC. t_∞ as defined in the text, to is defined by using the difference between original DSC isotherm and baseline

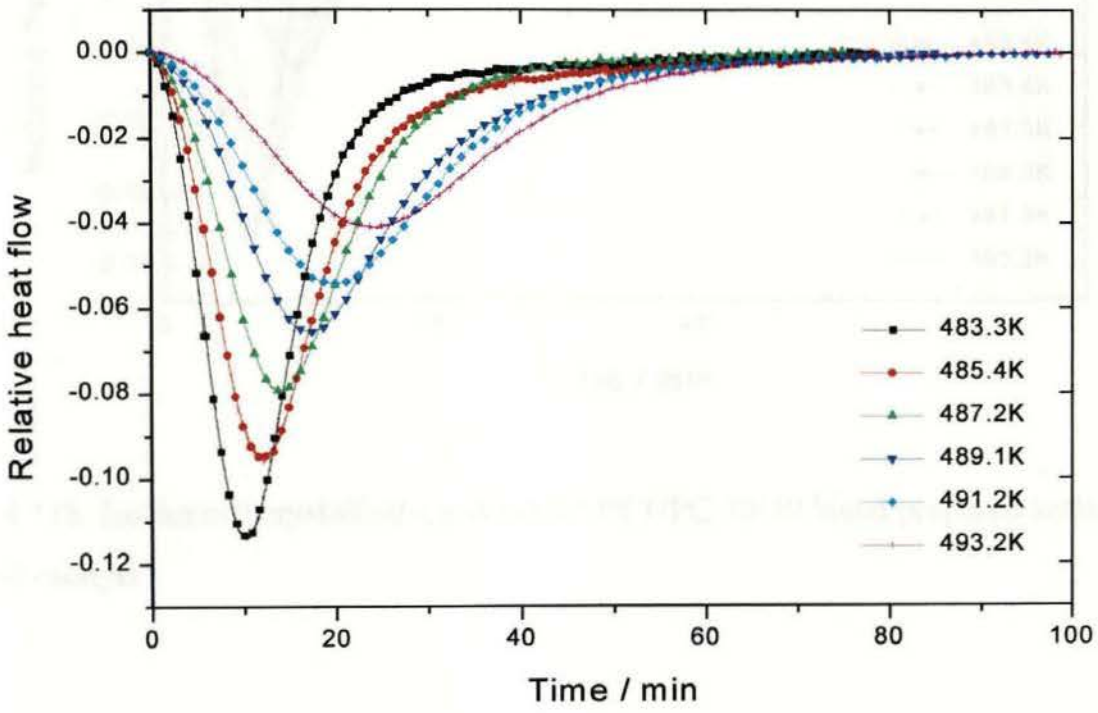

Fig. 4.11a DSC traces of PET isothermal crystallisation

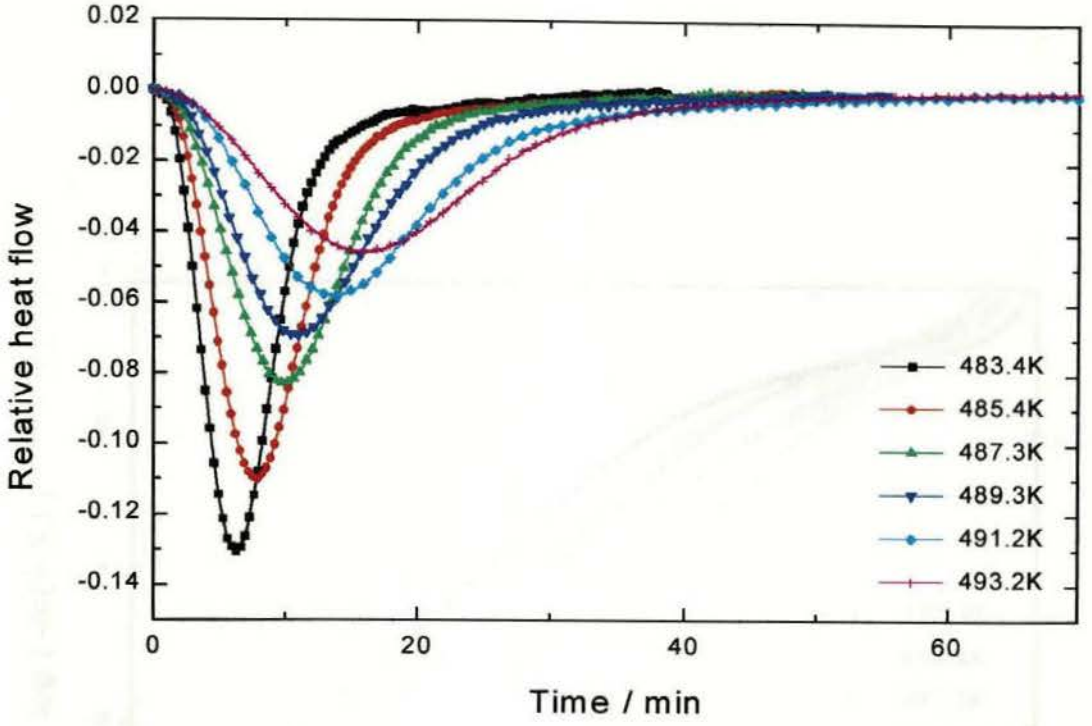

Fig. 4.11b Isothermal crystallisation traces of PET/PC 70/30 blend prepared without added catalyst

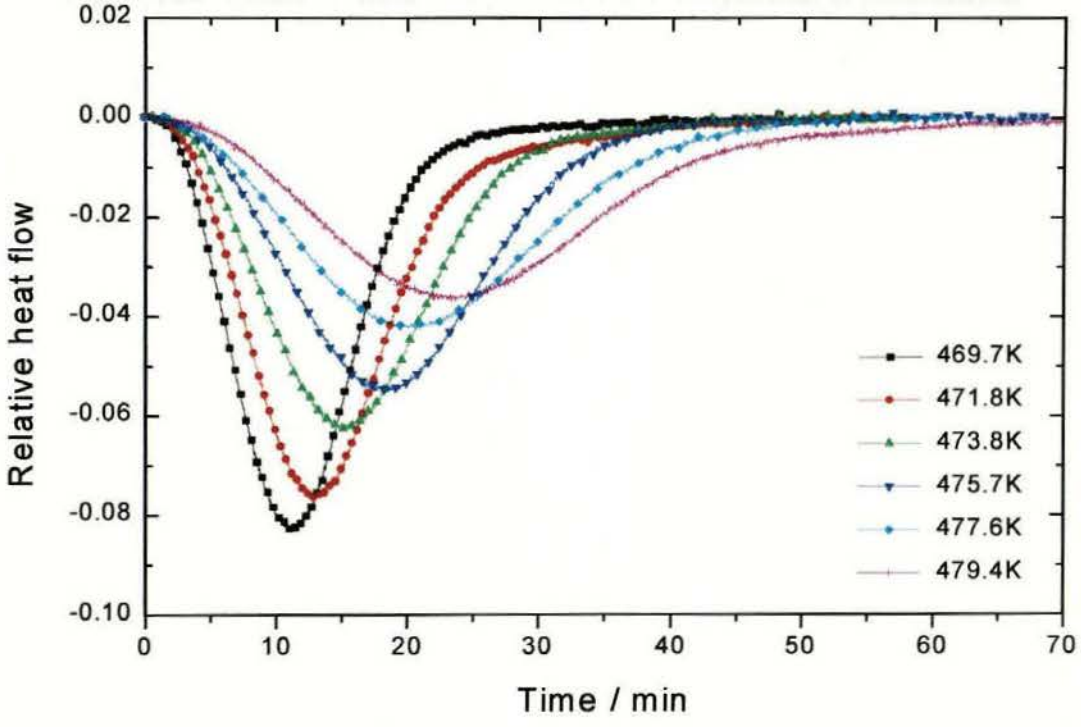

Fig. 4.11c Isothermal crystallisation traces of PET/PC 70/30 blend prepared in the presence of catalyst

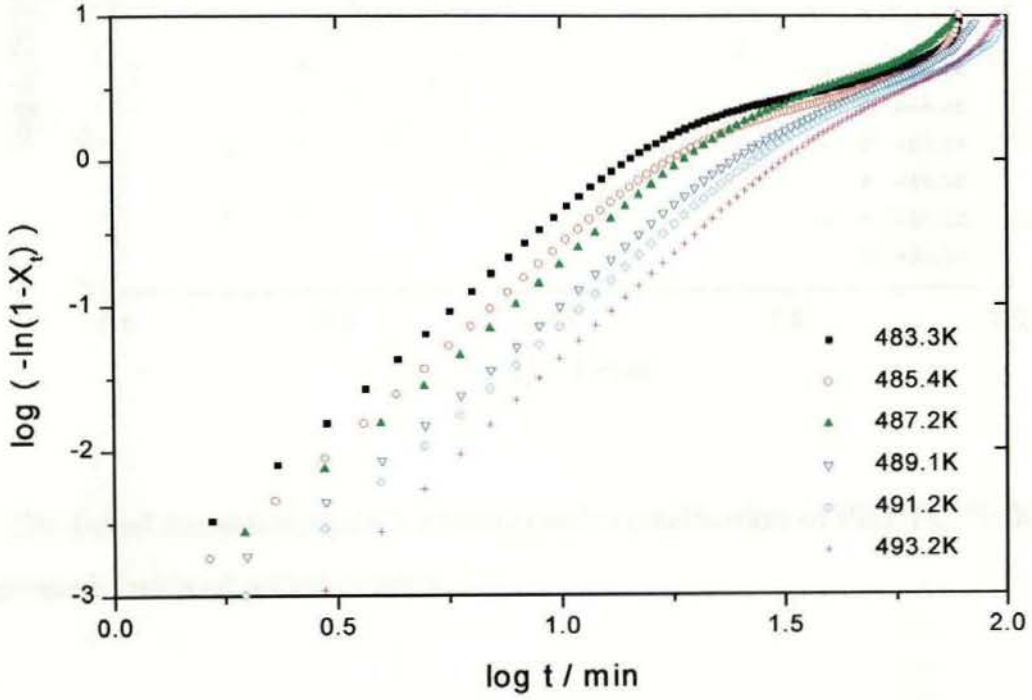

Fig. 4.12a Initial Avrami analysis for PET isothermal crystallisation

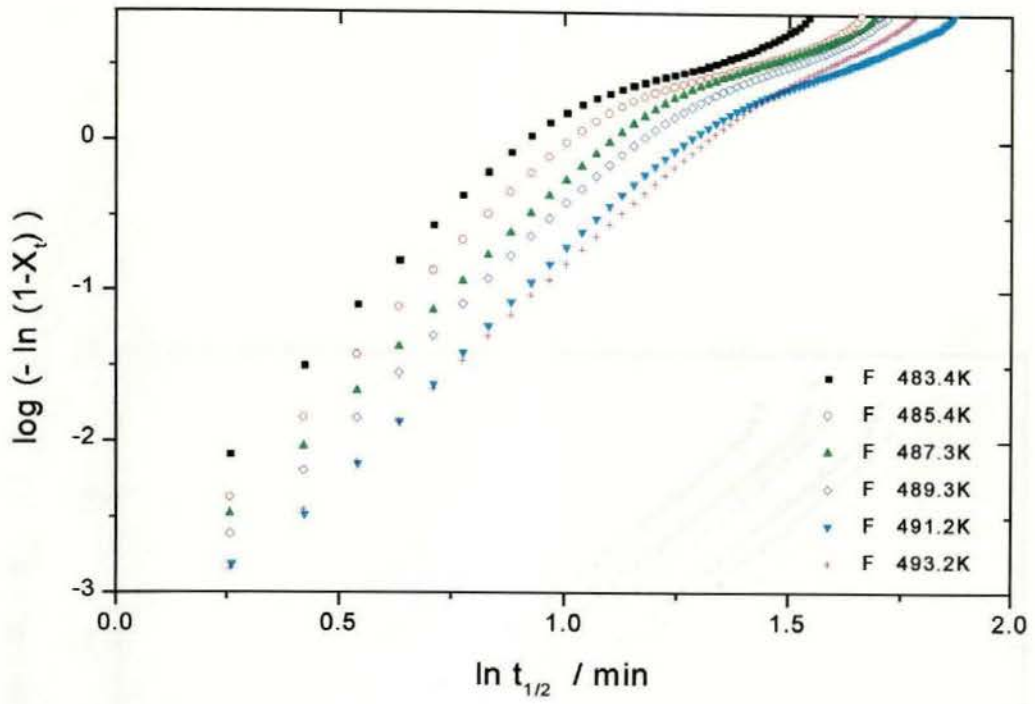

Fig. 4.12b Initial Avrami analysis for isothermal crystallisation of PET/PC 70/30 blend prepared without added catalyst

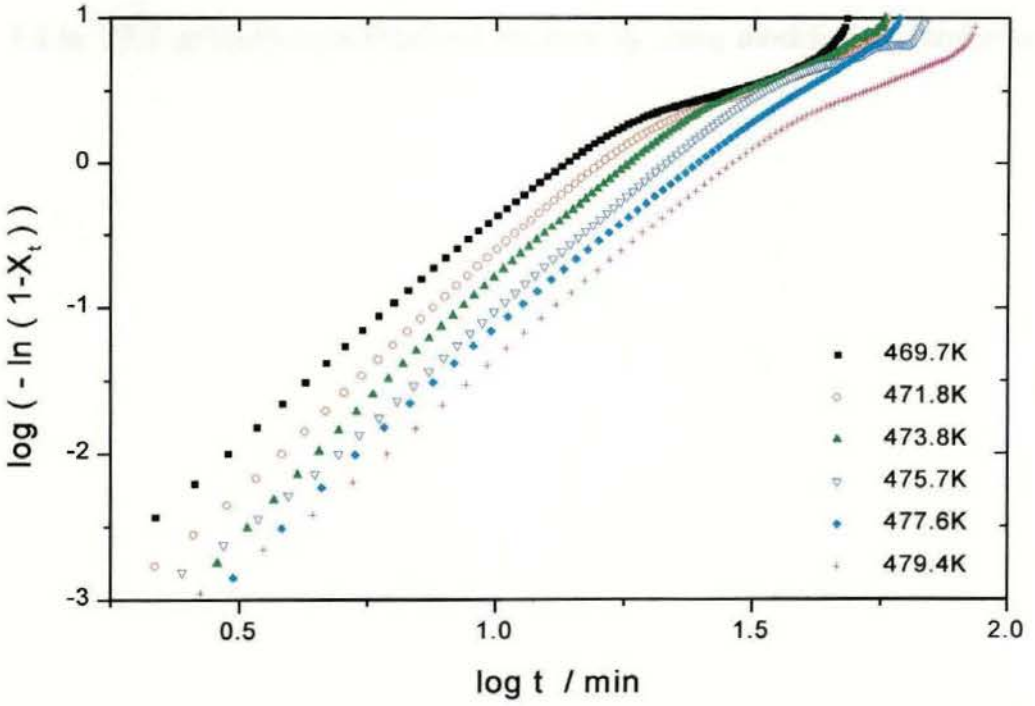

Fig. 4.12c Initial Avrami analysis for isothermal crystallisation of PET/PC 70/30 blend prepared in the presence of catalyst

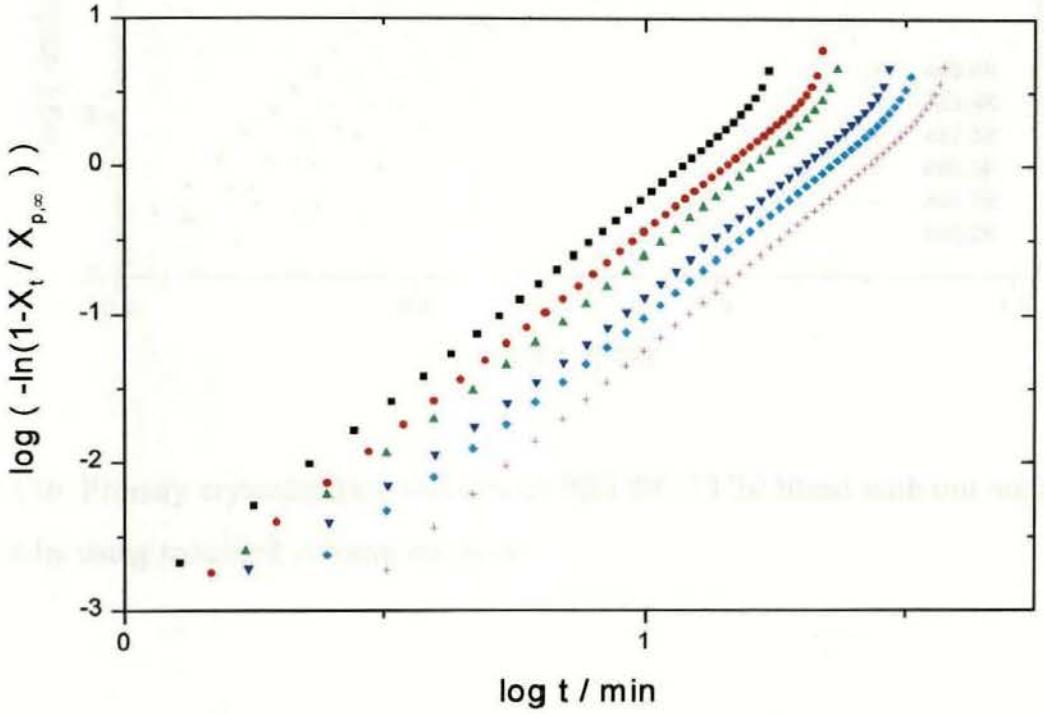

Fig. 4.13a PET primary crystallisation analysis by using modified Avrami equation

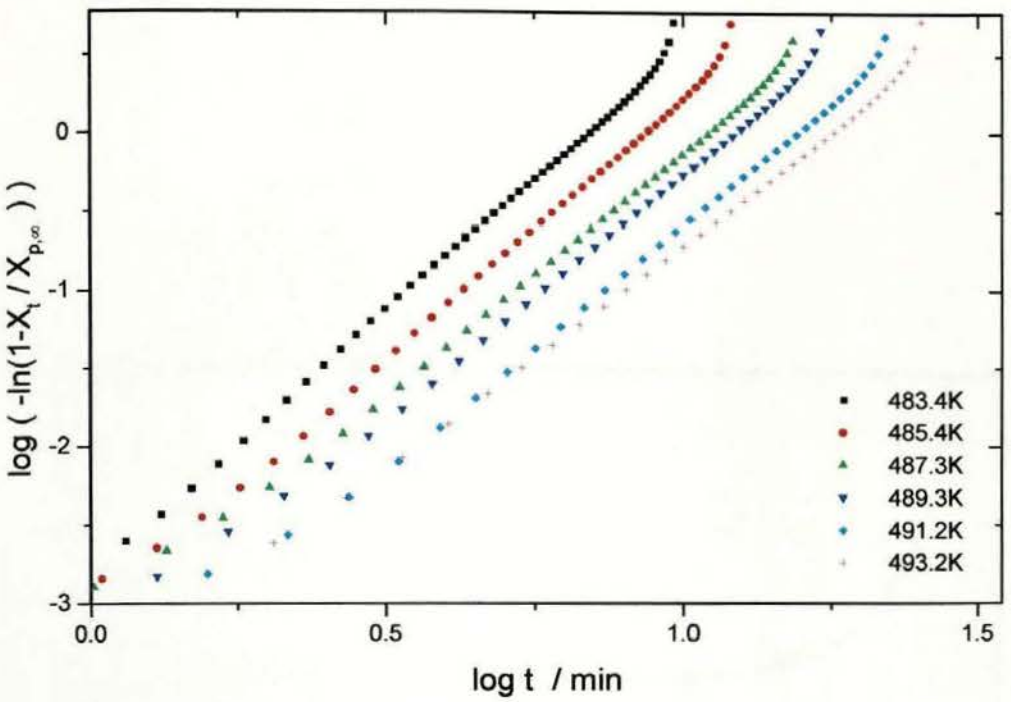

Fig. 4.13b Primary crystallisation analysis of PET/PC 73/30 blend with out added catalyst by using modified Avrami equation

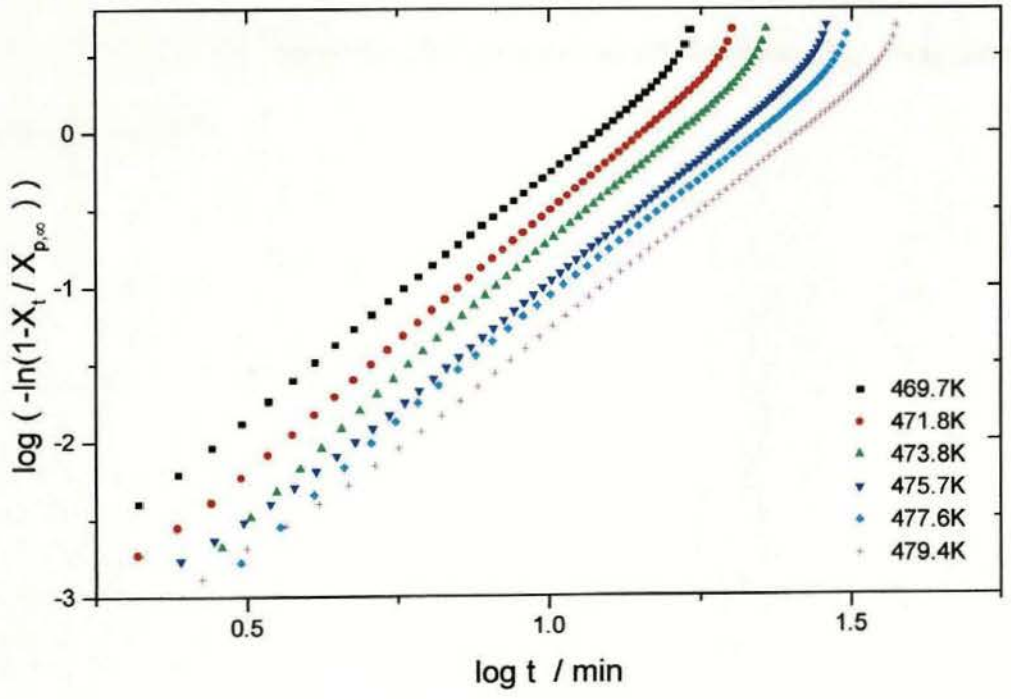

Fig. 4.13c Primary crystallisation analysis of PET/PC 73/30 blend prepared in the presence of catalyst by using modified Avrami equation

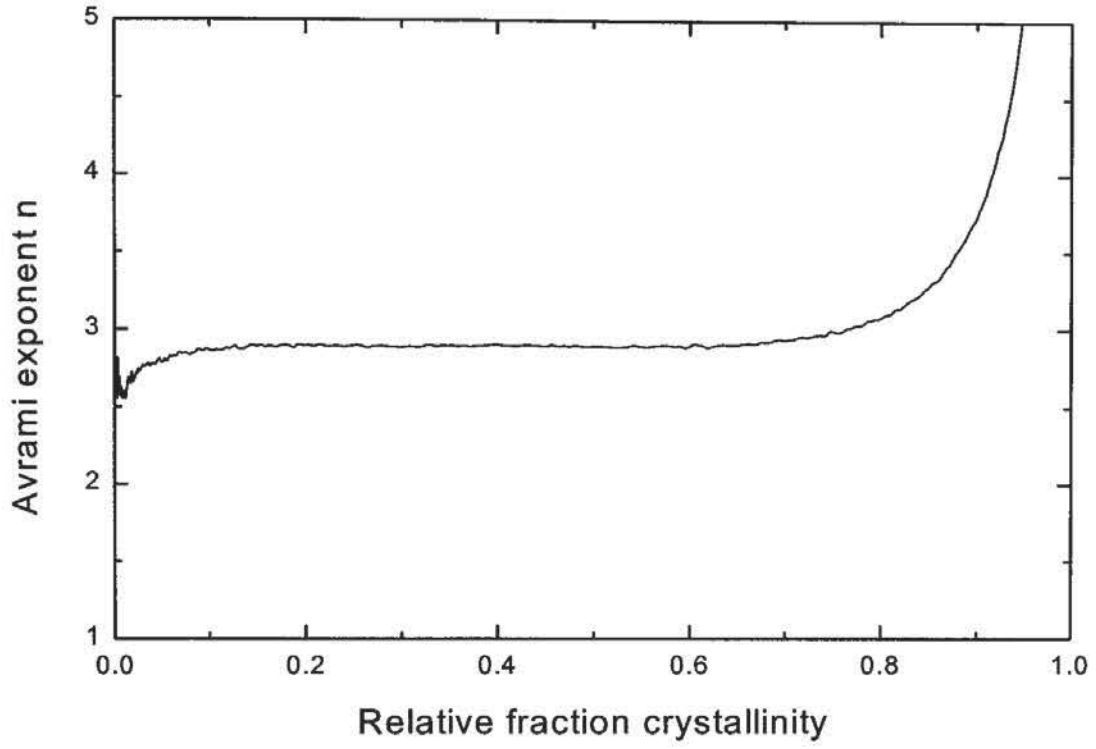

Fig. 4.14 Variation of n value for PET primary crystallisation. $X_{p,\infty}$ was determined as described in the text

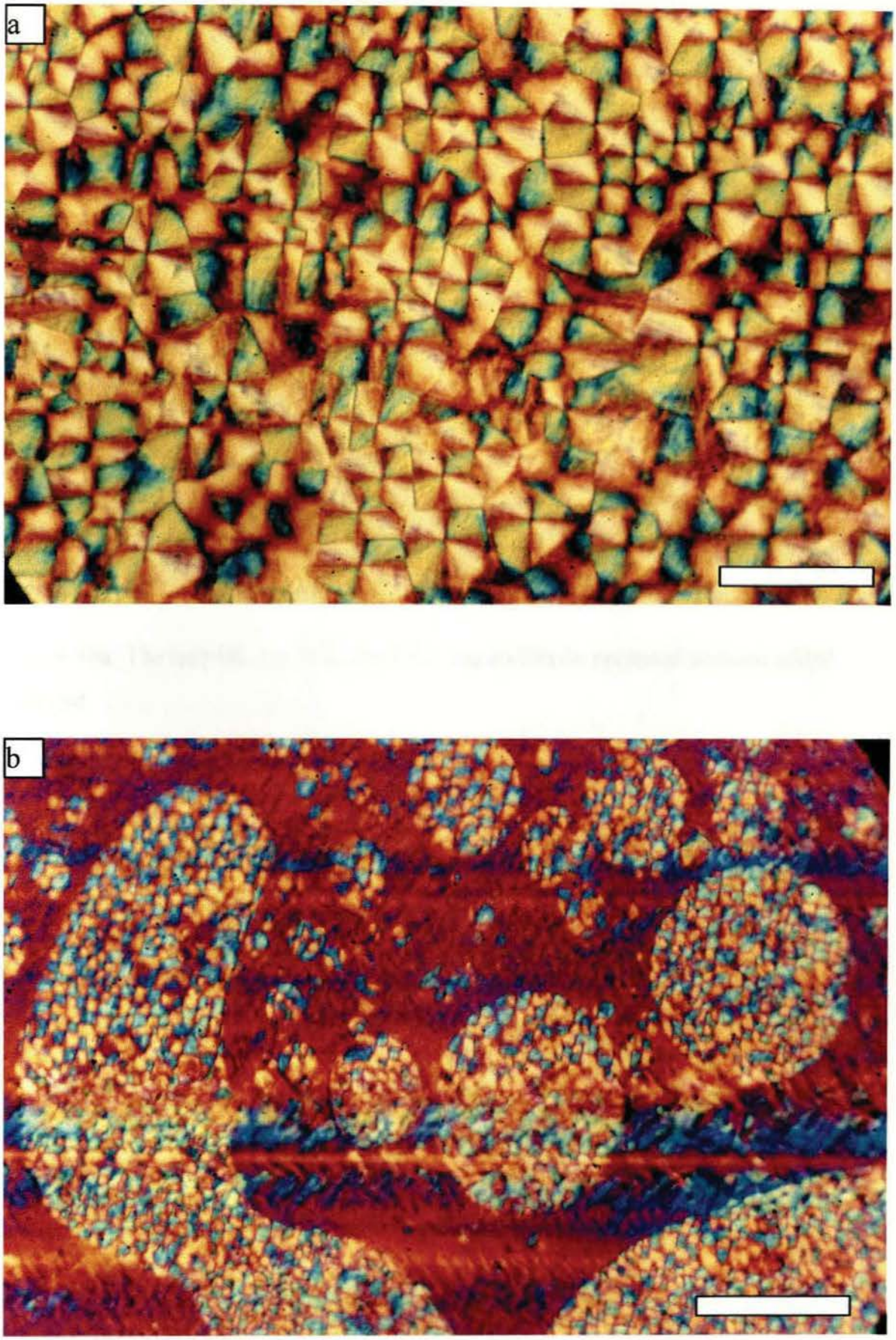

Fig. 4.15 Photographs of polarized light microscopy for hot crystallization, scale bar is 50 μm. a. PET and b. PET/PC 50/50 prepared without added catalyst

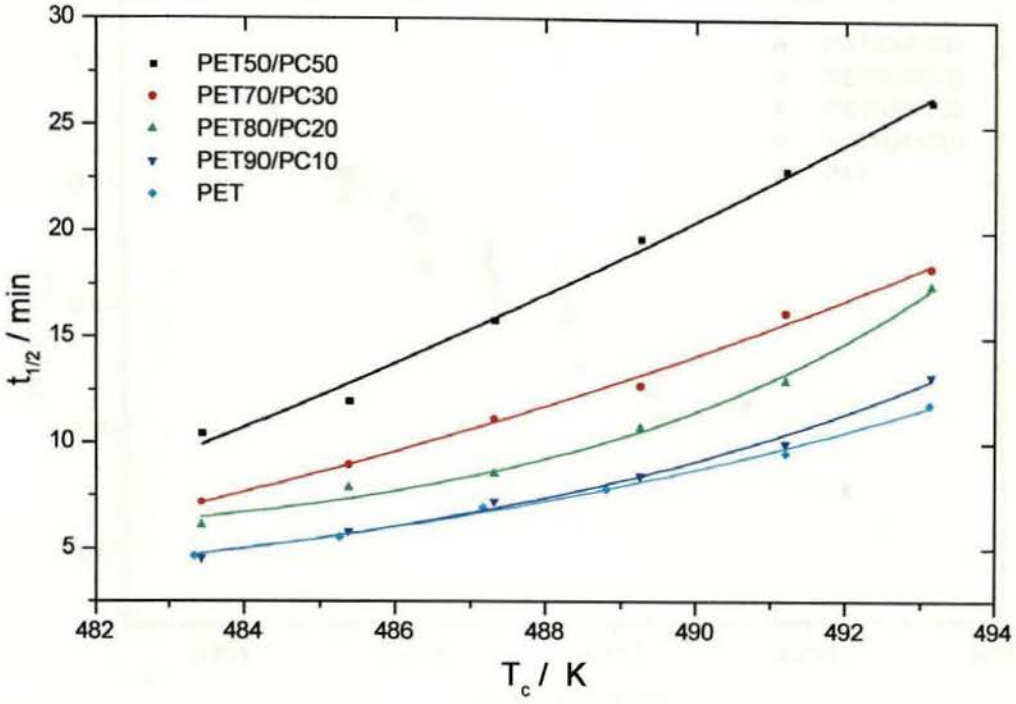

Fig. 4.16a The half-life, $t_{1/2}$ *vs* T_c for PET and its blends prepared without added catalyst

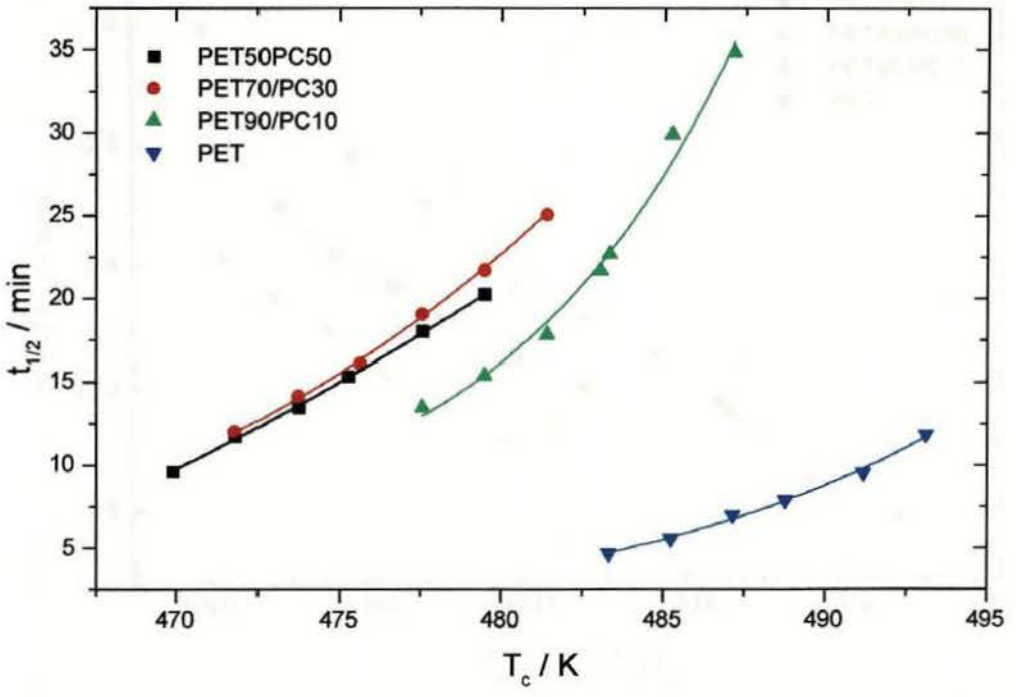

Fig. 4.16b The half-life, $t_{1/2}$ *vs* T_c for PET and its blends prepared with added catalyst

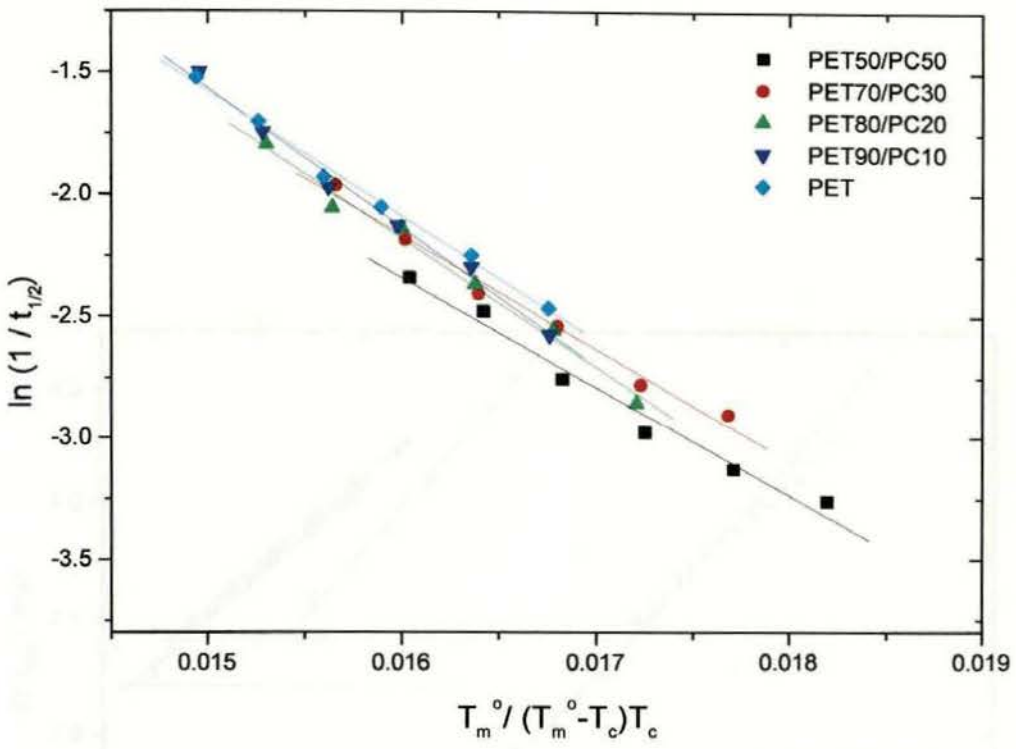

Fig 4.17a Temperature dependence of crystallisation rate for PET and its blends prepared without added catalyst

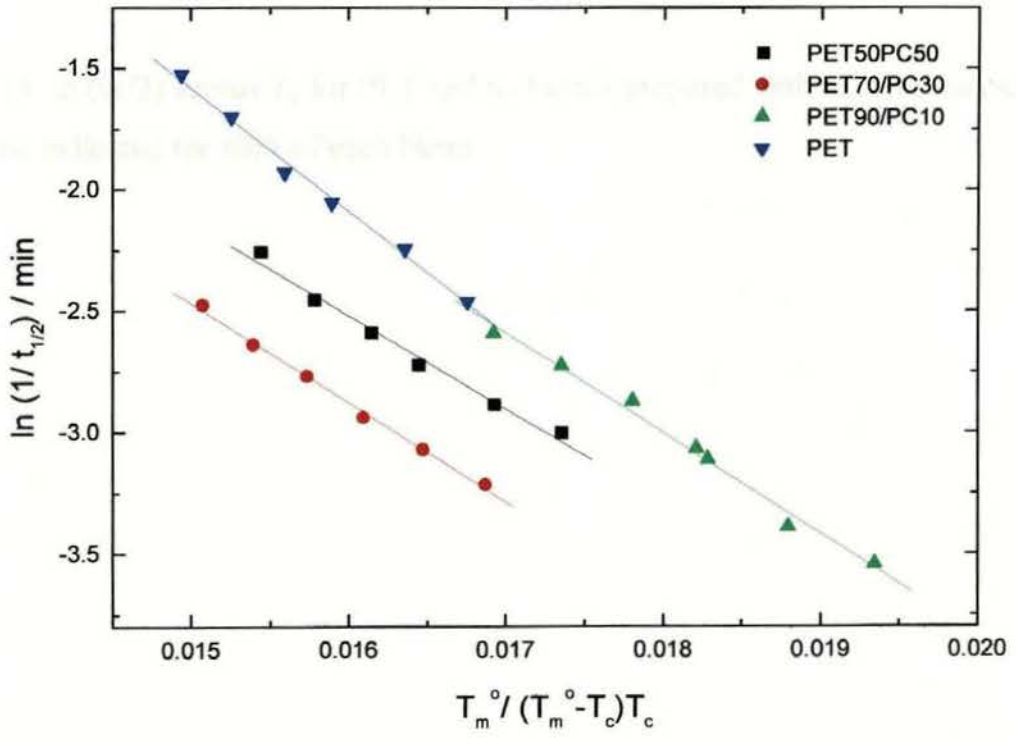

Fig 4.17b Temperature dependence of crystallisation rate for PET and its blends prepared with added catalyst

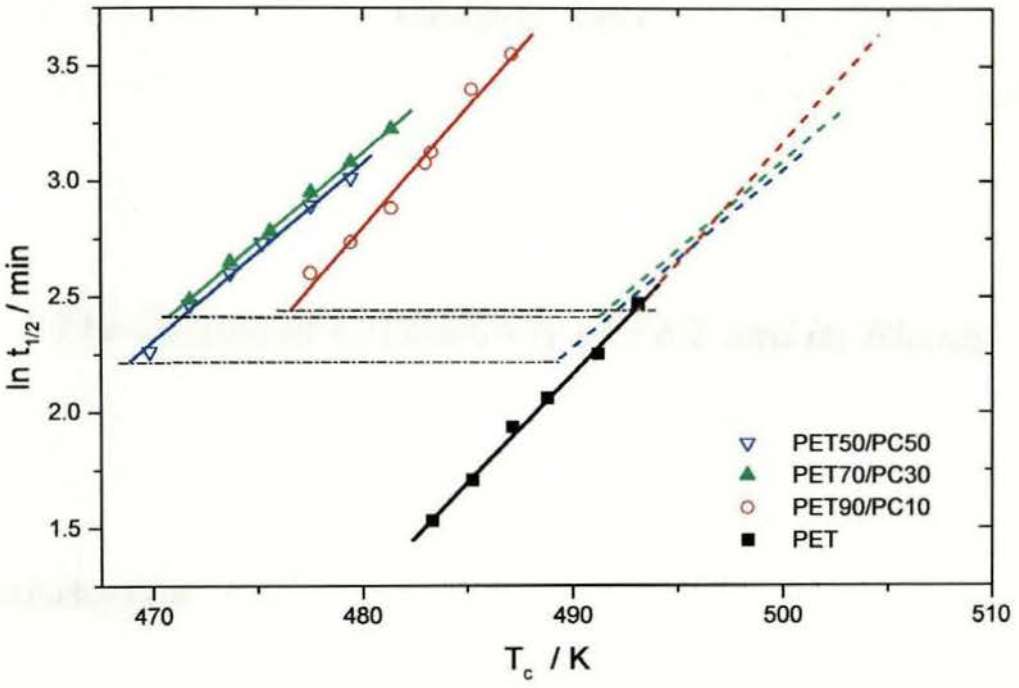

Fig. 4.18 ln (t1/2) *versus* T_c for PET and its blends prepared with added catalyst, the dash line indicated the shift of each blend

Chapter Five

The Degree of Crystallinity of PET and its Blends

5.1 Introduction

Molecular order has an important role in determining ultimate material properties, such as yield stress, elastic modulus and impact resistance, and is an important material characteristic[64,88]. In particular, amorphous polyethylene terephthalate (PET) is of little commercial value since it has poor mechanical properties, low dimensional stability and high gas permeation rate; on the other hand, crystalline PET has higher strength, good dimensional stability and chemical resistance. It is widely used as fibres and in carbonated beverage containers because of its low gas low permeability, especially to carbon dioxide and oxygen.

The various analytical methods used to determine the degree of crystallinity of a polymer namely, wide angle X-ray diffraction (WAXD), density, DSC, infrared (IR) vibration and nuclear magnetic resonance (NMR) spectroscopy have been reviewed by Runt[89]. DSC, however, is probably the most widely used technique. The degree of crystallinity of a polymer is temperature dependent and in comparing its effect on material properties it is vital to carry out these measurements at the same temperature, invariably at ambient temperature and not at the melting point.

In this chapter, the degree of crystallinity of PET and its blends have been studied by wide-angle X-ray diffraction (WAXD), DSC and density measurements.

5.2 The Degree of Crystallinity

5.2.1 Literature Review on the Crystallinity Measured by DSC

Although DSC is a widely used technique it is probably the most widely misused method[90-100]. The most usual wrong procedure in measuring the degree of crystallinity by DSC involves drawing a linear arbitrary baseline from the first onset of melting to the last trace of crystallinity and determining the enthalpy of fusion from the area between this endotherm and the arbitrary baseline, as can be seen from Fig. 5.1. The degree of crystallinity is then defined as

$$X_c = \Delta H_f (T_m) / \Delta H_f^o (T^o_m) \qquad (5.1)$$

where, X_c is the weight fraction extent of crystallinity, $\Delta H_f (T_m)$ is the so called enthalpy of fusion measured at the melting point, T_m, and $\Delta H^o_f (T^o_m)$ is the enthalpy of fusion of the totally crystalline polymer measured at the equilibrium melting point T^o_m which cannot be measured directly and normally obtained from reference data or by other means.

Some allowances have also been made for the sample crystallising on heating by separately integrating the exotherm on cold crystallisation and endotherm on melting over appropriate but different temperature regions. The degree of crystallinity is then defined as

$$X_c = (\Delta H_f - \Delta H_c)/ \Delta H_f^o \qquad (5.2)$$

where ΔH_f is the so called enthalpy of fusion, ΔH_C is the enthalpy of crystallisation and ΔH_f^o is the heat of fusion of the completely crystalline materials as defined above. All are measured at different temperatures and no corrections are made for the change in specific heat. This method has also appeared as a recommended method[99].

Both these methods define the degree of crystallinity close to the melting point rather than at room temperature where other analytical measurements are used, and there is little agreement between them. There are several things wrong in both procedures as outlined. The integration baseline separating exotherms and endotherms is drawn arbitrarily and does not reflect the specific heats of the crystalline or the liquid states and has no physical meaning[100,101]. The actual baseline should obey the heat capacity

variation with temperature by the following equation[102,103] if a two-phase model applied for crystalline polymers, i.e.

$$C_{p,x}(T) = C_{p,c}X_c(T) + C_{p,a}(1 - X_c(T)) \tag{5.3}$$

where $C_{p,x}(T)$ is the heat capacity of the semicrystalline sample at temperature T, which is the baseline of the sample, $C_{p,c}$ and $C_{p,a}$ are the heat capacity of the completely crystalline and amorphous phase respectively. $X_c(T)$ is the degree of crystallinity of the sample at temperature T. Because all these parameters are temperature dependent, in fact, it is impossible to draw this baseline before $X_c(T)$ is known as a function of temperature.

Secondly, the temperature range between the apparent end of crystallisation and the beginning of melting is not considered. It was assumed that no melting or recrystallisation occurred. Because of these effects the degree of crystallinity as measured by DSC conflicted with the values obtained by other methods[91]. Thirdly, the temperature difference of the enthalpy is not considered[104-106]. Therefore, it is usual for the values of ΔH_c and ΔH_f not to be equal even for amorphous samples, particularly for polymers with a large temperature difference between crystallisation and melting, such as PEEK[103,105]. Finally the enthalpy of fusion of 100% crystalline materials is invariably taken as the value at the equilibrium melting point, T_m^o, rather than in the temperature region of the measurement[102,103].

In measuring the degree of crystallinity of nylon-6, Khanna *et al.*[100] recommended a method, in which the DSC baseline was drawn between two set temperatures i.e., one

post-T_g and the other above T_m. Although as the authors admitted, the sample at the post-Tg was a mixture of liquid and solid and the observed specific heat was dependent on the degree of crystallinity, and so it cannot be equivalent to the specific heat of the liquid line, they still drew a linear baseline between the two temperatures. This separated the exotherm and endotherm due to recrystallisation and melting and determined the degree of crystallinity from equation 5.2.

Seguela[103] admitted that the melting enthalpy was temperature dependent, however, only for the enthalpy of fusion of 100% crystalline reference not for the enthalpy change of the actual sample. When calculating X_c, the value of the enthalpy of fusion of the actual sample was taken at the temperature of the transition peak for crystallisation and melting. Inevitably the crystallinity was treated as constant in order to establish the baseline from equation 5.3.

Some times ago, Gray[107] proposed a correct procedure to measure the degree of crystallinity by the DSC, later this procedure was called the total enthalpy method[108]. In this procedure a two-phase model was adopted along with the following assumptions:

(1) a semicrystalline polymer consists of only distinct crystalline and amorphous regions

(2) the polymer is free from stress, i.e. that stored energy influences due to orientation are absent

(3) the amorphous regions are "liquid-like"

If $X_c(T)$ is the weight degree of crystallinity at any temperature T, the enthalpy of the semicrystalline polymer is

$$H(T) = X_c(T)H_c(T) + (1 - X_c(T))H_a(T) \tag{5.4}$$

where H(T), $H_c(T)$ and $H_a(T)$ are the enthalpies of the semicrystalline polymer, 100% crystalline and amorphous at temperature T, respectively. This can be rearranged to

$$X_c(T) = \frac{H_a(T) - H(T)}{H_a(T) - H_c(T)} \tag{5.5}$$

As

$$\Delta H_f(T) = H_a(T) - H(T) \tag{5.6}$$

$$\Delta H_f^{\circ}(T) = H_a(T) - H_c(T) \tag{5.7}$$

where $\Delta H_f(T)$ and $\Delta H_f^{\circ}(T)$ are the enthalpies of fusion of the semicrystalline and 100% crystalline polymers at temperature T, respectively.

Since the enthalpy is a state function, enthalpy difference on the right hand side in the equation 5.6 can be changed to:

$$\begin{aligned} H_a(T) - H(T) &= H_a(T) - H(T) + H(T_r) - H(T_r) \\ &= [H(T_r) - H(T)] - [H(T_r) - H_a(T)] \end{aligned} \tag{5.8}$$

If T_r is taken as a temperature above melting point, T_m, then at T_r the sample is completely in the amorphous liquid state, therefore

$$H(T_r) = H_a(T_r) \tag{5.9}$$

On inserting equation 5.9 into 5.8

$$H_a(T) - H(T) = [H(T_r) - H(T)] - [H_a(T_r) - H_a(T)] \tag{5.10}$$

As can be seen from Fig 5.2, $[H(T_r) - H(T)]$ is the enthalpy change in the semicrystalline sample on heating from T to T_r, and $[H_a(T_r) - H_a(T)]$ is the enthalpy change of the amorphous liquid on heating over the same temperature range. These enthalpy changes are black and red shadowed areas respectively in Fig. 5.2. Therefore the enthalpy of fusion, $\Delta H_f(T)$, can be readily obtained without drawing a baseline, and $\Delta H_f^o(T)$ can be obtained from equation 5.23. But this method has appeared to be ignored by most polymer scientists for some considerable time. More recently, Blundell *et al.*[108] and Mathot *et al.*[109,110] recommended this procedure once more and they found that the crystallinity measured by this procedure was in good agreement with those estimated by other techniques.

Recently Hay *et al.*[104,105] independently proposed a similar method - a "First Law method", this evaluated the residual enthalpy of the sample at the lower temperature, T_1, which may be room temperature or just above the glass transition temperature. This measured crystallinity of the sample at T_1 closely reflected that at room temperature since the crystallinity will not change on heating to the glass transition.

5.2.2 DSC Analysis

5.2.2.1 Conventional Method

DSC normally measures the heat evolution to the sample against time, i.e.,

$$dH/dt = (dH/dT)(dT/dt) = C_p\beta \qquad (5.11)$$

where *dH/dt* is usually called heat flow, $C_p = dH/dT$ the "pseudo" heat capacity[102] and $\beta = dT/dt$ the heating/cooling rate. The term C_p includes the real heat capacity as well as the enthalpy change due to change of the crystallinity, i.e. the crystallisation or melting occurs during the heating process. This is because:

$$C_p = dH/dT = d[H_c X_c + H_a(1 - X_c)]/dT$$

$$= C_{p,c} X_c + C_{p,a}(1 - X_c) - \Delta H_f^o \frac{dX_c}{dT} \qquad (5.12)$$

where H_c and H_a are the enthalpies of completely crystalline and amorphous materials at temperature T, respectively. $C_{p,c} = dH_c/dT$ and $C_{p,a} = dH_a/dT$ are the heat capacity of completely crystalline and amorphous materials at temperature T. $\Delta H_f^o = H_a - H_c$ is the enthalpy of fusion of 100% crystalline material at temperature T. dX_c/dT is the crystallinity change with the temperature. Once again it was noted that all these parameters are temperature dependent. On inserting the equation 5.3 to 5.12 leads to

$$-dX_c = \frac{C_p - C_{p,b}}{\Delta H_f^o} dT \qquad (5.13)$$

As we know, at temperature T_1 where no crystallisation and/or melting occur the initial crystallinity is $X_c(T_1)$ and at T_2 where the semicrystalline material is completely melted the final crystallinity is 0. On integrating the above equation from T_1 to T_2 gives

$$X_c(T_1) = \int_{T_1}^{T_2} \frac{C_p - C_{p,b}}{\Delta H_f^o} dT \qquad (5.14)$$

This equation clearly indicates that if the conventional method – "baseline procedure" is used to measure the crystallinity, it must be calculated by each step point because the crystals actually melt at each different temperature. Normally, the polymer crystals melt

over a large temperature range during thermal analysis. This means that enthalpy of fusion can not be measured by simply drawing the arbitrary "tangential" baseline or even using the baseline defined by the equation 5.3, and then measuring the area enclosed by the DSC curve and baseline since there is no simple additivity in the enthalpy of fusion at different temperatures. The enthalpy dependence for any kind of physical transition is given by Kirchhoff's law[111]:

$$\Delta H_{f/c}(T_2) = \Delta H_{f/c}(T_1) + \int_{T_1}^{T_2} \Delta C_p(T) dT \tag{5.15}$$

where $\Delta H_{f/c}(T_2)$ and $\Delta H_{f/c}(T_1)$ are the changes of the enthalpy at temperature T_2 and T_1 due to fusion or crystallisation, and $\Delta C_p(T)$ is the difference of heat capacity as function of temperature.

Only when the sample was crystallised at very high temperature or annealed for very long time such that the melting finishes in a narrow temperature range could the enthalpy be approximately considered as temperature independent and ΔH_f^o can be put outside of the integration which changes the above equation into

$$X_c(T_1) = \frac{1}{\Delta H_f^o} \int_{T_1}^{T_2} (C_p - C_{p,b}) dT = \frac{\Delta H_f}{\Delta H_f^o} \tag{5.16}$$

where $\Delta H_f = \int_{T_1}^{T_2} (C_p - C_{p,b}) dT$ is the heat of fusion occurring from T_1 to T_2. It is only in such situations that the enthalpy of fusion for semicrystalline polymer can be directly measured from the area enclosed between the DSC curve and true baseline just as measuring the heat of fusion of low molecular weight materials. Although the equation 5.16 has a similar form to 5.1 the meanings of them are essentially different. It is also

worthwhile to point out that in the baseline procedure, by measuring the heat of fusion the crystallinity actually reflects the initial value prior to melting not at the melting point. However, Qiu *et al.*[112] concluded recently that the degree of crystallinity measured by DSC equals to the initial crystallinity plus an increasing value due to heat capacity change, i.e.

$$X_c^{dsc} = X_c^o + \Delta X_c \tag{5.17}$$

This is simply due to the temperature dependence of the enthalpy of fusion not being considered and a baseline incorrectly constructed.

This derivation obviously proved how and why the conventional method is wrong, and furthermore as $C_{p,b}$ as a function of temperature in the equations 5.14 and 5.16 is unknown as mentioned earlier, this method cannot be used to measure the degree of crystallinity. Therefore, another method is needed to measure the crystallinity correctly.

5.2.2.2 The First Law Method

The First Law method is an application of the First Law of Thermodynamics to recrystallisation and melting of a polymer sample on heating in a calorimeter, and involves 2 separate measurements. The first is that of determining the overall enthalpy changes in heating a partially crystalline polymer from T_1 to above its melt, T_2, i.e. a typical DSC trace. The second is a virtual experiment of measuring the enthalpy change on cooling from T_2 to T_1 without crystallisation occurring. For a closed system, the

difference between these two steps is the enthalpy of fusion the sample at T_1. The enthalpy changes for the whole process can be expressed as follows:

$$\Delta H_R = \Delta H_{12} + \Delta H_{21} \tag{5.18}$$

in which

$$\Delta H_{12} = \int_{T_1}^{T_2} C_p dT \tag{5.19}$$

and

$$\Delta H_{21} = \int_{T_2}^{T_1} C_{p,a} dT \tag{5.20}$$

where ΔH_R is the residual enthalpy of fusion at T_1, ΔH_{12} and ΔH_{21} are the changes in enthalpy due to heating and cooling process, respectively. ΔH_{12} includes all the enthalpy change due to the heat capacity and these due to crystallisation and recrystallisation, ΔH_c, as well as melting, and remelting ΔH_f. Therefore, for an initially amorphous sample ΔH_R should be zero. The DSC trace for a partially crystalline sample and the diagram of the enthalpy change of these processes are shown in Fig.s 5.3 and 5.4 respectively.

The amorphous liquid temperature dependence, $C_{p,a}$, can be obtained by several methods, i.e. by a linear extrapolation of the specific heat of the liquid measured in the melt; or measured on an amorphous sample above the glass transition temperature prior to the onset of crystallisation or by using reference data. In the first two cases heat flow measurements in the calorimeter can be used directly instead of the measured specific heat.

The weight fraction degree of crystallinity at T_1, $X_c(T_1)$, is then the ratio of the observed enthalpy of fusion of the sample to that of the completely crystalline material at T_1,

$$X_c(T_1) = \Delta H_f(T_1)/\Delta H^o_f(T_1) = \Delta H_R/\Delta H^o_f(T_1) \tag{5.21}$$

Normally, the ΔH_f^o is measured at equilibrium melting point T_m^o not at T_1, however,

$$d(\Delta H_f^o) = (C_{p,a} - C_{p,c})dT = \Delta C_{p,c}dT \tag{5.22}$$

where $\Delta C_{p,c}$ is the heat capacity difference between the completely liquid and crystalline solid. The enthalpy of fusion of 100% crystalline material at T_1 could be obtained by integrating the above equation from T_1 to T_m^o, i.e.

$$\Delta H_f^o(T_1) = \Delta H_f^o(T_m^o) - \int_{T_1}^{T_m^o} \Delta C_{p,c}dT \tag{5.23}$$

The enthalpy of fusion of 100% crystalline PET was calculated by using this equation and shown in Fig. 5.5. It is clear that ΔH^o_f is temperature dependent. Combining the equations 5.18 to 5.23 leads to

$$X_c(T_1) = \frac{\int_{T_1}^{T_2}(C_p - C_{p,a})dT}{\Delta H_f^o(T_m^o) - \int_{T_1}^{T_m^o}\Delta C_{p,c}dT} \tag{5.24}$$

By using this equation, the degree of crystallinity at T_1 could be readily obtained. For any other temperature T′ it could be conducted by simply changing lower integration limit T_1 to T′ no matter what state the sample is. In the First Law method the crystallinity is considered of each individual temperature point, therefore, the baseline is avoided.

5.2.3 Density and Wide-Angle X-ray Diffraction

The degree of crystallinity can be measured by density if a two-phase model for crystalline polymers are used. Both volume and weight fraction crystallinity can be obtained by this method. The volume of a semicrystalline polymer at any given temperature is

$$V = V_c + V_a \tag{5.25}$$

where V_c and V_a are the volume of the crystalline and amorphous regions, respectively. Therefore the volume fraction crystallinity, $X_{c,v}$, is

$$X_{c,v} = V_c/(V_c + V_a) \tag{5.26}$$

Similarly the total weight of a semicrystalline polymer, w, is given

$$w = w_c + w_a \tag{5.27}$$

Where w_c and w_a are the mass of crystalline and amorphous regions, respectively. The weight fraction crystallinity is

$$X_c = w_c/(w_c + w_a) \tag{5.28}$$

As density, ρ, equals

$$\rho = w/V \tag{5.29}$$

Therefore,

$$X_{c,v} = \frac{V_c}{V_c + V_a} = \frac{\rho - \rho_a}{\rho_c - \rho_a} \tag{5.30}$$

and

$$X_c = \frac{w_c}{w_c + w_a} = \frac{(\rho - \rho_a)\rho_c}{(\rho_c - \rho_a)\rho} = X_{c,v}\frac{\rho_c}{\rho} \tag{5.31}$$

where ρ_c and ρ_a are the densities of crystalline and amorphous regions, respectively.

WAXD measures the volume fraction crystallinity and involves subtracting the amorphous scattering from the intensity of semicrystalline sample to leave the crystalline lines as outlined in Chapter 2. By using the equation 5.31, the volume fraction crystallinity can be converted into the weight fraction crystallinity.

5.3 Results and Discussion

5.3.1 The Fractional Crystallinity of m-PE

Fig. 5.6 shows the DSC traces for water and slow-cooled m-PE samples. m-PE has good thermal stability above T_m and the temperature dependence of the amorphous heat capacity can be well defined. This is shown from the heat capacity – temperature plot measured above the melting point and extrapolated to ambient temperature. At room temperature the heat capacity of the partially crystalline sample was lower than that of the liquid but with increasing temperature and with the onset of melting it became greater than the liquid.

The enthalpy of fusion at 298 K was determined using the First Law method as 116 and 132 J g^{-1} for the water and slow-cooled sample respectively. The enthalpy of fusion of completely crystalline PE at 298 K was computed[113] to be 243.8 J g^{-1}, which is approximately 17% less than the more commonly used value of 293 J g^{-1} at the equilibrium melting point. The fractional crystallinities of the fast and slow cooled sample were 0.48 ± 0.02 and 0.54 ± 0.02, respectively. These values compared well

with the weight fraction crystallinity measured at 296 K by density are listed in Table 5.1.

Using the temperature dependent enthalpies of fusion, the change in the fractional crystallinity of the sample with the temperature was evaluated, as can be seen in Fig. 5.7 for slow cooled m-PE. It is clear that the fractional crystallinity is constant up to about 300 K and thereafter drops progressively to zero. This indicated that m-PE melting starts earlier in the heating process. Mathot *et al.*[110] found that melting occurred as low as –60°C for very low-density polyethylene. In this situation, the degree of crystallinity was measured at room temperature otherwise its value could not be compared with that measured by the density method.

5.3.2 The Fractional Crystallinity of PET

PET, amorphous by WAXD and density measurements, was observed by DSC to have a glass transition at about 353 K, see Fig. 5.8a and a large crystallisation exotherm at about 410 K. Melting finally occurred above 500 K, although a modulated temperature DSC study showed that melting and recrystallisation occur prior to the final melting endotherm[118]. Two temperature regions exist in which the liquid state is present alone – one post-T_g and prior to the onset of crystallisation and the other above T_m. Careful measurement of the heat capacities in these temperature regions indicated that they exhibited different temperature dependences and that PET was degrading above T_m. As a result, the post-Tg amorphous heat capacity - temperature dependence was chosen as the liquid heat capacity - temperature dependence to define on cooling process. The

areas of the exotherm and endotherm enthalpies around this liquid heat capacity – temperature plot between T_1 and T_2 were determined and the residual enthalpy of fusion determined at T_1. For an amorphous sample the residual enthalpy of fusion should be zero. This determination was repeated 10 times on the quenched amorphous sample. The average value of fractional crystallinity was 0.004 with a variation of ± 0.02 as shown in Table 5.2. This was considered to be excellent reproducibility and consistent with WAXD and density results.

PET samples crystallised in a vacuum oven at 383K for different period times and to different extents of crystallinity were similarly analysed. Their heat capacities against temperature are shown in Fig. 5.8b. They exhibited a less well-defined glass transition and smaller recrystallisation exotherm than previously observed with the amorphous samples. It was not possible in these samples to define the amorphous heat capacity - temperature dependence either from the post-T_m dependence for reasons discussed above or from the post Tg dependence since the material was partially crystalline. The amorphous heat capacity - temperature dependence of the sample determined separately on a quenched sample was used instead and the fractional crystallinity determined from the residual enthalpy of fusion at 375 K.

PET was also crystallised in a vacuum oven at different temperatures from 398 to 473 K for 18 hrs and their heat capacities are shown as a function of temperature in Fig. 5.8c. Multiple melting points were observed with the lowest about 20 K above the crystallisation temperature. The temperature corresponding to the last trace of crystallinity was almost constant and independent of crystallisation temperature. This

has been attributed to the melting of crystallites produced on heating[119-121]. The same amorphous heat capacity - temperature dependence as determined above was used and the degree of crystallinity was obtained as outlined above. These results are listed in Table 5.1 and compared with the weight fraction crystallinity as measured by density and WAXD. There is good agreement within experimental error between them.

The changing crystallinity of the various PET samples during DSC scans can be seen in Fig. 5.9. For amorphous PET it is zero up to above the glass transition but increases rapidly from 420 to 450 K. Poorly crystalline materials further crystallise at higher temperature, the crystallinity increasing rapidly on heating from 400 to 450 K and is followed by some initial melting up to about 490 K, and finally, melting is complete at about 530 K. For PET crystallized at higher temperatures, e.g. 448 K, the crystallinity was almost constant up to 450K, after which the crystallites melt and the crystallinity decreases to zero. Fig. 5.9 also shows that the maximum degree of crystallinity achieved relates closely to the thermal history of the sample.

From the above, it is apparent that during heating to determine the degree of crystallinity of a polymer, crystallisation, melting, recrystallisation and melting reorganisation can occur. The degree of crystallinity is not constant and is temperature and time dependent. The degrees of crystallinity measured by most other analytical methods, such as WAXD and density, are carried out at ambient temperature. Therefore, in comparing the degree of crystallinity measured by DSC it should be carried out under the same conditions. By using the First Law method it is possible to measure the crystallinity at room temperature although the sample doesn't melt at room temperature. In m-PE melting

starts close to room temperature and in PET crystallisation occurs at 50 K above glass transition temperature. Although PET crystallinity was measured at 375 K the value of crystallinity actually did not change below this temperature under normal DSC heating rate.

5.3.3 The Fractional Crystallinity of PET/PC Blends

PET and its blends were isothermally crystallised at different temperature for 8 - 10 times $t_{max,}$, the time to reach the maximum in the isothermal crystallisation curve. After that the samples were directly heated up to the melting point. The DSC traces of heating PET/PC 50/50 blends prepared without and with catalyst are shown in Fig.s 5.10 and 11, respectively. Except for samples crystallised at 498 K PET/PC blends showed multiple melting peaks which were similar to those observed with PET. The fractional crystallinities were calculated according to the First Law method and the results are listed in Table 5.3.

It is clear from Table 5.3 that all the samples showed nearly the same crystallinities 0.24 - 0.27 except for the 50/50 and 70/30 PET/PC blends prepared with added catalyst crystallised at 498 K which probably underwent further transesterification during the crystallisation process at this temperature. The transesterification reaction will be investigated further in a later chapter. Reinsch and Rebenfeld[122] also found that the degree of crystallinity was independent on the crystallisation temperature and the blend compositions except for those with PC content above 80%.

5.3.4 Crystallinity Effect on Tensile Properties of the Blends

The tensile properties of the PET/PC blends crystallised at 112°C for different time are presented in Tables 5.4 to 5.9. They showed compositional difference. Generally, for PET and its blends, the modulus, yield stress and extension at yield increased with increasing crystallisation time, while the elongation at break decreased. The degrees of crystallinity of these samples were measured by the density method. The results are shown in Table 5.10. It can be seen that the degree of crystallinity increased with crystallisation time especially within the primary crystallisation stage.

The effect of the dependence of crystallinity on tensile properties were illustrated in Fig 5.12. It was apparent that both PET and its blends showed the same trend, with increasing crystallinity the Young's modulus, yield stress and extension at yield increased while elongation at break dramatically decreased. This is due to the crystalline regions acting as cross-links in the polymer matrix which limits deformation of the amorphous regions.

5.4 Conclusions

The measurement of the degree of crystallinity in polymers by DSC has been reviewed. Since crystallisation, melting, recrystallisation and remelting occur during the heating of the sample to the melting point and as a result the degree of crystallinity changes. This makes it impossible to draw a baseline to separate exotherms and endotherms. Accordingly, the conventional method of comparing exothermic and endothermic enthalpies cannot be used to measure the degree of crystallinity. Instead a First Law method was used since it avoided drawing a baseline and the crystallinity of the samples could be measured at room temperature or just above glass transition temperature as well although the polymer did not melt at this temperature. Thus, the crystallinity measured by DSC becomes comparable with that measured by other techniques. Examples are taken from PET and m-PE to demonstrate this.

Although the PET crystallisation rate was depressed by the presence of PC in the PET/PC blends, the degree of crystallinity was found to be independent of composition and crystallisation temperature. The presence of crystalline regions makes the polymer brittle, i.e. the modulus, yield stress and extension at yield all increased with increasing crystallinity while the elongation at break decreased with increasing crystallinity. All are consistent with crystallinity making polymers and blends brittle.

Table 5.1 Density, residual enthalpy and fractional crystallinity measurement

Sample	Density	Residual enthalpy	Weight fraction crystallinity		
			Density	DSC	WAXD
	$g\ cm^{-3}$	$J\ g^{-1}$	±0.02	± 0.02	± 0.02
Water-cooled m-PE	0.923	116	0.51	0.48	-
Slow-cooled m-PE	0.931	132	0.57	0.54	-
PET					
amorphous	1.336	0.4	0.01	0.00	0
110 °C*1h	1.350	9.6	0.09	0.10	0.11
110 °C*2h	1.356	15.5	0.13	0.16	0.17
110 °C*5h	1.365	19.6	0.19	0.20	0.19
125 °C*18h	1.375	25.0	0.25	0.26	0.27
150 °C*18h	1.379	26.4	0.27	0.28	0.28
175 °C*18h	1.382	30.0	0.29	0.31	0.30
200 °C*18h	1.392	34.4	0.35	0.36	0.37

* Crystallinity calculated by density for m-PE, $\rho_a = 0.855\ g\ cm^{-3}$, $\rho_c = 0.999\ g\ cm^{-3}$; ref.113.

Crystallinity calculated by density for PET, $\rho_a = 1.335\ g\ cm^{-3}$, $\rho_c = 1.515\ g\ cm^{-3}$; ref.114.

Heat of fusion of PE at 298 K: $\Delta H_f^{\circ}(298) = 243.8\ J\ g^{-1}$; ref. 113.

Heat of fusion of PET at 375 K: $\Delta H_f^{\circ}(375) = 96.0\ J\ g^{-1}$; ref. 115-117.

Table 5.2 Residual enthalpy and weight fraction crystallinity of amorphous PET

Sample	Residual enthalpy $J\ g^{-1}$	Fraction crystallinity
1	-1.7	-0.018
2	-0.91	-0.009
3	2.3	0.024
4	1.9	0.019
5	-1.9	-0.020
6	2.8	0.029
7	3.7	0.038
8	-1.2	-0.012
9	-0.03	-0.000
10	-0.5	-0.005
Average		0.004 ± 0.020

Table 5.3 Enthalpies of fusion and weight fraction crystallinities of PET and its blends measured by DSC at different temperature

Sample		Enthalpy $J\ g^{-1}$	Crystallinity ± 0.02
PET	423 K	31.0	0.27
	448 K	30.6	0.26
	473 K	31.8	0.25
	498 K	34.6	0.26
PET/PC	423 K	14.0	0.25
50/50	448 K	14.8	0.25
without	473 K	15.5	0.25
catalyst	498 K	16.3	0.25
PET/PC	423 K	21.4	0.27
70/30	448 K	23.0	0.27
without	473 K	23.7	0.27
catalyst	498 K	23.7	0.26
PET/PC	423 K	26.9	0.26
90/10	448 K	27.7	0.26
without	473 K	28.4	0.25
catalyst	498 K	32.1	0.27
PET/PC	423 K	14.5	0.26
50/50	448 K	14.2	0.24
with	473 K	16.8	0.27
catalyst	498 K	13.3	0.20
PET/PC	423 K	21.2	0.27
70/30	448 K	21.4	0.26
with	473 K	22.8	0.26
catalyst	498 K	21.1	0.23
PET/PC	423 K	25.6	0.25
90/10	448 K	25.9	0.24
with	473 K	27.6	0.24
catalyst	498 K	31.5	0.27

*Enthalpies of fusion 100% crystalline PET are112.6 $J\ g^{-1}$ for 423 K, 119.75 $J\ g^{-1}$ for 448 K, 125.9 $J\ g^{-1}$ for 473 K and 131.2 $J\ g^{-1}$ for 498 K

Table 5.4 Tensile properties of physical ageing PC at 385 K for different time

Time h	Young's modulus GPa	Yield stress MPa	Extension at yield %	Breaking strength MPa	Elongation at break %
0	1.20 ± 0.01	53.5 ± 0.7	7.84 ± 0.23	53.7 ± 1.1	105 ± 6.1
0.25	1.16 ± 0.03	58.9 ± 0.6	7.89 ± 0.39	48.4 ± 2.5	46 ± 35
0.5	1.14 ± 0.04	61.2 ± 1.1	7.66 ± 0.38	55.1 ± 5.0	91 ± 30
1	1.12 ± 0.02	61.6 ± 1.0	7.76 ± 0.43	48.5 ± 1.2	29 ± 10
2	1.21 ± 0.01	63.4 ± 0.4	7.77 ± 0.23	49.1 ± 1.2	43 ± 28
5	1.20 ± 0.02	64.1 ± 1.1	7.49 ± 0.32	49.3 ± 1.7	36 ± 19
12	1.20 ± 0.03	65.4 ± 0.5	7.60 ± 0.27	49.1 ± 3.2	20 ± 17

Values given are the means of at least 5 samples and error limits are standard deviation.

Table 5.5 Tensile properties of PET/PC (50/50) blends prepared without added catalyst crystallised at 385 K for different time

Time h	Young's modulus GPa	Yield stress MPa	Extension at yield %	Breaking strength MPa	Elongation at break %
0	1.23 ± 0.02	53.0 ± 0.8	6.16 ± 0.17	42.9 ± 1.8	135 ± 32
0.25	1.21 ± 0.02	53.6 ± 0.8	6.32 ± 0.07	39.0 ± 0.8	24 ± 9.4
0.5	1.22 ± 0.02	56.8 ± 0.6	6.77 ± 0.17	44.2 ± 1.3	49 ± 22
1	1.29 ± 0.01	61.7 ± 1.8	7.15 ± 0.43	45.6 ± 1.3	16 ± 3.2
2	1.35 ± 0.03	64.1 ± 0.8	7.26 ± 0.20	47.1 ± 0.7	13 ± 5.2
5	1.31 ± 0.02	65.3 ± 2.0	7.03 ± 0.61	61.1 ± 7.4	8.0 ± 2.2
12	1.32 ± 0.02	64.2 ± 2.3	6.53 ± 0.88	64.2 ± 2.3	6.5 ± 0.9

Values given are the means of at least 5 samples and error limits are standard deviation.

Table 5.6 Tensile properties of PET/PC (70/30) blends prepared without added catalyst crystallised at 385 K for different time

Time h	Young's modulus GPa	Yield stress MPa	Extension at yield %	Breaking strength MPa	Elongation at break %
0	1.21 ± 0.02	51.7 ± 0.4	5.81 ± 0.08	44.3 ± 2.2	270 ± 30
0.25	1.22 ± 0.01	50.6 ± 0.4	5.60 ± 0.09	35.6 ± 0.7	120 ± 47
0.5	1.23 ± 0.02	57.0 ± 0.3	6.11 ± 0.17	44.8 ± 2.3	52 ± 29
1	1.36 ± 0.02	64.0 ± 1.7	6.97 ± 0.62	45.8 ± 1.9	33 ± 4.3
2	1.41 ± 0.03	65.1 ± 0.3	7.40 ± 0.14	56.6 ± 9.8	15 ± 9.1
5	1.35 ± 0.01	66.1 ± 1.3	7.17 ± 0.7	65.7 ± 1.4	7.5 ± 1.1
12	1.39 ± 0.01	64.3 ± 3.5	6.59 ± 1.2	56.8 ± 8.4	9.4 ± 4.8

Values given are the means of at least 5 samples and error limits are standard deviation.

Table 5.7 Tensile properties of PET/PC (80/20) blends prepared without added catalyst crystallised at 385 K for different time

Time h	Young's modulus GPa	Yield stress MPa	Extension at yield %	Breaking strength MPa	Elongation at break %
0	1.20 ± 0.02	51.6 ± 0.4	5.63 ± 0.11	48.6 ± 6.4	359 ± 68
0.25	1.22 ± 0.02	49.8 ± 0.8	5.52 ± 0.12	34.9 ± 2.5	168 ± 75
0.5	1.25 ± 0.05	54.0 ± 1.2	6.08 ± 0.22	40.1 ± 1.4	92 ± 5.5
1	1.41 ± 0.04	65.2 ± 0.6	7.33 ± 0.18	46.7 ± 1.4	51 ±. 36
2	1.44 ± 0.02	64.8 ± 0.7	7.25 ± 0.12	49.1 ± 8.9	22 ± 13
5	1.38 ± 0.03	67.6 ± 0.7	7.68 ± 0.32	67.5 ± 0.6	7.8 ± 0.5
12	1.40 ± 0.01	66.1 ± 0.8	7.25 ± 0.52	58.3 ± 11	19 ± 18

Values given are the means of at least 5 samples and error limits are standard deviation.

Table 5.8 Tensile properties of PET/PC (90/10) blends prepared without added catalyst crystallised at 385 K for different time

Time h	Young's modulus GPa	Yield stress MPa	Extension at yield %	Breaking strength MPa	Elongation at break %
0	1.18 ± 0.03	50.5 ± 0.54	5.46 ± 0.19	50.0 ± 4.1	448 ± 43
0.25	1.21 ± 0.02	48.9 ± 0.72	5.47 ± 0.10	35.1 ± 2.2	209 ± 85
0.5	1.33 ± 0.05	60.0 ± 1.1	6.66 ± 0.25	45.0 ± 1.3	110 ± 24
1	1.43 ± 0.02	65.1 ± 0.53	7.10 ± 0.35	47.1 ± 1.0	88 ± 44
2	1.45 ± 0.03	64.9 ± 0.62	7.23 ± 0.34	46.2 ± 1.5	79 ± 52
5	1.39 ± 0.02	66.5 ± 0.80	7.71 ± 0.20	45.7 ± 0.8	17 ± 4.1
12	1.43 ± 0.03	65.9 ± 0.62	7.15 ± 0.26	45.6 ± 1.3	50 ± 25

Values given are the means of at least 5 samples and error limits are standard deviation.

Table 5.9 Tensile properties of PET crystallised at 385 K for different time

Time h	Young's modulus GPa	Yield stress MPa	Extension at yield %	Breaking strength MPa	Elongation at break %
0	1.23 ± 0.02	49.3 ± 1.0	4.97 ± 0.17	54.0 ± 6.8	529 ± 59
0.25	1.25 ± 0.04	48.3 ± 1.7	5.07 ± 0.31	44.4 ± 5.4	402 ± 68
0.5	1.30 ± 0.07	56.7 ± 1.8	6.13 ± 0.66	43.9 ± 2.9	197 ± 96
1	1.44 ± 0.05	59.3 ± 2.9	5.95 ± 0.54	43.0 ± 2.2	132 ± 51
2	1.45 ± 0.09	63.5 ± 2.0	6.71 ± 0.47	46.0 ± 3.2	119 ± 71
5	1.46 ± 0.05	66.6 ± 1.3	7.38 ± 0.36	44.9 ± 1.5	59 ± 49
12	1.42 ± 0.03	64.8 ± 0.7	7.28 ± 0.44	45.4 ± 1.0	119 ± 54

Values given are the means of at least 5 samples and error limits are standard deviation.

Table 5.10 Degree of crystallinity of PET and its blends prepared without added catalyst crystallised at 385 K for different time

Crystallisation time, min	Sample	Density g cm^{-3}	Volume crystallinity, %
15	PET50/PC50	1.258	1.0
	PET70/PC30	1.289	1.5
	PET80/PC20	1.305	1.6
	PET90/PC10	1.321	1.5
	PET	1.339	2.2
30	PET50/PC50	1.260	3.5
	PET70/PC30	1.292	4.1
	PET80/PC20	1.308	3.8
	PET90/PC10	1.326	4.6
	PET	1.346	6.1
60	PET50/PC50	1.265	9.8
	PET70/PC30	1.298	9.2
	PET80/PC20	1.317	10.4
	PET90/PC10	1.335	10.3
	PET	1.354	10.6
120	PET50/PC50	1.268	13.6
	PET70/PC30	1.302	12.9
	PET80/PC20	1.320	12.6
	PET90/PC10	1.338	12.2
	PET	1.359	13.3
300	PET50/PC50	1.270	16.2
	PET70/PC30	1.306	16.1
	PET80/PC20	1.325	16.3
	PET90/PC10	1.343	15.4
	PET	1.364	16.1
720	PET50/PC50	1.271	17.5
	PET70/PC30	1.308	17.9
	PET80/PC20	1.326	17.0
	PET90/PC10	1.346	17.3
	PET	1.367	17.8

Density values are the means of 3 samples, $\rho_{PC} = 1.188$ g cm^{-3} ,

ρ_{PET} of amorphous and crystalline PET are 1.335 and 1.515 g cm^{-3} respectively.

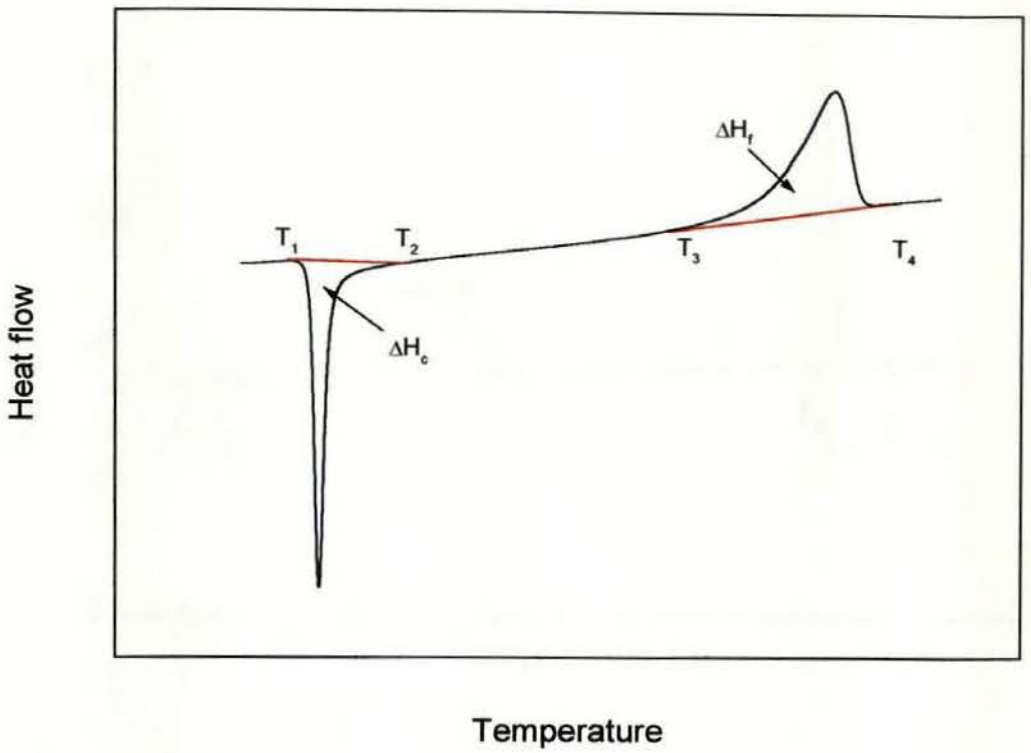

Fig. 5.1 Schematic representation of the enthalpy changes by misused method, red line is arbitrarily drawn baseline

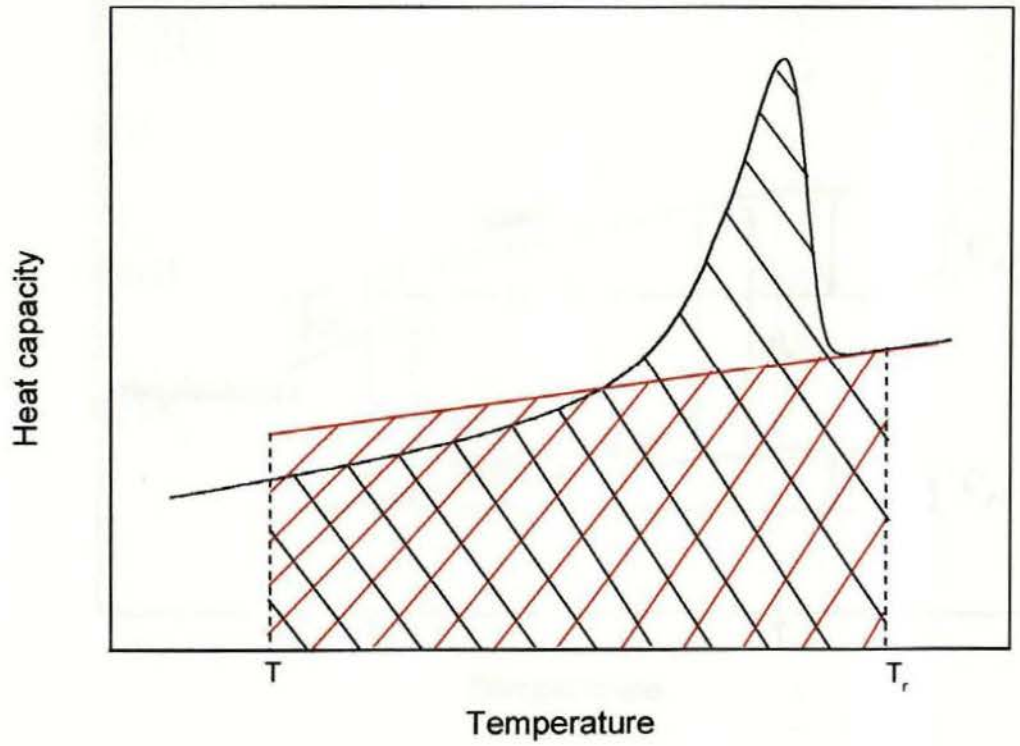

Fig. 5.2 Schematic representation of the enthalpy of fusion measured by Gray's method. Black shadow area is the enthalpy change heating for semicrystalline sample from T to T_r, i.e. $H(T_r) - H(T)$; red shadow area equals the enthalpy change for amorphous liquid heating from T to Tr, i.e. $H_a(Tr) - H_a(T)$

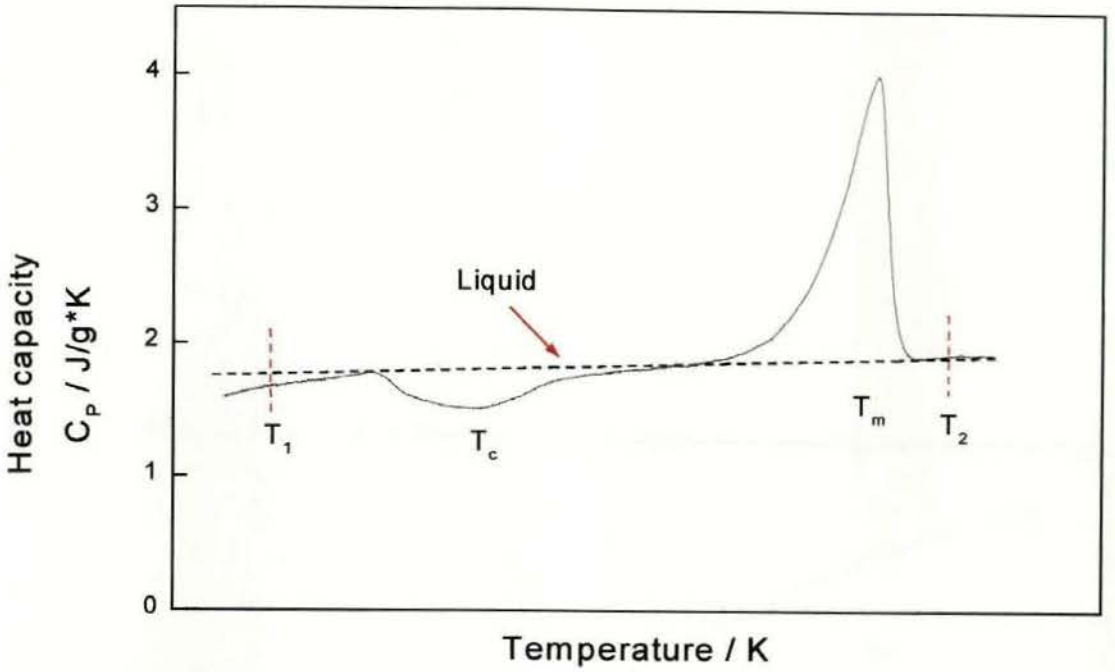

Fig.5.3. DSC trace of poor crystalline sample showing recrystallisation and melting

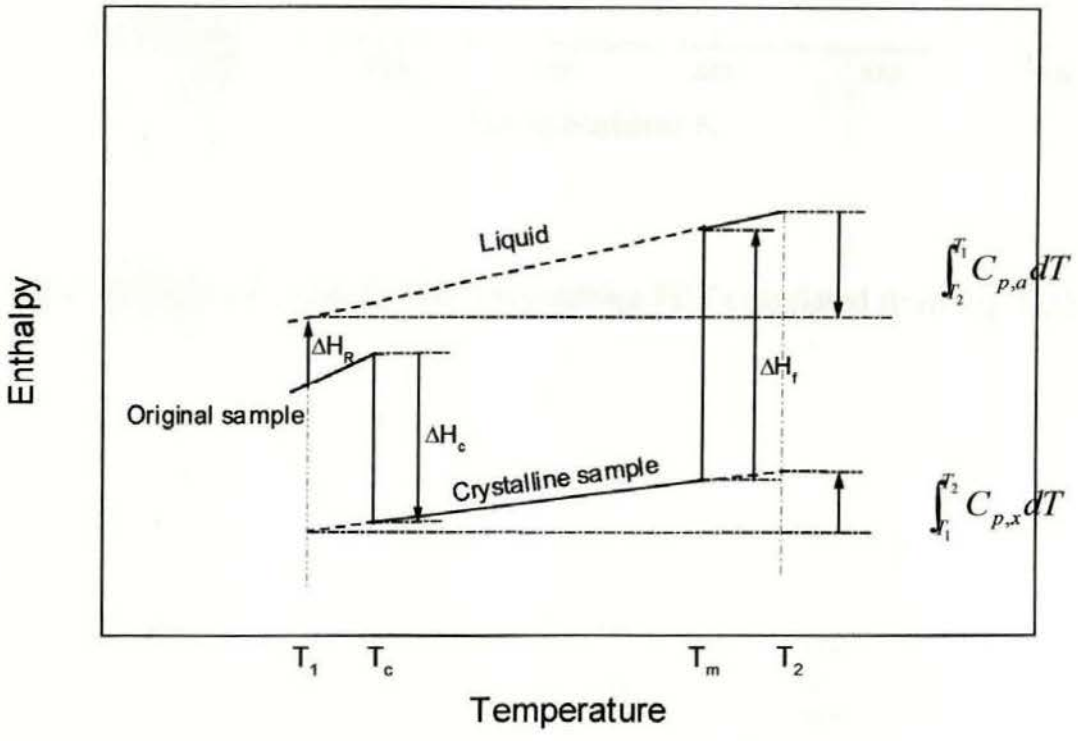

Fig. 5.4. Schematic changes in enthalpy on heating and cooling between T_1 and T_2. The scheme has been simplified by summing the enthalpies of crystallisation and melting at T_c and T_m respectively. Actually, the crystallisation, melting, recrystallisation and remelting may occur over a large temperature range, but this does not affect summary

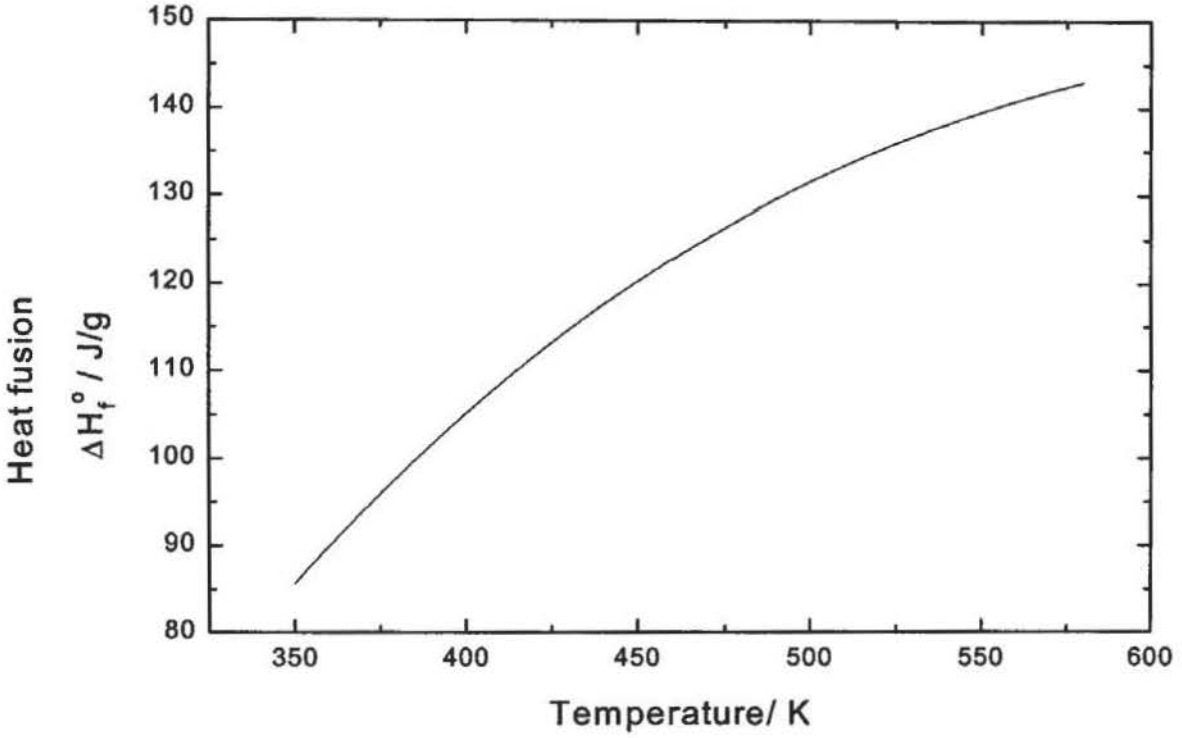

Fig. 5.5. The enthalpy of fusion of 100% crystalline PET calculated from Eq. 5.23.

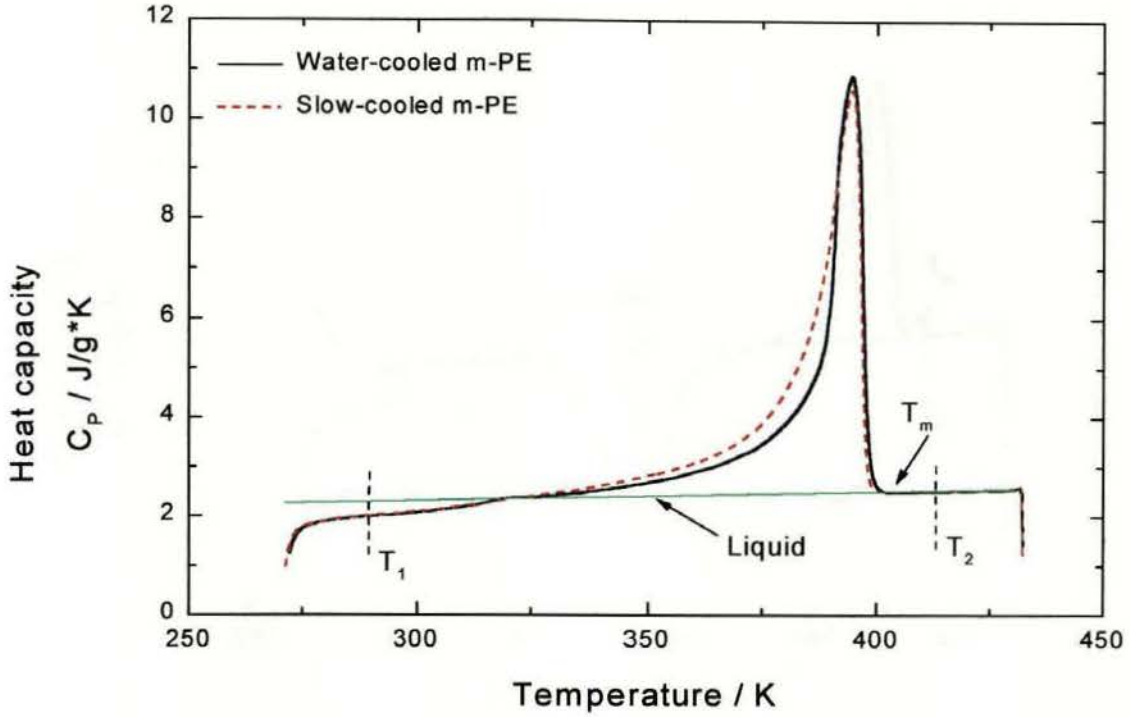

Fig.5.6 DSC traces of m-polyethylene and amorphous heat capacity temperature dependence extrapolated from the molten state

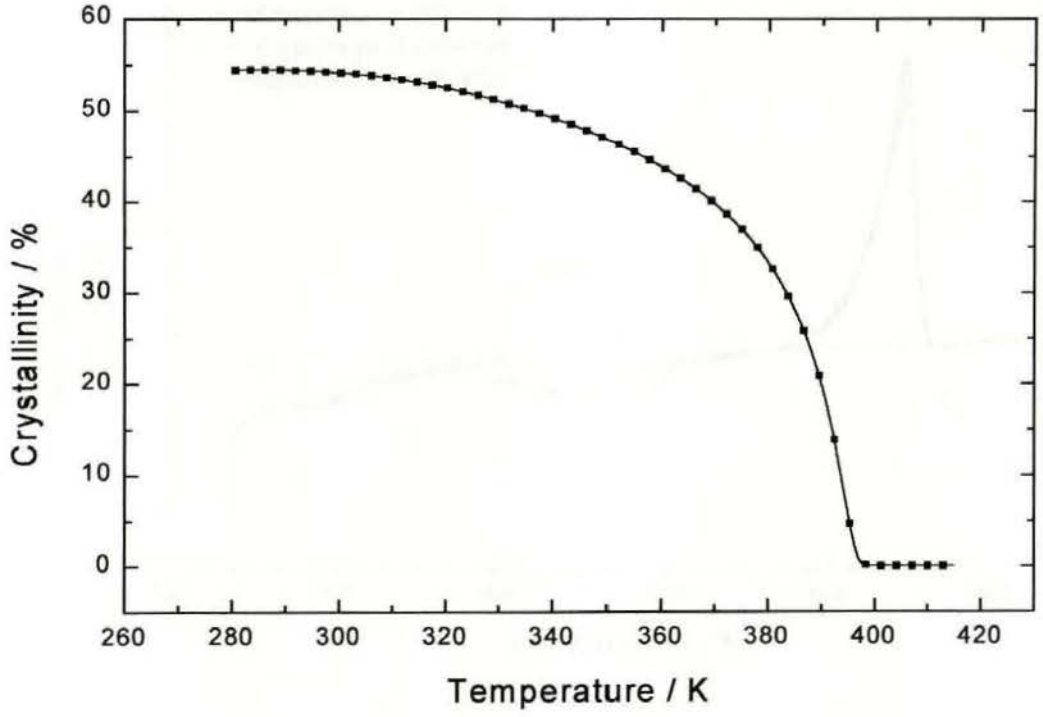

Fig. 5.7. The degree of crystallinity depends on temperature during heating for slow-cooled m-PE

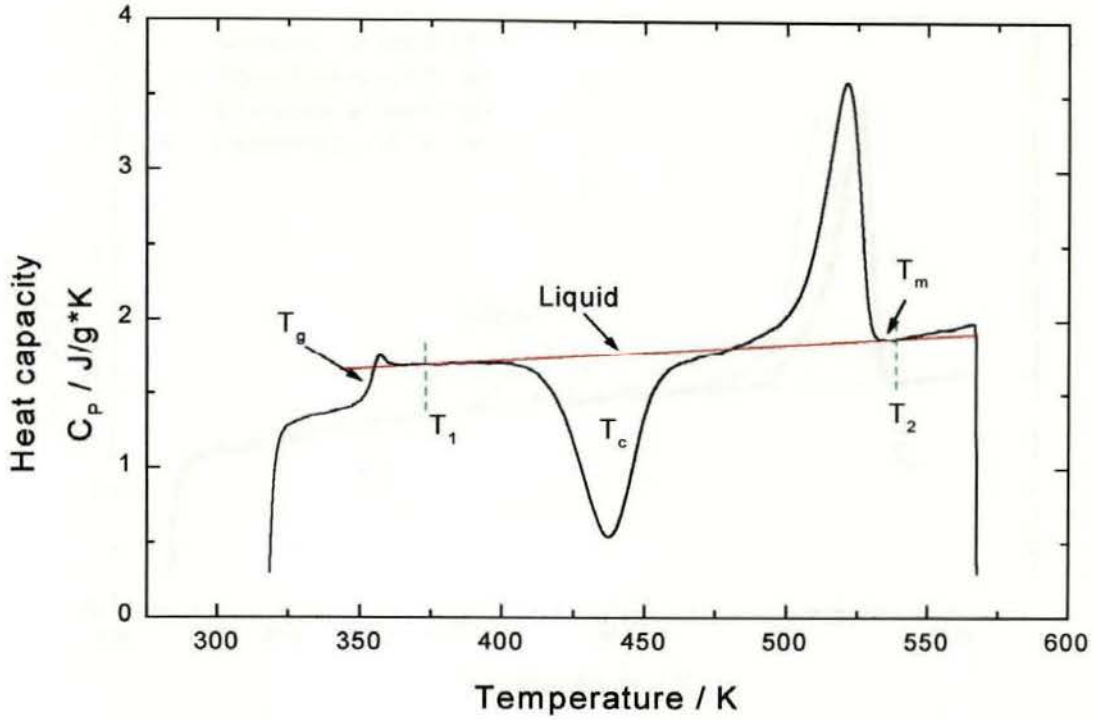

Fig. 5.8a. DSC traces of amorphous PET and amorphous heat capacity temperature dependence extrapolated from post-T_g

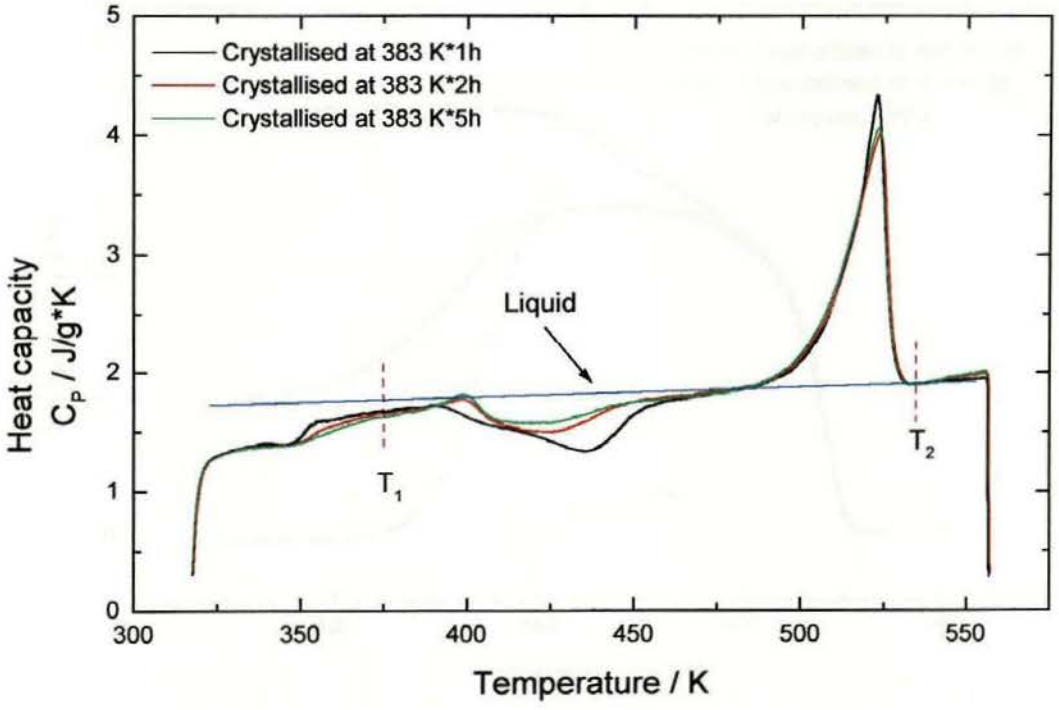

Fig. 5.8b. DSC traces of PET crystallised at 383 K for various periods and amorphous heat capacity temperature dependence obtained separately from quenched PET sample

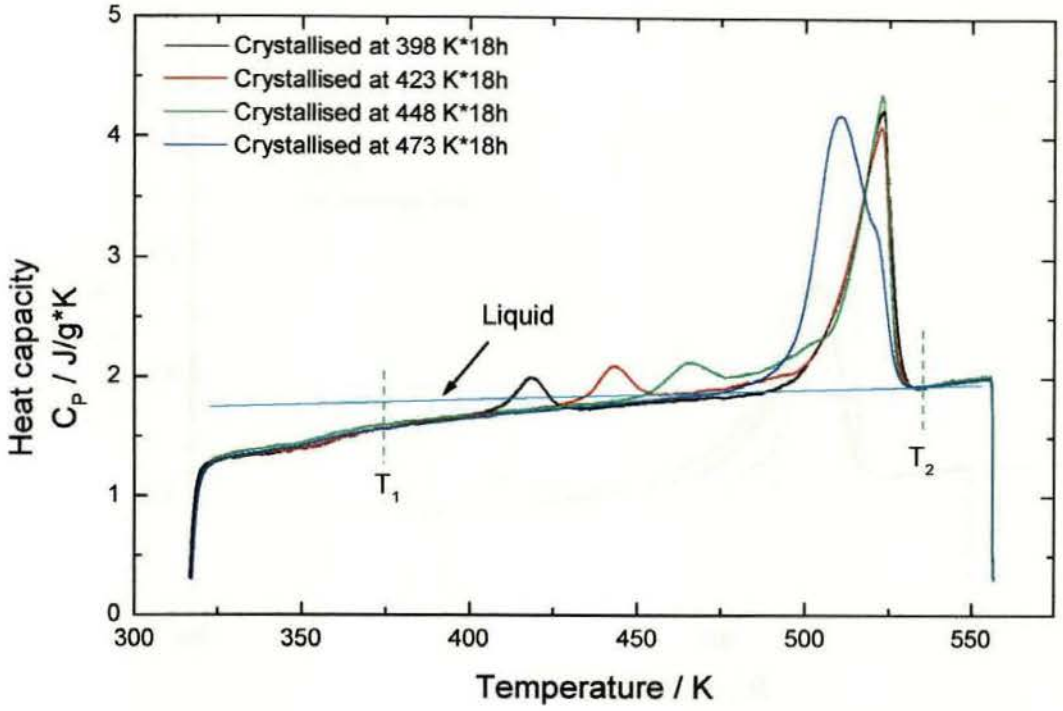

Fig.5.8c. DSC traces of PET crystallised for 18 hrs at different temperature and amorphous heat capacity temperature dependence obtained as Fig.5.8b

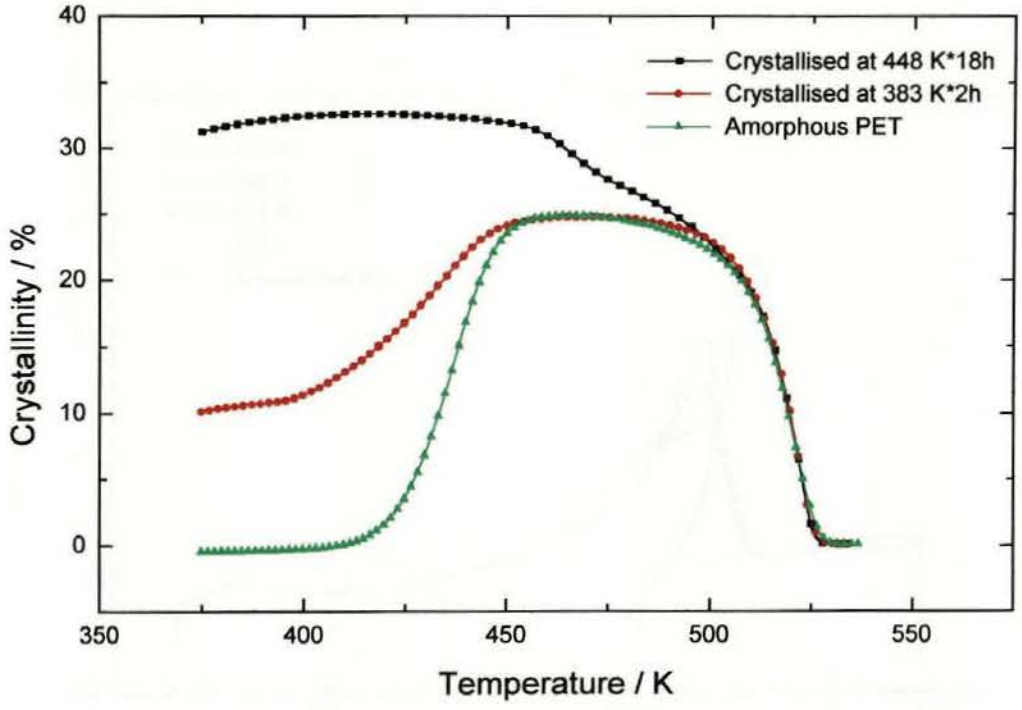

Fig. 5.9. The temperature dependence of the degree of crystallinity on heating. PET samples - amorphous and crystallised at 383 K for 2 hrs and 448 K for 18 hrs.

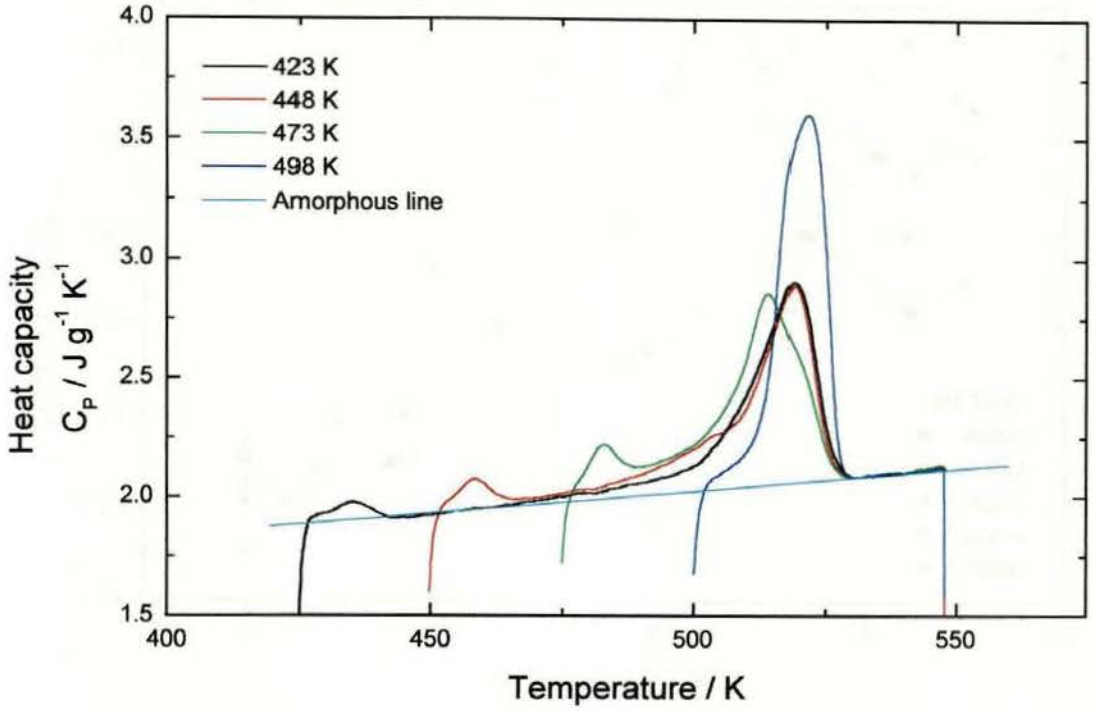

Fig. 5.10 DSC traces of PET/PC 50/50 blends prepared without added catalyst after crystallised at indicated temperature for 8-10 times t_{max} and heated at 10 K/min. Amorphous liquid line obtained separately from amorphous sample

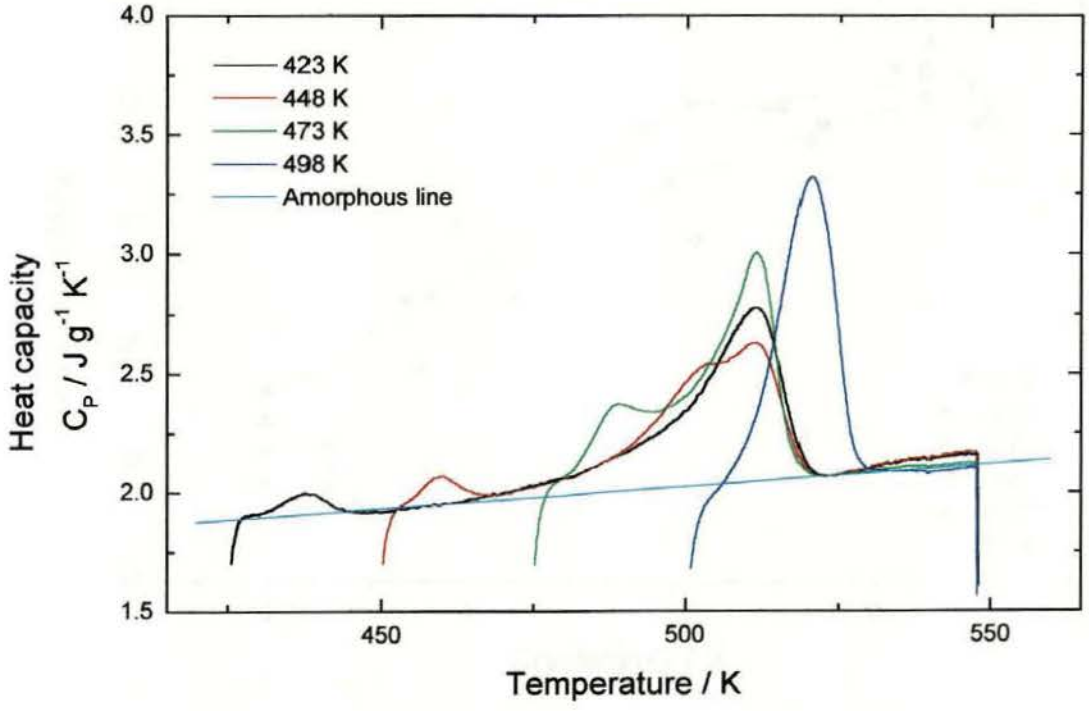

Fig. 5.11 DSC traces of PET/PC 50/50 blends prepared with added catalyst after crystallised at indicated temperature for 8-10 times t_{max} and heated at 10 K/min. Amorphous liquid line obtained separately from amorphous sample

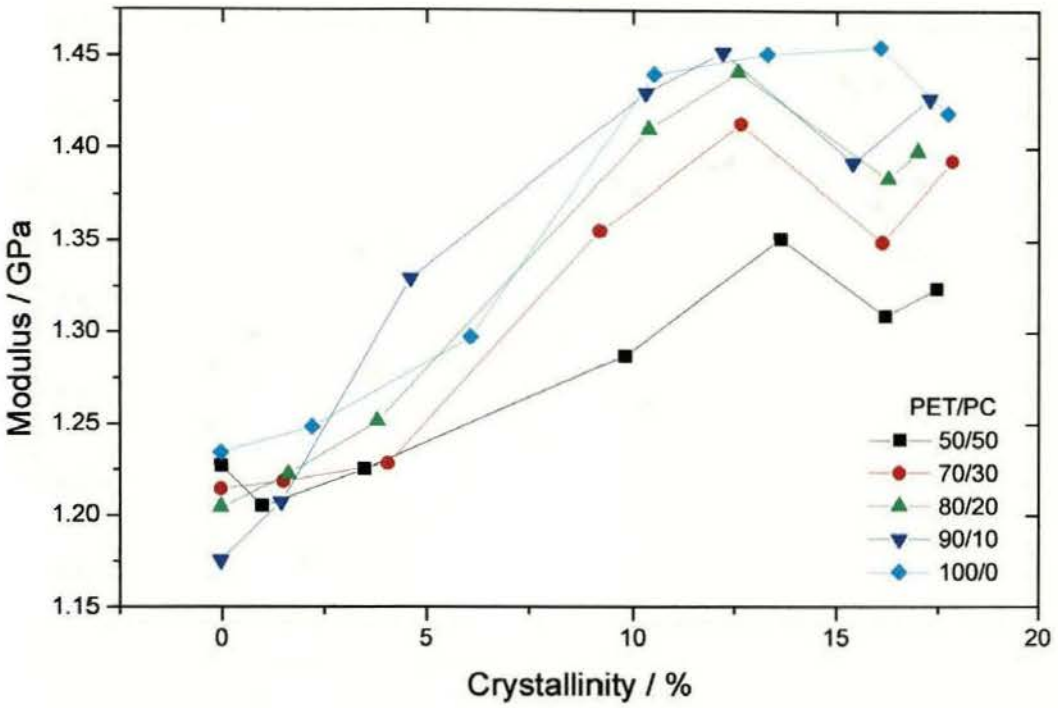

Fig. 5.12a Modulus change with crystallinity

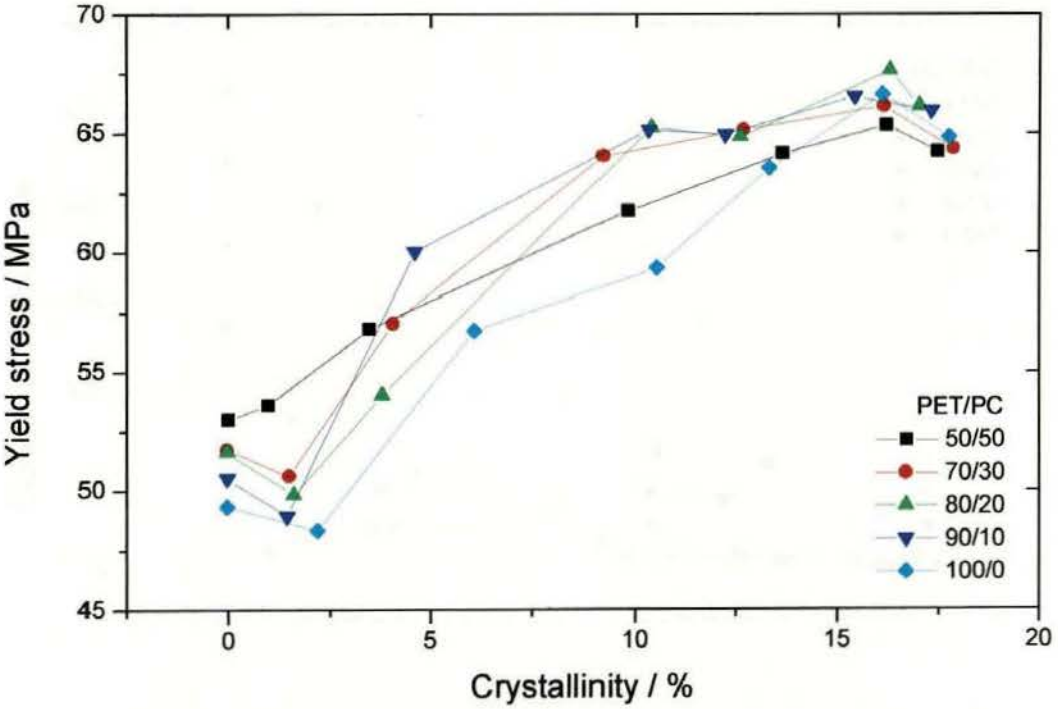

Fig. 5.12b Yield stress change with crystallinity

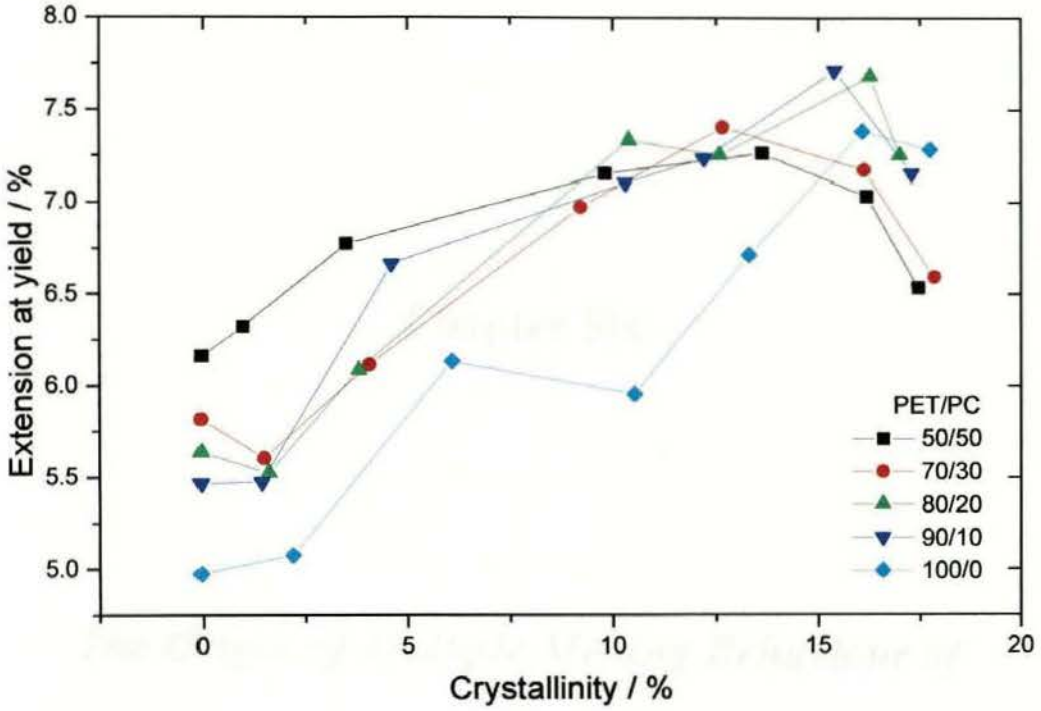

Fig. 5.12c Extension at yield change with crystallinity

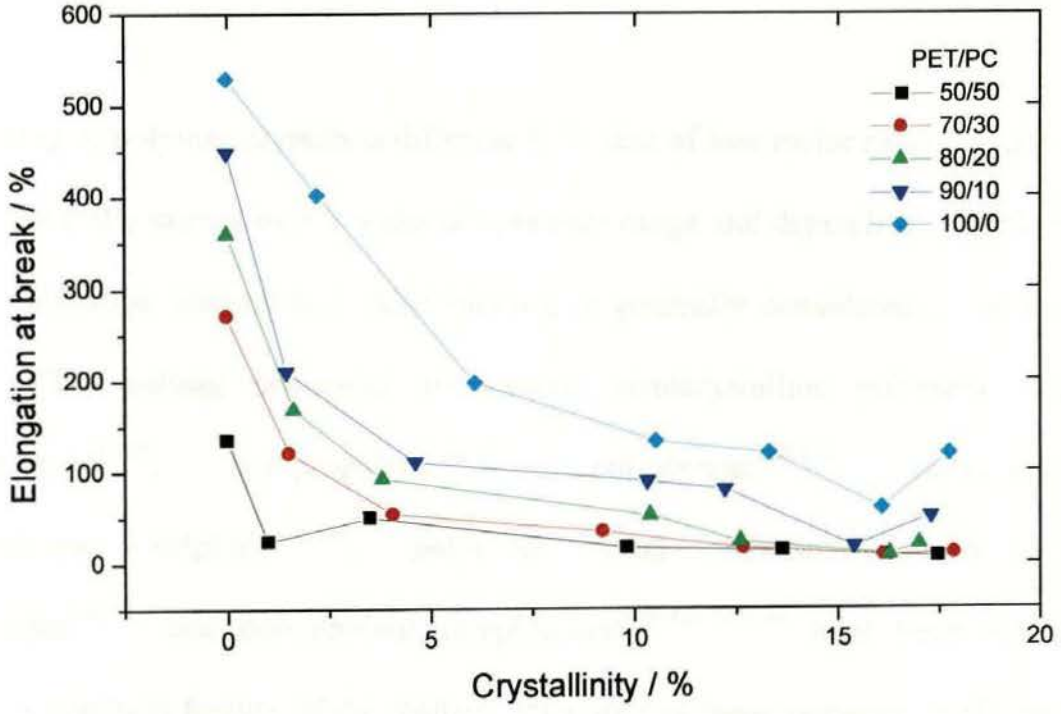

Fig. 5.12d Elongation at break change with crystallinity

Chapter Six

The Origin of Multiple Melting Behaviour of PET and Blends

6.1 Introduction

The melting of polymer crystals is different from that of low molar mass crystals in that melting generally occurs over a wider temperature range and depends on sample history and crystallisation temperature. Also melting is generally considered to be a kinetic process. The melting behaviour of various semicrystalline polymers, such as polyethylene[123-126], polypropylene[127-129], polystyrene[130-132], polyamide[133,134], polyphenylene sulphide[135,136], polyether ether ketone[137-139], polybutylene terephthalate[140,141] and polyethylene terephthalate[119-121,142-144] have been extensively studied. A common feature of the melting behaviour of these polymers is the presence of multiple melting peaks during a normal DSC scan (i.e. heating rates between 2.5 and 20 K min^{-1}). This phenomenon has been widely studied for many years, but there is no

consensus regarding its origin. It has instead been attributed to a variety of effects: (1) the presence of more than one crystallographic form (polymorphism), (2) melting, recrystallisation and remelting, (3) changes in the morphology, such as lamellar thickening and perfection, and (4) fractionation of the polymer by molecular weight during crystallisation.

In this chapter the influence of thermal history on the melting behaviour and the origin of multiple melting in PET and blend samples have been investigated by DSC and WAXD techniques.

6.2 Melting and Melting Theory

6.2.1 A Review of the Melting Behaviour of PET

The melting behaviour of PET has been studied by different techniques and it was found that PET crystallised over a wide range of temperatures frequently exhibited multiple melting regions, the number depending on the thermal history of samples. Normally two melting endoderms were present. The one at higher temperature was constant, and the other at lower temperature and relative smaller varied with crystallisation temperature. However, with increasing crystallisation temperature or crystallisation time, the melting endotherm, initially at lower temperature, moved to higher temperature and increased in size. At the same time the former decreased in size and eventually disappeared.

By using differential thermal analysis (DTA), electron microscopy, birefringence and dynamic mechanical measurements, Bell *et al*[133,145] proposed that the lower melting endotherm represented the melting of imperfect or small crystals with partially extended chains. The other endotherm was associated with the melting of folded chain crystal. They considered that the folded chain crystals were kinetically preferred, and the more extended crystals were thermodynamically preferred. Further annealing allowed the folded chain crystals to convert to extended chain crystals. On the other hand, Robert[146] attributed the lower melting endotherm to the melting of folded chain crystals and the higher one to bundle-like crystals. Both proposals were based on the assumption that melting endotherms were directly related to the structures that developed on crystallisation, and they did not consider that crystalline structures would change on heating.

A different and frequently cited conclusion introducing the idea that heating in DTA instruments changed the morphology was considered by Holderworth and Turner-Jones[119]. They suggested that partial melting and recrystallisation took place during heating and they proposed that the first endotherm, appearing at lower temperature, was due to the melting of crystals formed at the crystallisation temperature T_c and the other melting endotherm, appearing at higher temperature, was associated with the melting of the crystals produced by the recrystallisation process which occurred during heating. Therefore the DSC scan did not directly reflect the crystalline structure produced during the crystallisation. This view was also taken up by Bell et al.[147], who, in addition, examined PET samples cooled at various rates from the melt. These samples showed similar recrystallisation behaviour to samples annealed for different lengths of time. On

annealing PET at various temperatures and times, Alfonso *et al.*[148] observed that a linear increase in density with logarithm annealing time. They confirmed that partial melting and recrystallisation occurred during annealing occurred.

A detail study of PET isothermal crystallisation from the glass state was performed by Groenickx *et al.*[92] using DSC, WAXD and SAXS and transmission electron microscopy (TEM). They concluded that the first endotherm at the lower temperature corresponded to the melting of crystals formed at the crystallisation temperature, T_c, and the second endotherm at higher temperature originated from the melting of a fraction of the original crystalline materials reorganised during heating. Reorganisation was either due to crystal perfection or crystal thickening. Groeninckx and Reynaers[142] also annealed PET by using different heating rates and they concluded that this process involved a solid–state transformation of the original crystalline structure including crystal perfection without thickening or melting followed by recrystallisation with crystal perfection and crystal thickening.

One of the first studies on reporting triple melting endotherms in PET was due to Zhou and Clough[121], although triple melting endotherms had been observed earlier in other materials[149, 150]. Zhou and Clough[121] labelled the PET melting endotherms as I, II and III in order of increasing melting point. They considered that endotherm I which normally appeared about 10 K above the crystallisation temperature corresponded to the melting of secondary crystals. Endotherm II was due to the melting of crystals formed at T_c by the primary crystallisation process and III was due to fusion of crystals formed as

a result of recrystallisation during heating. Triple melting behaviour was also studied by Al Reheil[151]. He came to the same conclusion as Zhou and Clough[121].

More recently, Medellin-Rodriguez *et al.*[120, 152] have studied the melting behaviour of PET by using DSC, polarized optical microscopy and SAXS. They found that melting was the morphological reverse of isothermal crystallisation process with respect to primary and secondary structural elements. On this basis, they suggested that spherulites consisted of dominant lamellae and subsidiary branches. The first melting endotherm was due to the melting of small metastable branches and the second melting endotherm to the melting of main metastable branches. The upper one was associated with primary crystals which underwent some recrystallisation on heating. They also found that the recrystallisation process (thickening rather than crystal perfection) developed progressively but not in proportion to the greater increase in long periodicity. As a consequence, the melting of secondary branches was associated with an increased in periodicity.

By using real time resolved synchrotron SAXS and faster heating technique, Hsiao *et al.*[153, 154] confirmed that isothermal crystallisation involved two discrete stages producing two different crystal size distributions - primary and thinner secondary lamellae. Both lamellar types can undergo a great deal of crystal perfection and rearrangement on heating with time. The first (lower) endotherm is related to the melting of secondary crystals, the middle endotherm to the melting of primary crystals, and the upper endotherm to the melting of crystals that had reorganized on heating.

6.2.2 Melting Theory

Melting is a first-order phase transition, accompanying by discontinuities in the thermodynamic functions such as enthalpy and entropy. On melting the overall change in free energy, ΔG_f, is

$$\Delta G_f = \Delta H_f - T_m \Delta S_f \tag{6.1}$$

where ΔH_f and ΔS_f are the changes in enthalpy and entropy at the melting temperature T_m, respectively. For a thin chain-folded lamella with lamellar thickness l and other dimensions x, as shown in Fig.6.1, the overall change in free energy on melting is given by

$$\Delta G = lx^2 \Delta G_f - 4lx\sigma - 2x^2\sigma_e \tag{6.2}$$

where σ_e and σ are the free energy of the fold and lateral surfaces, respectively. At the equilibrium melting point, T_m°, $\Delta G_f = 0$ and $l \to \infty$,

$$\Delta S_f^o = \Delta H_f^o / T_m^o \tag{6.3}$$

If melting occurs at T_m close to T_m°, ΔH_f and ΔS_f can be considered to be independent of temperature and therefore equation 6.1 can be changed to

$$\Delta G_f = \Delta H_f^o - T_m \Delta S_f^o = \Delta H_f^o - T_m \frac{\Delta H_f^o}{T_m^o} = \frac{\Delta H_f^o \Delta T}{T_m^o} \tag{6.4}$$

On inserting this into equation 6.2 gives

$$\Delta G = lx^2 \frac{\Delta H_f^o \Delta T}{T_m^o} - 4lx\sigma - 2x^2\sigma_e \tag{6.5}$$

At the melting point T_m, $\Delta G = 0$ such that,

$$l\Delta H_f^o \frac{\Delta T}{T_m^o} = 4\sigma \frac{l}{x} + 2\sigma_e \tag{6.6}$$

For thin lamella $x >> l$ and σ_e is 5 - 10 times greater than σ, the first term on the right hand side can be ignored. After simplification the above equation can be rearranged to

$$T_m = T_m^o(1 - \frac{2\sigma_e}{l\Delta H_f^o}) \tag{6.7}$$

It is clear from above equation that for crystals of finite thickness, T_m is always less than T_m^o by an amount of $2\sigma_e/l\Delta H_f^o$.

Hoffman *et al.*[155] defined the melting point, T_m, as the temperature at which the last detectable trace of crystallinity disappeared. From nucleation theory, the initial thickness of a chain-folded lamella, l_g^*, which is controlled by secondary nucleation and kinetically determined, is of the form[156]

$$l_g^* = (2\sigma_e / \Delta G_f) + \delta = (2\sigma_e T_m^o / \Delta H_f^o \Delta T) + \delta \tag{6.8}$$

where $2\sigma_e/\Delta G_f$ is equal to a critical size of secondary surface nucleus, and δ is a quantity that is a weak function of the undercooling near the equilibrium melting point and for most polymer it is 10 – 40 Å [75]. It is clear that the initial lamellar thickness is a function of the undercooling and also must be larger than the critical size otherwise the crystal will melt at the temperature where it formed.

For the crystals crystallised for various lengths of time t, the thickness increases with the logarithm of time, i.e.[157, 158]

$$l(t) = l_g^* + B\log t \tag{6.9}$$

where $l(t)$ is the lamellar thickness at time t and B is a coefficient and only changes with crystallisation temperature. For simplicity, the thickness achieved at the end of crystallisation is considered to be γ times larger than the initial thickness l_g^*, i.e.

$$l = \gamma l_g^* \tag{6.10}$$

When the undercooling is lower it is a good approximation to assume that $2\sigma_e/\Delta G_f >> \delta$. In this case on inserting equation 6.10 into 6.7 leads

$$T_m = T_m^o(1-\frac{1}{\gamma}) + \frac{T_c}{\gamma} \tag{6.11}$$

This expression indicates that the observed melting point of a polymer that has thickened by a factor γ during crystallisation at T_c is approximately a linear function of T_c. Therefore, the thin crystals formed at the low crystallisation temperature melt lower on heating than the thick ones formed at a high crystallisation temperature. The equilibrium melting point T_m° can be obtained by plotting T_m *vs.* T_c and extrapolating to intercept $T_m = T_c$.

6.3 Results and Discussion

6.3.1 The Influence of Crystallisation Temperature

Fig. 6.2 shows the DSC analyses of PET samples crystallised isothermally at different temperatures for different times. In Fig.6.2a triple melting endotherms of PET are present for samples crystallised at intermediate crystallisation temperatures from. 448 to 473 K. Below 448 K two endotherms are present on melting and above 473 K only one endotherm is present. The initial melting endotherm temperature, T_{ml}, increased with crystallisation temperature. On the other hand, the temperature corresponding to the last trace of melting appeared to be independent of the crystallisation temperature below 473 K. In Fig. 6.2b, samples crystallised at higher temperature for 10 hrs showed only one

melting peak and the melting temperature increased with crystallisation temperature. The T_{ml} *vs.* T_c of PET crystallised for 2 hrs from the melt is plotted in Fig. 6.3. It is obvious that T_{ml} increases linearly with the crystallisation temperature T_c.

6.3.2 The Influence of Crystallisation Time

The DSC analyses of PET samples crystallised from 398 to 498 K for different times and then directly heated to melt are shown in Fig.s 6.4 to 6.9, respectively. The T_{ml} shifted to higher temperatures and increased in size with increasing crystallisation time at all temperature, see Fig. 6.10. Samples crystallised at 398 and 423 K showed two melting endotherms and the final endotherms were similar regardless of crystallisation time, see Fig.s 6.4 and 6.5. Samples crystallised at 448 K exhibited three endotherms, the middle one was much smaller than the final, and increased in size with increasing crystallisation time. The final endotherm was invariant with crystallisation time. Samples crystallised at 473 K showed three endotherms. However they were completely different from the samples crystallise at 448 K. The middle endotherms were more obvious than the final which developed as a shoulder and eventually disappeared with increasing crystallisation time. Samples crystallised at 483 K for 1 min showed no melting endotherm. After 5 min, only one appeared in the final melting temperature range. At longer times, the samples showed two melting endotherms. The DSC analyses of PET samples crystallised at 498 K are shown in Fig. 6.9. Sample crystallised for 15 min only shows one very small endotherm but samples crystallised for longer periods displayed a small shoulder on the melting endotherm. As with the samples crystallised at 483 K, the endotherms increased gradually with crystallisation time.

The T_{ml}s of the above samples are plotted against the crystallisation temperature, T_c, in Fig.6.10. As can be seen, T_{ml} increased linearly with logarithm time, a feature of secondary crystallisation[75]. The slope of the line increased from 2.5 at 398 K to 4.1 at 448 K, and eventually to 7.1 and 7.5 at 473 and 483 K, respectively. This indicates that T_{ml} increased faster at higher T_c than at lower T_c. Similar results have been observed by Alfonso *et al.*[148]. The dependences of the temperature corresponding to the last trace crystallinity on crystallisation temperature and crystallisation time are shown in Fig. 6.11. For samples crystallised below 473 K, these temperatures were constant within experiment error; for the samples crystallised at 483 K, the melting temperature decreased slightly with increasing crystallisation time. However, for samples crystallised at 498 K the melting temperature increased markedly with increasing crystallisation time. This suggests that when crystallised below 473 K the last trace of melting is recrystallisation dominated, and above 498 K the last trace of melting is dominated by thickness of crystals produced on crystallisation[135]. From the equation 6.11, it is clear that the higher the crystallisation temperature the greater is the lamellar thickness, the higher the melting temperature, and the less recrystallisation occurs on heating. The evolution of the WAXD pattern of PET as functions of the crystallisation temperature and time are shown in Figs 6.12 and 6.13, respectively. It is obvious that the effect of increasing the crystallisation temperature and time does not change the crystal structure but only improves crystal perfection.

6.3.3 The Effect of Heating Rate

Fig. 6.14 shows the DSC analyses of PET crystallised at 473 K for 1 hr and then immediately heated to melt at different heating rates. The melting endotherms changed from apparently three endotherms at heating rates of 2.5 and 5 K min^{-1} to two endotherms with a shoulder at the final melting temperature at 10 K min^{-1}. Eventually two endotherms were observed with the disappearance of the final shoulder. Corrections were made for the thermal lags at the different heating rates. The lags were measured for the differences in the glass transition temperature of the samples at these rates of heating. Since T_g is independent of heating rate, the differences in T_gs are thermal lags. The T_g was measured on a standard glass produced at the same cooling rate, i.e. 40 K min^{-1} and thermal lags of 0.5, 1, 1.8, 3.8, and 8.5 K were measured for heating rates of 2.5, 5, 10, 20 and 40 K min^{-1}, respectively. On correcting for thermal lag, the start of the melting temperatures was the same for every sample. However, T_{ml} increased with increasing heating rate. On the other hand, the melting temperature of the middle endotherm was constant and the last trace of melting decreased with increasing heating rate. As has been pointed out by Holdsworth *et al.*[119] the crystals undergo continuous reorganisation during heating, i.e., the crystallites formed at low temperature melt and recrystallise with increased perfection during the thermal scan. Using higher heating rates progressively less recrystallisation takes place, and the last endotherm decreases to a shoulder and eventually disappears. At lower heating rates, however, the overall endotherm is due to the sum of melting and recrystallisation. The observed position of the endotherm maximum depends not only on the original distribution of lamellar thickness but also on extent of melting and recrystallisation.

Fig. 6.15 shows the DSC analyses of PET samples crystallised at 225°C for 2 hrs and on immediate heating at different rates. There is only one endotherm at the higher heating rates, an endotherm with a shoulder at the intermediate rates and two overlapping endotherms at the slowest heating rates. On the contrary with samples crystallised at 473 K, the last trace of melting was constant independent of heating rate, due to more stable crystals forming at 498 K and not annealing on heating.

The DSC analyses of sapphire and PET samples measured at high heating rates are shown in Fig. 6.16. It can be seen from Fig. 6.16a that the DSC analyses become constant after 30 seconds with sapphire heated at 320 K min^{-1}, and there are no spurious spikes as claimed by Medellin-Rodriguez et al.[120]. Normally, as the heating rate increases the thermal lag and temperature gradient across the sample increase due to its poor thermal conductivity. This will increase a tendency for the lamellae of different thickness to melt simultaneously, broaden the melting peak and reduce the resolution if more than one melting endotherms exist. If there is no well defined separation between the two lamellar thickness distributions and no further lamellar thickening during heating, the melting curve will be present as a single broad melting endotherm. It was observed that at the extreme heating rate of 160 K min^{-1}, there were two melting endotherms rather than one single broad melting endotherm, as seen in Fig. 6.16b. It took about 1 min from the onset (445 K) to the end of melting (595 K), and so it is reasonable to neglect any recrystallisation in this situation. Thus, it would seem that there were two distinct lamellar thickness distributions in the original sample.

To reduce thermal lag and temperature gradient within the sample, very thin PET films (100 μm) were used instead of the normal sample cut from moulded plaques (0.8 mm). Using the above procedure, the thermal lag for this film at 160 K min^{-1} was 17 K. DSC analyses of the PET films at fast heating rates are shown in Fig. 6.17 after correcting for thermal lag. It can be seen from Fig. 6.17a that samples crystallised at 423 and 448 K exhibited two distinct endotherms, while samples crystallised at 473 K showed an endotherm with a shoulder. However, when the thickness of the film was reduced to 50 μm, the shoulder became more distinct, see Fig. 6.17b. Since near the melting point even low molecular weight materials require several minutes to attain equilibrium conditions[101] and also DSC does not response instantaneously, obviously, the end of melting of PET samples can not be considered as the melting point under these conditions even though the thermal lags were corrected.

6.3.4 The Influence of Annealing

Annealing is generally considered to be a process of increasing crystallinity, improving perfection of the crystals[72]. Fig. 6.18 shows the DSC analyses of PET samples crystallised at 398 K for 1 hr and then annealed at different temperatures for 1 hr. Except for samples annealed at 498 K two endotherms were present and the final endotherm was invariant in all cases. The DSC analyses of PET samples crystallised at 398 K for 1 hr, annealed 498 K for 1 hr, and then annealed at 473, 448, 423 and 398 K for 1 hr separately and consequently are shown in Fig. 6.19. It is clear that the final endotherm is almost the same since the highest annealing temperature and time were the same. However, the lower temperature endotherms are related to the lower annealing

temperatures. As can be seen, the lower temperature melting endotherms of stepwise annealed samples occurred in the same temperature range as those annealed in a single-step. It is worth noting that the size of the initial endotherm in the stepwise annealed samples was relatively small compared to those annealed in a single-step at that temperature, as shown in Fig. 6.14 inset. This also indicated even for the well-crystallised sample which can continuously crystallise at temperature much lower than the temperature previously crystallised.

6.3.5 The Effect of Stepwise Heating

On heating, the measured DSC specific heat can be divided into two parts, one completely due to the baseline heat capacity change and the other to crystallinity changes, i.e.

$$C_p = dH/dT = C_{p,c}X_c + C_{p,a}(1 - X_c) - \Delta H_f^o \frac{dX_c}{dT} \qquad (6.12)$$

where $C_{p,c}$ and $C_{p,a}$ are the heat capacity of the completely crystalline and amorphous materials respectively, X_c is the weight fraction crystallinity and ΔH^o_f is the heat of fusion of 100% crystalline at temperature T. dX_c/dT is the rate of the change of crystallinity with temperature. If dX_c/dT is equal to zero the DSC analysis will only show the change in specific heat of the samples with temperature. As expected in the step heating of sapphire the specific heat was linear with temperature even at a 10-fold enlargement scale, seen in Fig. 6.20.

DSC analyses of the melting of the PET samples crystallised at 423 K for 30 min are shown in Fig. 6.21. On continuous heating, A, it seems that no change occurs between the initial endotherm and the final endotherm since the DSC analyses was smooth over this interval. During step heating, B to E, the first scan was exactly the same as A. However, the differences were seen on immediate rescan - a small endotherm occurs at the temperature at which the previously scan was stopped, and the specific heat increases over that obtained in the previous heating scan. This clearly indicated that there must be some changes in crystallinity between the two scans, melting and recrystallisation must occur between the two endotherms on heating. Therefore, the difference in C_p between the two immediate scans could be as an indicator of the extent of melting and recrystallisation.

DSC analyses of step heating of the samples crystallised at different temperatures are shown in Fig. 6.22 – 26. After each step, the samples were cooled to 10 K lower than the temperature at which heating was stopped and heated up immediately. These steps were: A. 415 to 450 K; B. 440 to 470 K; C. 460 to 490 K; D. 480 to 510 K; E. from 500 K to melt. The rate of cooling was 160 K min^{-1} and rate of heating was 10 K min^{-1}. The C_p differences were present between all steps for the sample crystallised at 423 K, see Fig.6.22. However, when the sample was crystallised at 473 K, the differences only existed between C/D and D/E steps. At prolonged crystallisation times, i.e. from 30 min to 5 hrs, the C_p difference between C/D steps decreased to some extent, but on the contrary, the C_p difference of D/E steps increased greatly. The C_p difference in the sample crystallised at 498 K for 3 hrs exhibited the same tendency as the samples crystallised at 473 K but both the C_p differences of C/D and D/E were much smaller.

From the C_p differences it could be concluded that the extent of melting and recrystallisation decreased with increasing crystallisation, annealing temperatures and time, as the crystals become perfect. It can be concluded that melting and recrystallisation take place on heating when the temperature is above T_c especially for T_c below 473 K.

Fig.6.27 shows the DSC analyses of step heating samples which were initially stepwise annealed for 5 hrs at 10 K increments from 398 to 498 K at a slow heating rate of 0.31 K min^{-1} and reannealed at 125 K for 5 hrs. It can be seen that there is no C_p differences between each step with temperatures below 500 K, indicating that the crystals were perfect under this conditions. However considerable differences were present between D / E steps, indicating a great change in crystallinity between these two steps. On comparing this with continuously heating F, it can be seen that a greater amount of fusion took place about 512 K, while a large amount of fusion occurred at 523 K for the samples isothermally crystallised at 498 K for 3 hrs, see Fig. 6.25. Comparison is easier from Fig 6.28. This clearly indicates that average lamellar thickness in isothermal crystallisation sample is much larger than that in slow annealed samples although the annealed sample was held at 498 K for as long as 5 hrs. Fontaine et al.[143] have also observed that the average long periods were 171, 152 and 126 Å for the samples isothermally crystallised at 518 K, crystallised at 373 K and then quickly and slowly heated to 518 K respectively, although the fractional crystallinity was nearly the same. This was due to the absence of completely melting imperfect crystals during slow annealing.

In Fig. 6.28, the DSC analysis of slow annealed sample shows two distinct melting endotherms corresponding two lamellar thickness distributions. As the sample was originally crystallised at a large supercooling with a large amount of nuclei present, therefore, most of the crystals are imperfect[156]. During slow annealing, these imperfect crystals can be partially melted and recrystallised to more stable structures. These formed crystals may undergo melting and recrystallisation several times until the final annealing temperature is reached[142]. The initial large melting endotherm at around 512 K was associated with these imperfect crystals that had gradually recrystallised, on the other hand, the final small endotherm at 520 K was related to the melting of recrystallised primary crystals.

As mentioned above a small endotherm appears on step heating at the temperature at which previous heating was stopped. This has been observed by the several researchers, however, it has never been fully explained[121,134,152]. There are two reasons for this. One is melting of the crystals newly formed on heating, the other is melting of the crystals produced in isothermal crystallisation. In Fig.s 6.23 – 25 there are not such endotherms in step A, however, they are present in step B. Since T_cs were 473 and 498 K, the small endotherms appeared from 450 to 463 K must be due to melting of the crystals newly formed during heating. But the size of the endotherm is quite small in this case, therefore, the relatively large sizes of the endotherms in Fig. 6.22 and 23 must be mainly due to melting of the crystals formed during isothermal crystallisation. At this one may wonder why the small enotherm does not appear on continuous heating. During continuous heating, melting and recrystallisation take place simultaneously and uninterruptedly, and endothermic and exothermic are probably comparable before the

final melting occurs, thus, no net endotherm appears between the initial and the final melting endotherms, see A in Fig6.21. But it should not be forgotten that the occurrence of recrystallisation should always occur after the (partially) melting, thus, the initial melting endotherm is usually observed on continuous heating. On step heating temperature was stopped at a certain point, the melting temperatures of all crystals in sample are higher than this point. On the next heating, the crystals with melting temperature just above this point will, of course, start to melt at this temperature. Thus, the small endotherm on step heating has a similar origin to the initial melting endotherm on continuous heating.

6.3.6 Equilibrium Melting Point

The equilibrium melting point is the temperature which corresponds to the melting of infinitely thick lamellae[155]. The equilibrium melting point, T_m^o, can be conveniently measured by Hoffman-Weeks' procedure[155], according to which, a plot of T_m *vs.* T_c is a linear relationship and the same thickening coefficient γ should be obeyed. This is shown in Fig. 6.29 and from which an extrapolated value of T_m^o was obtained. The value of T_m^o is 561 ± 2 K in good agreement with the literature values[92, 144].

6.3.7 Melting Behaviours of Blends

In the PET/PC blend, only PET was crystallisable but the blends also exhibited multiple melting endotherms similar to that of PET, see Fig.s 6.30 and 6.31. However, the shapes of the endotherms were slightly different from that of PET as the blends were less

readily crystallised. The DSC analyses of the PET/PC 50/50 blend crystallised from the melt for 1 hr at different temperature are exhibited in Fig. 6.32. A distinct exotherm was present in samples crystallised at 398 and 498 K. These samples did not completely crystallised within 1 hr at these temperatures.

The equilibrium melting points of the blends were also determined as above and are listed in Table 1. The values of the blends prepared without added catalyst showed only slight depression of that of PET which was proportional to PC composition, indicating little compatibility between PC and PET. On the other hand, the T_m^o of the blends prepared with added catalyst were depressed considerably, in line with the amount of PC dissolving in PET. The value of the lamellar thickening coefficient, γ, was about 2.0 indicating that the maximum lamellar thickness was close to the critical size of the primary nucleus.

6.3.8 Discussion

Chain-folded lamellae tend to have broader melting range because of the distribution of lamellae present[156]. The mean value of the distribution is $l_g^* = (2\sigma_e / \Delta G_v) + \delta$. If the thickness is $(2\sigma_e / \Delta G_v)$, the lamellae will be melted at its own T_c. If the thickness is rather larger than l_g^*, the growth rate is also quite slow. Only those with the thickness around l_g^* have the maximum growth rate. Therefore the lamellar thickness is controlled by kinetics. During the crystallisation process, and also during heating to melt, lamellar thickening leads to an increase in the melting point and this is reflected in $\gamma > 1$ in the Hoffman-Weeks plot.

From a broad initial lamellar thickness distribution and incorporating with melting and recrystallisation model, Qiu et al.[112] produced simulated DSC traces. They found that there was a good agreement between the simulated traces and the measured DSC analysis. The stepwise heating clearly shows that melting and recrystallisation take place during heating even below the crystallisation temperature for well-crystallised samples. TMDSC[154,159] also shows that partial melting and recrystallisation occur above T_c during heating.

Fast heating is, however, successful in minimizing the reorganization and recrystallisation of metastable polymer crystals[160]. Heating PET samples at fast rates demonstrates that double melting endotherms are due to two distinct lamellar thickness distributions. In Fig. 6.8, it can be seen that samples crystallised at 483 K for 5 min exhibited only one melting endotherm corresponding to the highest temperature endotherm. This was also the case with samples crystallised at 498 K for 15 min. However, with increasing crystallisation time double melting endotherms were observed, indicating that the final melting endotherm appeared earlier in the crystallisation than the lowest temperature melting endotherm[120,135,151]. For PET crystallised isothermally at 483 and 498 K, the times required to reach a maximum in the exotherm, t_{max}, were about 11 and 40 min, respectively. The lowest temperature melting endotherms were observed at 10 and 30 min, respectively. These times are shorter than the corresponding t_{max}. Usually, in PET the primary crystallisation process appeared to stop at about 75% conversion[161]. This means that the thinner lamellae start to form much earlier - before the primary crystallisation stop. Recently Hsiao *et al.*[153] observed that the average long period and lamellar thickness decreased with isothermal

crystallisation time particularly in the primary crystallisation stage. This decrease was explained by the formation of two populations of lamellar thickness with the thinner lamellar thicknesses causing the average value to drop.

PET samples crystallised at 473 K show three melting endotherms. With increasing heating, rate, the middle endotherm increase in size at the expense of the highest temperature endotherm. On comparing samples crystallised at 473 K for 30 min and melted at 10 K min^{-1} with that melted at 160 K min^{-1} in Fig. 6.17, it can be seen that the highest temperature endotherm has completely disappeared in the highest heating rate. Similarly, it was found[153] that the melting point of the PET sample crystallised at 473 K for 2 hrs without further recrystallisation was 518 K, much lower than the observed melting point 530 K. This indicates that the highest temperature melting endotherm is associated with melting of the thickest crystals from recrystallisation during the heating process.

6.4 Conclusions

The multiple melting endotherms of PET have been studied by DSC and the WAXD. They are usually determined by the experiment conditions adopted, i.e. crystallisation temperature, time, and heating rate. The origin of this is due to a combination of recrystallisation and dual lamellar distributions. The first melting endotherm is due to the melting of the thinner lamellae. With the temperature continuously rising, the lamellae undergo melting and recrystallisation process, the middle and highest melting endotherms are determined by this process. On the highest heating rate, the third endotherm is absence and the middle endotherm is due to melting of the primary lamellae. On normal heating rate, it is clear that the highest melting endotherm is associated with the melting of the recrystallised primary lamellae. The middle endotherm is probably related to the melting of the recrystallised thinner lamellae.

Table 6.1 The equilibrium melting point of PET and blends

Sample	T_m^o ± 2 K	γ ± 0.2
PET	561	2.1
Without catalyst		
PET90	561	1.9
PET80	558	2.0
PET70	557	2.0
PET50	555	2.0
With catalyst		
PET90	545	2.2
PET70	549	2.1
PET50	545	2.2

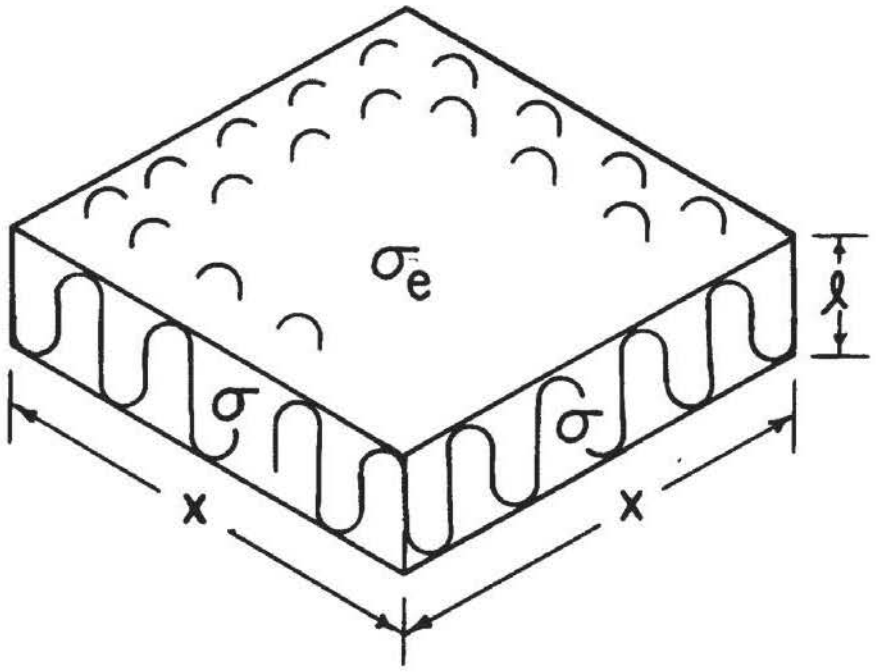

Fig. 6.1 A schematic representation of thin chain-folding lamella with the thin dimension of l and the large dimension x. σ_e and σ are the free energy of the fold surface and the lateral surface, respectively[75].

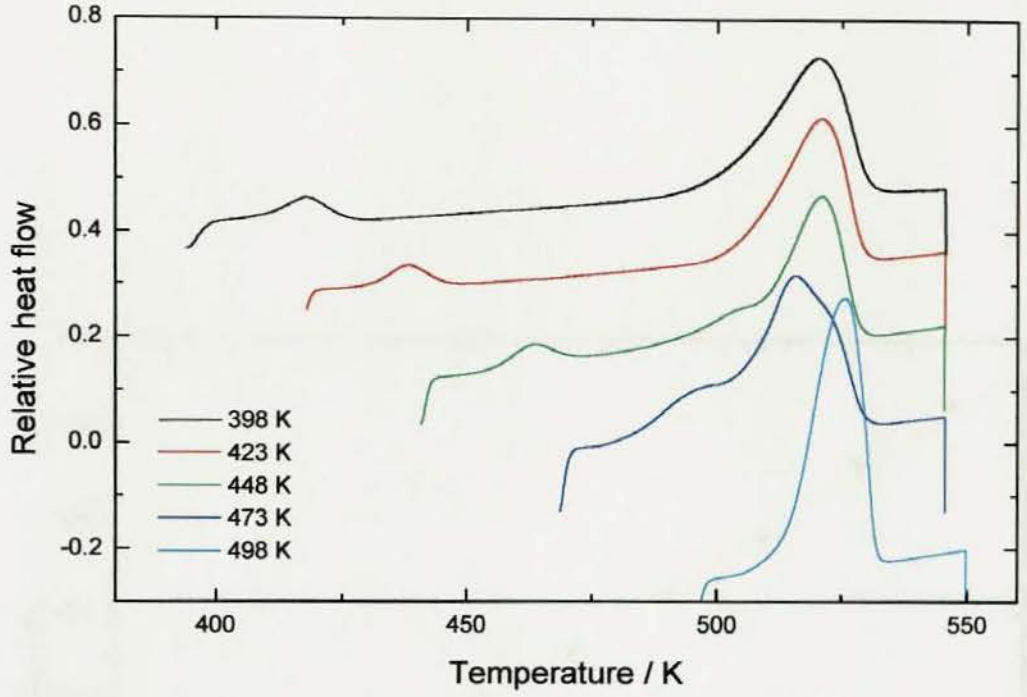

Fig. 6.2a DSC analyses of the melting of PET heated immediately after being crystallised for 2 hrs. Heating rate 10 K min^{-1}

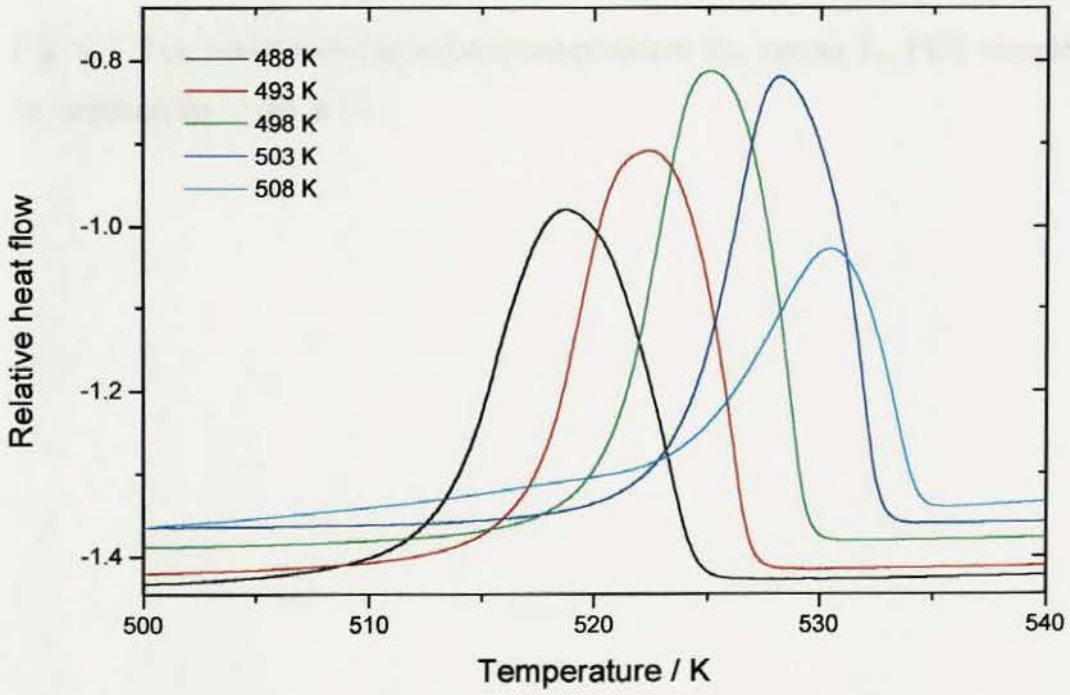

Fig. 6.2b DSC analyses of the melting of PET crystallised for 10 hrs. Heating rate 5 K min^{-1}

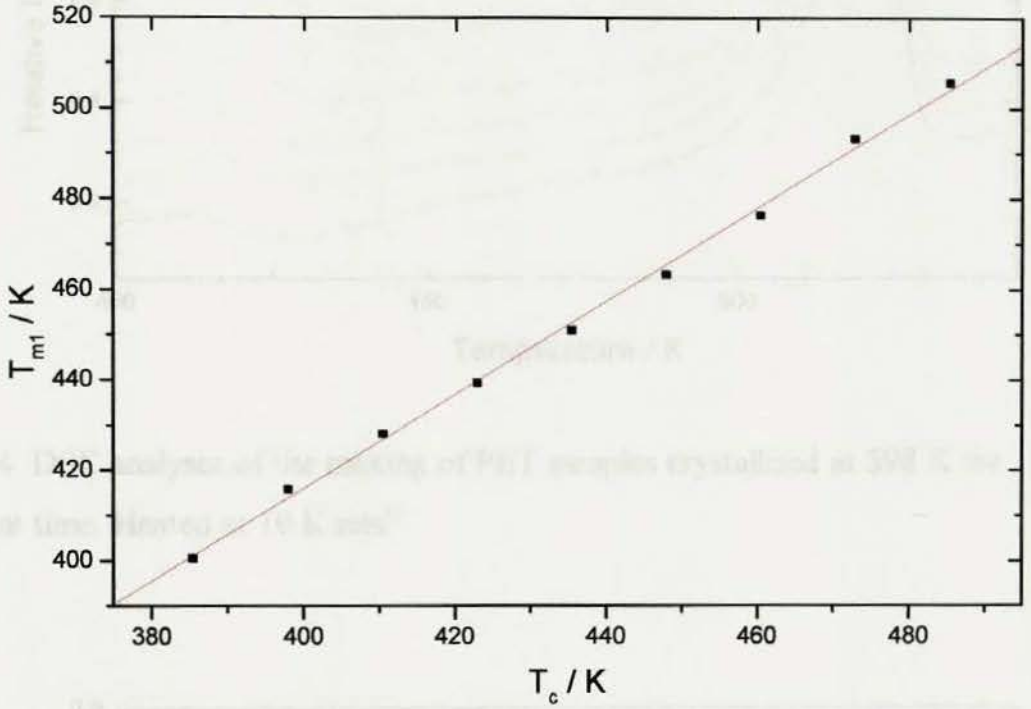

Fig. 6.3 The initial endotherm peak temperature T_{m1} *versus* T_c. PET samples crystallised for 2 hrs at T_c

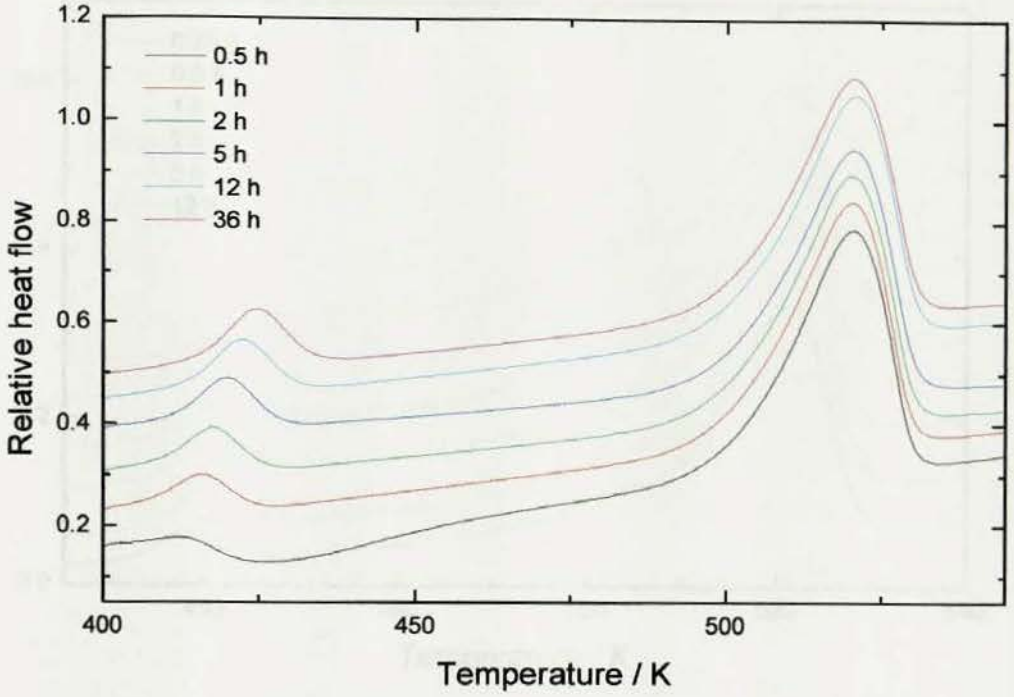

Fig. 6.4 DSC analyses of the melting of PET samples crystallised at 398 K for different time. Heated at 10 K min^{-1}

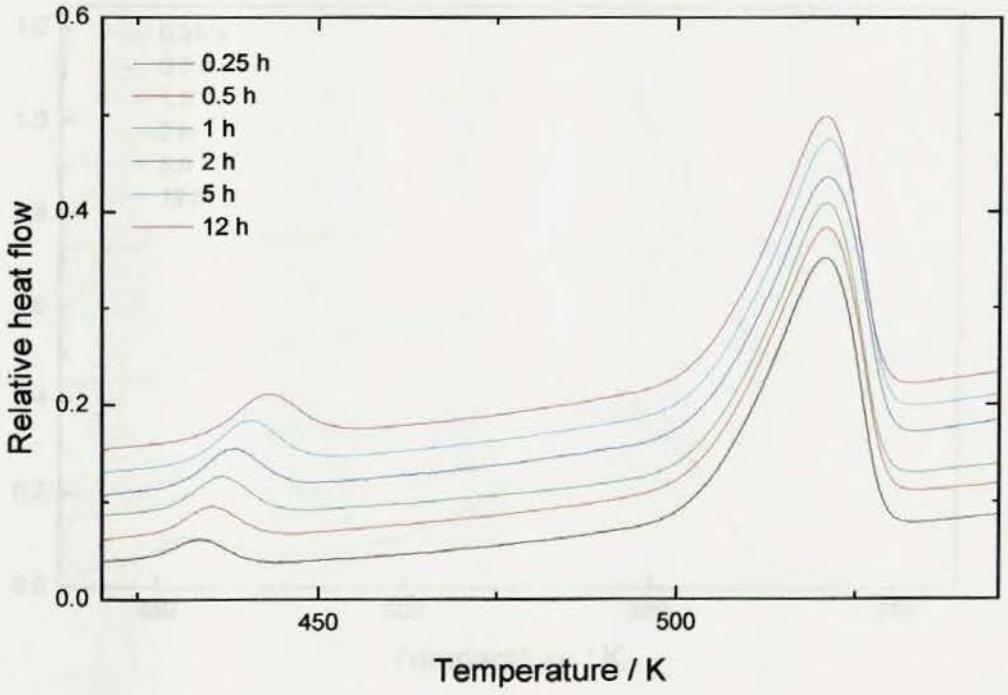

Fig. 6.5 DSC analyses of the melting of PET samples crystallised at 423 K for different time. Heated at 10 K min^{-1}

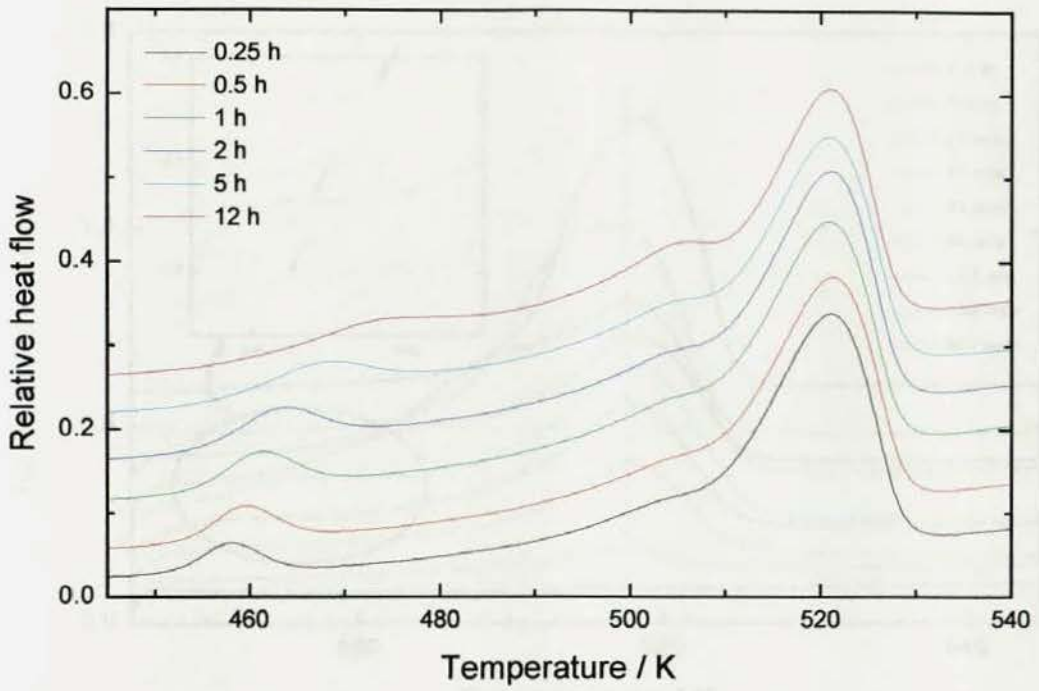

Fig. 6.6 DSC analyses of the melting of PET samples crystallised at 448 K for different time. Heated at 10 K min^{-1}

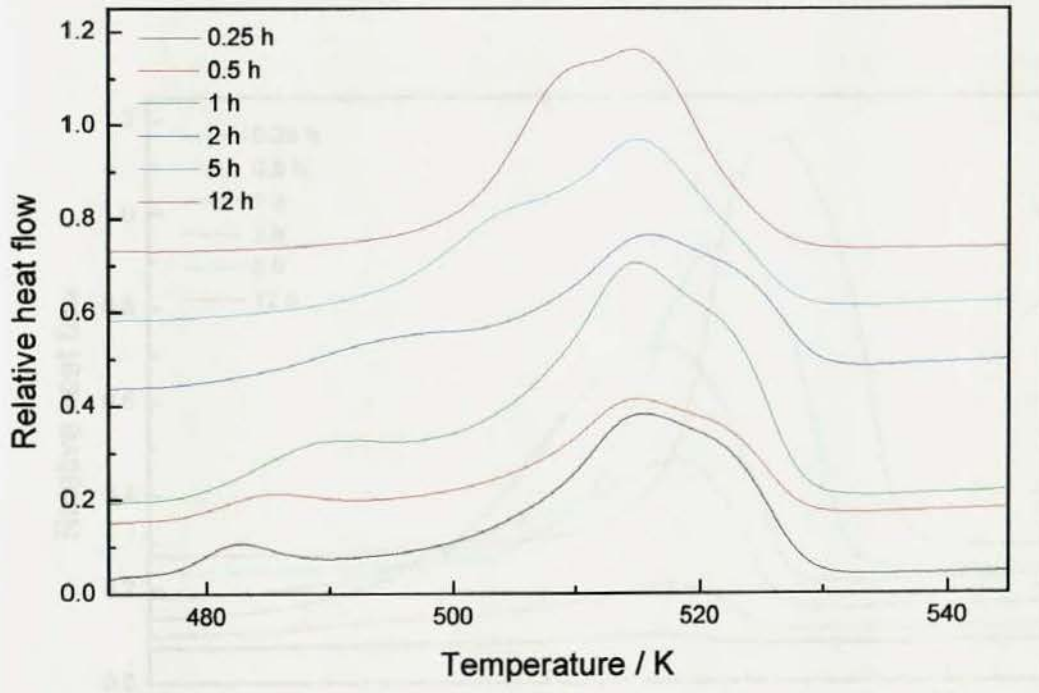

Fig. 6.7 DSC analyses of the melting of PET samples crystallised at 473 K for different time. Heated at 10 K min^{-1}

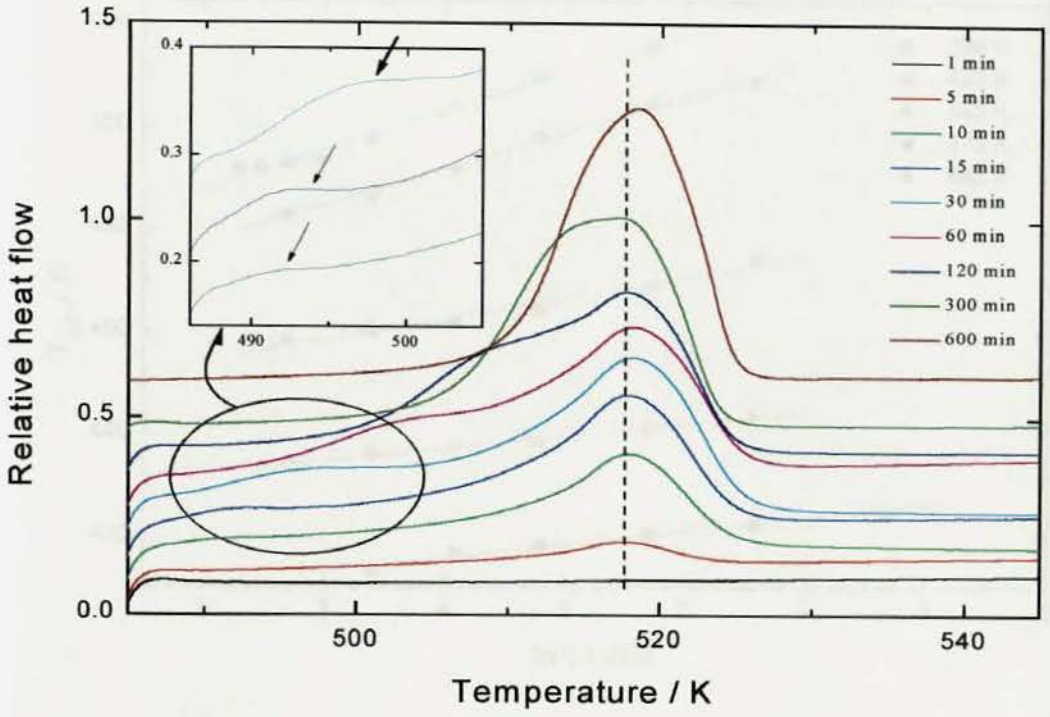

Fig. 6.8 DSC analyses of the melting of PET samples crystallised at 483 K for different time. Heated at 10 K min^{-1}

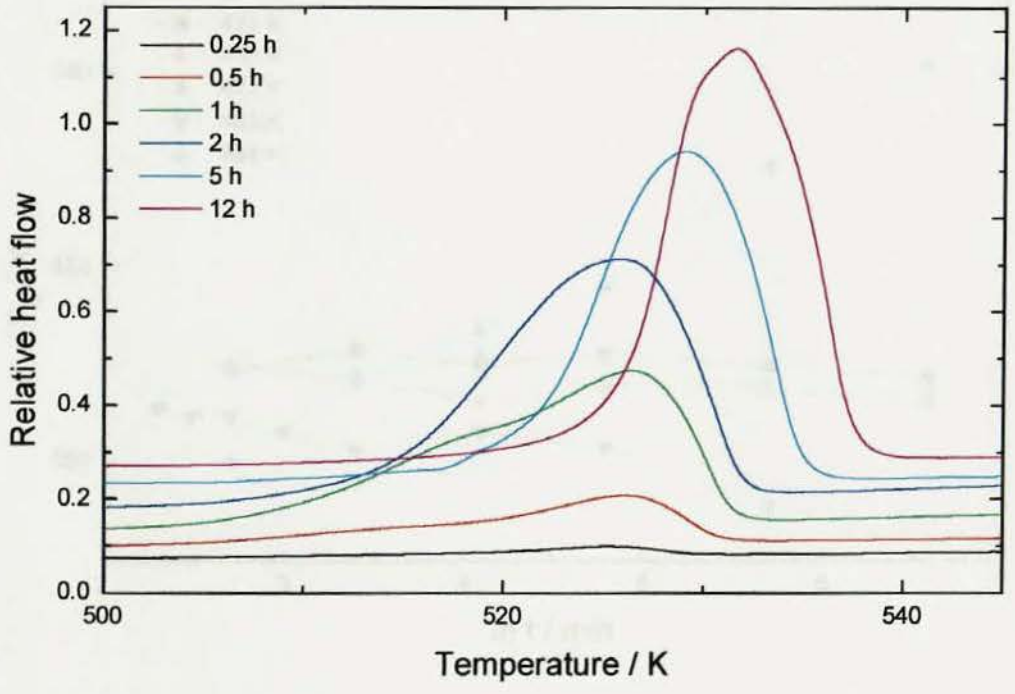

Fig. 6.9 DSC analyses of the melting of PET samples crystallised at 498 K for different time. Heated at 10 K min^{-1}

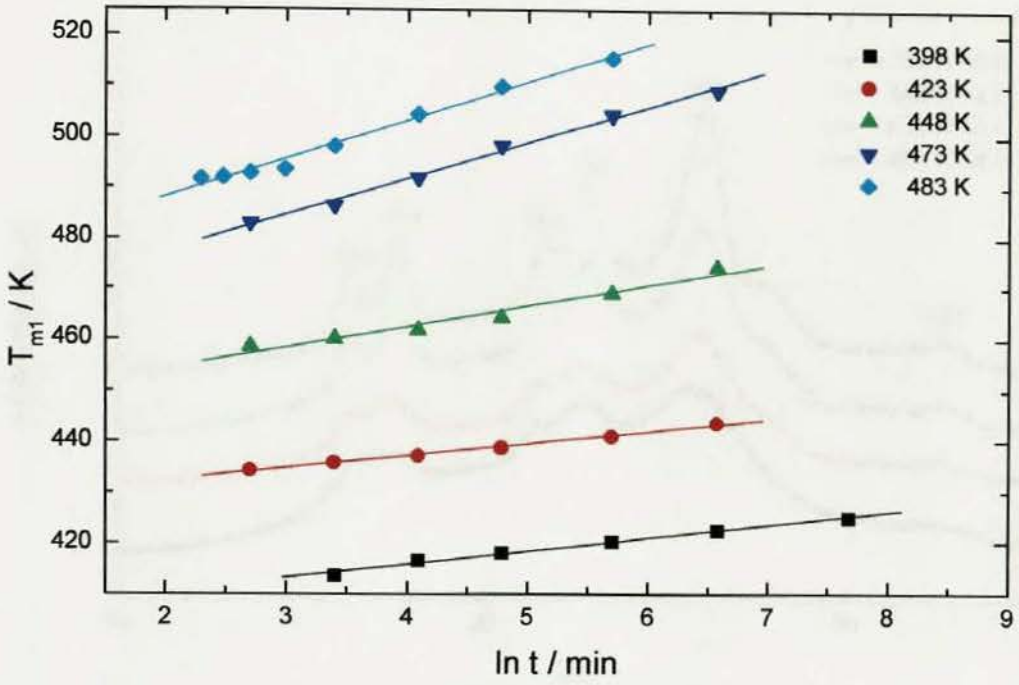

Fig. 6.10 The dependence of T_{m1} on crystallisation temperature and time

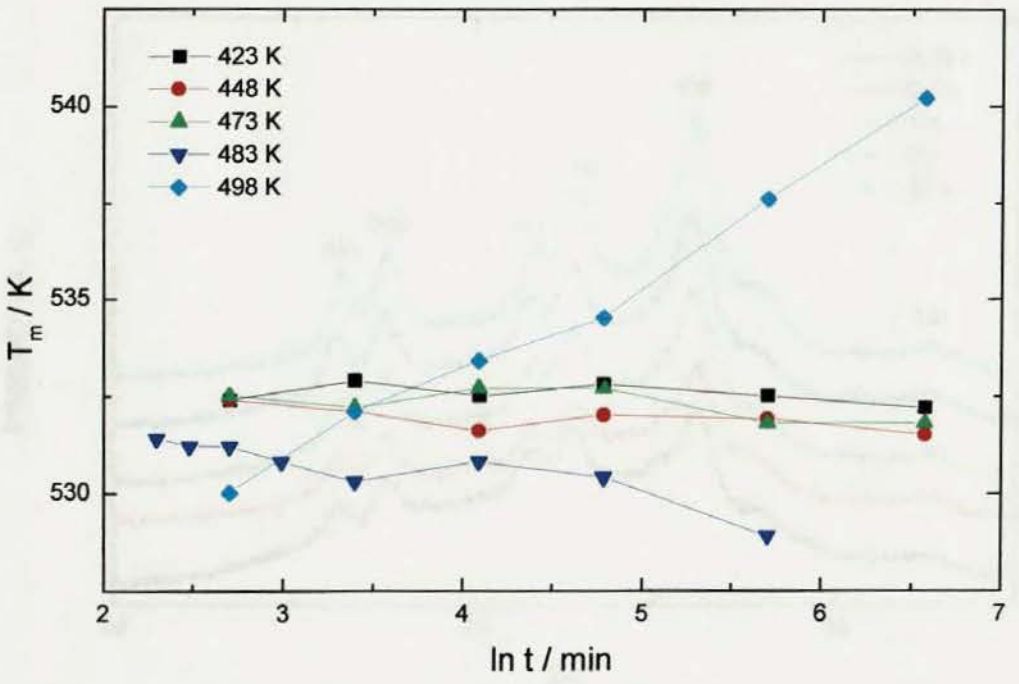

Fig. 6.11 The dependence of the final melting temperature on crystallisation temperature and time

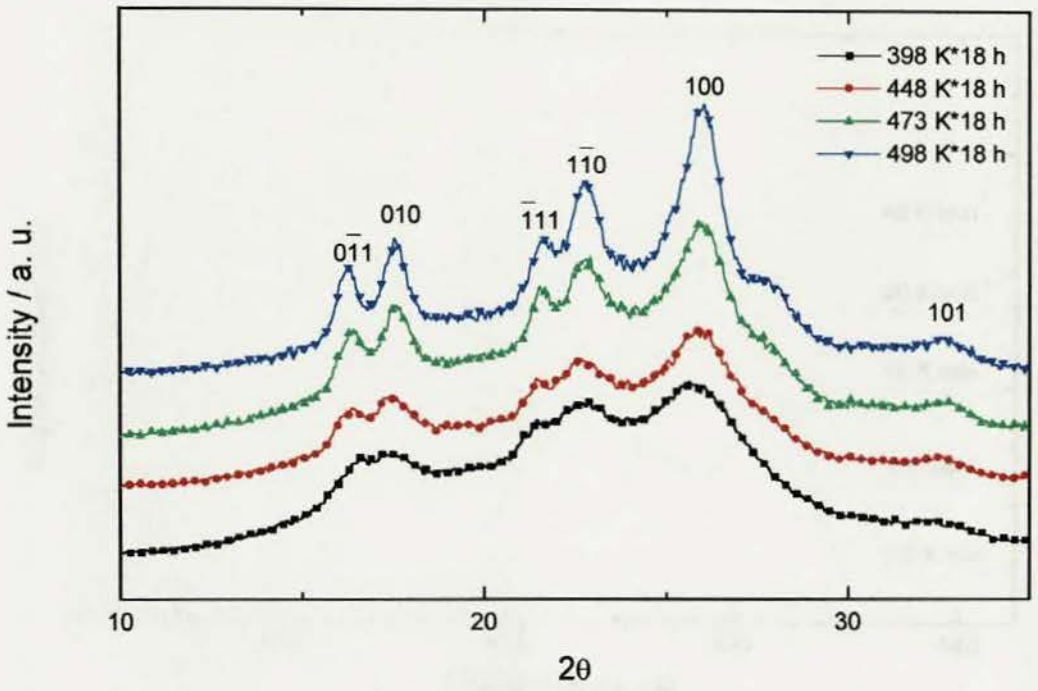

Fig. 6. 12 The evolution of the WAXD pattern of PET as a function of crystallisation temperature

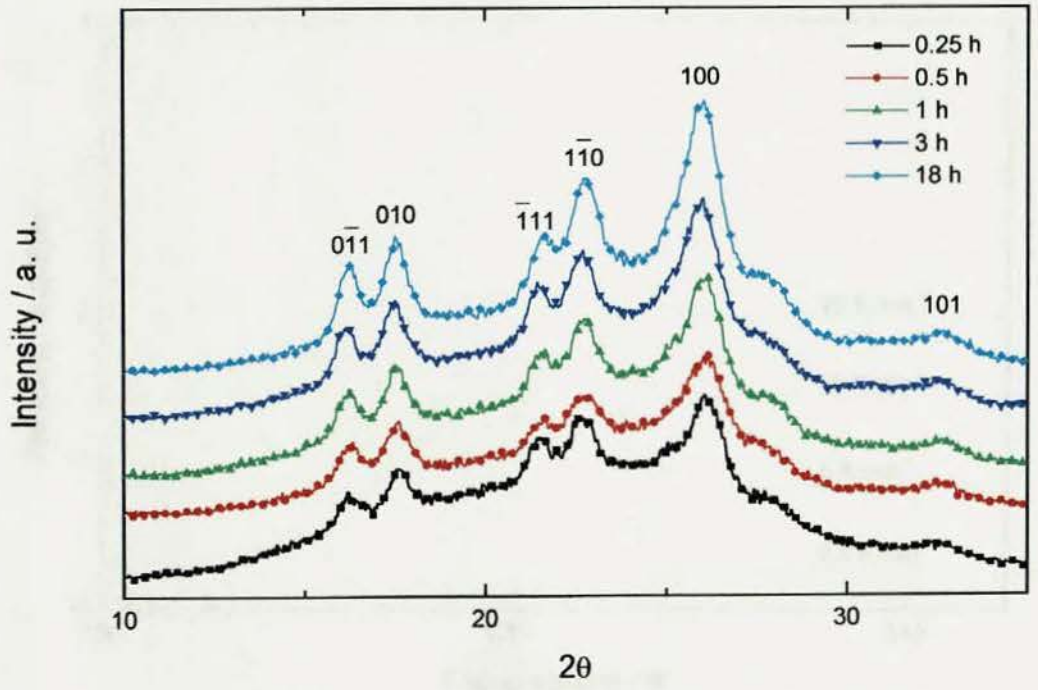

Fig. 6. 13 The evolution of the WAXD pattern of PET as a function of crystallisation time. Samples crystallized at 498 K

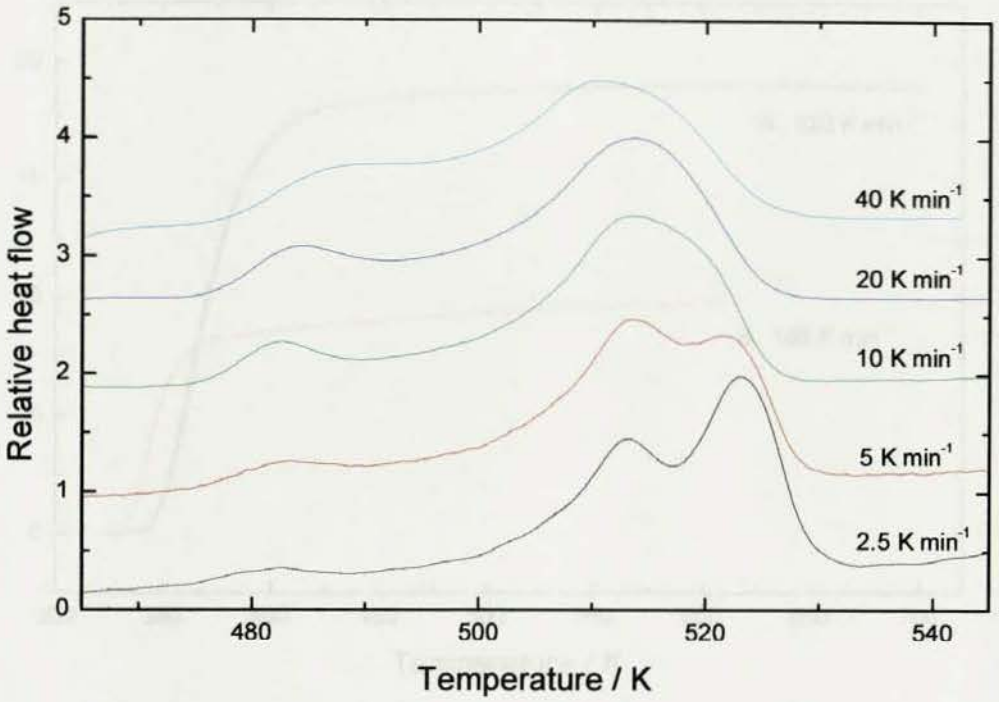

Fig. 6.14 DSC analyses of the melting of the PET crystallised at 473 K for 1 hr at different heating rates

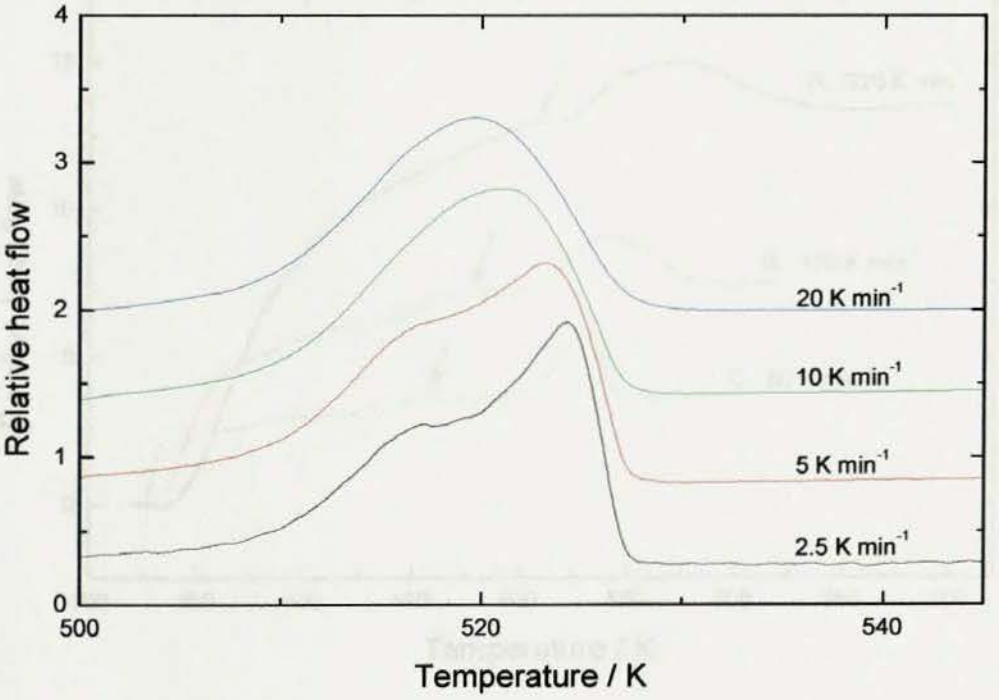

Fig. 6.15 DSC analyses of the melting of the PET crystallised at 498 K for 2 hrs at different heating rates

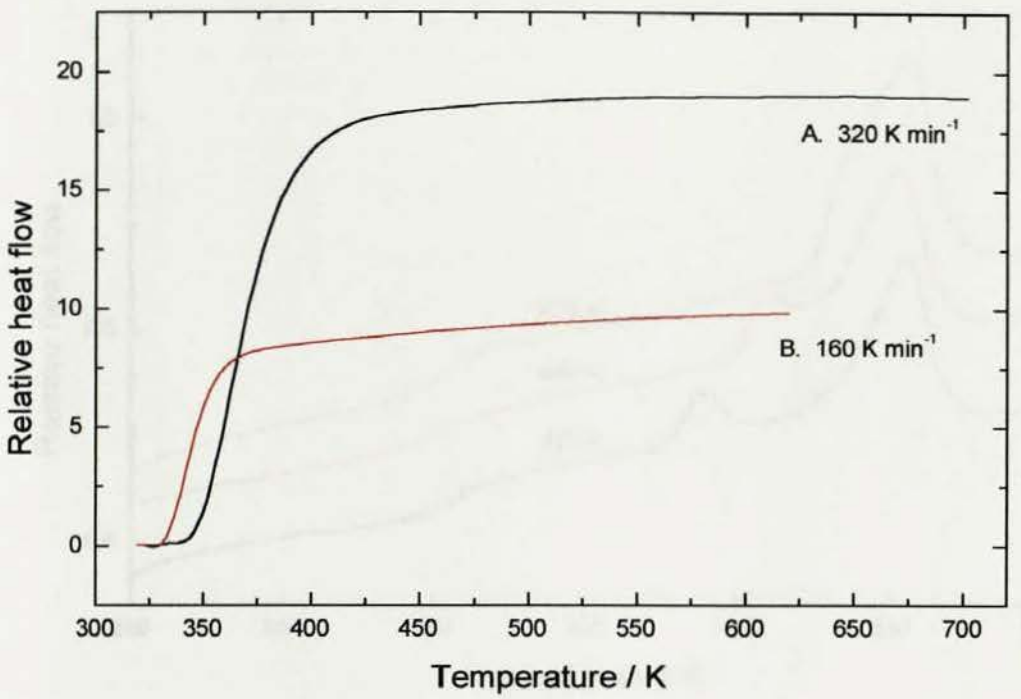

Fig. 6.16a DSC analyses of sapphire at various high heating rates

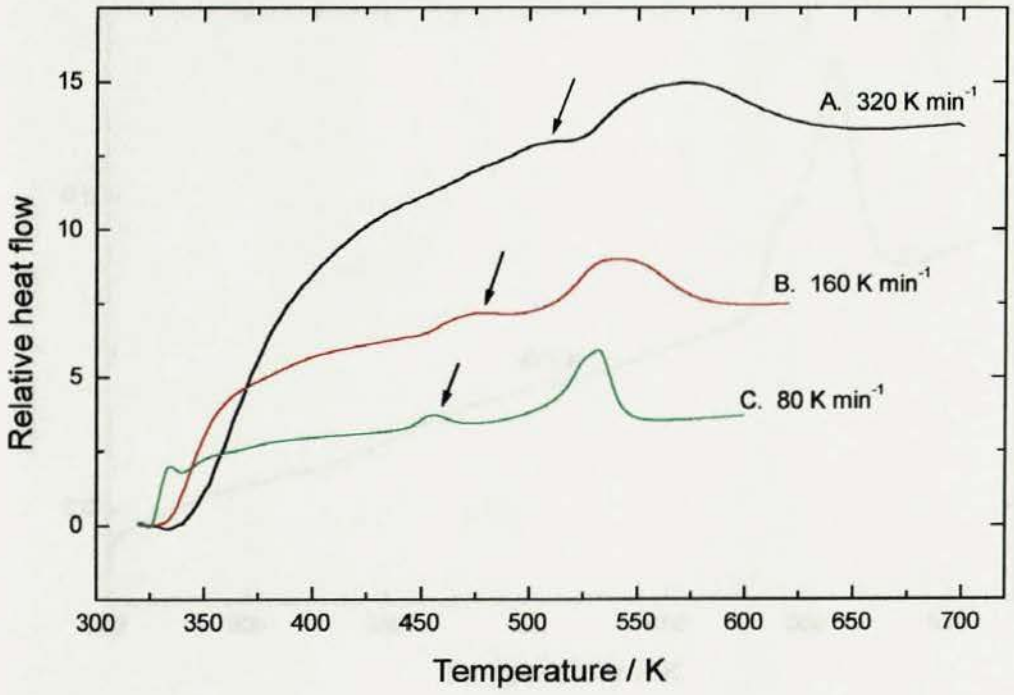

Fig. 6.16b DSC analyses of the melting of PET crystallised at 423 K for 30 min, at very high heating rates

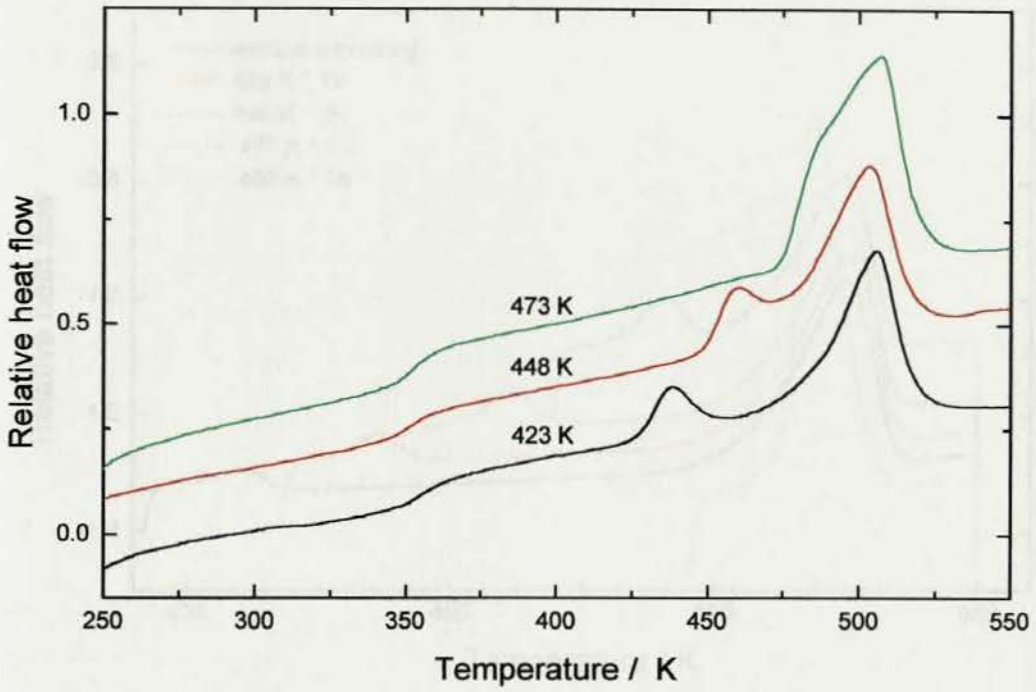

Fig. 6. 17a DSC analyses of the melting of thin film (100 μm) of PET after correcting for thermal lags. Samples crystallised at 423, 448 and 473 K for 30 min. Heating rate 160 K min^{-1}

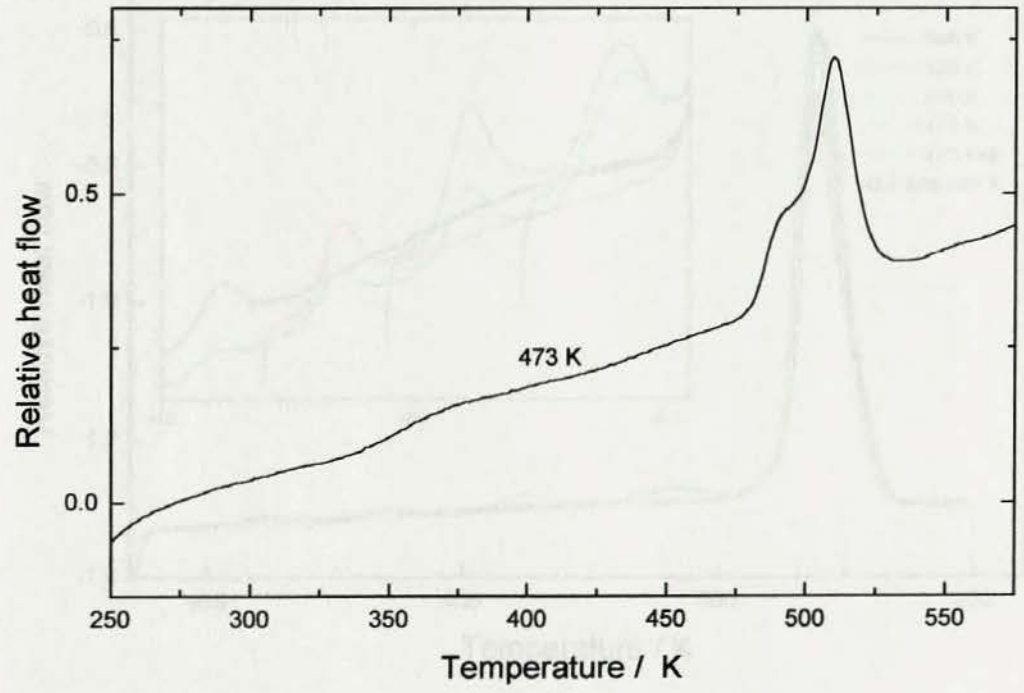

Fig. 6. 17b DSC analysis of thin film (50 μm) of PET after correcting for thermal lag. Samples crystallised at 473 K for 30 min. Heating rate 160 K min^{-1}

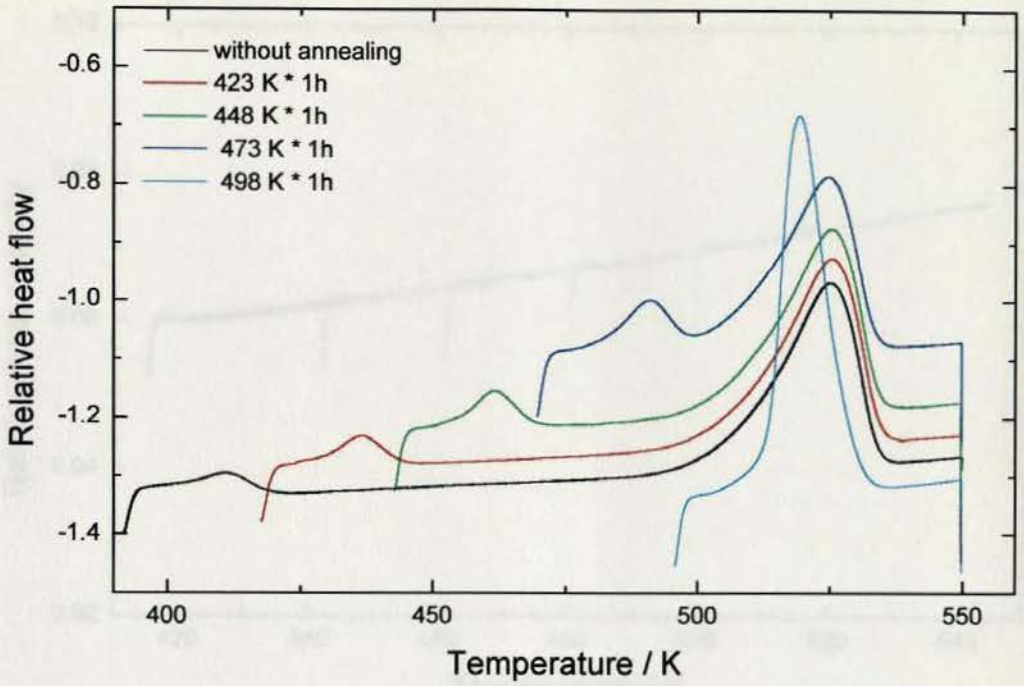

Fig.6.18 DSC analyses of the melting of PET, first crystallised at 398 K for 1hr and annealed at different temperature for 1hr. Heating rate 10 K min^{-1}

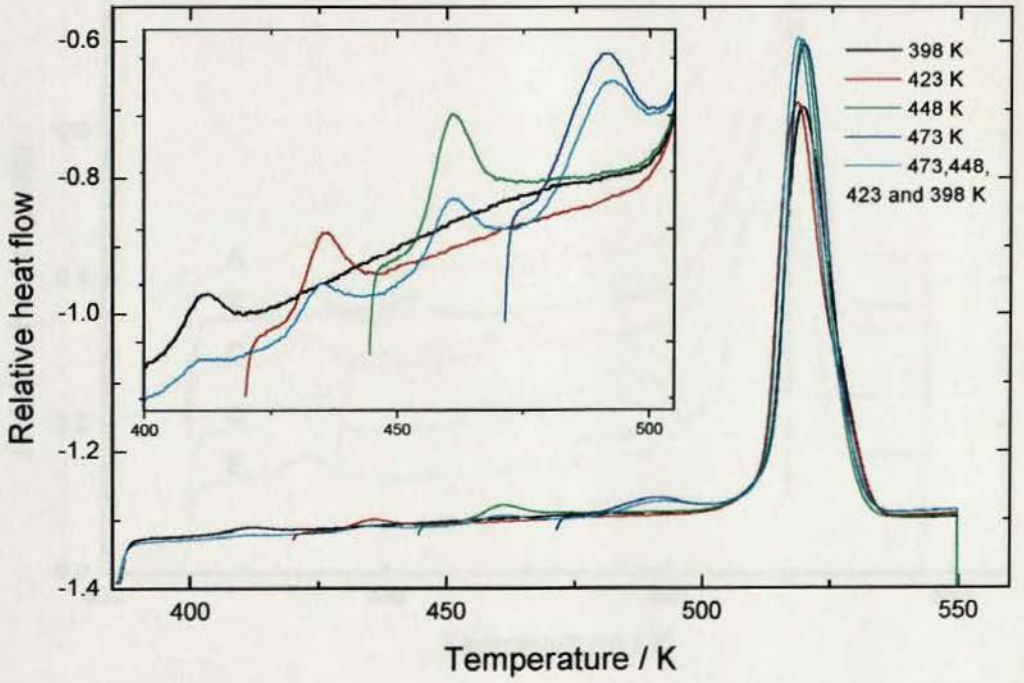

Fig. 6.19 The DSC analyses of the melting of PET, first crystallised at 398 K for 1hr, annealed at 498 K for 1hr,and subsequently annealed at various other temperatures

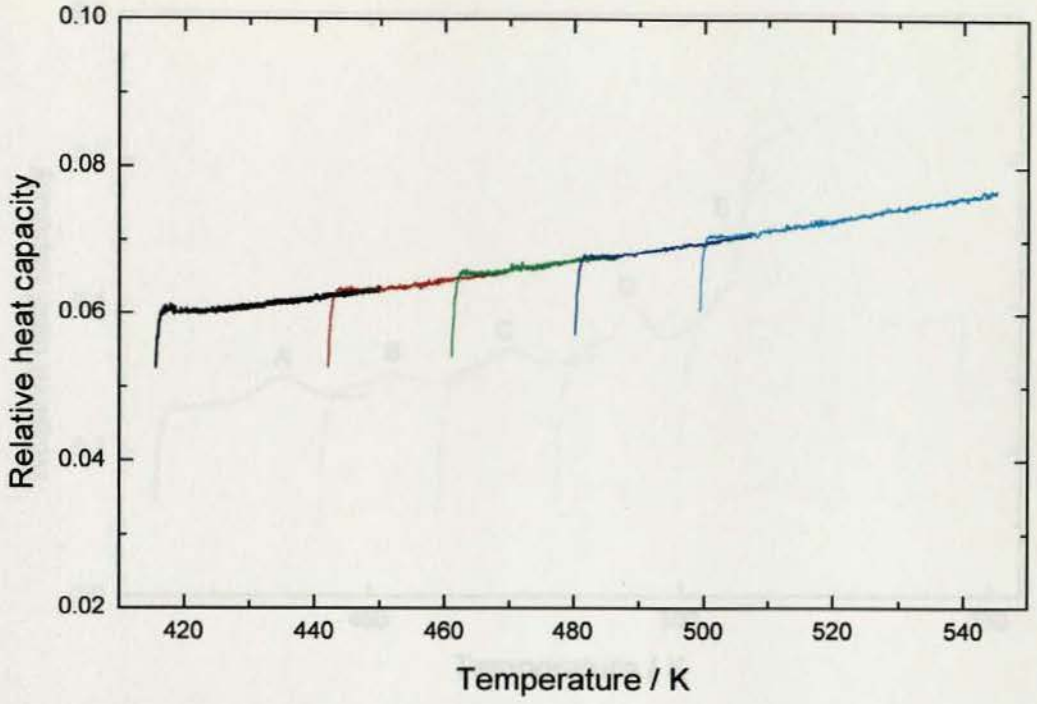

Fig. 6.20 DSC analyses of sapphire by heating in steps. Heating rate 10 K min^{-1}

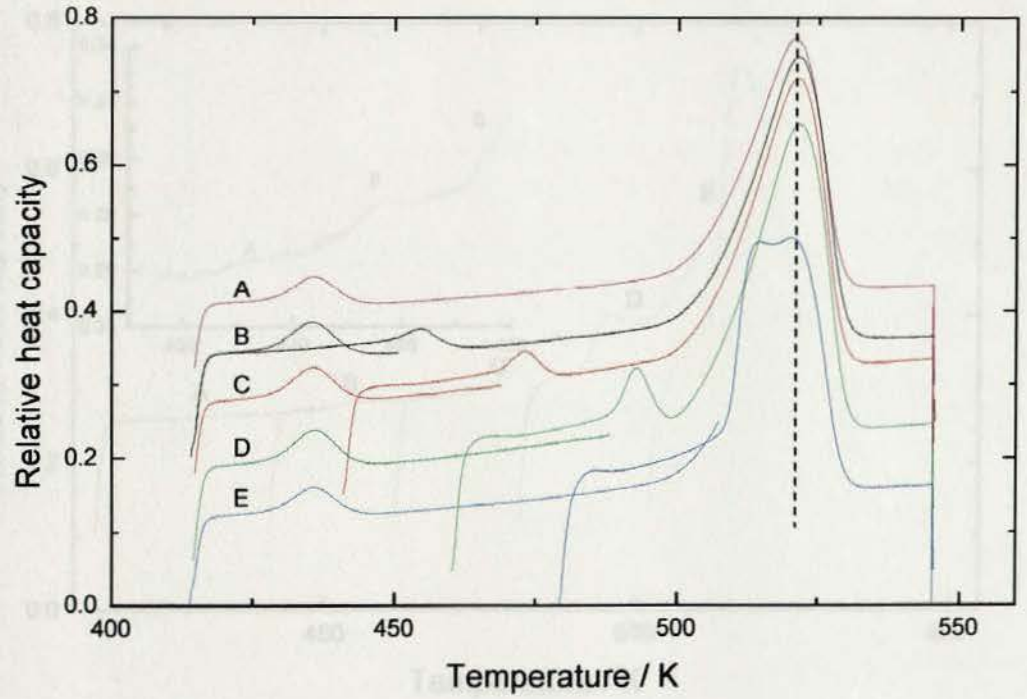

Fig. 6.21 DSC analyses of the melting of PET, crystallised at 423 K for 30 min. After initially heating, then cooling 30 K lower and then heating immediately. A. directly heating; B. initially heating to 450 K; C. initially heating to 470 K; D. initially heating to 490 K; E. initially heating to 510 K. Heating rate 10 K min^{-1}

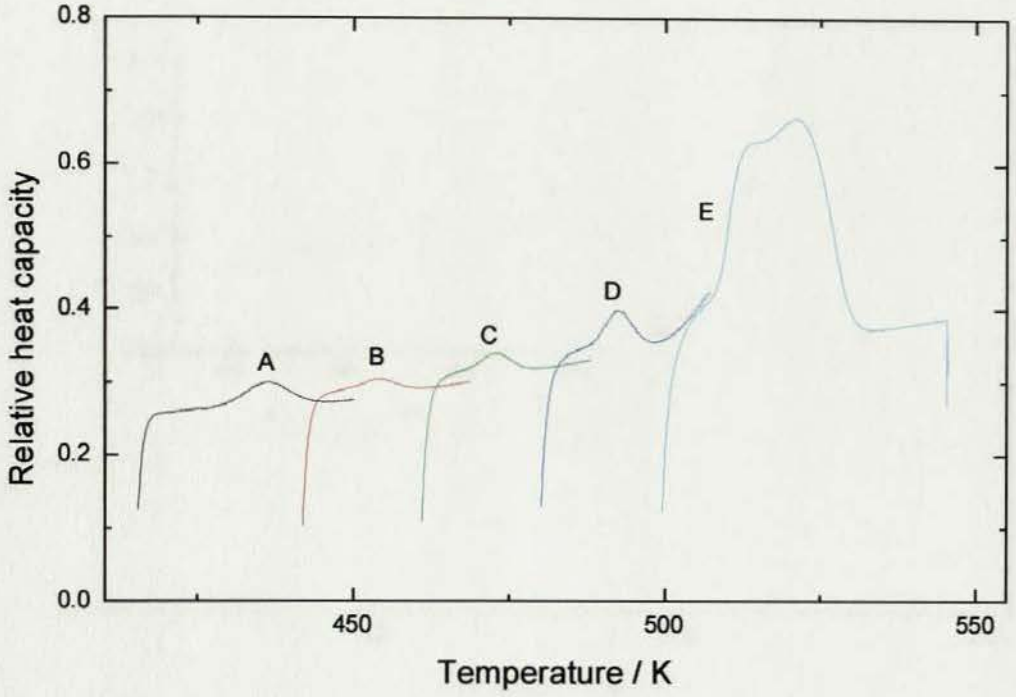

Fig. 6.22 DSC analyses of the stepwise melting of PET crystallised at 423 K for 30 min. After each step heating, cooled 10 K lower and then heated immediately. A. 415 to 450 K; B. 440 to 470 K; C. 460 to 490 K; D. 480 to 510 K; E. from 500 K to melt. The rate of cooling is 160 K min^{-1} and heating rate 10 K min^{-1}

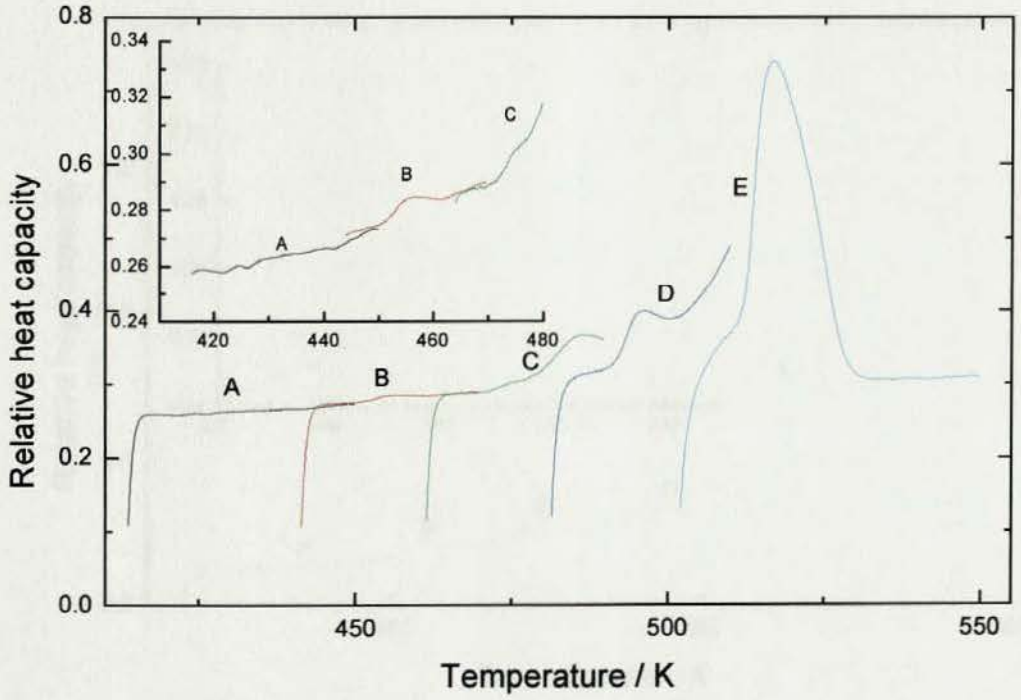

Fig. 6.23 DSC analyses of the stepwise melting of PET crystallised at 473 K for 30 min. After each step heating, cooled 10 K lower and then heated immediately. A. 415 to 450 K; B. 440 to 470 K; C. 460 to 490 K; D. 480 to 510 K; E. from 500 K to melt. The rate of cooling is 160 K min^{-1} and heating rate 10 K min^{-1}

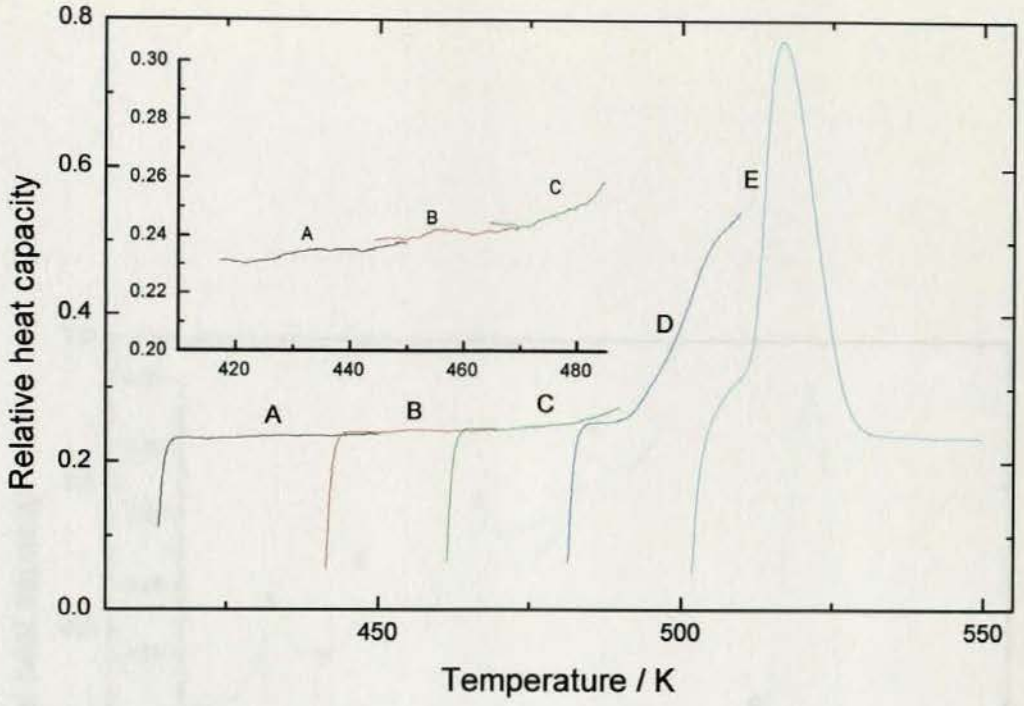

Fig. 6.24. DSC analyses of the stepwise melting of PET crystallised at 473 K for 5 hrs. After each step heating, cooled 10 K lower and then heated immediately. A. 415 to 450 K; B. 440 to 470 K; C. 460 to 490 K; D. 480 to 510 K; E. from 500 K to melt. The rate of cooling is 160 K min^{-1} and heating rate 10 K min^{-1}

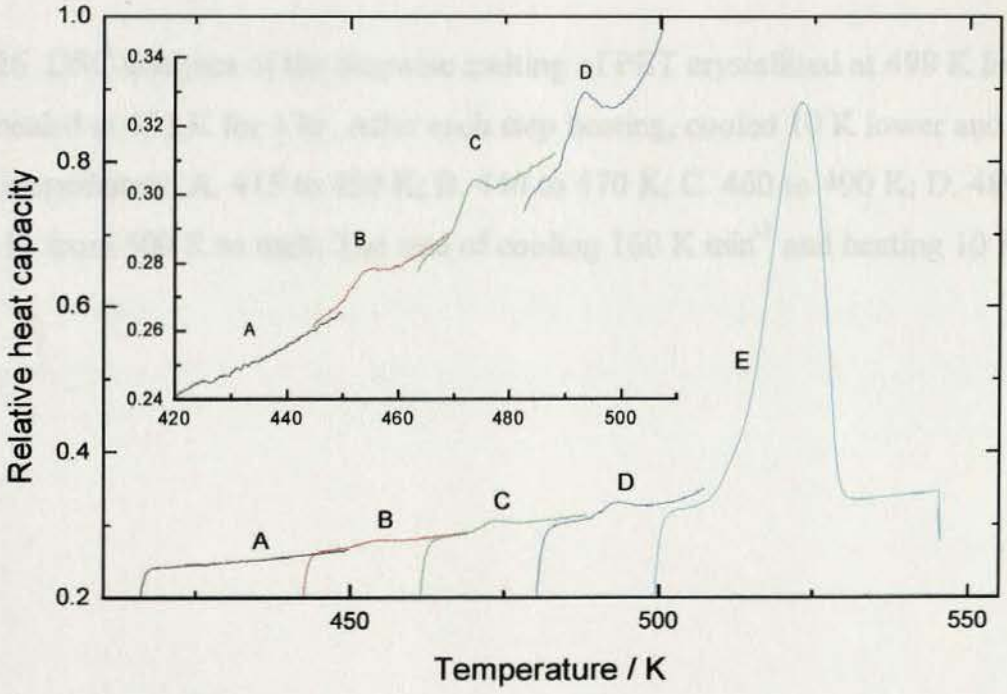

Fig. 6.25 DSC analyses of the stepwise melting of PET crystallised at 498 K for 3 hrs. After each step heating, cooled 10 K lower and then heated immediately. A. 415 to 450 K; B. 440 to 470 K; C. 460 to 490 K; D. 480 to 510 K; E. from 500 K to melt. The rate of cooling is 160 K min^{-1} and heating rate 10 K min^{-1}

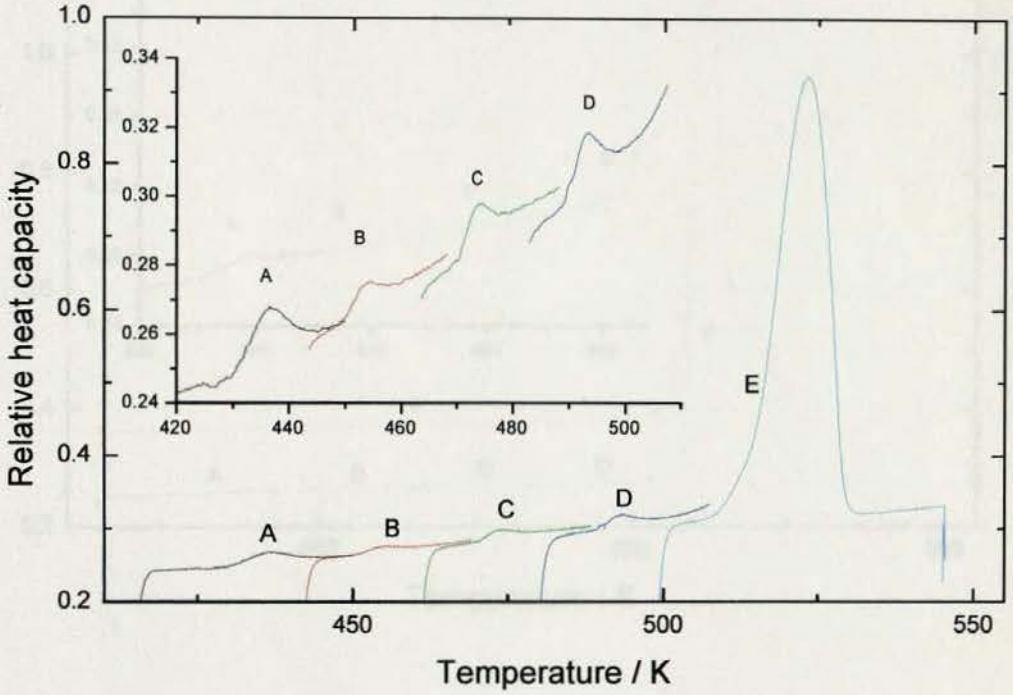

Fig. 6.26 DSC analyses of the stepwise melting of PET crystallised at 498 K for 3 hrs and annealed at 423 K for 1 hr. After each step heating, cooled 10 K lower and then heated immediately. A. 415 to 450 K; B. 440 to 470 K; C. 460 to 490 K; D. 480 to 510 K; E. from 500 K to melt. The rate of cooling 160 K min^{-1} and heating 10 K min^{-1}

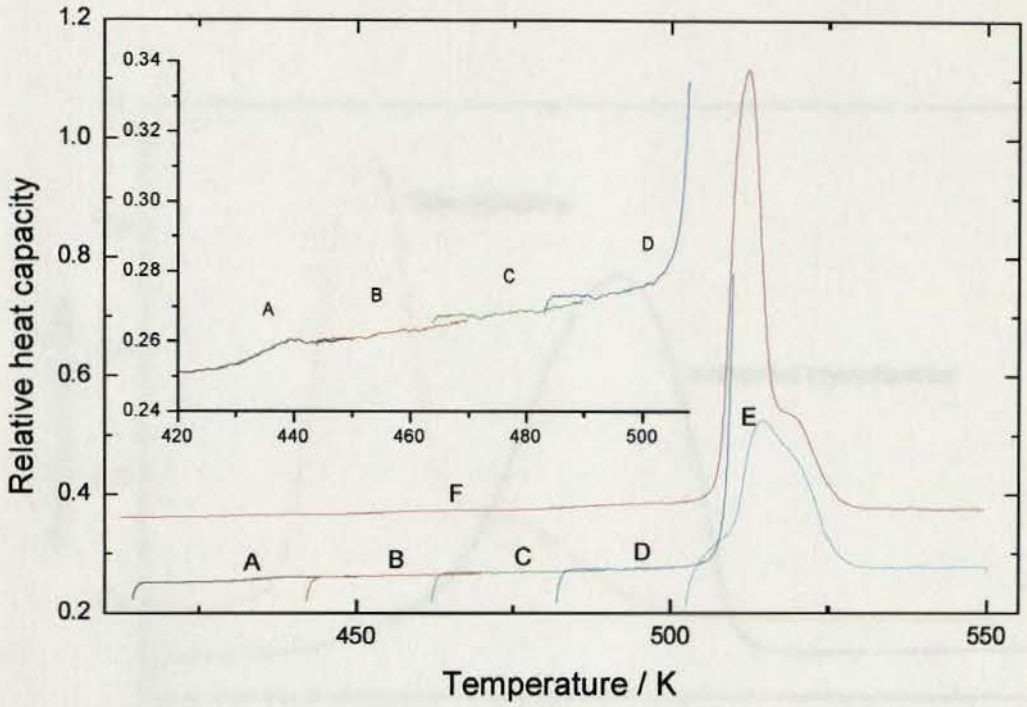

Fig. 6.27 DSC analyses of the melting of PET directly and stepwisely. PET samples were crystallised at 398 K for 30 min, and annealed from 398 to 498 K (heating rate 0.31 K min^{-1}, held at every 10 K increment and annealed for 5 hrs). Stepwise melting sample was cooled to 423 K, held for 5 hrs and stepwisely melting. After each step sample was cooled by 10 K and immediately heated. A. 415 to 450 K; B. 440 to 470 K; C. 460 to 490 K; D. 480 to 510 K; E. from 500 K to melt. Directly melting sample was heated from 400 K to the melt. Cooling rate 160 K min^{-1} and heating rate 10 K min^{-1}

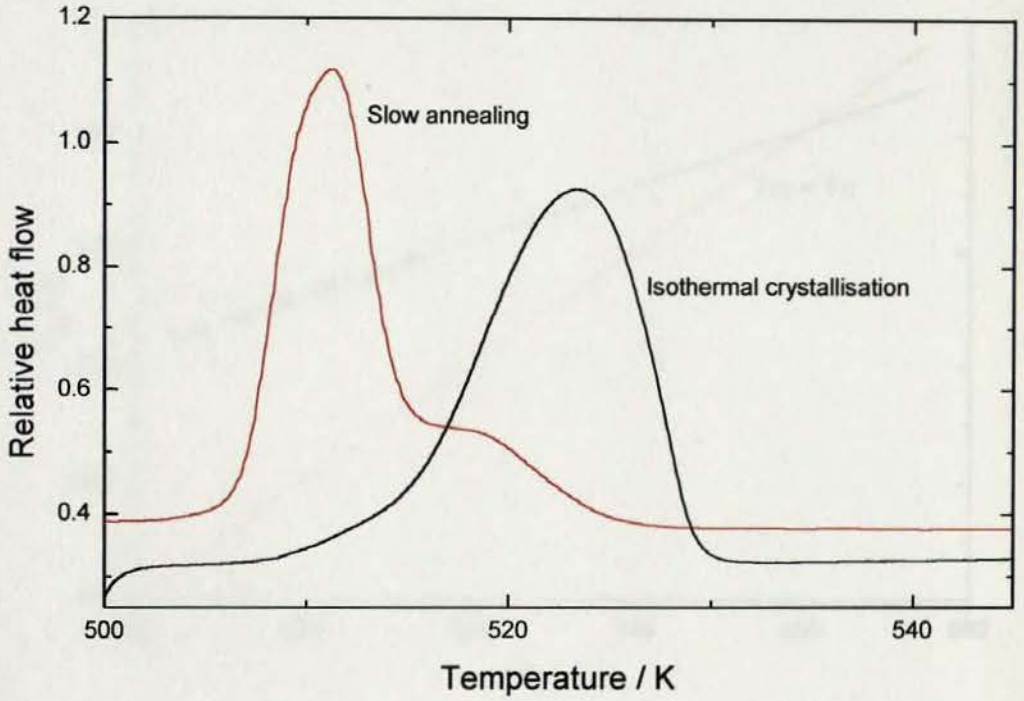

Fig. 6.28 DSC analyses of the melting of the PET with different thermal histories. Isothermal crystallisation sample is the sample E in Fig 6.25; slow annealing sample is the sample F in Fig.6.27. Heating rate 10 K min^{-1}

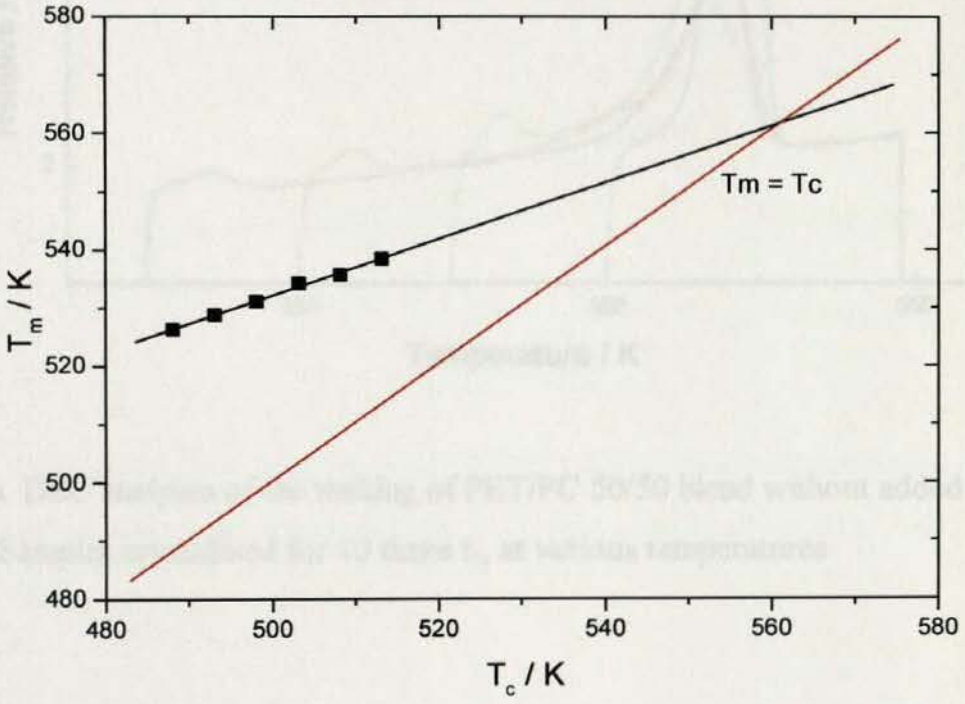

Fig. 6.29 Hoffman-Weeks' plot for PET of observed melting temperature against crystallisation temperature

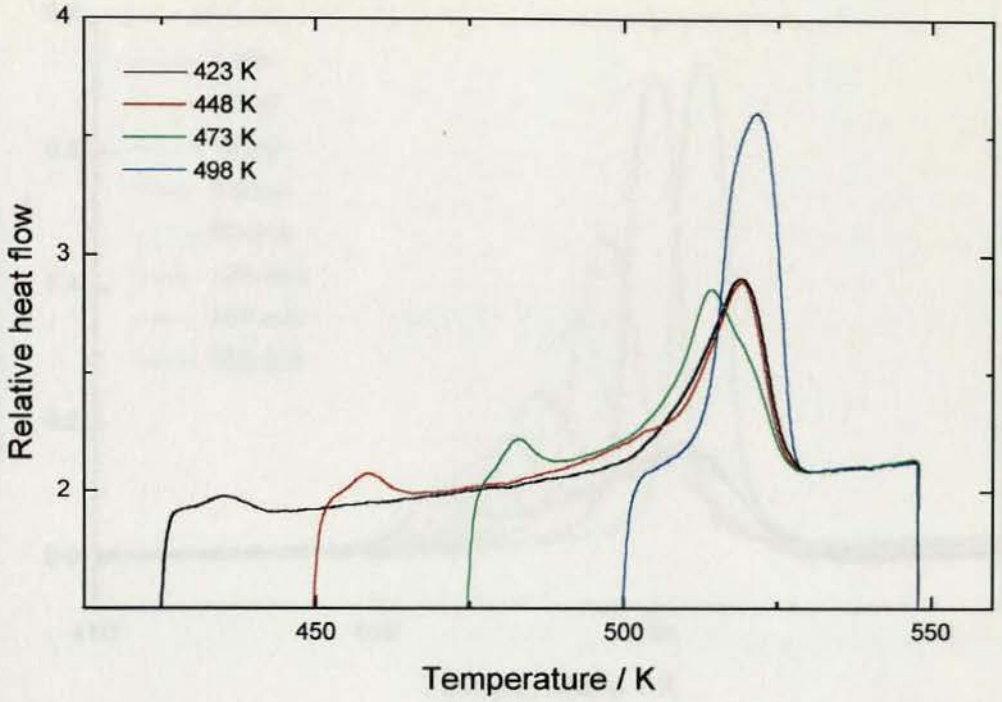

Fig.6.30a DSC analyses of the melting of PET/PC 50/50 blend without added catalyst. Samples crystallised for 10 times $t_{½}$ at various temperatures

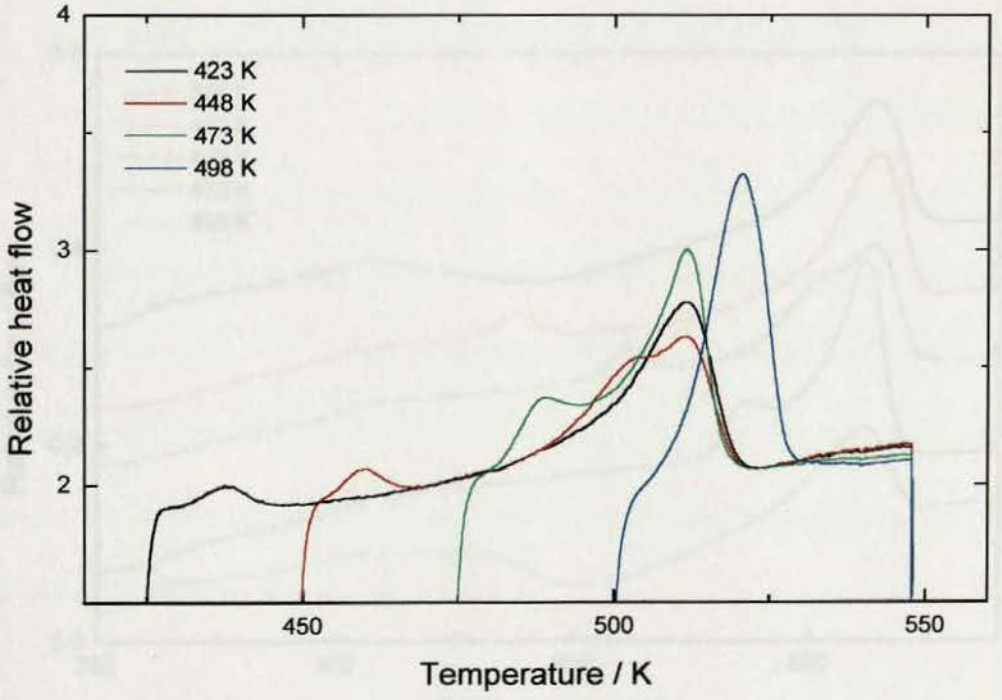

Fig.6.30b DSC analyses of the melting of PET/PC 50/50 blend with added catalyst. Samples crystallised for 10 times $t_{½}$ at various temperatures

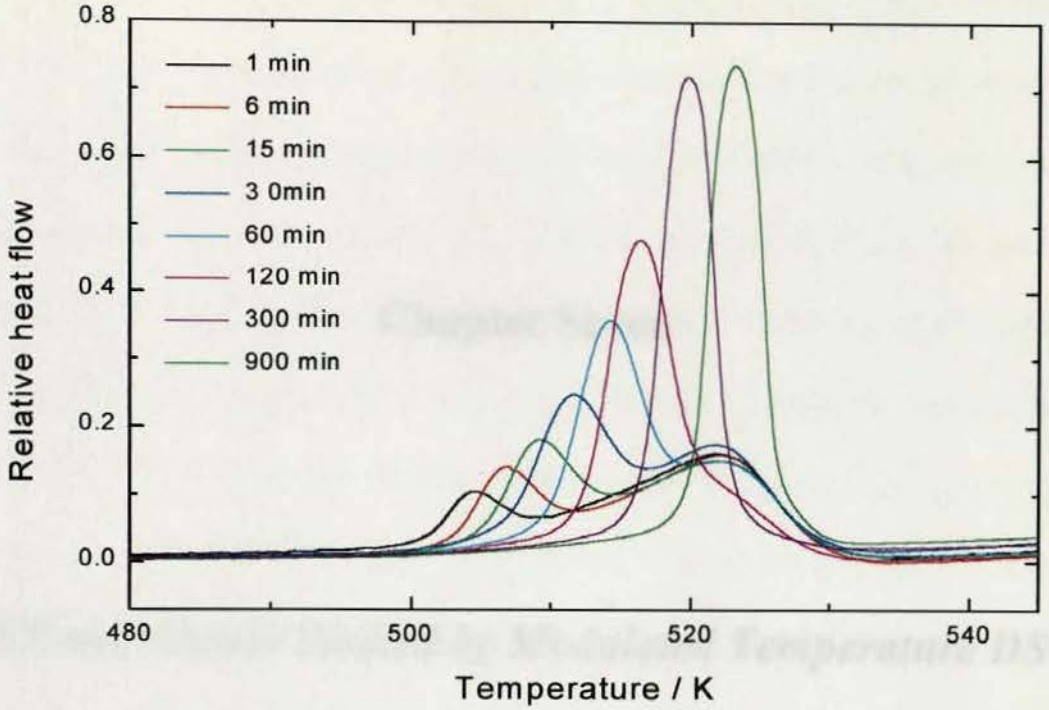

Fig.6.31 DSC analyses of the melting of PET/PC 50/50 blend without added catalyst. Samples heated from room temperature at 20 K min^{-1} and crystallised at 498 K for different times

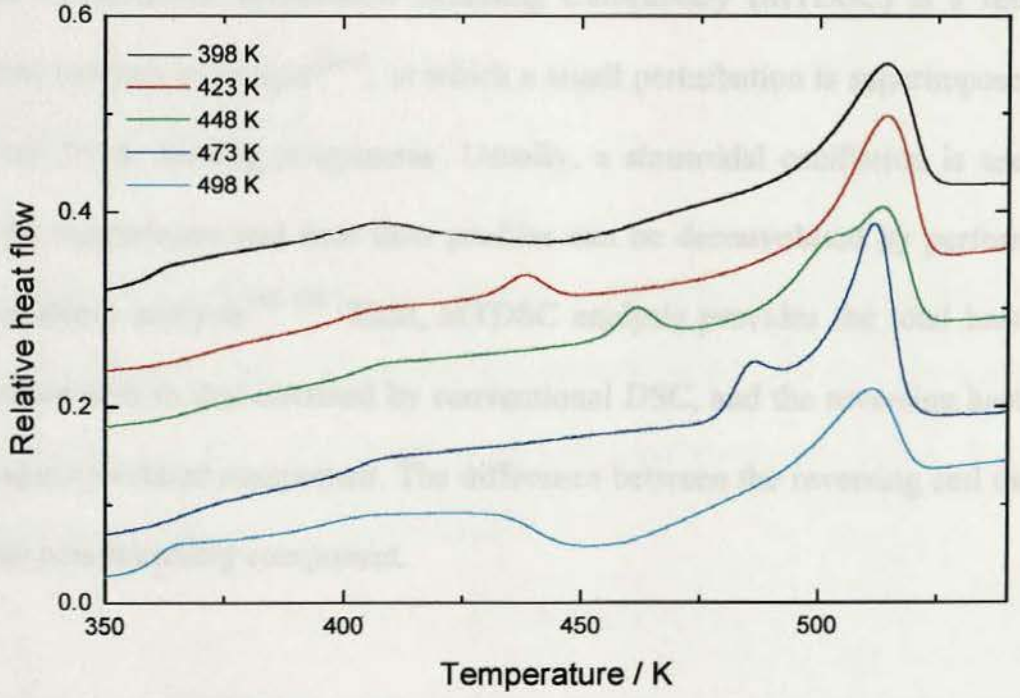

Fig.6.32 DSC analyses of the melting of PET/PC 50/50 blend with added catalyst. Samples crystallised for 1 hr at each temperature

Chapter Seven

PET and Blends Studied by Modulated Temperature DSC

7.1 Introduction

Modulated Temperature Differential Scanning Calorimetry (MTDSC) is a relatively new thermal analysis technique[46-48], in which a small perturbation is superimposed on a conventional linear heating programme. Usually, a sinusoidal oscillation is used, see Fig.7.1. The temperature and heat flow profiles can be deconvoluted by performing a Fourier transform analysis[162-164]. Thus, MTDSC analysis provides the total heat flow, which is equivalent to that obtained by conventional DSC, and the reversing heat flow, the heat capacity-related component. The difference between the reversing and the total signal is the non-reversing component.

At the concept of MTDSC it was claimed that it might become the preferred calorimetric technique for polymer characterisation[47,163] in that compared to

conventional DSC it had an improved sensitivity, was more efficient and accurate in the determination of heat capacities as well as the separation of reversible transitions from irreversible processes. It could separate the glass transition from enthalpy relaxation and recrystallisation. It was also suggested that TMDSC gave better insight into the melting and recrystallisation phenomena of polymers because of these potential capabilities, MTDSC has been used in a wide variety of fields and particularly in the study of polymers, such as absolute heat capacity determination[165,166], thermal conductivity[167,168], glass transition region[169-172], reaction resin curing[173], blend miscibility[174-176] as well as crystallisation and melting[177-185]. From these points of view, MTDSC can undoubtedly be regarded as a valuable extension of conventional DSC.

In this chapter MTDSC prepared from a power compensation DSC has been used to investigate the glass transition of the PET/PC blends, quasi-isothermal crystallisation and the melting behaviour of PET.

7.2 MTDSC Background

The response of DSC under conditions where no significant temperature gradients exist in the sample is a combination of a signal that depends on the heat capacity and kinetic component of the heat flow. The former is reversible and the latter is often, though not always, irreversible. This can be expressed as[162,163]

$$dQ/dt = C_{p,r}dT/dt + dq(t,T) \qquad (7.1)$$

where dQ/dt is the heat flow into the sample, $C_{p,r}$ is the reversing heat capacity of the sample due to its molecular structure and dq(t,T) is some irreversible heat change due to

a irreversible kinetic response, which is a function of time and temperature. In MTDSC, as mentioned above, the temperature programme consists of an underlying change in temperature that is modulated by small sinusoidal perturbation, i.e.

$$T = T_0 + Bt + A_T \sin(\omega t) \tag{7.2}$$

where T_0 is the start temperature, B is the heating rate, A_T is the amplitude of the temperature modulation and ω is the frequency equal to $2\pi/p$ with p the period of the modulation. On differentiating the above equation with respect to time, the rate of heating is

$$dT/dt = B + A_T \omega \cos(\omega t) \tag{7.3}$$

If the experiment is carried out at a sufficient small underlying heating rate and an equally small temperature amplitude, then the measured heat flow is a superposition of two independent signals – an underlying and an oscillating heat flow, i.e.[186]

$$dQ/dt = BC_{p,r} + dq'(t,T) + \omega BC_{p,r} \cos(\omega t) + A_K \sin(\omega t) \tag{7.4}$$

where dq'(t,T) is the average of dq(t,T) over the interval of one cycle when doing so the oscillating effect is eliminated. A_K is the amplitude of the kinetic response to the modulated temperature.

7.2.1 Deconvolution Procedure

By using the Fourier transformation analysis, the modulated signal can be deconvoluted and there are two main methods used. The first method proposed by Reading *et al.*[48] involved deconvoluting the average heat flow into reversing and non-reversing components. The other one by Schawe[164] involved obtained the complex heat capacity

that was separated into the storage (real part) heat capacity and loss (imaginary part) heat capacity.

7.2.1.1 Reading's Method

After deconvolution the average heat flow, $BC_{p,r} + dq'(t,T)$, is the total heat flow which is equivalent to that obtained from conventional DSC. Reversing heat capacity, $C_{p,r}$, is calculated from the modulation amplitudes of heat flow and heating rate, which is analogous to normal heat capacity measurement $C_p = (dQ/dt)/(dT/dt)$, i.e.[165]

$$C_{p,r} = A_{HF} / A_T\omega \tag{7.5}$$

where A_{HF} and $(A_T\omega)$ are the amplitudes of heat flow and heating rate modulations, respectively. By multiplying with the heating rate the reversing heat flow can be obtained. The non-reversing heat flow is the difference between the total heat flow and the reversing heat flow, i.e.

$$\text{non-reversing heat flow} = \text{the total heat flow} - BC_{p,r}$$

$$= dq'(t,T) \tag{7.6}$$

It is obvious that in the above method information on the phase lag (δ), the difference of phase angles between heat flow and heating rate, is neglected. Thus, the method may also be called "simple" deconvolution procedure[186]. Later Reading et al.[187,188] developed this method by introducing a complex heat capacity which is separated into in-phase and out-phase heat capacities using the phase lag. This makes no difference to Schawe' method[164,186].

7.2.1.2 Schawe's Method[164]

Schawe' method is based on "the well-known linear response theory" as he claimed. To simplify, the heat flow under modulation ω and A_T can be expressed as

$$dQ/dt = C_{p,B}B + \omega A_T |C^*| \cos(\omega t - \delta) \tag{7.7}$$

with

$$|C^*| = \sqrt{C'^2 + C''^2} \tag{7.8}$$

where $C_{p,B}$ corresponds to the apparent heat capacity which, in conventional DSC measurement, is determined at a heating rate B. The term $C_{p,B}B$, the average heat flow in Schawe's, is the essentially same as the term $BC_{p,r} + dq'(t,T)$ in Reading's. |C*| is the modulus of complex heat capacity C*. C' and C" are the real and imaginary parts heat capacity respectively. δ is , as mentioned above, the phase angle difference between the heat flow and the heating rate profiles.

The modulus of complex heat capacity, |C*|, can be obtained as $C_{p,r}$ in Reading's by

$$|C^*| = A_{HF} / A_T \omega \tag{7.9}$$

From this value and the phase lag, the real and imaginary parts of heat capacity can be calculated

$$C' = |C^*| \cos\delta \tag{7.10}$$

$$C'' = |C^*| \sin\delta \tag{7.11}$$

In general both components are dependent on the measurement frequency ω. If the phase lag is very small, i.e. $\delta \rightarrow 0$ and then $\cos\delta \approx 1$, thus, the real part of the heat capacity approximates to the reversing heat capacity in Reading's procedure.

7.2.2 Phase Lag

Although in MTDSC it is assumed that the sample responds instantaneously to the sinusoidal temperature change in the range where there is no time dependent phenomenon, this is a somewhat idealised picture. In practice, thermal lags always exist because heat flow requires time. A thermal lag develops among furnace, pan and sample temperatures and it is sample size and heating rate dependent. The observed phase lag can be considered to be superposition of that due to heat transfer (thermal lag) and that of relaxation processes in the sample[189]. To correct for the thermal lag, subtracting the straight line between the starting and the end point of transition was performed[190]. Thus, the phase lag due to transition can be obtained. The experimentally measured phase lag varies in sign for different transitions. Glass transition and melting, typical endothermic events, cause phase lag with positive deviation, whereas the exothermic events, such as crystallisation, lead a phase lag with negative deviation[191].

In this study, the phase lag was determined by shifting heat flow data one point at a time onto the heating rate profile until the best fit is achieved [118].The deconvolution procedure has been used according to Reading's procedure. As already pointed out[164,187,188], the procedure is valid only when the phase lag is small. Normally, this is the case for materials in temperature regions where no transition occurs, or over the glass transition region, during crystallisation and in hindrance of a chemical reaction, but not for melting which usually exhibited a large phase lag. Nevertheless, the data obtained on melting may still be useful in a qualitative fashion[190, 192].

7.3 Results and Discussion

7.3.1 MTDSC Calibration

It has been proposed that the symmetry of the Lissajous diagrams measured under quasi-isothermal conditions can determine whether heating and cooling during MTDSC measurements are reversible[165]. Fig. 7.2a shows Lissajous diagrams of quasi-isothermal heating of sapphire over different modulation periods. It is clear that except for p = 10 s the ellipses are symmetrical and centred around the set-point temperature. The right-hand side of the ellipse represents cooling and the left-hand side for heating. It is obvious for p = 10 s that cooling is poorly controlled, in contrast to heating which is carried out under control. The deconvolution results measured at the other periods are plotted in Fig.s 7.2b to d. The apparent relative reversing heat capacities increased with modulation period, while uncorrected phase lag decreased with modulation period. Obviously the phase lag of sapphire should not contain a materials component and must be completely due to thermal lag since there is no transition occurrence. Thus, the longer modulation period the more time for heat transferring and the less thermal lag. Non-reversing heat flows are independent on modulation period and their values are about 0 as no transition occurring.

Measurements of the C_P values for sapphire by MTDSC at different modulation temperature are shown in Fig.7.3. At all experimental modulation amplitudes the instrument was under control in reversing heating and cooling since the Lissajous diagrams were symmetrical ellipses with a common centre. Measured apparent

reversing signal is almost independent of the modulation amplitude, uncorrected phase lag decreased slightly with decreasing modulation amplitude and like in Fig. 7.2d non-reversing heat flows are zero.

One of the proposed benefits of MTDSC is that heat capacity can be measured more accurately. In conventional DSC, three runs are needed to determined heat capacity – an empty pan, a standard and the sample runs. In MTDSC only one step is needed since $C_{p,r} = A_{HF}/A_T\omega$. Specific heat capacities of sapphire in quasi-isothermal and dynamic heating conditions were measured from 320 to 520 K and the results are shown in Fig.7.4. As can be seen, both MTDSC processes gave similar results and two fit line are parallel to each other and both correlation coefficients are 0.997. By using these calibration equations the heat capacity of the other materials under the same conditions can be obtained.

7.3.2 Glass Transition Study

Polycarbonate (PC) is normally amorphous due to its rigid molecular chains[31]. It is convenient to study its glass transition by MTDSC. Fig. 7.5a is an example of MTDSC analyses of PC at an underlying heating of 2.5 K min^{-1} with p = 60 s and A_T of 1.0 K. The glass transition is readily seen in the modulated analyses. The deconvoluted results are shown in Fig.s 7.5 b to d. The reversing specific heat capacities were independent of the underlying heating rate, and the values of heat capacity were in good agreement with the ATHAS value[193]. Phase lag at constant heating rate went into a maximum at the glass transition region but the increase was little more than the experimental

accuracy i.e. ± 0.03 rad, see Fig. 7.5d. The non-reversing heat flow showed a small endotherm within the glass transition regions, whose size increased with the underlying heating rate. This endotherm is related to enthalpic relaxation – a non-reversing kinetic process also known as physical ageing. Bailey *et al.*[118] have measured the kinetics of enthalpic relaxation by means of the non-reversing specific heat in PET, and found that there were larger errors in MTDSC than conventional DSC due to much lower heating rate required in MTDSC.

The effect of the modulation period on the temperature of the glass transition of PC at an underlying heating rate 2.5 K min^{-1} with A_T = 1.0 K is shown in Fig. 7.6. The glass transition temperature in the reversing curve shifted to lower temperature with increasing modulation period consistent with the cooling rate deceasing with increasing modulation period. The corresponding enthalpy relaxation peak also shifts to the lower temperature. Normally the observed T_g and the cooling rate, C_R, can be described by Arrhenius equation[60], i.e.

$$\ln C_R = A - \frac{\Delta E}{RT_g} \tag{7.12}$$

In MTDSC, the modulation amplitude is $A_T\omega$ thus the plot of ln ($A_T\omega$) *vs.* ($1/T_g$) should be linear with the slope of $\Delta E/R$. The activation energy of PC glass transition obtained from Fig. 7.6d is 850 ± 50 kJ/mol. Bailey[49] found that the frequency dependence of PET measured by MDTSC exhibited a similar dependence to that of DETA and DMTA and all these data can be fitted in the same master curve. In Fig. 7.6c the maximum values of phase lag were constant with changing period. The same conclusion was drawn by Schawe for polystyrene when the modulation periods were not too small[183].

Fig. 7.7 is the deconvoluted MTDSC analyses of PET/PC 70/30 blend prepared without added catalyst. The total heat flow was equivalent to that measured by conventional DSC. Only one glass transition was observed which can be ascribed to that of PET alone, as the other glass transition ascribed to PC was obscured by PET crystallisation[161]. However, the latter transition can readily be observed in the reversing heat capacities of the blends because crystallisation appears in the non-reversing signal only. PET, PC and the blends prepared without and with catalyst are shown in Fig 7.8. For blends prepared without added catalyst two T_gs which were almost the same as those of PET and PC alone were observed. On the other hand, two T_gs which shifted with composition were observed in the blends prepared with added catalyst. Once again it can be seen that blends prepared without added catalyst are completely immiscible and the others are partially miscible. Nevertheless, only one run was required in MTDSC analysis and at least two runs by conventional DSC[161].

7.3.3 Quasi-isothermal Crystallisation

In MTDSC with the underlying heating rate set to zero the process is said to be quasi-isothermal with the average temperature held constant at $T = T_0 \pm A_T$.

Fig.7.9a shows typical heat flow and temperature profiles of quasi-isothermal crystallisation of PET. The deconvoluted results are plotted in Fig.s 7.9b and c. The total and non-reversing heat flows are identical see Fig. 7.9b. Initially, the reversing heat capacity showed a gradual increase with time, reached a maximum value nearly at the end of crystallisation and then decreasing with time. Toda *et al.*[194] have reported

similar changes in PET and Scherrenberg *et al.*[195] in PE. However, the absolute variation in PET is much smaller than in PE. From the change in baseline heat capacity $C_{p,b}$ with crystallisation a progressive decrease in baseline heat capacity with crystallisation would be expected since the heat capacity of the crystalline is smaller that of the amorphous. This implies the reversing heat capacity is not only determined by the baseline heat capacity but also comprised an additional instantaneous excess heat capacity[195]. An explanation for the presence of an excess heat capacity is, as suggested by Wunderlich *et al.*[159,178], that a fraction of the crystalline material present undergoes melting and crystallisation at a specific time and temperature as a consequence of the temperature modulation.

The non-reversing heat flows of PET during quasi-isothermal crystallisation at different temperature are shown in Fig. 7.10. The crystallisation rate of quasi-isotheral decreased with increasing crystallisation temperature. Using the kinetic analysis described in Chapter 4, the crystallisation time dependences were analysed, and the results are listed in table 7.1. There were compared with samples rate measurement made under normal isothermal crystallisation condition. It can be seen that the Avrami exponent was constant at 2.5 ± 0.1 for both quasi-isothermal and isothermal crystallisation, indicating the same crystallisation mechanism was present, and the half-life and composites rate constant showed similar temperature dependence. From Fig. 7.11, it can be clearly seen that the half-lives of isothermal crystallisation were approximately equal within the experiment error to samples crystallised at different DSC block temperatures. The half-lives of quasi-isothermal were different from the isothermal crystallisation only at the

higher temperature. The crystallisation rates were slower in quasi-isothermal and this may reflect some underlying melting/recrystallisation occurring in modulation.

The half-life is usually related to the crystallisation temperature using the relationship[86]

$$\ln(1/t_{1/2}) = C - (\frac{4\sigma\sigma_e}{R\Delta H_f})\frac{T_m^o}{T_c(T_m^o - T_c)} \qquad (7.13)$$

Such a plot of $\ln(1/t_{1/2})$ *vs* $\frac{T_m^o}{T_c(T_m^o - T_c)}$ should be linear with a slope equal to $\frac{4\sigma\sigma_e}{R\Delta H_f}$.

These plots are shown in Fig.7.11. The surface energy, σ_e, was obtained from the slope by assuming[87] $\sigma = 0.1\Delta H_f$. Values of 16.3 ± 1.4 and 11.3 ± 1.0 kJ/mol for quasi-isothermal and isothermal crystallisation were obtained respectively. However, the larger surface energy observed for the quasi-isothermal crystallisation process was attributed to melting and recrystallisation occurring in the quasi-isothermal process, consequently, the apparent increase in surface energy is not considered significant. Goderis *et al.*[196] have found that reversible reversing melting and crystallisation did not take place on the lateral surface, i.e. the crystal growth surface, but on the fold surface of lamellar crystallites. Thus, the crystallisation rate was affected by the modulation temperature.

An attempt was made to relate crystallisation rate and modulation parameters. However, the results indicated that the crystallisation appears to be independent of the modulation parameters, see Table 7.2. This might be due the instability of PET or some other reasons that is not clear at present but needs to be further investigated.

7.3.4 Melting Studied By MTDSC

7.3.4.1 Effect of Modulation Period and Temperature on Melting

Fig. 7.13 shows the effect of modulation period on the melting of PET, as can be seen the total heat flow was independent of the oscillation periods. Similar to conventional DSC, a very small endotherm appeared just above the crystallisation temperature and two other endotherms appeared above 500 K. The reversing heat capacity increases linearly with temperature up to 475 K, thereafter an endotherm which increases in size with the period is present. In Fig. 7.13c a very small non-reversing endotherm was present just above T_c and with increase temperature an exotherm appeared, which also increased in size with periodicity. On the contrary, the final melting endotherm decreases in size with increasing periodicity. This is obviously due to an increase in reversing component during the melting process with increasing the modulation periods. Thus when p was equal to 75 s even no melting endotherm was observed in no-reversing melting signal. As mentioned previously phase lag increases largely in the melting zone, indicating mismatch between heating and cooling.

The effects of modulation amplitude on the melting are shown in Fig.s 7.14 to 7.16 for modulation periods of 30, 60 and 90 s respectively. At each period the total heat flow was invariant with the change of modulation temperature. On the other hand, the reversing heat capacity increased with decreasing modulation amplitude from above T_c. In the non-reversing signal the recrystallisation exotherm increased and final melting endotherm decreased in size with decreasing temperature amplitude. When p = 30 s

small recrystallisation exotherm was observed only at A_T = 0.2 K because of too small periodicity leading to less recrystallisation. When p = 60 s recrystallisation exotherm can be observed in each of A_T, and at A_T = 0.2 K the final melting endotherm was completely disappear and large exotherm was exhibited, see Fig.7.15c. When p = 90 s even more large recrystallisation exotherms were present and the final melting endotherm can be observed only at A_T = 1 K, clearly due to too large modulation period causing large amount of recrystallisation.

The above experiments demonstrate that change of modulation parameters will shift the kinetic behaviour of the reversing melting and recrystallisation. Increasing the modulation period or decreasing modulation amplitude increases the reversing heating and cooling, thus, increase the reversing heat capacity and non-reversing exotherm.

7.3.4.2 The Effect of Crystallisation on Melting

MTDSC analyses of the PET samples crystallised at different temperatures for 1 hr are shown in Fig. 7.17. Average heat flows showed different features because of the difference in the crystallisation temperature, T_c, but the reversing heat capacity was the same for temperatures below 400 K, the lowest T_c. Thereafter, it showed gradual deviation up to 475 K but the deviation was less than 15%. Above 475 K considerable deviation occurred. For the sample crystallised at 498 K this deviation did not take place until above 500 K. Non-reversing heat flow showed differences. A small endotherm appeared just above the T_c. The net exotherms were present at around 500 K except for the sample crystallised at 498 K. The phase lag exhibited an identical tendency to the

reversing heat capacity. This clearly indicated that reversing melting and recrystallisation started above T_c, but most of it occurred above 475 K, especially at about 500 K.

MTDSC analyses of the sample crystallised at 495 K for different times are shown in Fig. 7.18. All the samples exhibited two endotherms in their average heat flow, and an endotherm at lower temperature shifts to higher temperature increasing in size with crystallisation time. It is interesting to note that the temperature of reversing heat capacity deviating from linearity, the temperature of exotherm and the temperature of phase lag increasing obviously all jointly shift to higher temperature with prolonging crystallisation time. This change was related to sample histories. With prolonging crystallisation time the crystals become more perfect, and the temperature of the onset of melting and recrystallisation moved to high temperature. At the longest crystallisation time, 900 min, there was no exothermic peak in the non-reversing signal, indicating crystal perfection was much higher.

Fig. 7.19 shows the MTDSC analyses of stepwise crystallised PET samples. Several quite small endotherms, corresponding to each crystallisation temperature appeared in the non-reversing signal. The much smaller deviation (less than 5%) in the reversing heat capacity was observed at temperatures below 475 K, which were exactly the same as Fig. 7.17b. Once again, it was found that the reversing heat capacity and phase lag increase considerably from 500 K.

In MTDSC the reversing heat capacity consisted of a baseline heat capacity ($C_{p,b}$) and an excess heat capacity($C_{p,e}$)[195]. The baseline heat capacity is the sum of each component heat capacity[181], i.e.,

$$C_{p,b} = \sum_i W_i C_{P,i} \tag{7.14}$$

where $C_{p,i}$ is the heat capacity of the i^{th} individual phase with weight fraction W_i. Normally the baseline heat capacity shows a linear relationship with temperature. Therefore, the deviatation from linearity represents the excess heat capacity, i.e. the heat capacity due to melting and recrystallisation. For PET the excess heat capacity is always small at temperatures below 475 K and increased greatly as the temperature increased above 500K although this depended on sample history. This clearly indicated that only a small part of the crystals underwent reversing melting and recrystallisation below 475 K while a large amount underwent this process above 500 K. It confirmed the conclusion drawn in the last chapter of a dual population of crystals present in PET. Thinner lamellae melt at lower temperature (just above T_c) as shown by the small endotherm in the non-reversing signal, in the mean time partial melting and recrystallisation occur, with appearance of slowly increasing $C_{p,e}$ and phase lag. At higher temperature, the primary lamellae also start to reorganize in the appearance of considerably increasing $C_{p,e}$ and phase lag as well as a net exotherm peak in non-reversing signal.

7.4 Conclusions

Under all experimental conditions chosen except for p = 10 s the Lissajous diagrams were symmetrical and the glass transition temperature of PC measured by MTDSC was in good agreement with the value of ATHAS databank. This indicated that the power compensation DSC could be successfully adapted to MTDSC. MTDSC was also proved to be a powerful tool to separate the glass transition from other thermal events. The study of PET/PC blends confirmed that the blends prepared without added catalyst are completely immiscible while the blends prepared with added catalyst are partially miscible.

The kinetics of quasi-isothermal crystallisation was affected by modulation. It was found that the crystallisation rate of quasi-isothermal PET is slower than the normal isothermal crystallisation, although the Avrami exponent is the same as for normal crystallisation. The exact crystallisation mechanism and the modulation parameter effect on the quasi-isothermal crystallisation need to be further investigated.

Increasing the modulation period or decreasing modulation temperature improve the reversing heating and cooling, thus increase the reversing heat capacity and decreasing non-reversing melting. Although it is a problem that quantitatively explains melting by MTDSC, it still clearly indicates that reversing melting and recrystallisation take place in the melting process. At relatively lower temperatures a small amount of reorganization process is present mainly due to the thinner lamellae, and at higher temperature a large amount of reorganization occurs which is due to the primary lamellae.

Table 7.1 Comparison of the Avrami parameters of PET obtained quasi-isothermally with isothermal crystallisation

Sample	Temperature K	$t_{1/2}$ min	n ±0.1	Z $min^{-n}.10^{-4}$
Quasi-isothermal	488.2	6.1	2.4	90.4
	490.0	8.2	2.5	36.0
	491.8	12.4	2.6	9.95
	493.7	15.5	2.6	5.57
	495.6	19.9	2.6	2.91
Isothermal	487.0	5.6	2.5	93.4
	489.1	6.6	2.5	61.5
	491.1	10.0	2.4	27.6
	493.0	11.0	2.4	22.0
	495.1	13.5	2.5	10.3
	497.0	17.4	2.4	7.35

* DSC block temperature is 243 K.

For quasi-isothermal crystallisation p = 60 s and A_T = 1.0 K

Table 7.2 Avrami parameters for PET quasi-isothermal crystallisation under different amplitudes and periods

A_T K		P s	45	60	75	90
	T_c, K		490.10	490.11	490.15	490.00
1	n		2.4	2.4	2.3	2.2
	$t_{1/2}$, min		11.7	10.8	9.8	10.7
	T_c, K		490.13	490.14	490.14	490.05
0.5	n		2.4	2.2	2.2	2.2
	$t_{1/2}$, min		8.2	11.9	7.7	7.8
	T_c, K		490.13	490.14	490.00	490.07
0.25	n		2.4	2.3	2.1	2.1
	$t_{1/2}$, min		10.9	11.8	7.6	10.4

* DSC block temperature 243 K

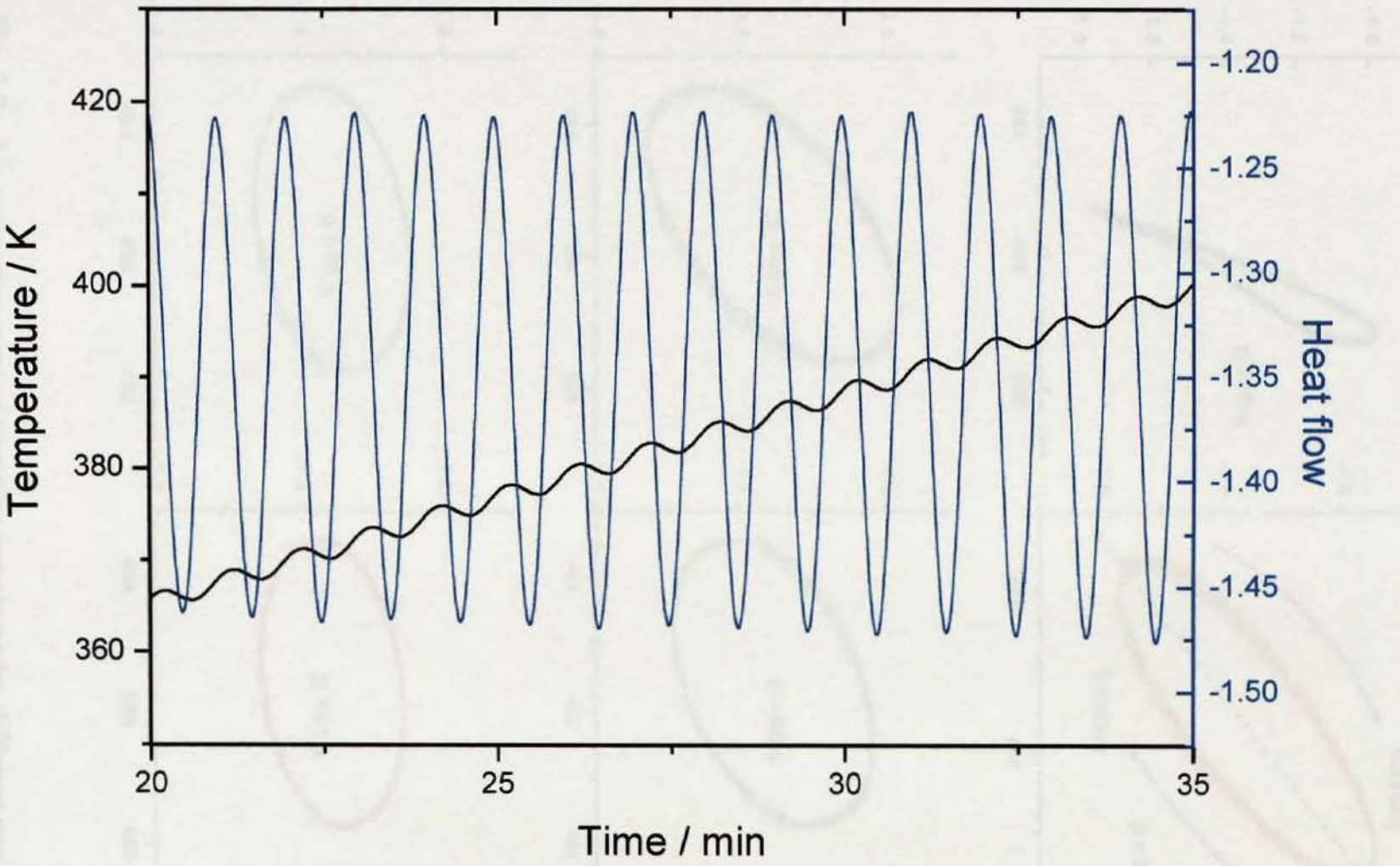

Fig. 7.1 MTDSC signals change with heating

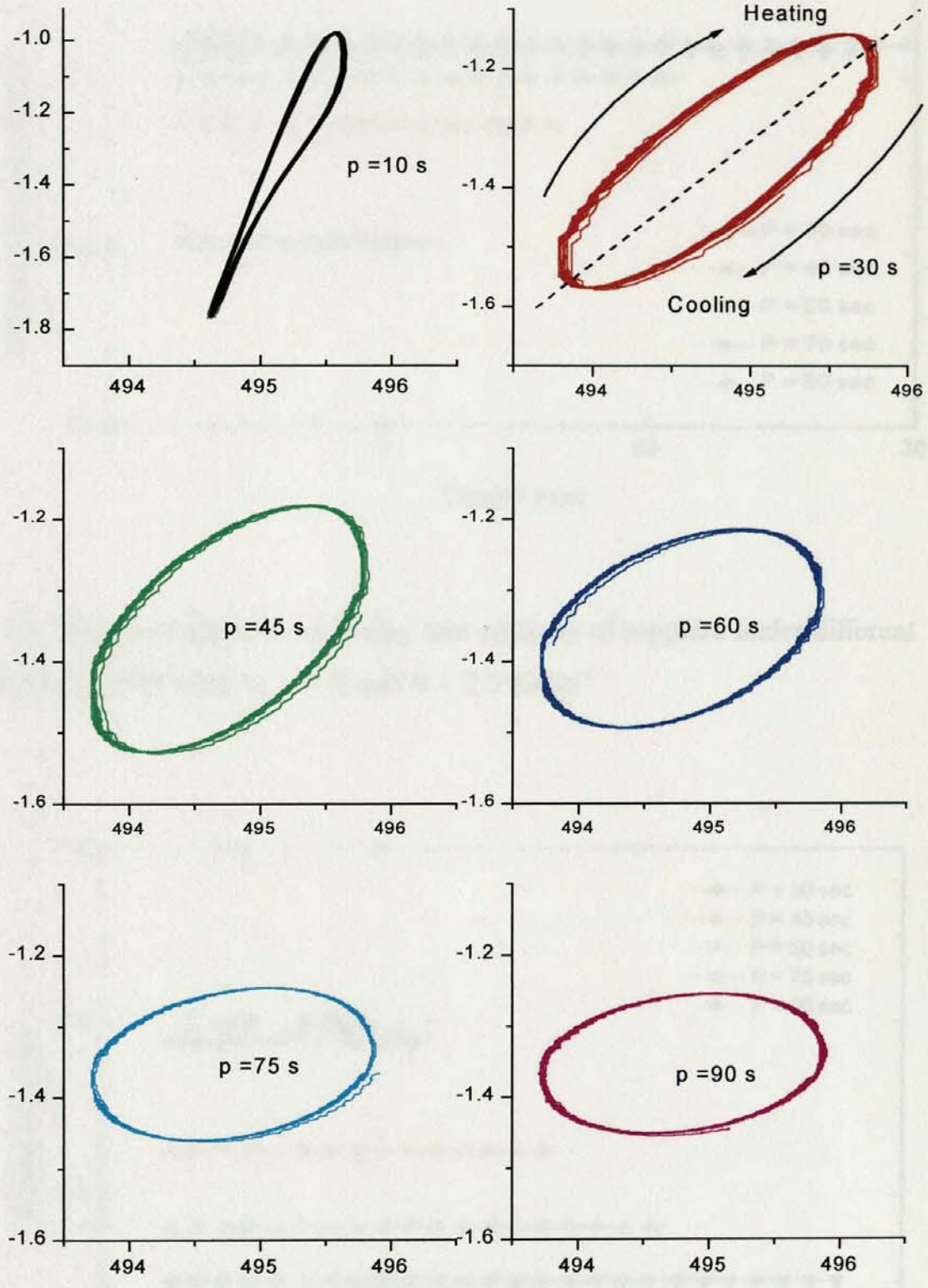

Fig. 7.2a. Lissajous diagrams of sapphire sample under different periods

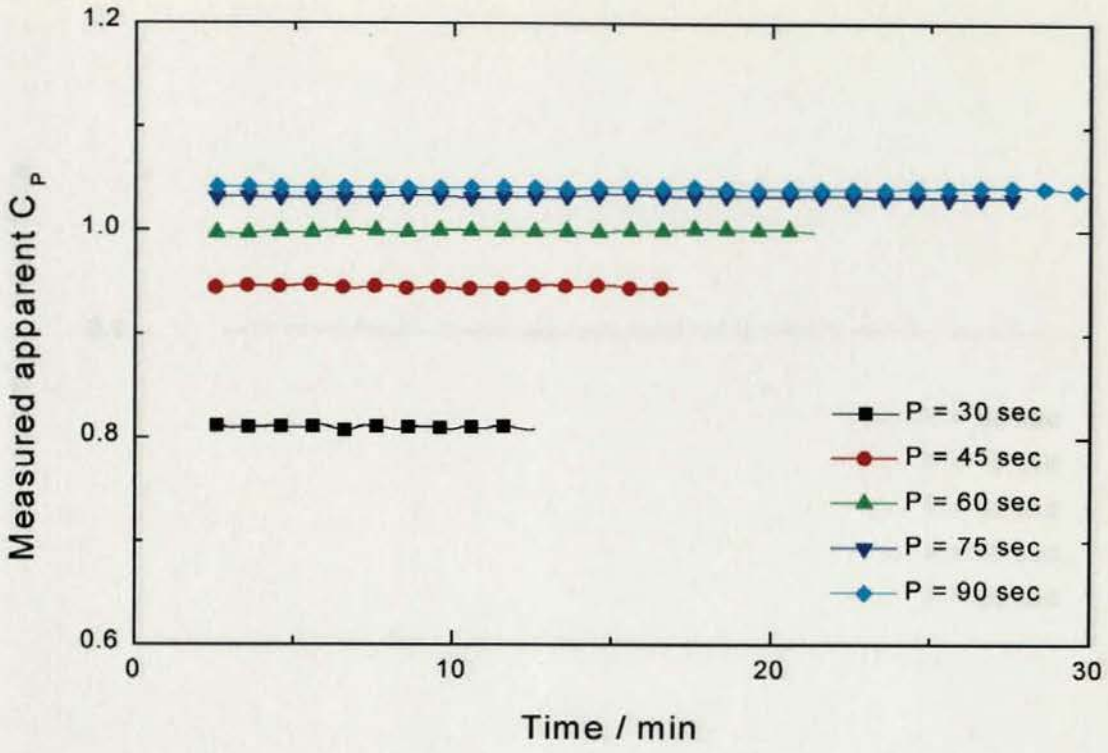

Fig. 7.2b Measured apparent reversing heat capacity of sapphire under different modulation periods with A_T = 1 K and B = 2.5 $Kmin^{-1}$

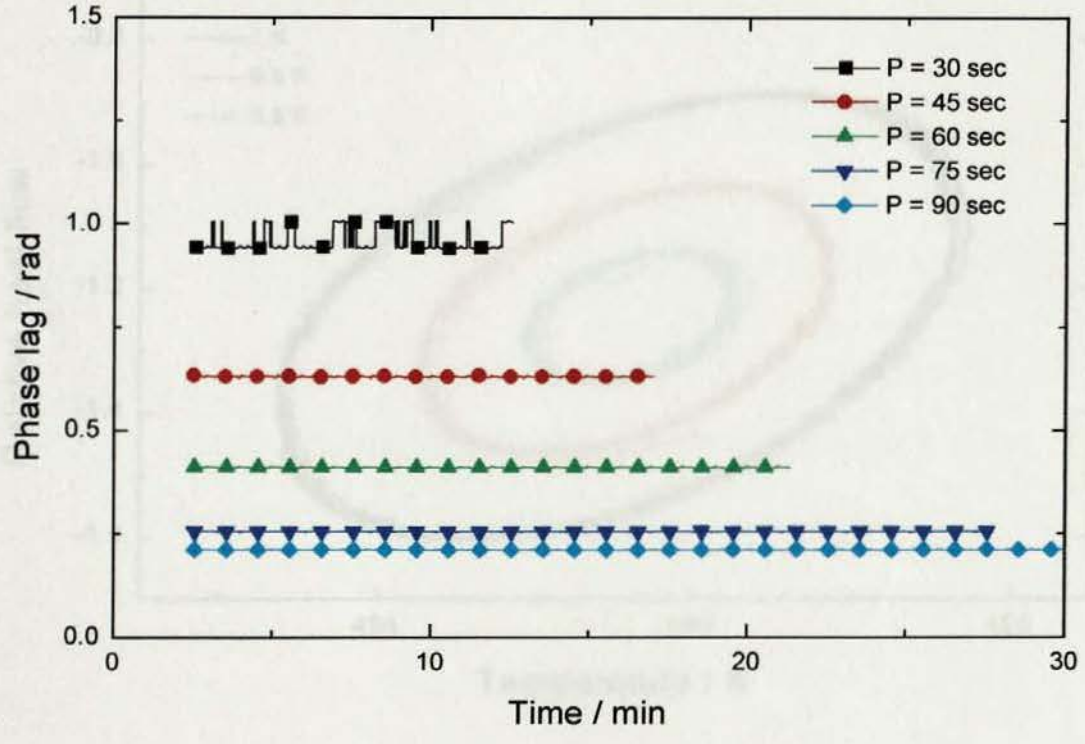

Fig. 7.2c Uncorrected phase lag of sapphire under different modulation periods with A_T = 1 K and B = 2.5 $Kmin^{-1}$

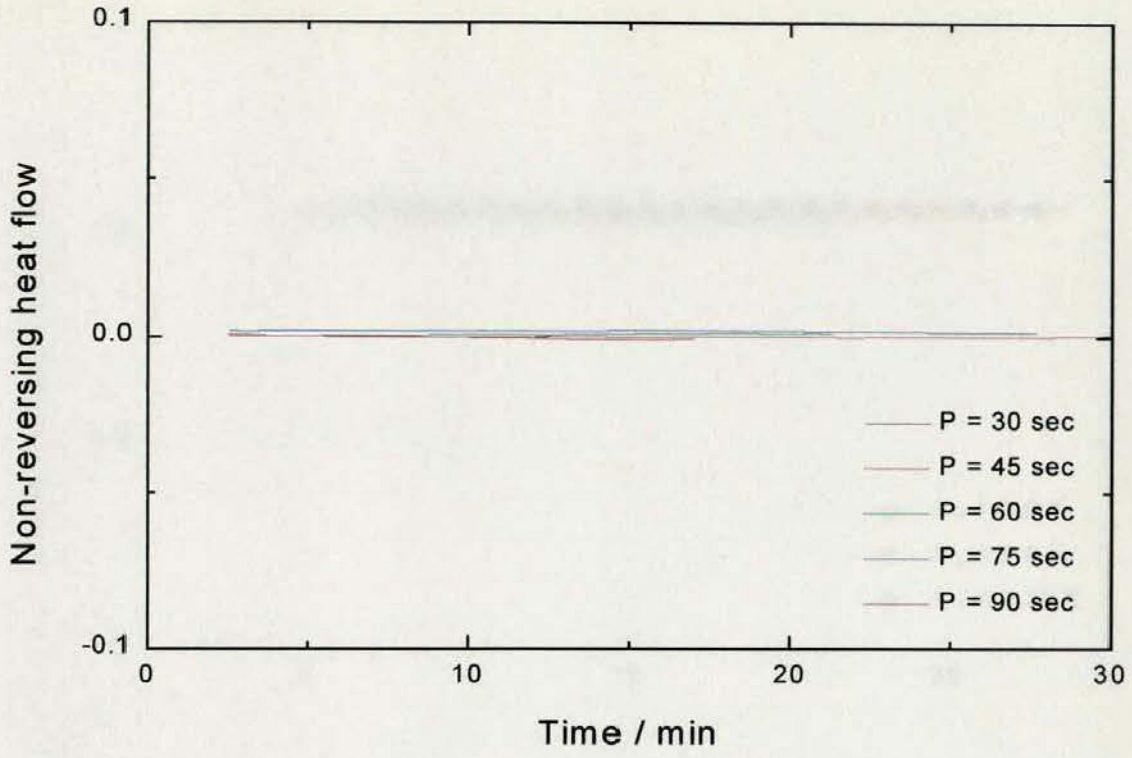

Fig. 7.2d Non-reversing heat flow of sapphire under different modulation periods with A_T = 1 K and B = 2.5 $Kmin^{-1}$

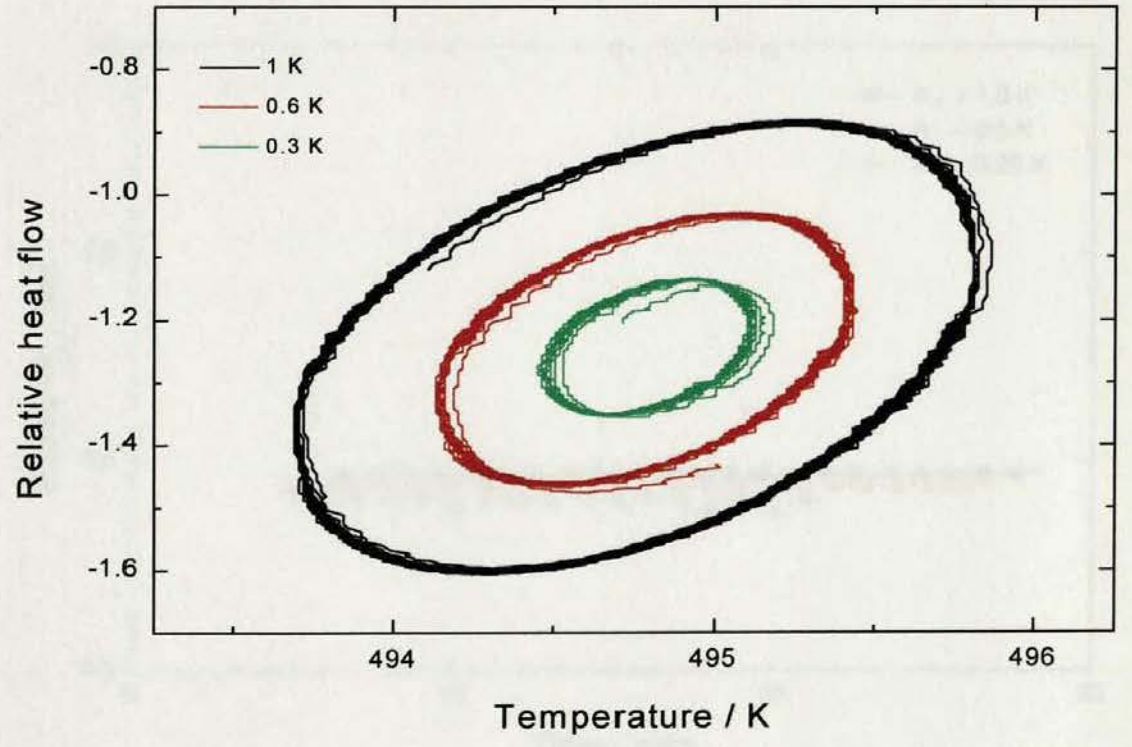

Fig. 7.3a Lissajous diagrams of sapphire sample under different amplitudes with p = 60 s and B = 2.5 K min^{-1}

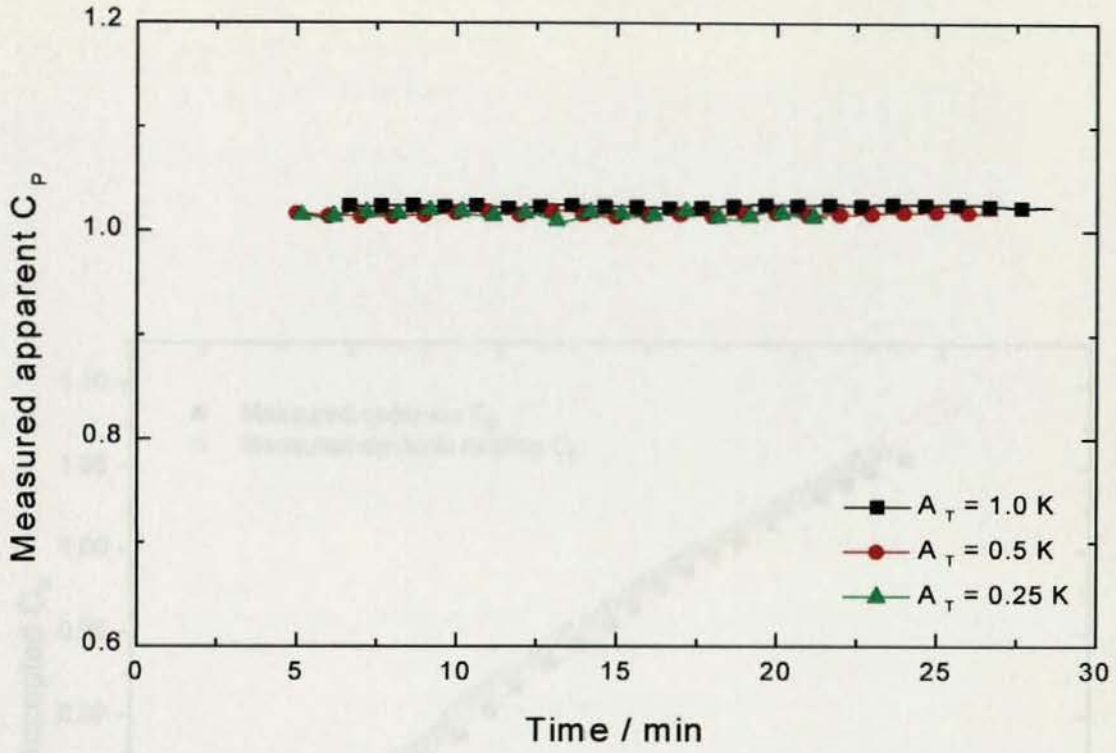

Fig. 7.3b Measured apparent reversing heat capacity of sapphire under different modulation amplitudes with p = 60 s and B = 2.5 K min^{-1}

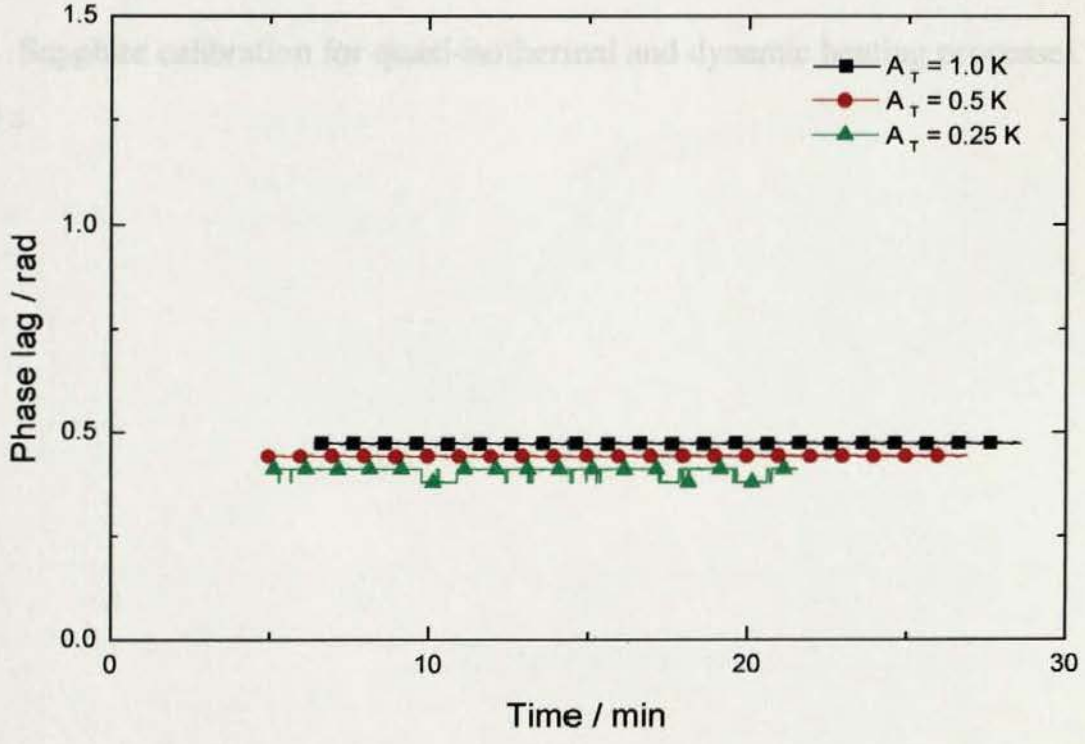

Fig. 7.3c Uncorrected phase lag of sapphire under different modulation amplitudes with p = 60 s and B = 2.5 K min^{-1}

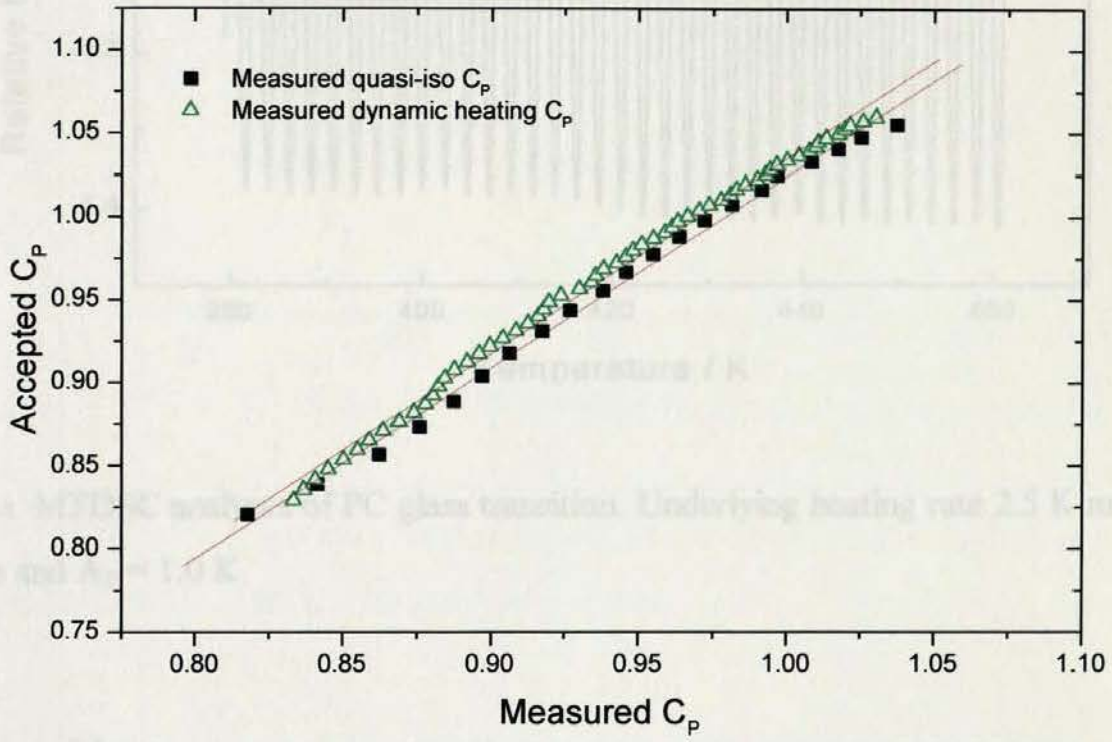

Fig7.4 Sapphire calibration for quasi-isothermal and dynamic heating processes with p = 60 s

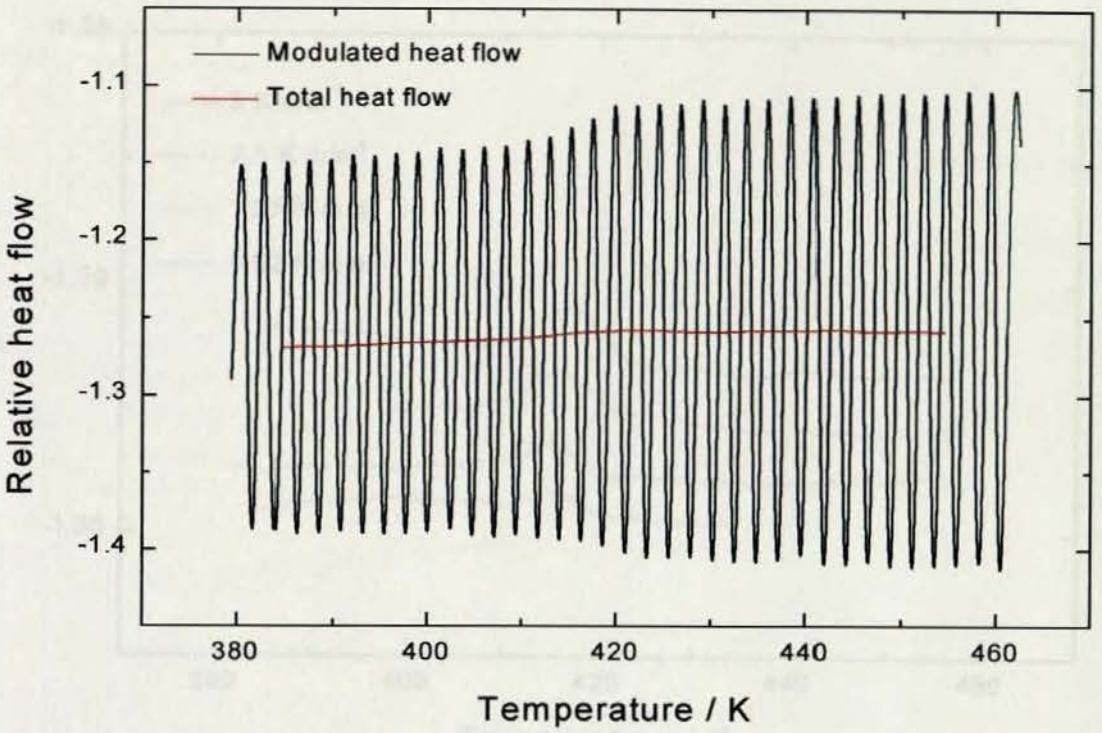

Fig. 7.5a MTDSC analyses of PC glass transition. Underlying heating rate 2.5 K min^{-1}, p = 60 s and A_T = 1.0 K

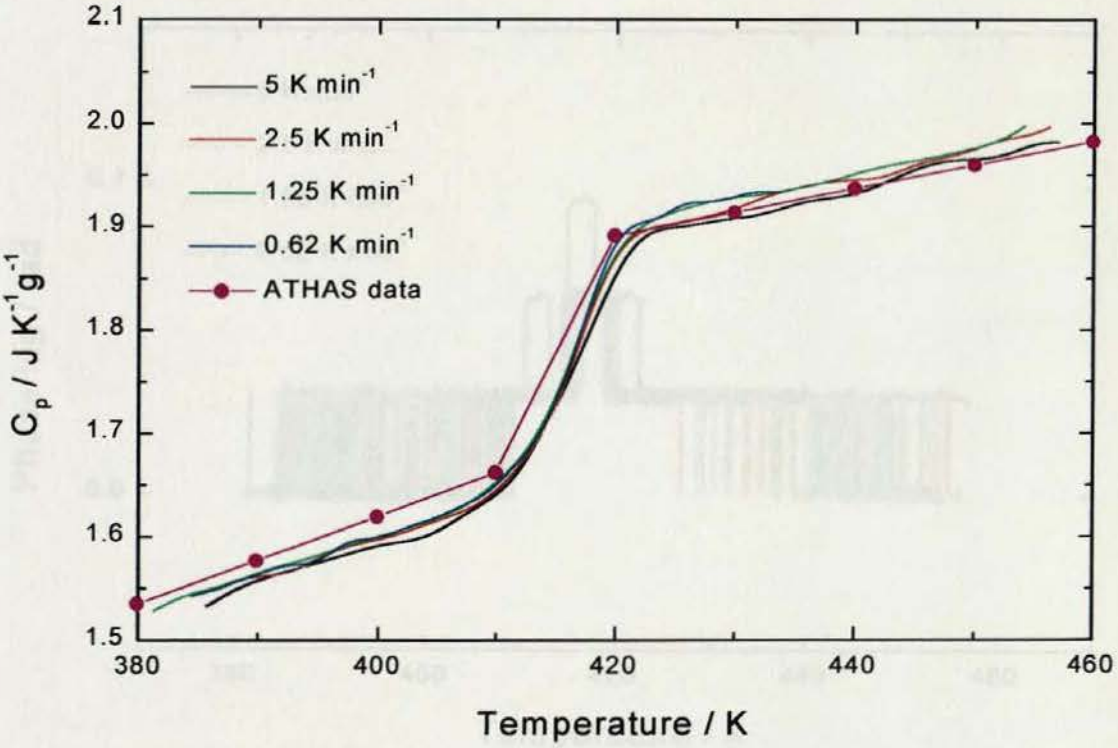

Fig. 7.5b Heat capacity in glass transition region as a function of different underlying heating rate with p = 60 s and A_T = 1.0 K

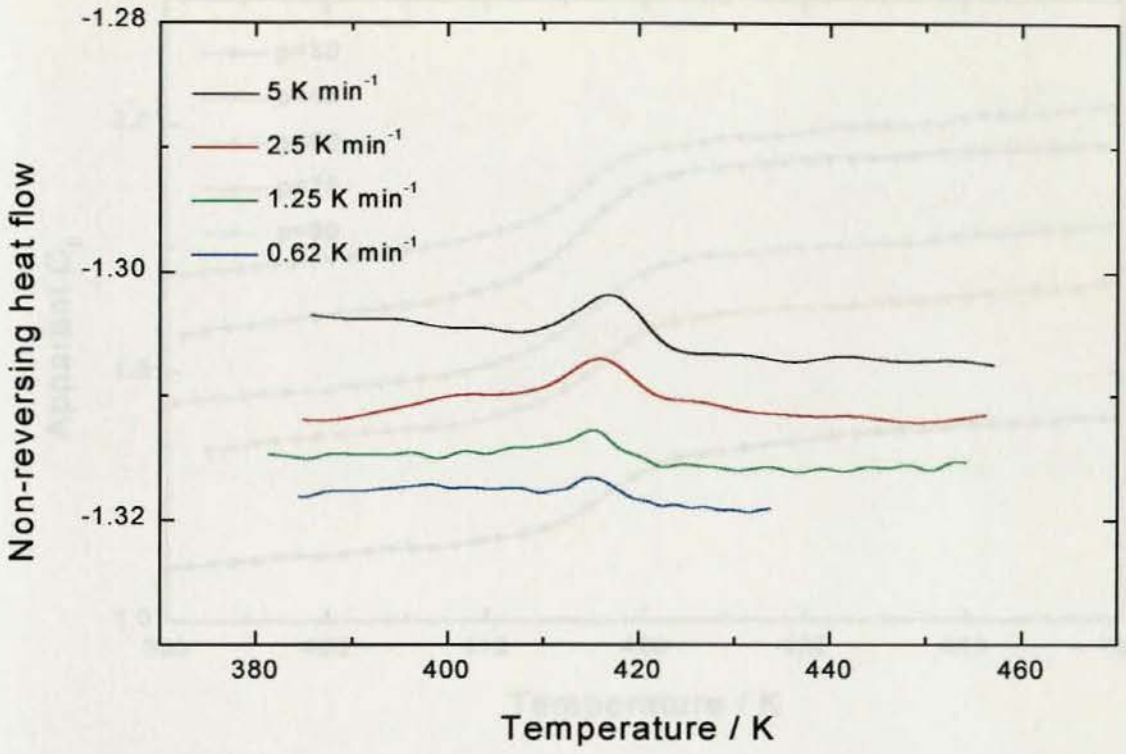

Fig. 7.5c Non-reversing heat flow in glass transition region of PC at different underlying heating rate with p = 60 s and A_T = 1.0 K

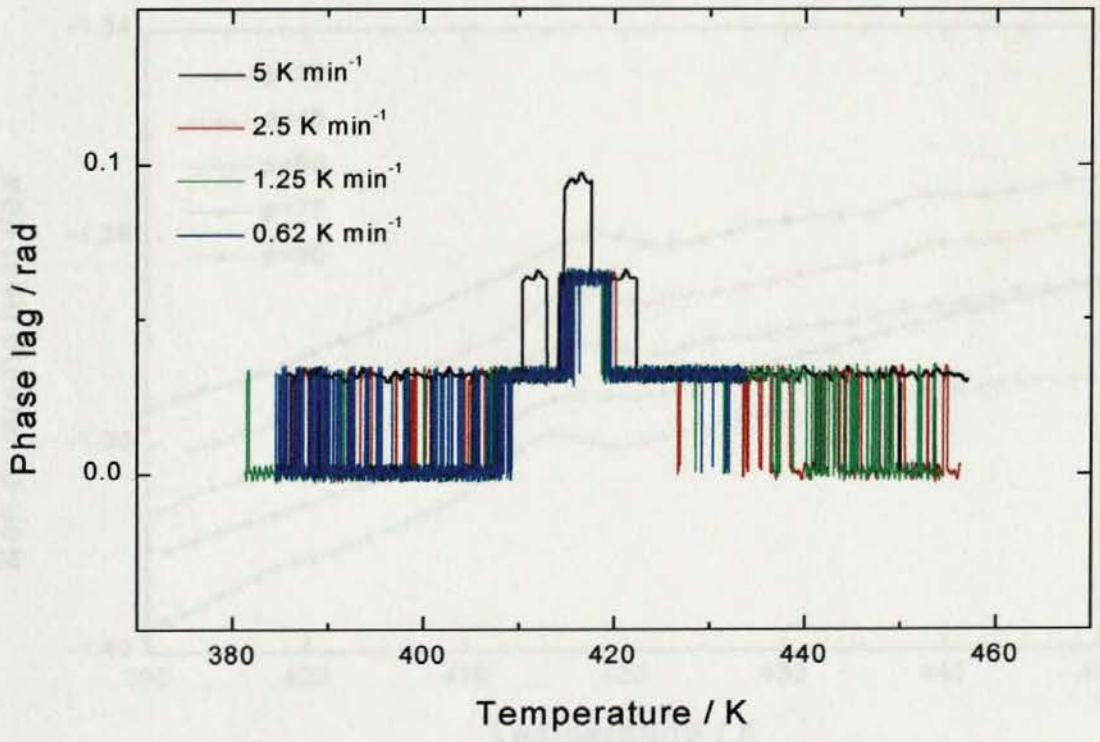

Fig. 7.5d Corrected phase lag of PC in glass transition region as a function of underlying heating rate with p = 60 s and A_T = 1.0 K

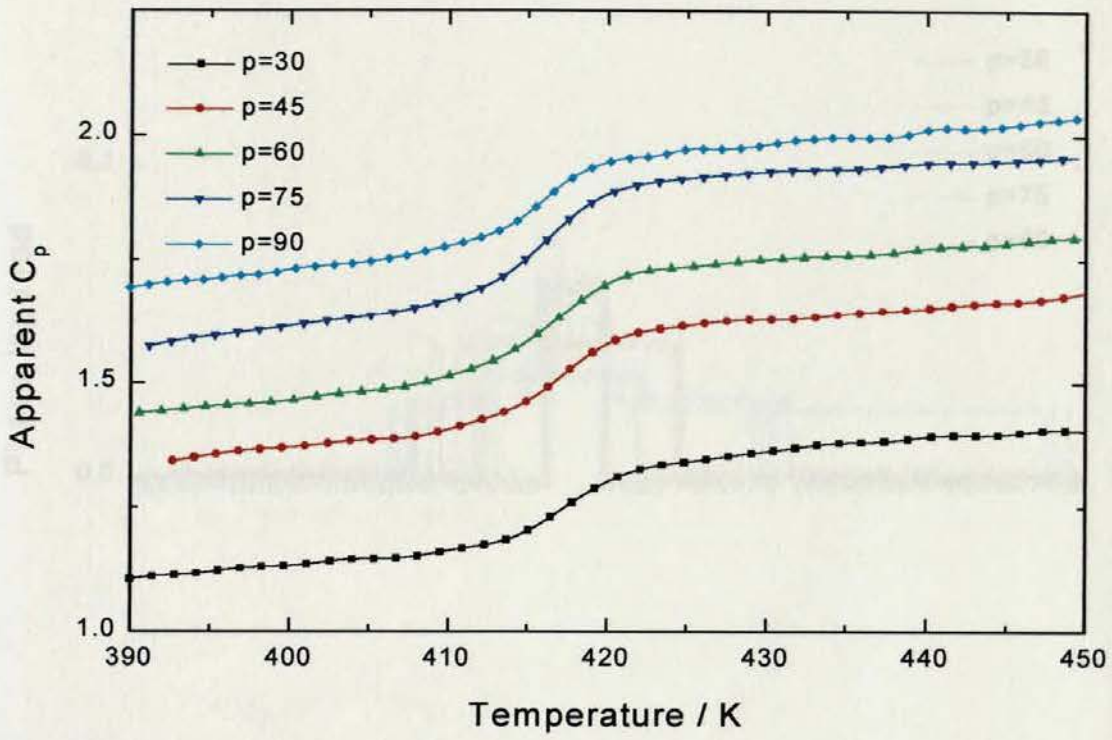

Fig. 7.6a Reversing heat capacity in glass transition region of PC as a function of modulation periods with B = 2.5 K min^{-1} and A_T = 1.0 K

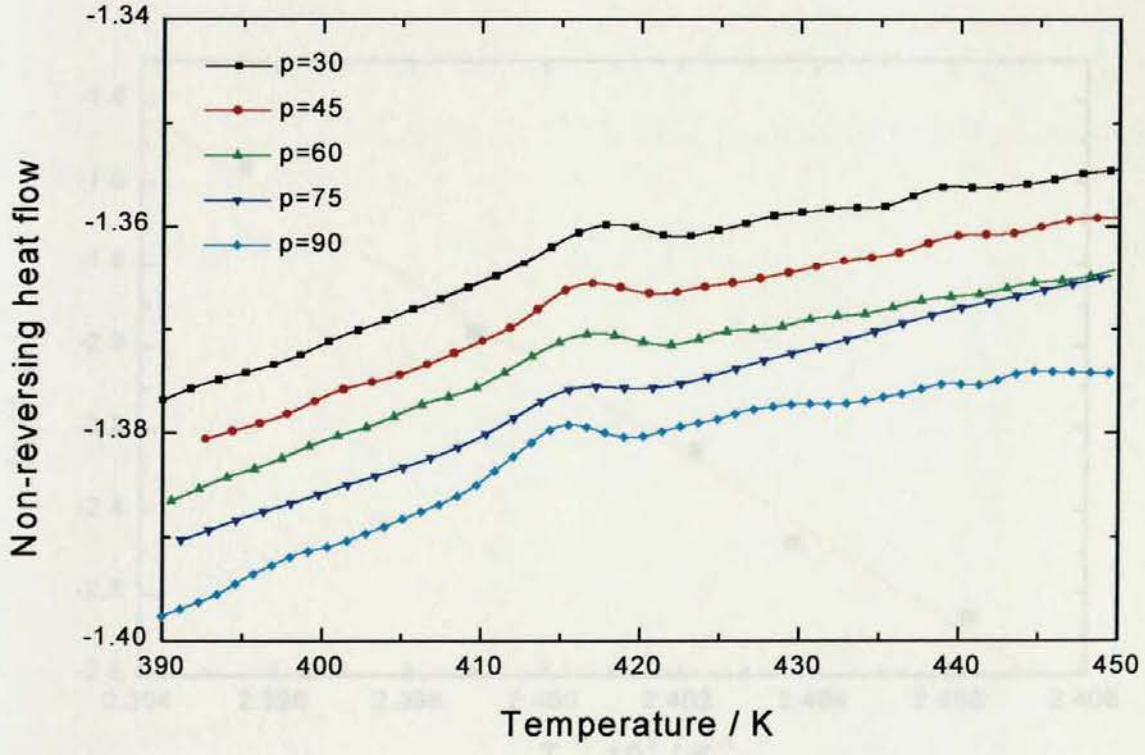

Fig. 7.6b Non-reversing heat flow in glass transition region of PC as a function of modulation periods with B = 2.5 K min^{-1} and A_T = 1.0 K

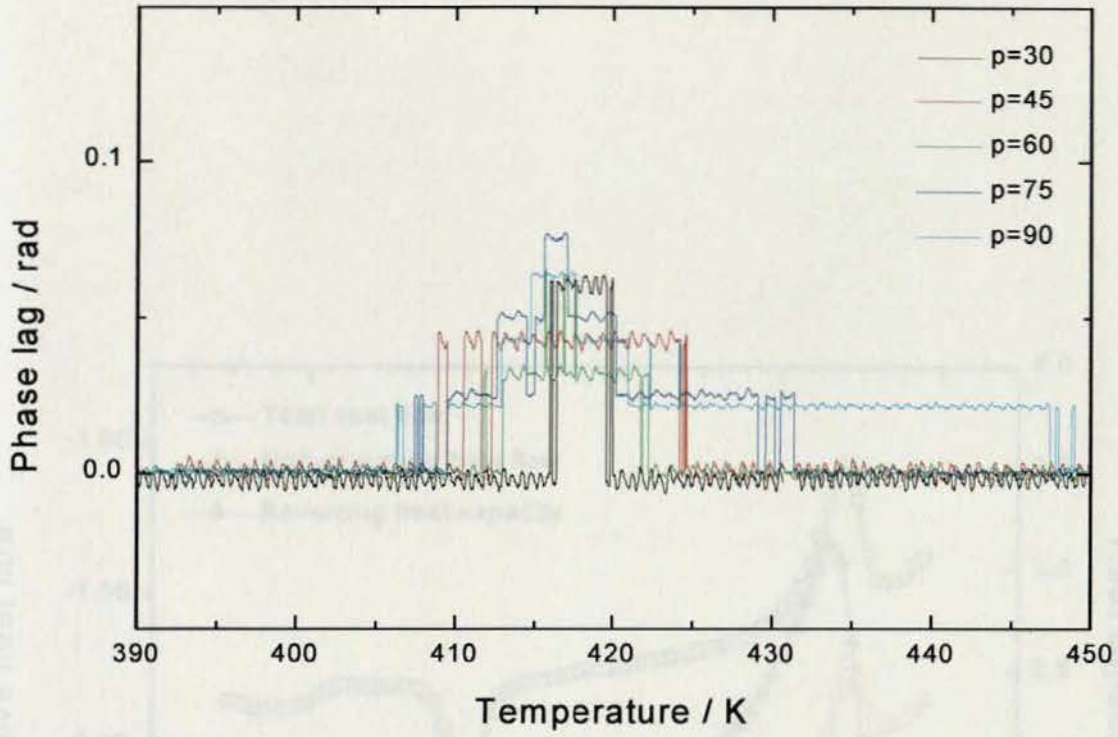

Fig. 7.6c Corrected phase lag change over the glass transition region of PC as a function of modulation periods with B = 2.5 K min^{-1} and A_T = 1.0 K

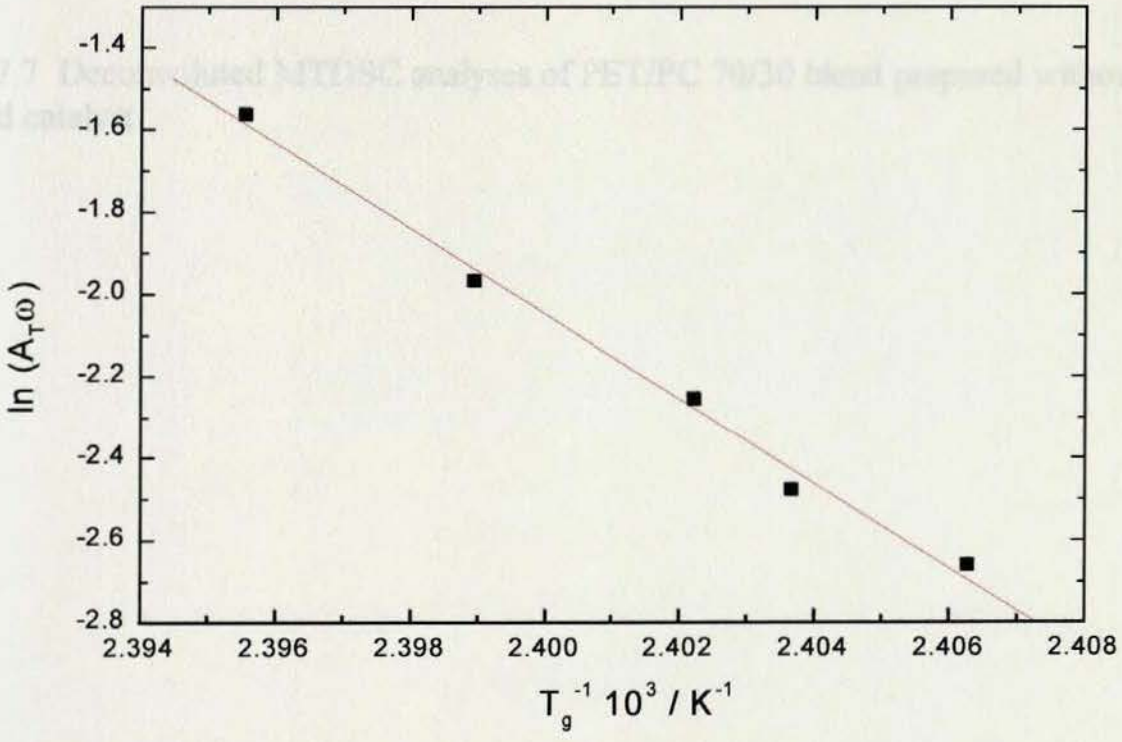

Fig. 7.6d The modulation frequency dependence of glass transition temperature

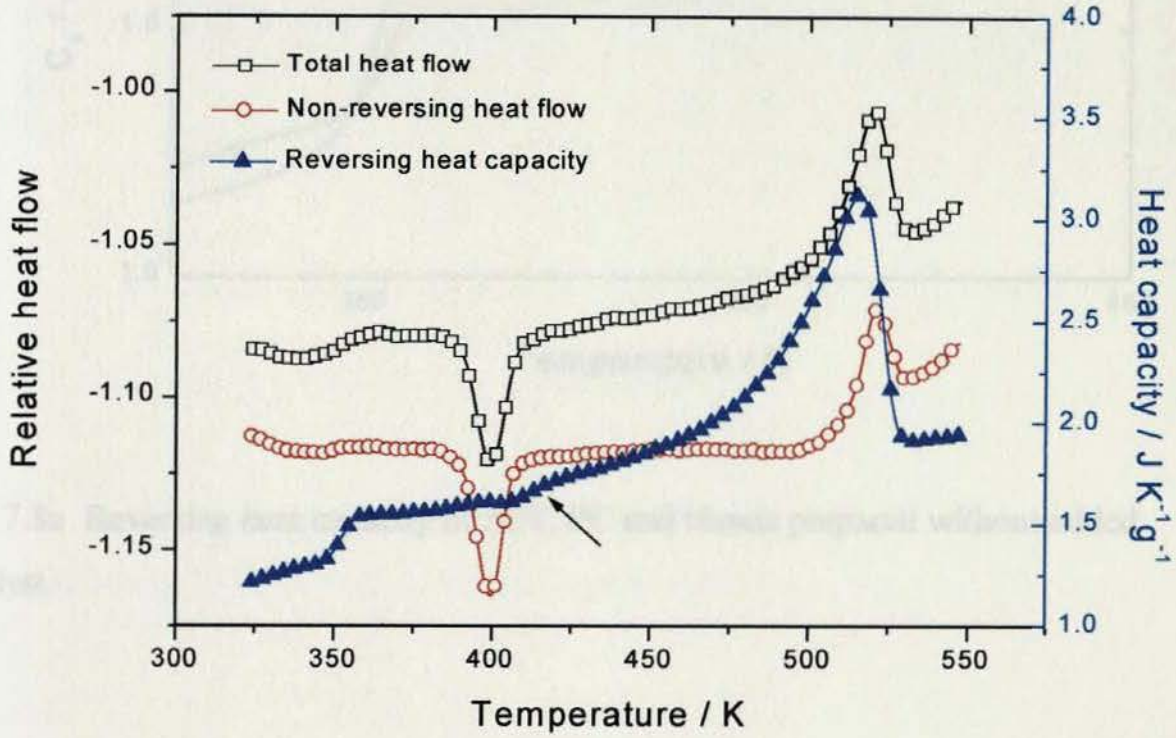

Fig. 7.7 Deconvoluted MTDSC analyses of PET/PC 70/30 blend prepared without added catalyst

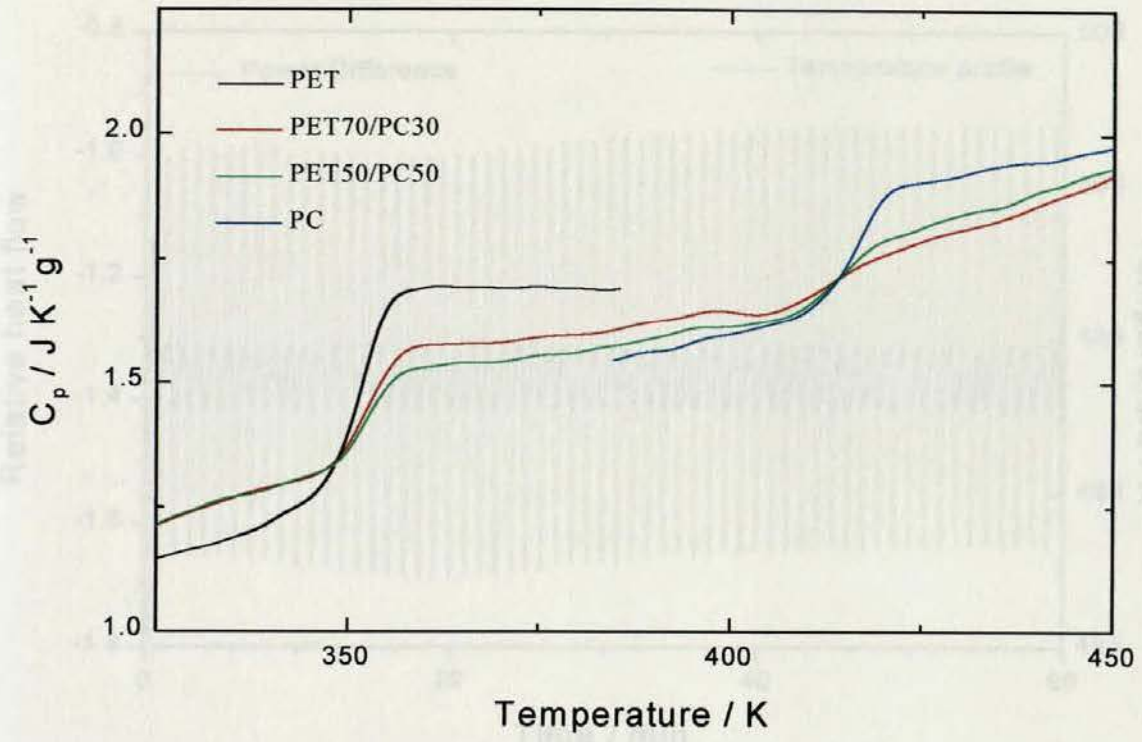

Fig. 7.8a Reversing heat capacity of PET, PC and blends prepared without added catalyst

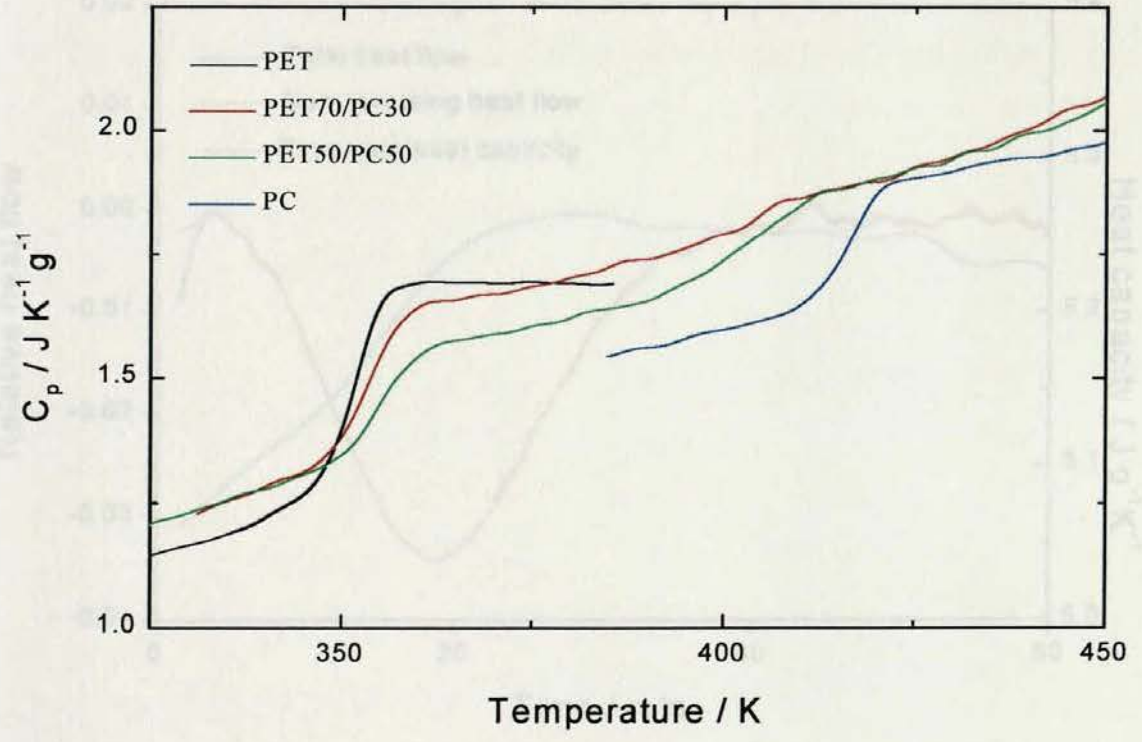

Fig. 7.8b Reversing heat capacity of PET, PC and blends prepared with added catalyst

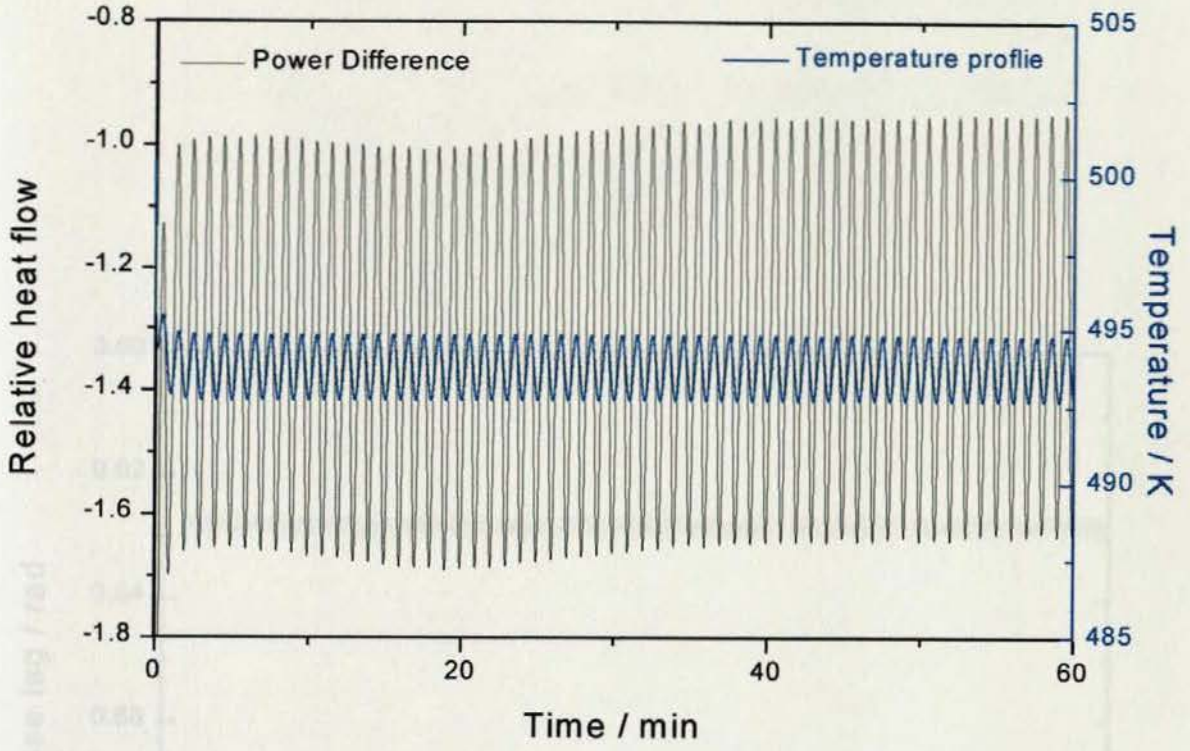

Fig. 7.9a Heat flow and temperature profiles of PET during quasi-isothermal crystallization at 493.7 K with A_T = 1.0 K and p = 60 s

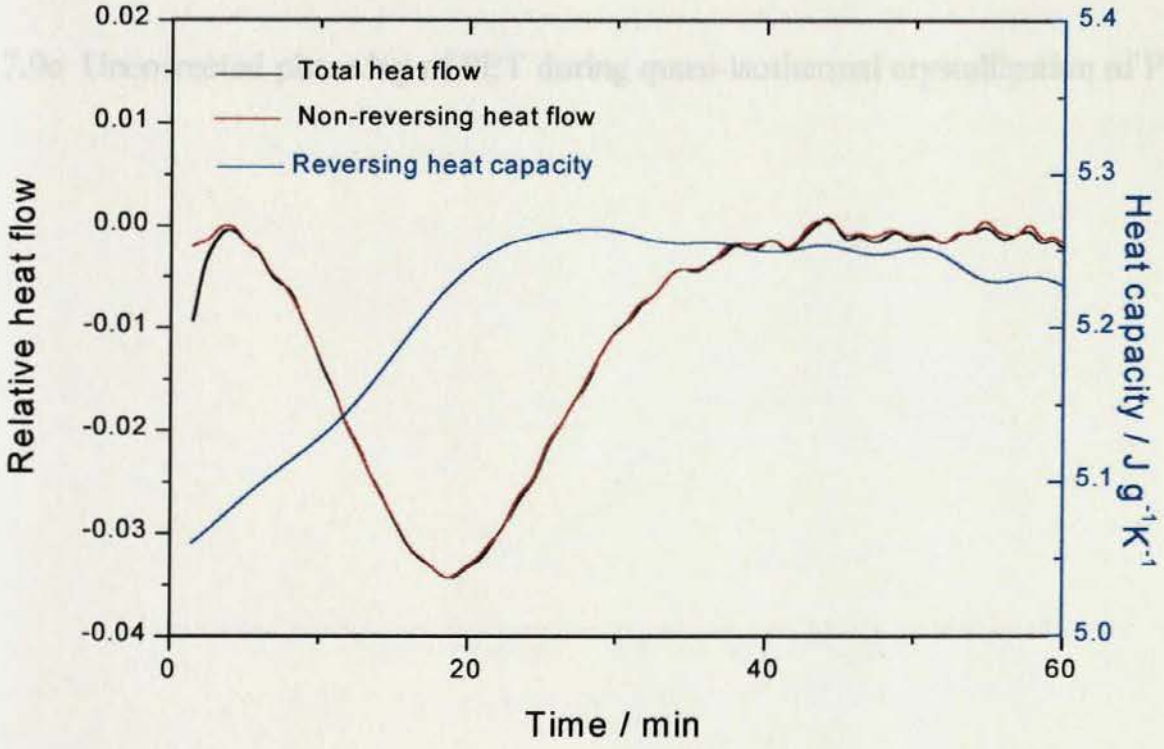

Fig. 7.9b Deconvoluted analyses of MTDSC into total, non-reversing heat flow and reversing heat capacity

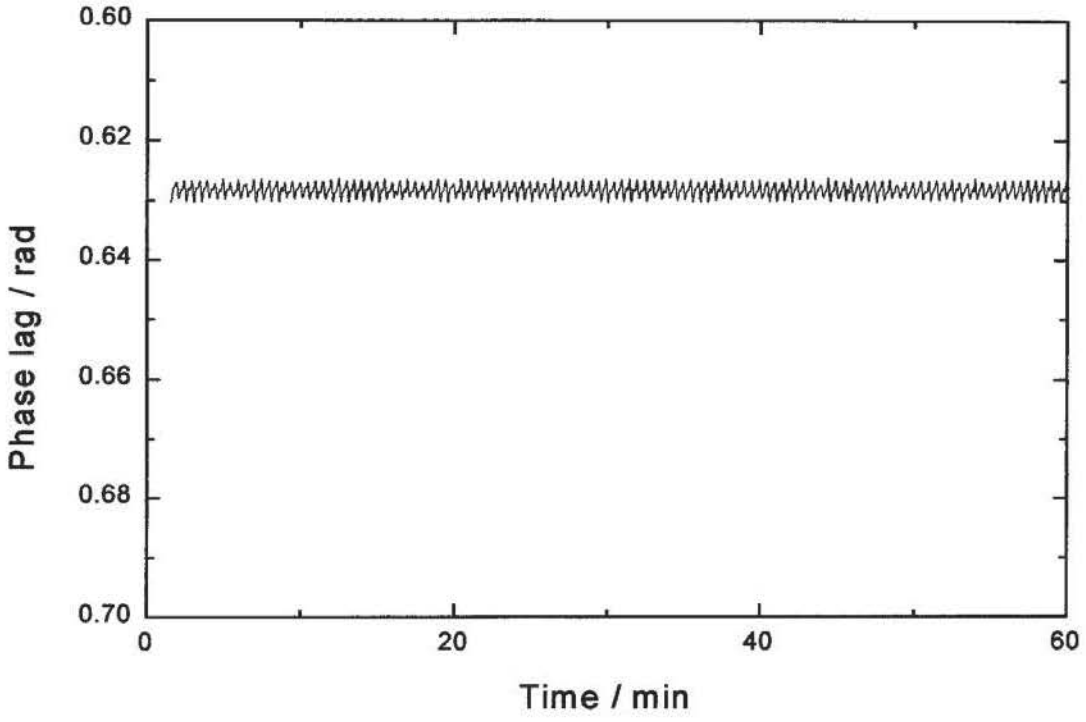

Fig. 7.9c Uncorrected phase lag of PET during quasi-isothermal crystallization of PET

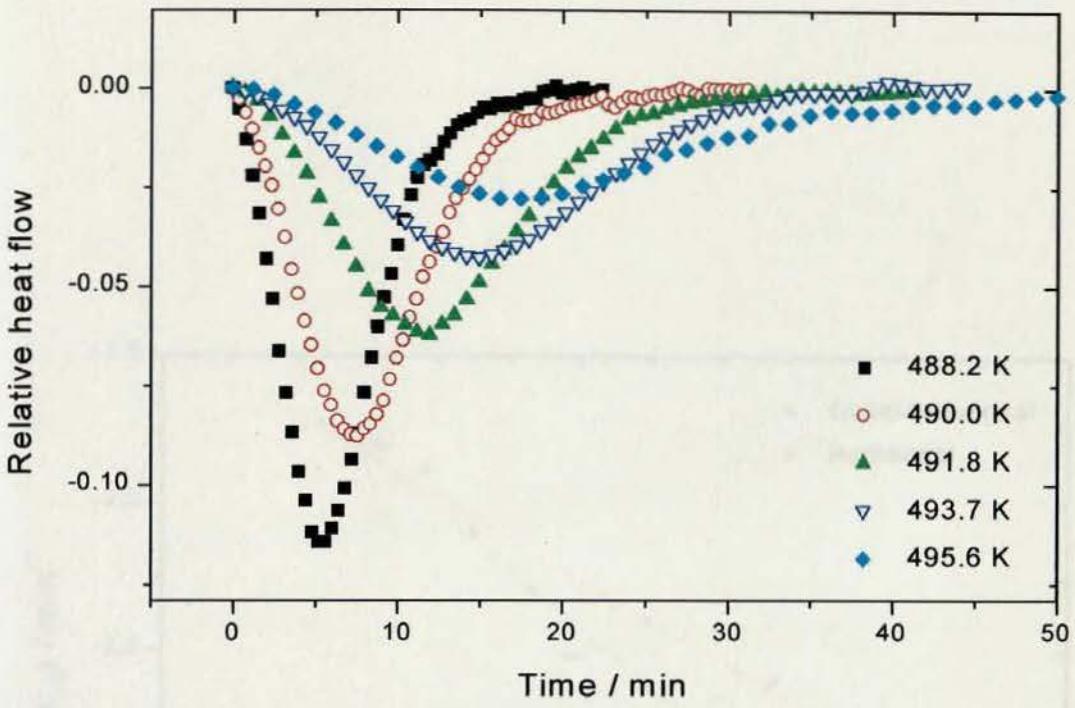

Fig. 7.10 Non-reversing response of PET quasi-isothermal crystallisation with A_T = 1.0 K and p = 60 s

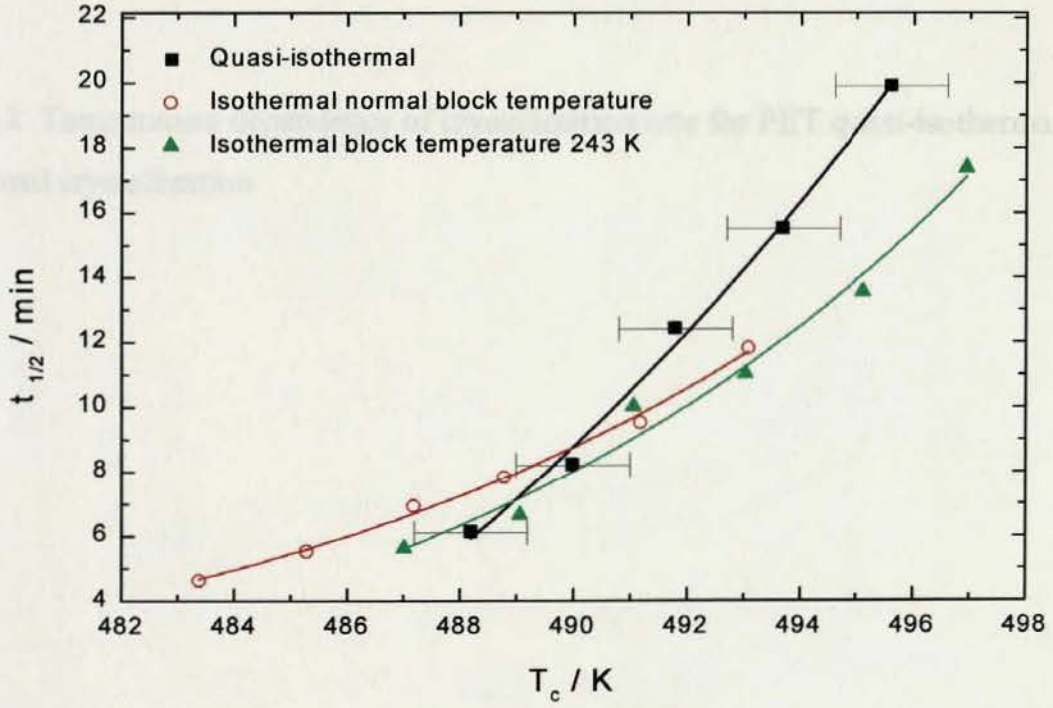

Fig7.11 The $t_{1/2}$ vs. T_c for PET under the different conditions

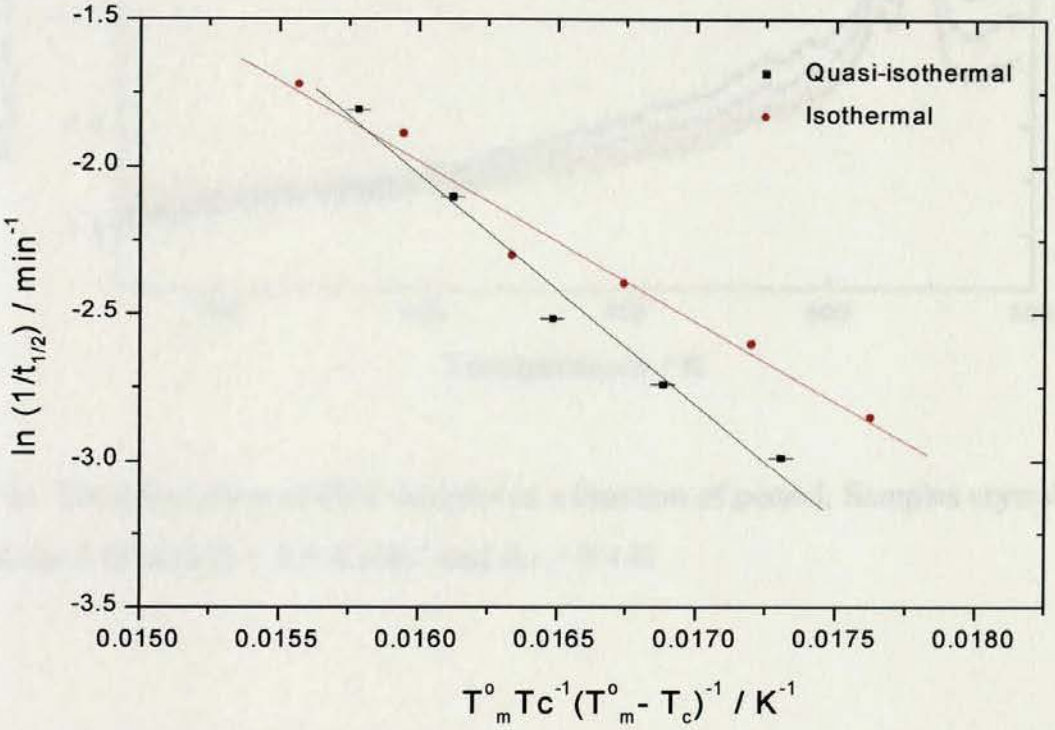

Fig 7.12 Temperature dependence of crystallization rate for PET quasi-isothermal and isothermal crystallization

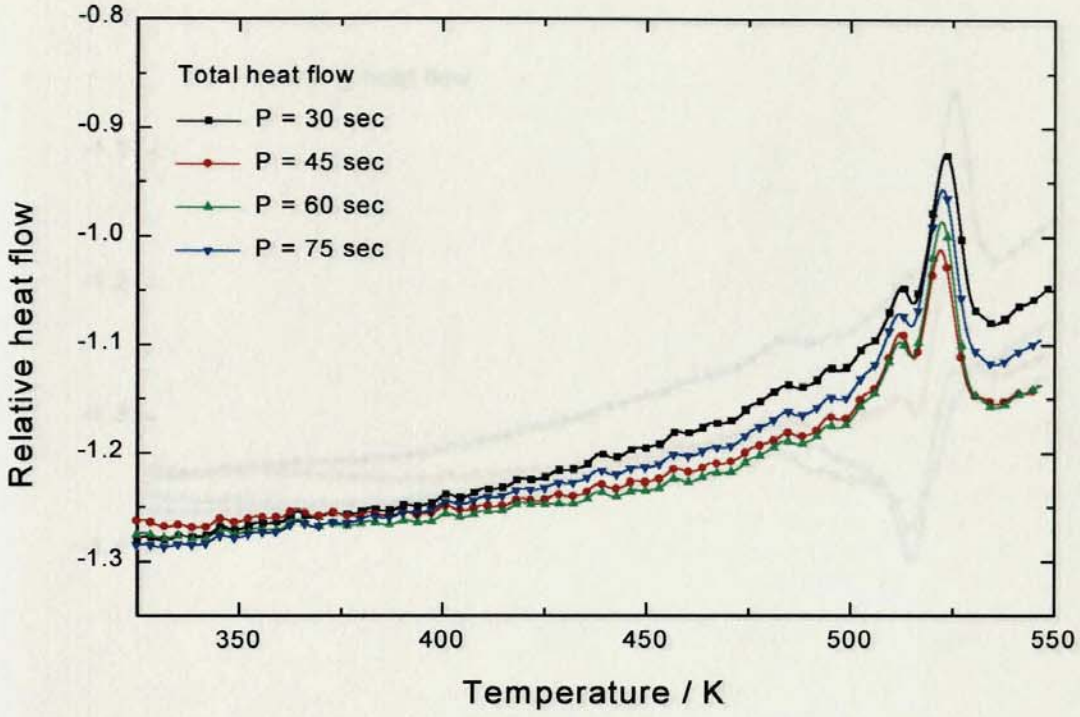

Fig. 7.13a Total heat flow of PET samples as a function of period. Samples crystallised at 473 K for 1 hr with B = 2.5 K min^{-1} and A_T = 0.4 K

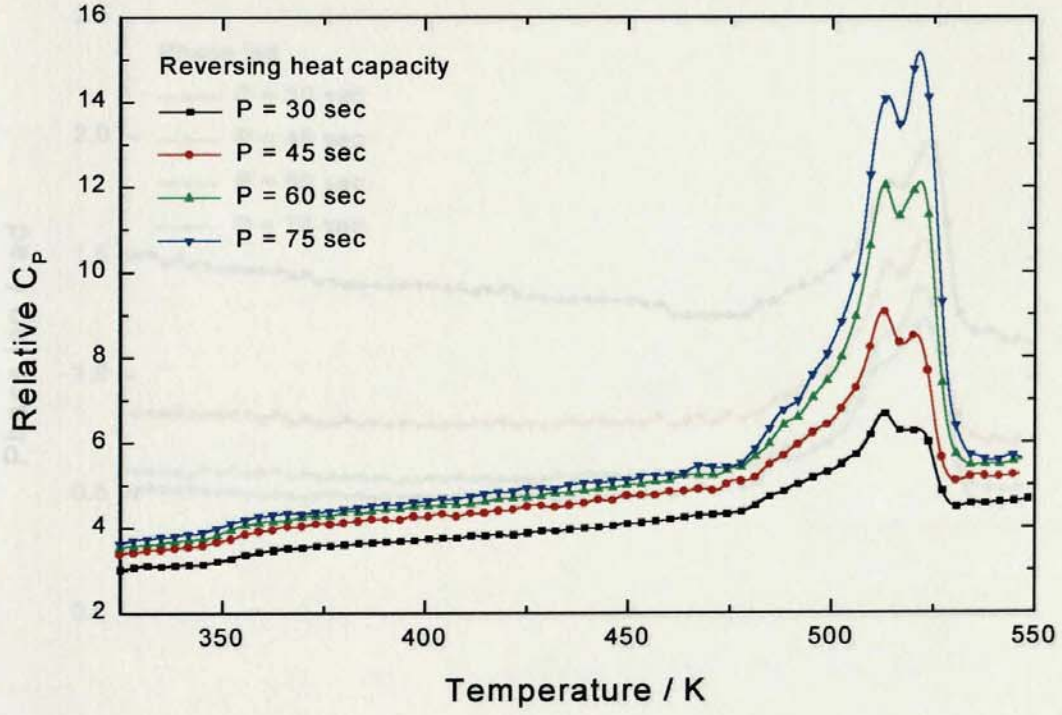

Fig. 7.13b Reversing heat capacity of PET samples as a function of period. Samples crystallised at 473 K for 1 hr with B = 2.5 K min^{-1} and A_T = 0.4 K

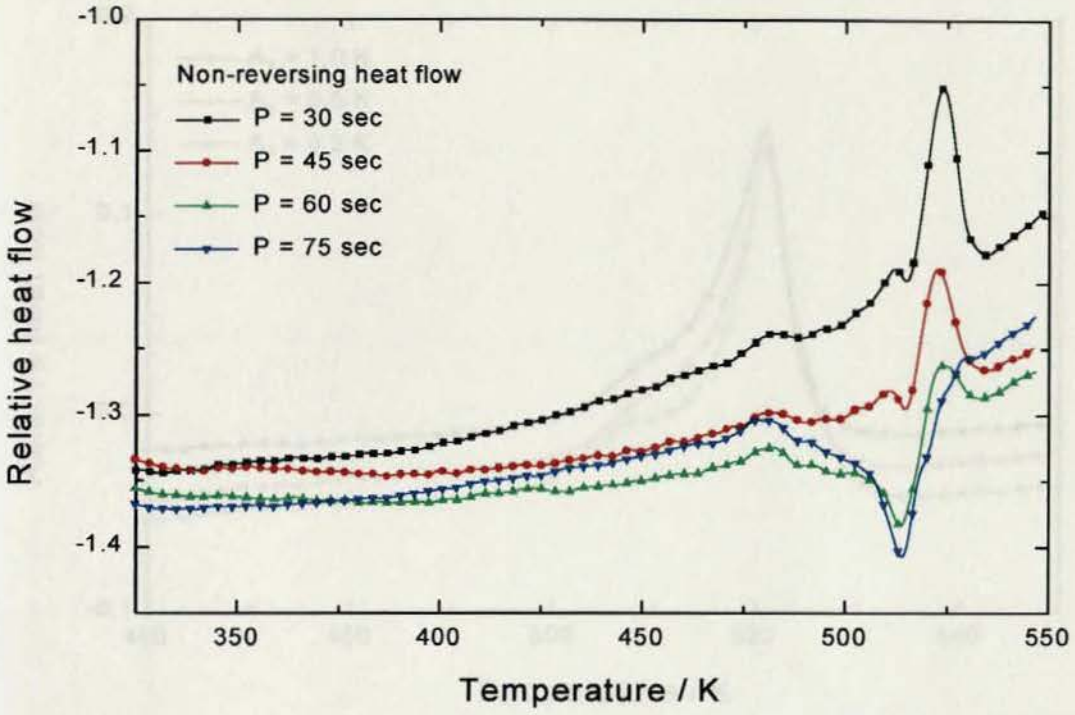

Fig. 7.13c Non-reversing heat flow of PET samples as a function of period. Samples crystallised at 473 K for 1 hr with B = 2.5 K min^{-1} and A_T = 0.4 K

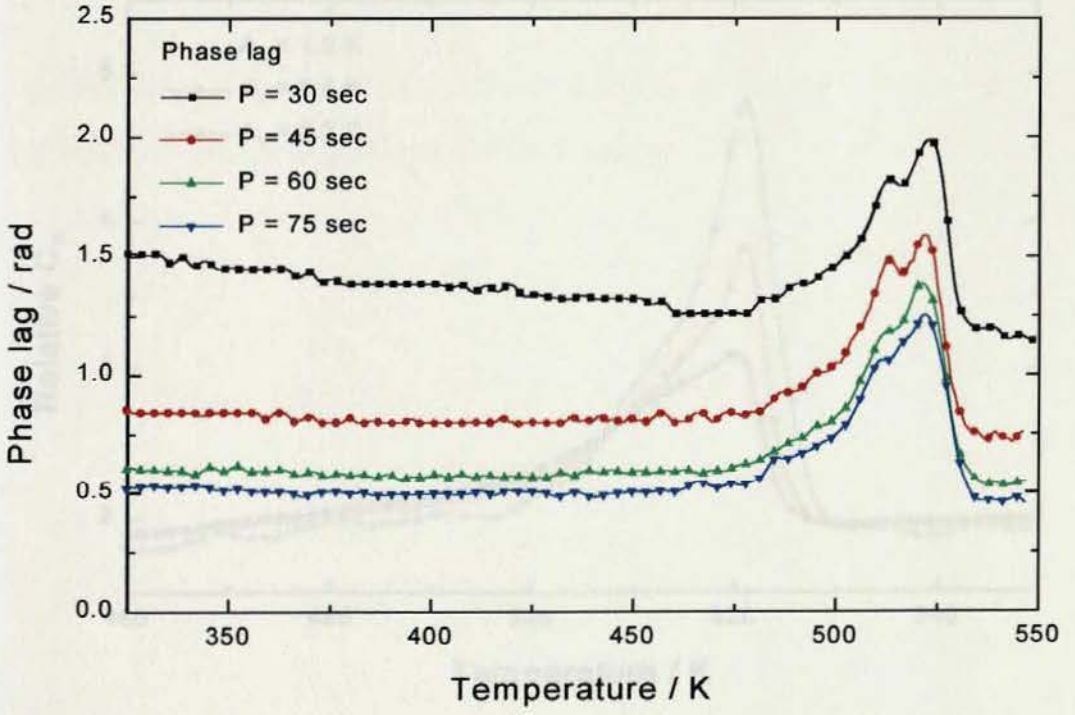

Fig. 7.13d Phase lag of PET samples as a function of period. Samples crystallised at 473 K for 1 hr with B = 2.5 K min^{-1} and A_T = 0.4 K

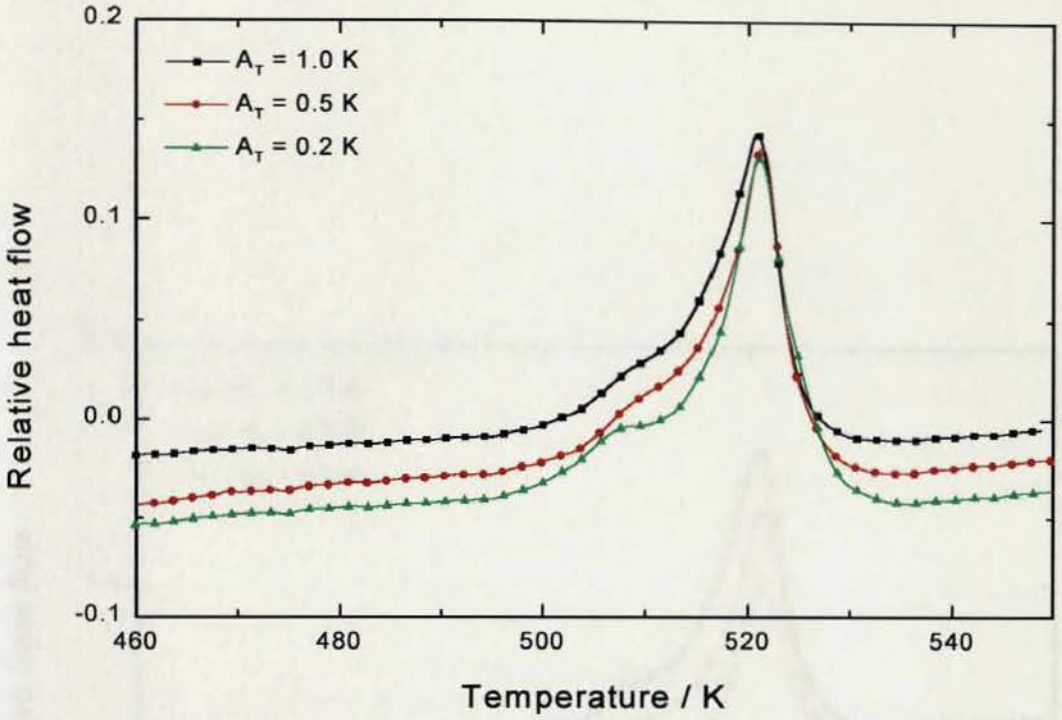

Fig. 7.14a Total heat flow of PET at different amplitude with p = 30 s and B = 2.5 K min^{-1}. Samples crystallized at 496 K for 1h

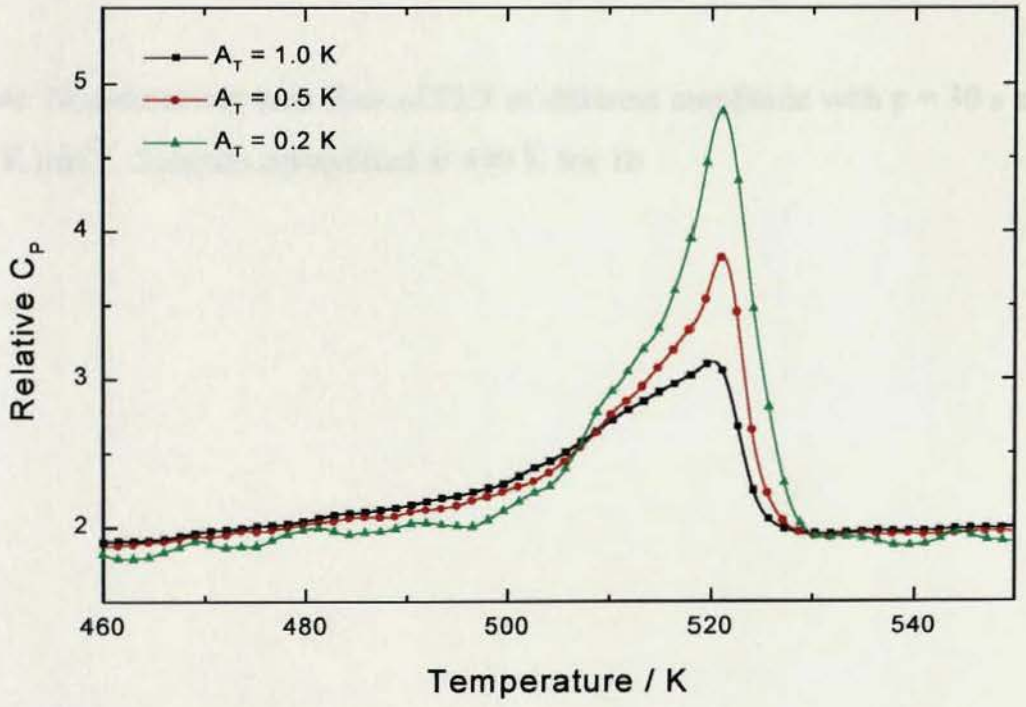

Fig. 7.14b Reversing heat capacity of PET at different amplitude with p = 30 s and B = 2.5 K min^{-1}. Samples crystallized at 496 K for 1h

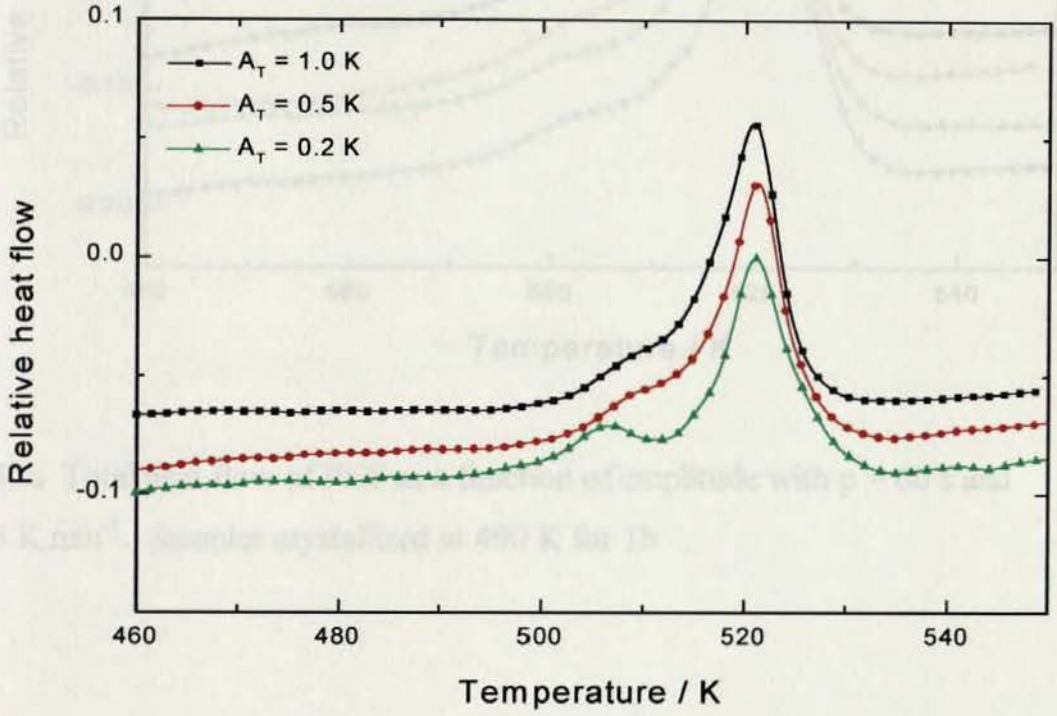

Fig. 7.14c Non-reversing heat flow of PET at different amplitude with p = 30 s and B = 2.5 K min^{-1}. Samples crystallized at 496 K for 1h

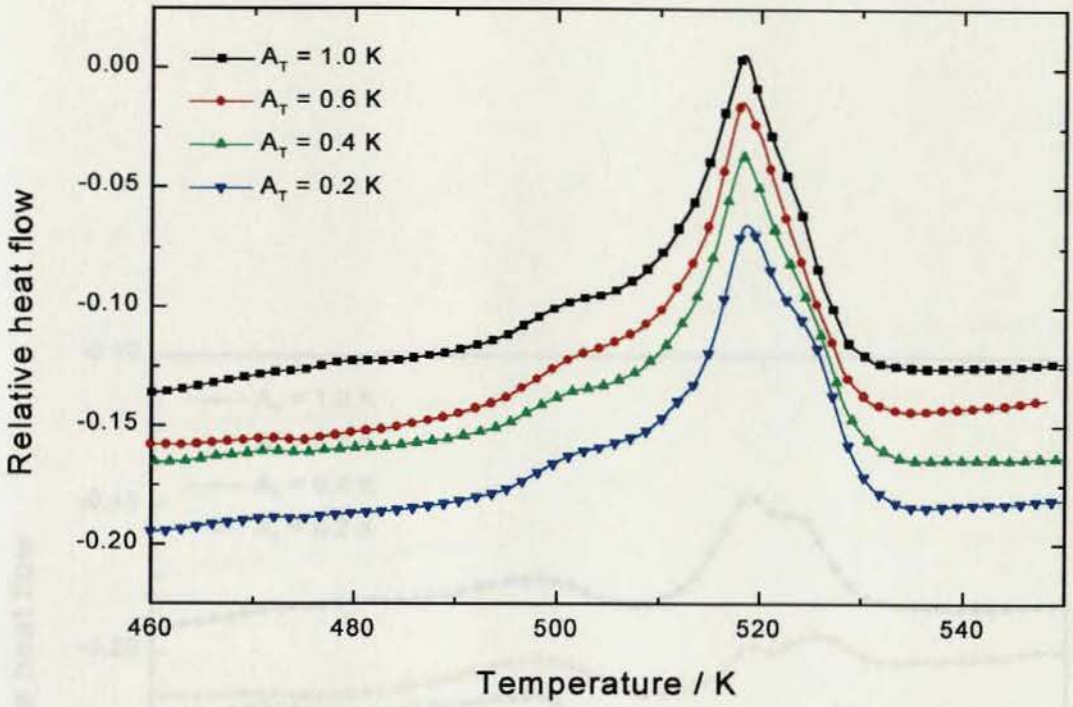

Fig. 7.15a Total heat flow of PET as a function of amplitude with p = 60 s and B = 2.5 K min^{-1}. Samples crystallized at 490 K for 1h

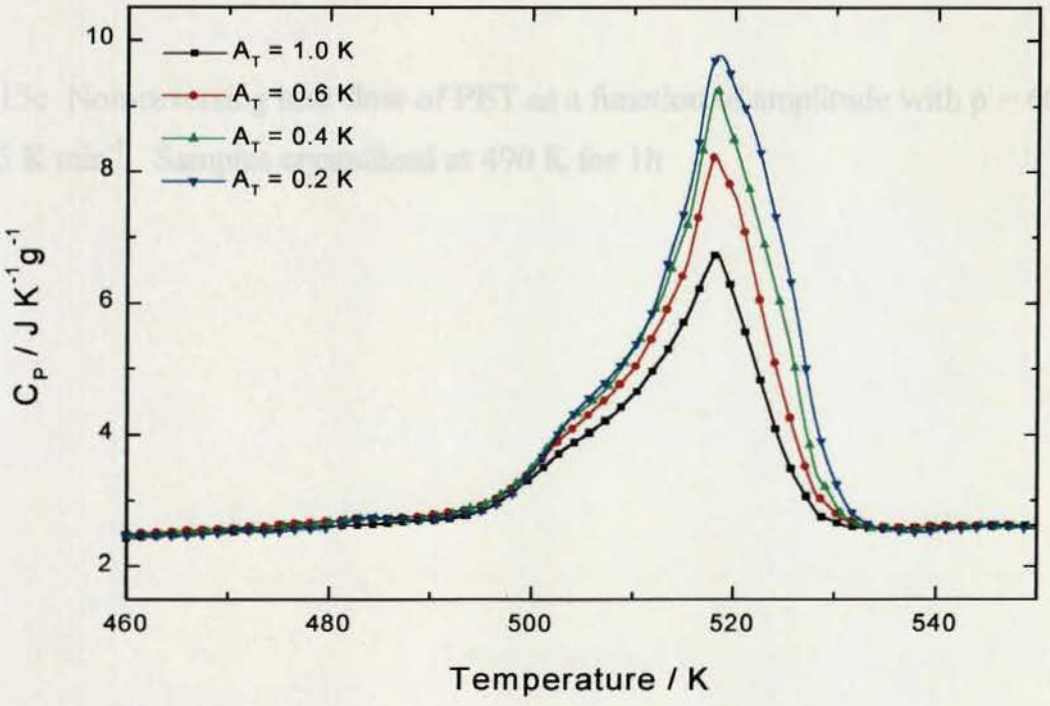

Fig. 7.15b Reversing heat capacity of PET as a function of amplitude with p = 60 s and B = 2.5 K min^{-1}. Samples crystallized at 490 K for 1h

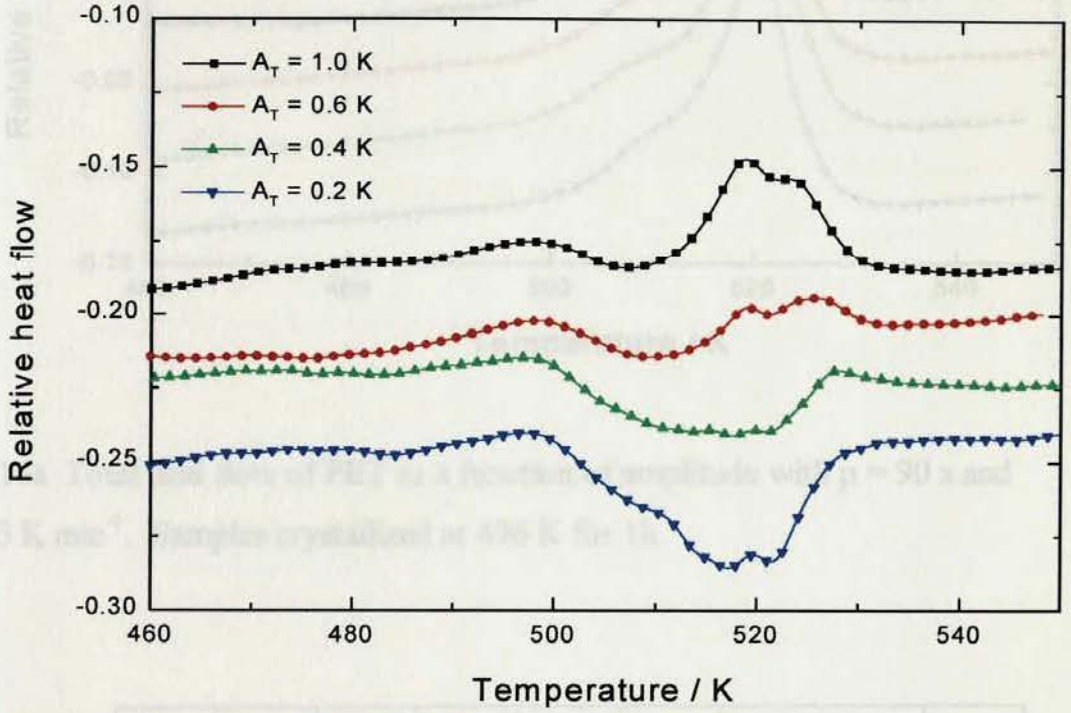

Fig. 7.15c Non-reversing heat flow of PET as a function of amplitude with p = 60 s and B = 2.5 K min^{-1}. Samples crystallized at 490 K for 1h

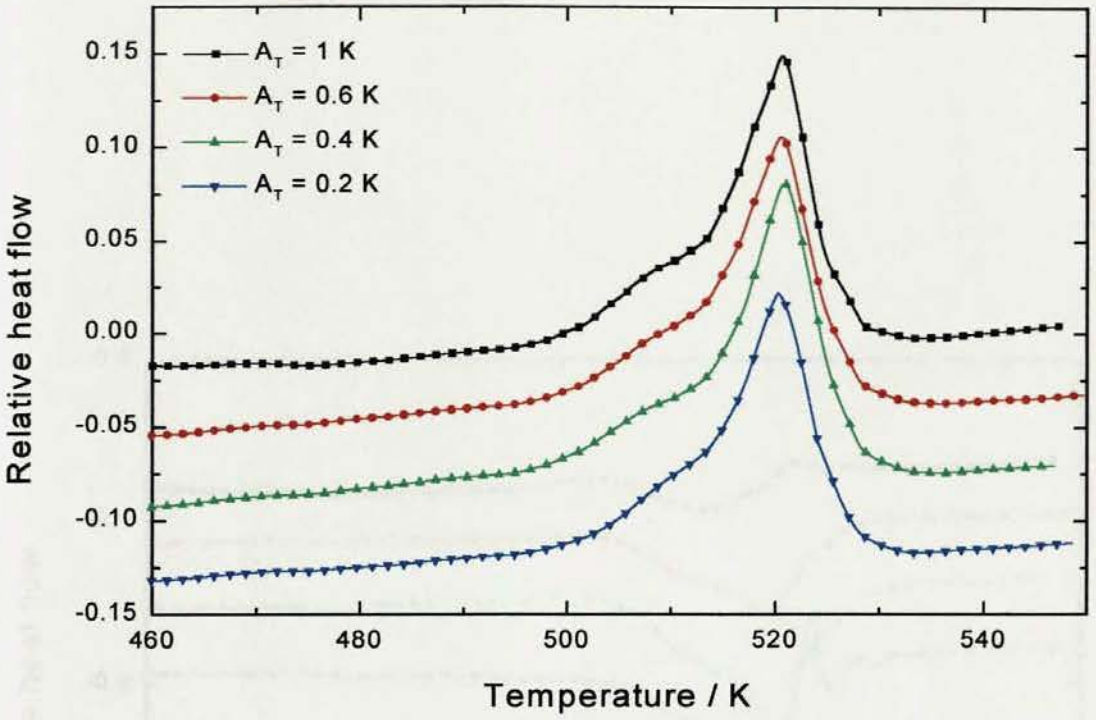

Fig. 7.16a Total heat flow of PET as a function of amplitude with p = 90 s and B = 2.5 K min^{-1}. Samples crystallized at 496 K for 1h

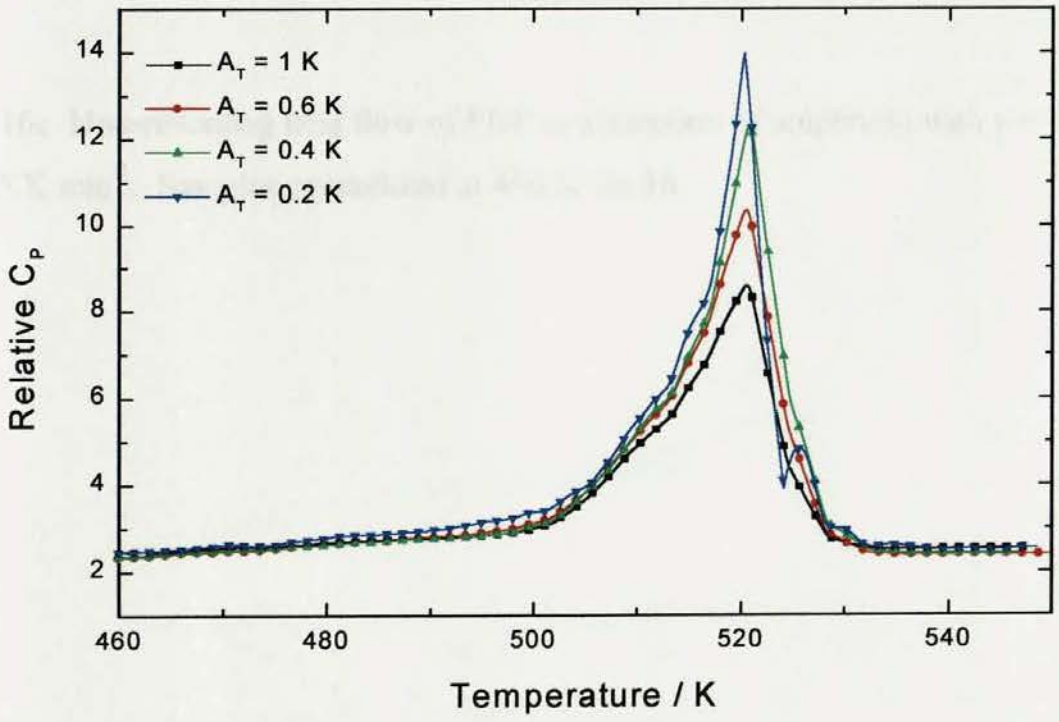

Fig. 7.16b Reversing heat capacity of PET as a function of amplitude with p = 90 s and B = 2.5 K min^{-1}. Samples crystallized at 496 K for 1h

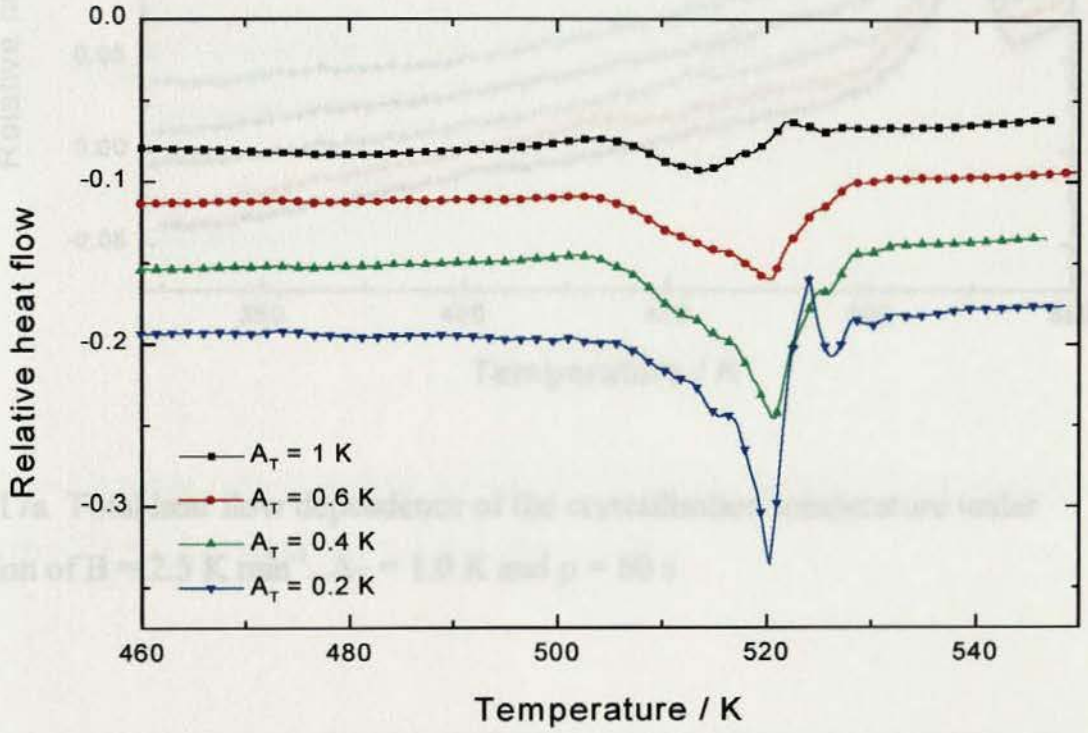

Fig. 7.16c Non-reversing heat flow of PET as a function of amplitude with p = 90 s and B = 2.5 K min^{-1}. Samples crystallized at 496 K for 1h

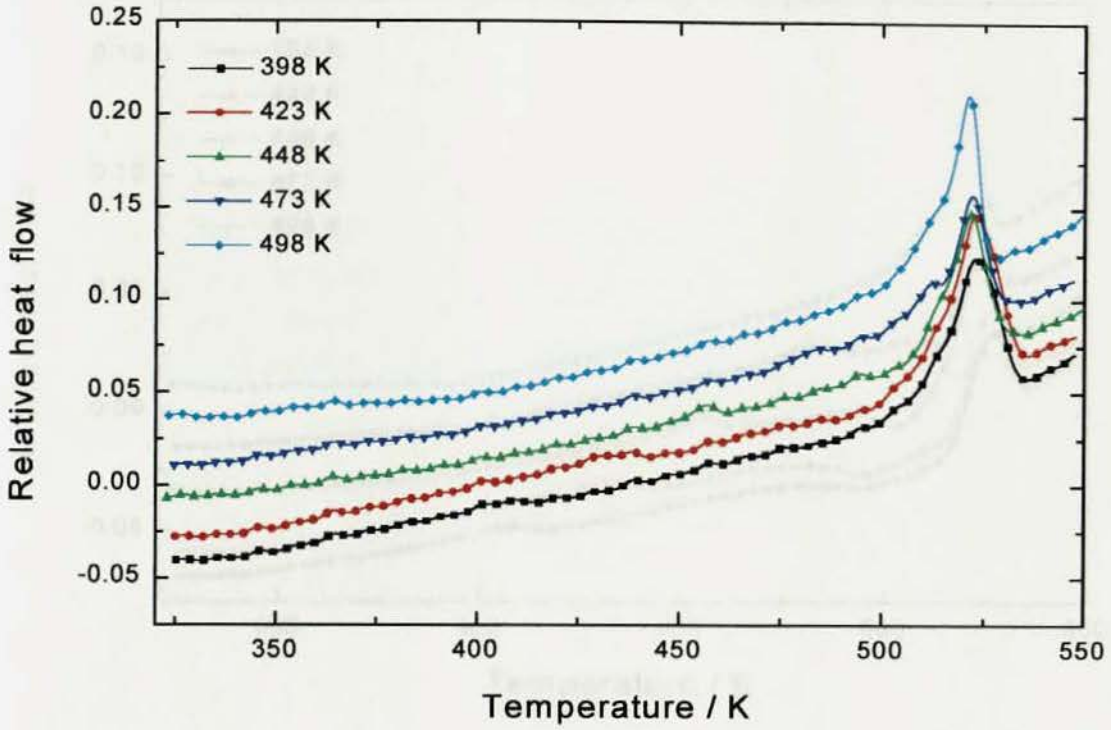

Fig. 7.17a Total heat flow dependence of the crystallisation temperature under condition of B = 2.5 K min^{-1}, A_T = 1.0 K and p = 60 s

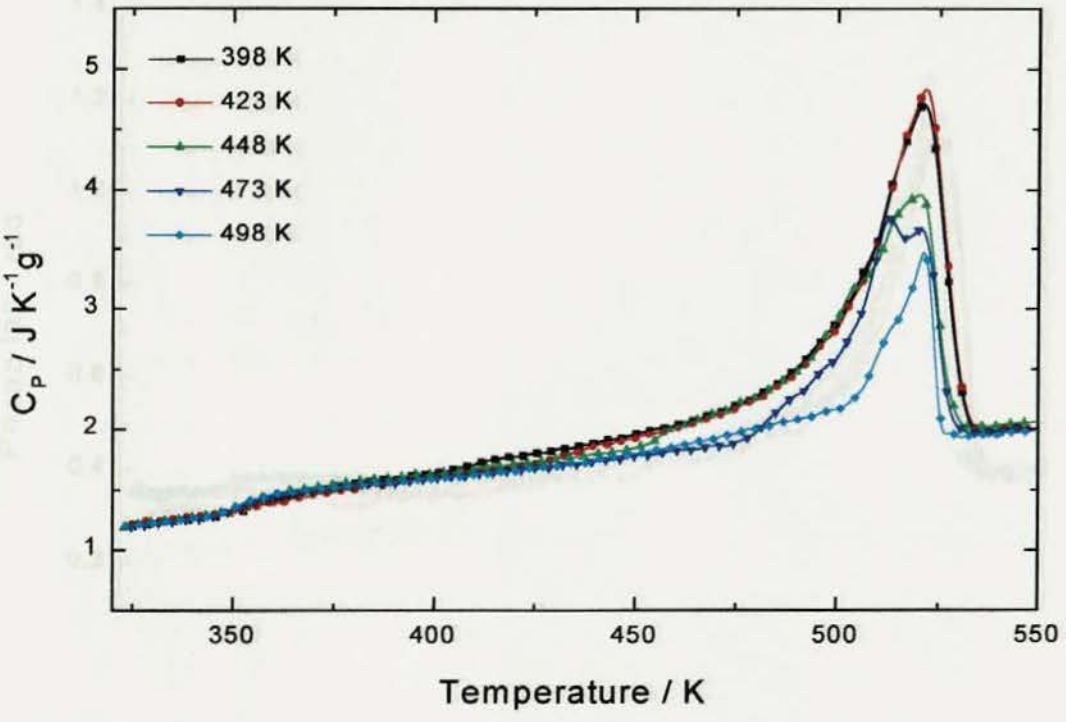

Fig. 7.17b Reversing heat capacity dependence of the crystallisation temperature under condition of B = 2.5 K min^{-1}, A_T = 1.0 K and p = 60 s

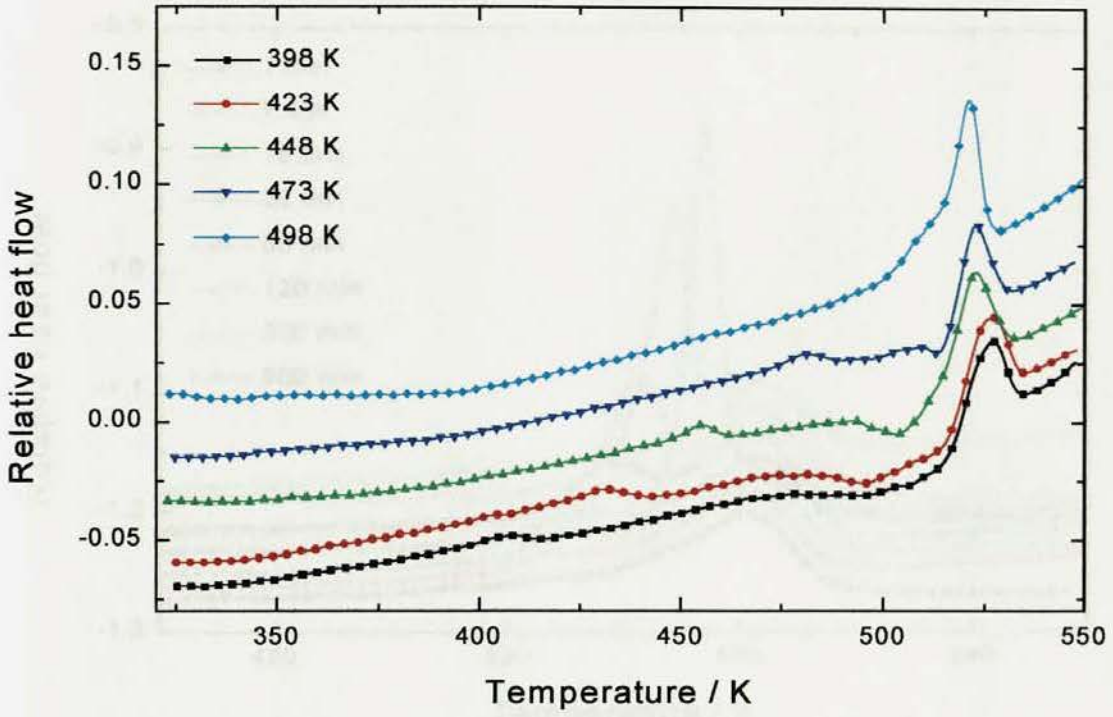

Fig. 7.17c Non-reversing heat flow dependence of the crystallisation temperature under condition of B = 2.5 K min^{-1}, A_T = 1.0 K and p = 60 s

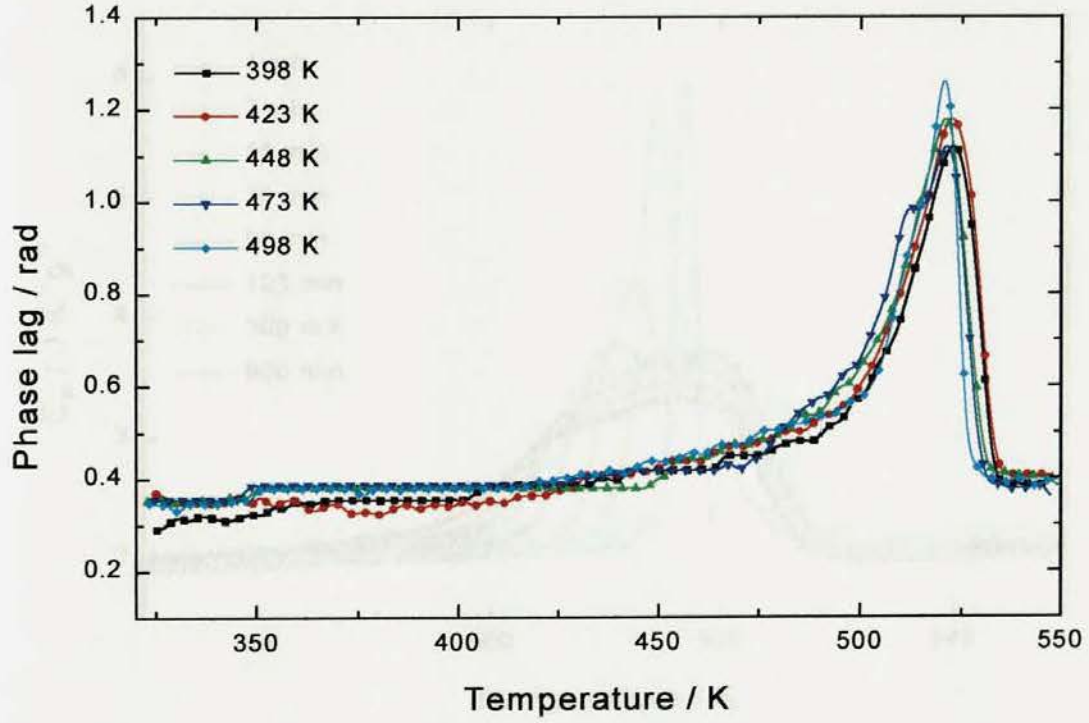

Fig. 7.17d Uncorrected phase lag dependence of the crystallisation temperature under condition of B = 2.5 K min^{-1}, A_T = 1.0 K and p = 60 s

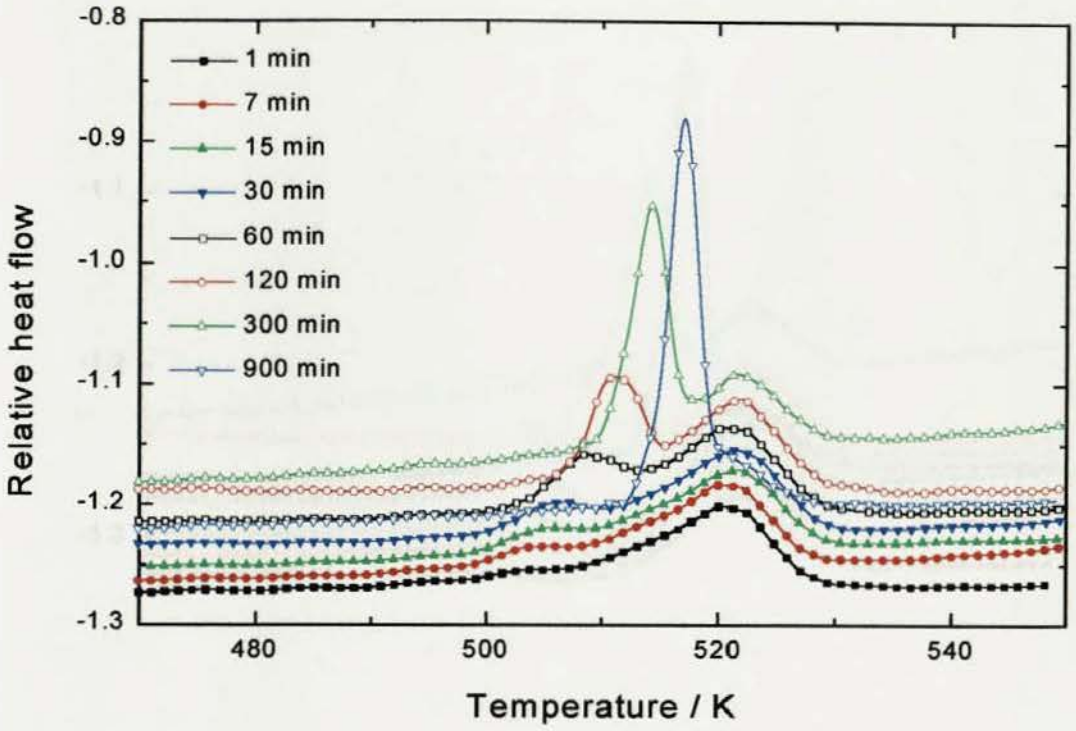

Fig. 7.18a Total heat flow dependence of the crystallisation time(495 K) under condition of B = 2.5 K min^{-1}, A_T = 1.0 K and p = 60 s

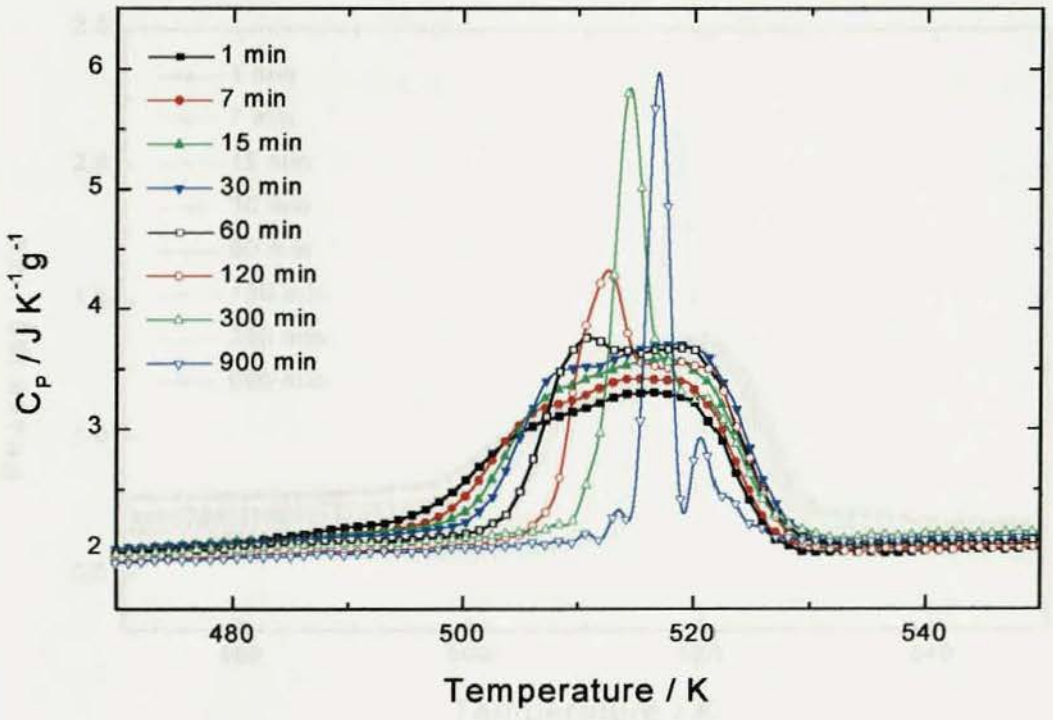

Fig. 7.18b Reversing heat capacity dependence of the crystallisation time(495 K) under condition of B = 2.5 K min^{-1}, A_T = 1.0 K and p = 60 s

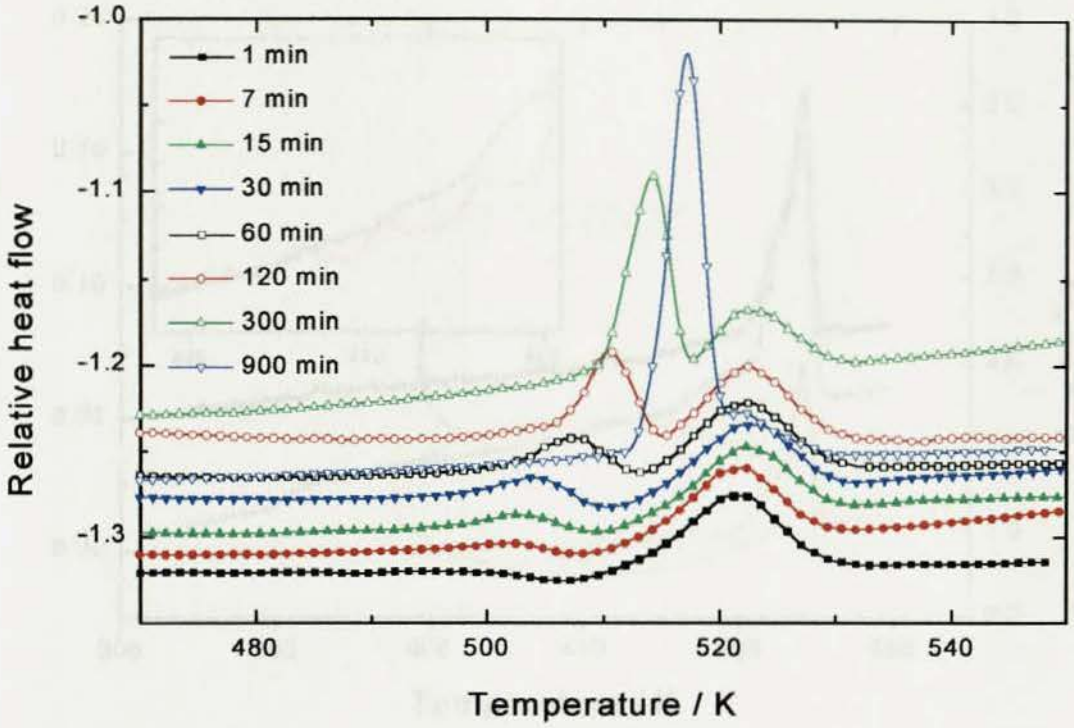

Fig. 7.18c Non-reversing heat flow dependence of the crystallisation time(495 K) under condition of B = 2.5 K min^{-1}, A_T = 1.0 K and p = 60 s

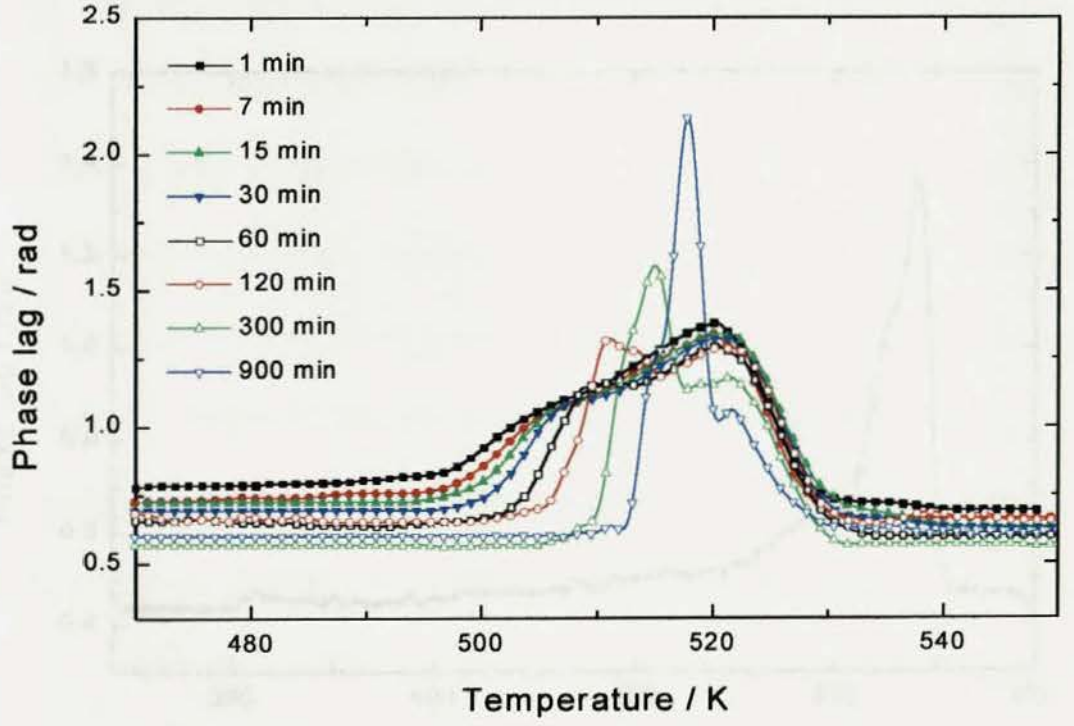

Fig. 7.18d Uncorrected phase lag dependence of the crystallisation time(495 K) under condition of B = 2.5 K min^{-1}, A_T = 1.0 K and p = 60 s

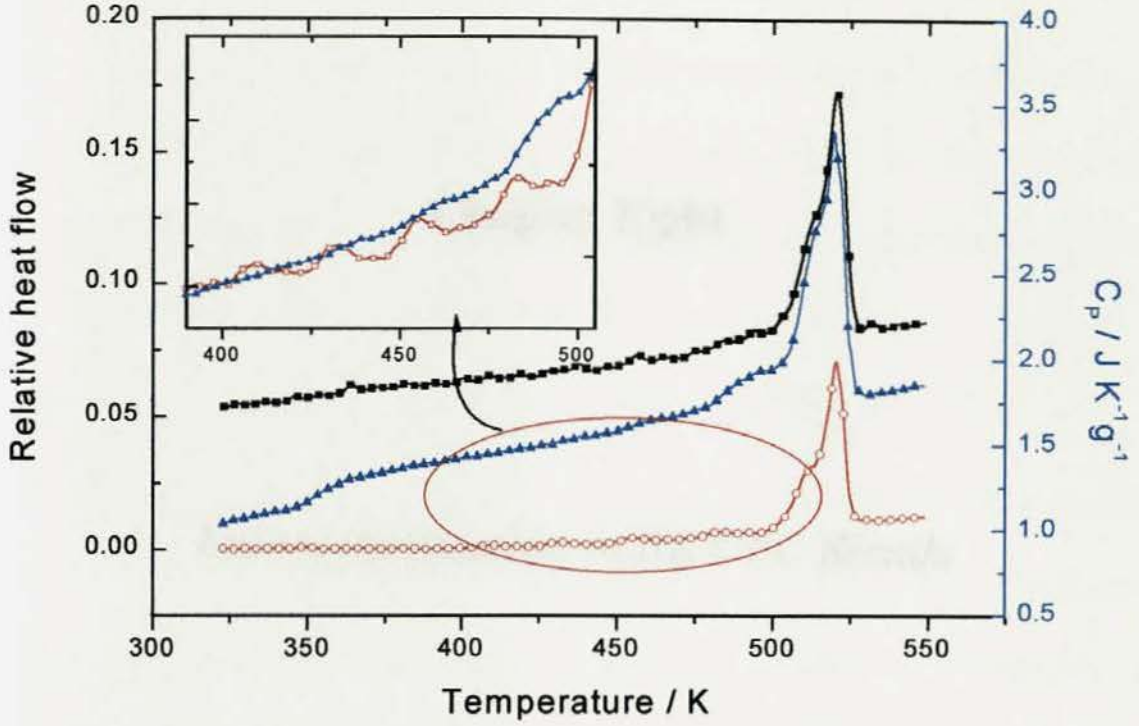

Fig. 7.19a MTDSC analyses after deconvoluted into total heat flow(solid square), reversing heat capacity(solid up triangle) and non-reversing heat flow(open circle). Sample stepwisely crystallised at 498, 473, 448, 423 and 398 K for 1 hr with A_T = 1.0 K B = 2.5 Kmin^{-1} and p = 60 s

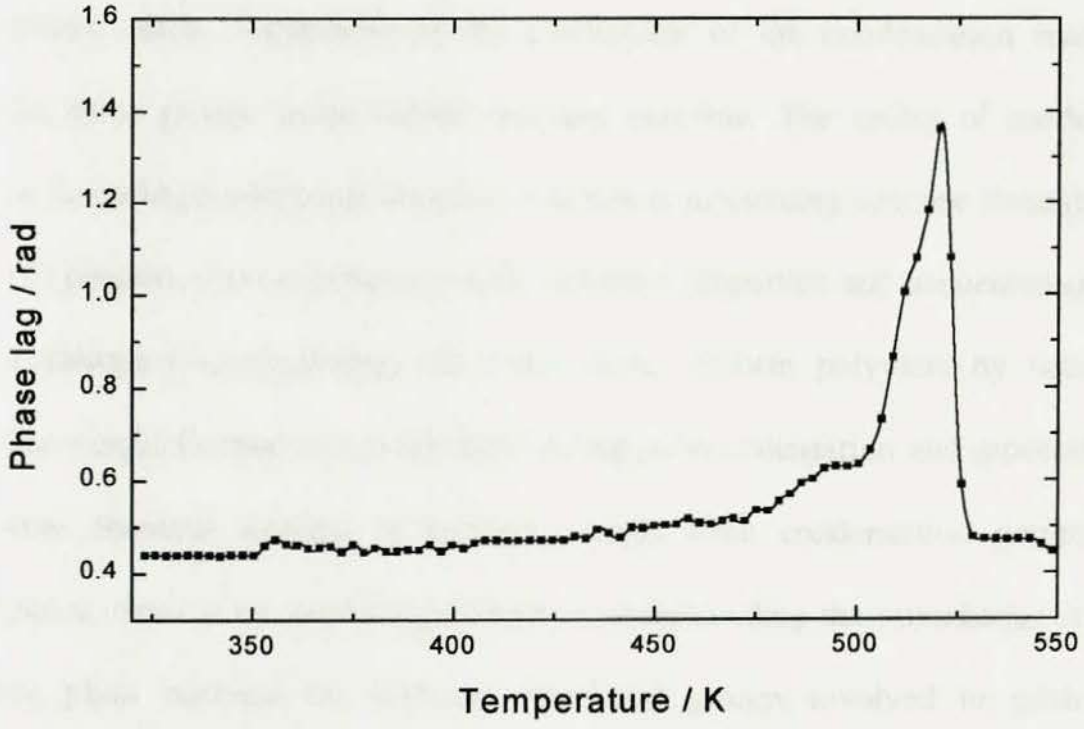

Fig. 7.19b Uncorrected phase lag as a function of temperature. Experiment as above

Chapter Eight

Transesterification in PET/PC Blends

8.1 Introduction

The inherent property of condensation polymers, in contrast to polyolefins, is due to the presence of functional groups, such as ester, amide, urethane and carboxyl *etc.*, along the molecule chain. Regardless of the mechanism of the condensation reaction in synthesis, these groups make further reactions possible. The ability of condensation polymers to undergo additional chemical reaction is fascinating because these reactions can[197] (1) prepare novel copolymers with desirable properties and sequential order, as well as enhanced compatibility, (2) make more uniform polymers by minimising molecular weight fluctuations in the melt during polycondensation and processing and (3) enable chemical healing of laminates made from condensation polymers. In consequence, there is an increasing interest in understanding the interchange reactions that take place between the different functional groups involved in mixtures of polycondensation polymers.

Interchange reactions take place at elevated temperatures (most frequently in the melt) between functional groups inter- or intra-molecule chains. Normally these reactions are reversible and can achieve equilibrium. They include acidolysis, alcoholysis, amidolysis and esterolysis reactions[43]. The last one is also called transesterification and occurs between two polyesters as shown in equation 8.1.

$$RCO_2R'+R''CO_2R'''\Leftrightarrow RCO_2R'''+R''CO_2R' \qquad (8.1)$$

As transesterification proceeds, the initial homopolymers convert to block copolymers and finally into random copolymers[38]. The resultant block and random copolymers are expected to enhance mutual miscibility over the original unreacted components[6].

In this chapter the properties' changes which accompany transesterification and phase coarsening in both blends prepared with and without catalyst have been studied as a function of time and temperature by DSC, SEM and FTIR spectroscopy. The kinetics of transesterification have been determined as well.

8.2 Review of Transesterification in the PET/PC Blends

Polyester blends have been studied both for industrial and academic interest. Many commercial polyester blends based on PET, PBT, PEN and PC have been studied and mainly used for moulded automobile parts. These have been reviewed by Utracki primarily in patents[2]. More general reviews of transesterification have been given by Kotliar[43] and Porter *et al.*[6]. The former author discussed the statistics of three different exchange reactions where the chains are terminated by hydroxyl or carboxyl groups, while Porter *et al.*[6] pointed out that the miscibility of blends is influenced by transesterification.

It is well known that several interchange reactions involving transesterification between PET/PC blends can take place in molten PET/PC at elevated temperature, during prolonged annealing in the absence or in the presence of catalyst[38, 43-45,198]. The most important of these reactions are as following:

(1) the reaction between hydroxyl end groups of PET and carbonate groups of PC (alcoholysis)

$$\sim \text{Ar-COO-Alk-OH} + \sim \text{Ar}'\text{-OCOO-Ar}' \sim \rightarrow$$

$$\sim \text{Ar}'\text{-OH} + \sim \text{Ar-COO-Alk-OCOO-Ar}' \sim \qquad (8.2)$$

where Ar-COO represents a terephthalate unit, -Alk- an alkenyl and Ar′ a bisphenyl one.

(2) the reaction between carboxyl end groups of PET and carbonate groups of PC (acidolysis)

$$\sim \text{Ar-COOH} + \sim \text{Ar}'\text{-OCOO-Ar}' \sim \rightarrow$$

$$\sim \text{Ar}'\text{-OCOOH} + \sim \text{Ar-COO Ar}' \sim \qquad (8.3)$$

(3) the ~OCOOH end group produced in the above reaction will undergo decomposition

$$\sim \text{Ar}'\text{-OCOOH} \rightarrow \sim \text{Ar}'\text{-OH} + \text{CO}_2 \uparrow \qquad (8.4)$$

(4) the phenol groups formed in the above reactions can also decompose to bisphenol-A

$$2 \sim \text{OCOO- Ar}'\text{-OH} \rightarrow \sim \text{OCOO-Ar}'\text{-OCOO} \sim + \text{HO- Ar}'\text{-OH} \uparrow \qquad (8.5)$$

(5) the reaction between ester and carbonate groups (transesterification)

$$\sim \text{Ar-COO-Alk} \sim + \sim \text{Ar}'\text{-OCOO-Ar}' \sim \rightleftharpoons$$

$$\sim \text{Ar-COO-Ar}' \sim + \sim \text{Alk-OCOO-Ar}' \sim \qquad (8.6)$$

The ethylene carbonate group may react with PET continuously

$$\sim \text{Ar-COO-Alk} \sim + \sim \text{Alk-OCOO-Ar}' \sim \rightleftharpoons$$

$$\sim \text{Ar-COO-Ar}' \sim + \sim \text{Alk-OCOO-Alk} \sim \qquad (8.7)$$

(6) the degradation of ethylene carbonate will release CO_2 with the formation of ether groups

$$\sim \text{Alk-OCOO-Ar}' \sim \rightarrow \sim \text{Alk-O-Ar}' \sim + CO_2\uparrow \quad (8.8)$$

$$\sim \text{Alk-OCOO-Alk} \sim \rightarrow \sim \text{Alk-O-Alk} \sim + CO_2\uparrow \quad (8.9)$$

(7) the formation of cyclic ethylene carbonate ($\overline{OCH_2CH_2O\text{-}CO}$) (EC)

From FTIR and NMR spectra and mass spectroscopy, Berti et al.[198] found EC as one of important volatile by-products. In principle there are three different types of intramolecular reactions which produce EC, i.e.

$$\sim \text{OCOO-Alk-OH} \rightarrow \sim \text{OH} + \text{EC}\uparrow \quad (8.10)$$

$$\sim \text{OCOO-Alk-OCO} \sim \rightarrow \sim \text{OCO} \sim + \text{EC}\uparrow \quad (8.11)$$

$$\sim \text{O-Alk-OCOO-Alk-O} \sim \rightarrow \sim \text{O-Alk-O} \sim + \text{EC}\uparrow \quad (8.12)$$

However, the conclusion cannot be drawn as to which one or all of these reactions are responsible for EC formation.

Pilati *et al.*[44] investigated these reactions in the presence and absence of transesterification catalyst, by selective degradation of PC sequences, solubility tests, and IR spectroscopy. They found that the chemical structure of the final blend was strongly dependent both on the mixing time and on the kind of interchange catalyst used with these polymers. Tetrabutylorthotitanate $Ti(OBu)_4$, a transesterification catalyst, gave fast exchange reactions which involve transesterification, alcoholysis and acidolysis reactions, but, at the same time, side reactions took place, leading to discoloration and gas evolution. Without the titanium catalyst, the exchange reaction between ester and carbonate groups proceeded at a much lower rate with neither discoloration nor gas evolution.

By using IR and NMR spectroscopy as well as TGA, Godard *et al.*[45] have studied the reactions taking place in molten mixtures and measured the kinetics of the exchange reaction. They found that the main reaction was that of transesterification, which could be described as a second-order reaction. They also observed that ethylene carbonate produced as a product was unstable and ultimately disappeared. It was suggested that this degradation played an important role in the transesterification process. As a consequence of the irreversible decomposition of the ethylene carbonates, the exchange reaction was far from equilibrium.

Montaudo *et al.*[199] studied the mechanism of the ester exchange in PET/PC blends with capped or reactive chain end groups. They found that the exchange process occurred by two different mechanisms: (1) a direct exchange reaction between functional groups located within the polymer chains (inner-inner) and (2) by the attack of reactive chain ends with inner groups (outer-inner). The inner–inner mechanism occurs only in the reaction between end-capped or high molar mass PET/PC blends. On the other hand, the outer-inner mechanism occurred in the presence of hydroxyl or carboxyl reactive chain ends in PET samples. The reaction proceeded by the attack of the reactive end groups on the PC chains, producing block copolymers and lower mass PC with terminated by phenol group. The reaction stopped after the reactive end groups were consumed. The amount and the composition of the copolymers generated in the reactions were constant as a function of time.

Ignatov and co-worker[200-202] systematically investigated the catalytic activity on the exchange reactions. They compared the reactivity of various lanthanide compounds

(based on europium, cerium, samarium, terbium and erbium), and titanium- and calcium/antimony-based catalysts. Lanthanide catalysts, especially those based on samarium, europium and cerium, offered several advantages over the traditional catalysts, because they allowed exchange reactions to be controlled more easily, and at the same time they did not promote side reactions. They also found that alkaline earth catalysts possessed some activity in exchange reactions, which increased with increasing atomic number of the metal. Using samarium acetylacetonate as a catalyst the miscible blends, a transparent amorphous glass with a single T_g, were produced at 275°C by blending in a twin-screw extruder.

8.3 Results and Discussion

8.3.1 Thermal Properties Change with Transesterification

DSC analyses of the PET50/PC50 blends, both with and without added catalyst and annealed at different temperature and time, are shown in Fig.s 8.1 – 8.6. The glass transition temperature, crystallisation and melting temperatures (peak values) are summarised in Fig.s 8.7 and 8.8. In both blend systems, the T_gs of the PET rich phase shifted to higher temperature, while the T_gs of the PC rich phase shifted to lower temperature with prolonging periods of time. Finally only one T_g was observed except in blends without added catalyst annealed at 513 K. The time to observe only one T_g decreased markedly with increasing annealing temperature especially in the blend system with added catalyst. The change was much slower without catalyst being present. For example, at 523 K it took 22.5 hrs to observe only one glass transition with

the transition spread over about 40 K in the blends without added catalyst, and only 5 hrs to observe one glass transition with the transition spread over 18 K in the blends with catalyst. A single T_g at about 375 – 379 K for PET50/PC50 blend was consistent with that calculated according to Fox equation[19] for the miscible blend. With only one T_g present the blends did not show any crystallisation or melting on heating, indicating that a random copolymer was formed at this stage.

In the blends prepared with added catalyst, the crystallisation temperature initially decreased to some extent, and then increased to higher temperature, see Fig. 8.7b. The decrease was up to 20 K for annealing at 503 and 513 K. The crystallisation temperature changed insignificantly in the blends without added catalyst. Initially the crystallisation temperature did not decrease but shifted to higher temperature; after annealing for 5 to 12 hrs (depending the annealing temperature), it then dropped to some extent but the final value was still higher than the initial one, see Fig. 8.8b. The decreases changed from 16, 12 and 5 K with increasing annealing temperature.

Melting temperature showed a general tendency to decrease with annealing (Fig.s 8.7b and 8.8b). However, for blends with added catalyst the melting temperature exhibited an increase at the point where the crystallisation temperature dropped. For blends without added catalyst such increase was observed only at lower annealing temperature, i.e. 513 K.

The relative enthalpies of fusion for the blends prepared with and without added catalyst are shown in Fig.s 8.9 and 8.10 respectively. Each curve was obtained by integrating the

DSC response from above the T_g of PC to the last trace of melting. There was a maximum in relative enthalpy change that represented the greatest degree of crystallinity reached during the heating process. It is cleat that in the blends with catalyst the greatest crystallinity increased to a maximum value and then decreased to nearly zero. In the blends without added catalyst, the greatest crystallinity was present in the sample without annealing and it decreased monotonically with annealing time.

Sample weights were also measured before and after annealing. The weight loss from the blends annealed at different temperature and periods of time are shown in Fig. 8.11. It is apparent that the weight losses were proportional to annealing temperature and time. It was assumed that the reaction mechanism did not change under these experimental conditions and the overall rate constant was obtained from the weight loss, see Fig. 8.12. This followed a first-order reaction since the plot of *ln w vs.* t was found to be linear. From this rate constant, the activation energies of the overall decomposition reaction were obtained as the slope of Arrhenius plot in Fig. 8.13. Their values were 88 ± 13 and 160 ± 25 kJ mol^{-1} for blends with and without catalyst, respectively. These results were consistent with the change rate of T_g for different blends.

8.3.2 Morphology of the Blends

The above results indicated that with prolonging annealing time the original polymers change gradually into block copolymers, and finally to random copolymers with a loss in their ability to crystallise. During annealing the crystallisation temperature and ability

to crystallise did not decrease monotonously, especially for blends with added catalyst. It must be related to changes in microstructure.

Fig.s 8.14 and 8.15 show the optical micrographs of PET50/PC50 blends (prepared with added catalyst) annealed at 523 K for different periods of time. The occurrence of transesterification and further phase coarsening can be seen clearly from changes in the domain sizes. Phase coarsening dominated the first 15 min of annealing during which there was an obvious increasing in domains and after which transesterification dominated with the domains decreasing in size. The boundaries and contrast between the domains become less obvious, and finally (at 45 min) it was difficult to distinguish between them. In Fig. 8.15 spherulites are distributed uniformly at the beginning, but after annealing for 20 min obvious bicontinuous domains (one crystalline and the other amorphous) were observed. On further annealing, smaller spherulites were observed, and after 60 min the spherulites could not be seen. The lack of birefringence implied that the samples were amorphous.

For blends prepared without added catalyst, the polarised light micrographs are shown in Fig.s 8.16 and 8.17. Although phase coarsening was not so obvious as with the blends with added catalyst, it was still present in the initial 20 min. Thereafter transesterification began to dominate and during which other characteristics of transesterification were present. The crystallised sample showed that the PET50/PC50 blend was bicontinuous at the beginning but after annealing for 60 min the sample crystallised extremely slowly at 453 K and took 120 min to crystallise fully. This would normally take PET only a few minutes at this temperature.

The morphologies of the bulk samples annealed at 523 K for different time were also examined by SEM. The micrographs of the cryo-fracture surfaces for blends prepared with and without added catalyst are shown in Fig.s 8.18 and 8.19 respectively. These were similar to the optical micrographs in that phase coarsening and transesterification were also reflected in the changes observed in the microstructures. Nevertheless, due to the much higher magnification used in SEM the microstructure was clearer in comparing Fig.s 8.14a, 8.15a and 8.18a. SEM images of the blends with catalyst apparently showed that the microstructure prior to annealing consisted of fine bicontinuous domains. These underwent further phase coarsening, probably up to 30 min under the annealing condition. The uniform microstructure observed on annealing for 5 hrs was consistent with the DSC result (Fig. 8.3b), in that no crystallisation, no melting peak and only one T_g was observed. SEM micrographs of the blends without added catalyst indicated that less phase coarsening occurred in these blends because the original structure was already coarse bicontinuous phases. A homogeneous structure was obtained only after annealing for 20 hrs, indicating that transesterification rate was much slower than in blends with added catalyst.

8.3.3 FTIR Spectra of the PET50/PC50 Blends

Fig.s 8.20 and 8.21 show the FTIR spectra of solvent-cast films of PET50/PC50 blends prepared with and without added catalyst and annealed at 523 K for different times. The most important absorption bands of PET and PC as well as their assignment are listed in table 8.1. The spectrum of PC is dominated by a C=O stretching absorption band at 1775 cm^{-1} which progressively decreased and eventually disappeared on annealing. The

ester C(O)-O absorption bands of PC at 1205 and 1162 cm^{-1} also decreased in intensity and shifted to higher wavenumbers. At the same time, a band progressively appeared and finally became well-defined at 1076 cm^{-1}. This represents a complex vibration of a diphenyl ester as following[206]:

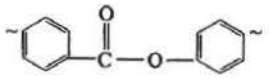

The appearance of this group, bearing evidence of a transesterification reaction, should be accompanied by the appearance of new C=O stretching band that is distinguishable from the existing carbonyl group stretching band. It has been shown that the new carbonyl band should be at 1740 cm^{-1} for poly(bisphenol-A terephthalate)[206]. However, it was not observed in the spectra of PET50/PC50 blends annealed under any condition. This may be due to it overlapping with the aromatic/aliphatic carbonate group (1764 cm^{-1}) and the aliphatic/aliphatic carbonate group (1745 cm^{-1}) [198]. Thus, the original ester band of PET (1723cm^{-1}) broadens and becomes an intense strong band at 1738 cm^{-1}. The main difference between the two blends (Fig.s 8.20 and 8.21) was that the transesterification rate was much faster in the blends with added catalyst.

8.3.4 Determination of Transesterification Kinetics

As has already been pointed out[45], the main reaction occurring on annealing the PET/PC blends at high temperature in the molten state is transesterification. This can be described by a second-order reaction (first order with respect to each component). From both FTIR spectral change and weight loss results the transesterification reaction kinetics can be measured. The main reaction is

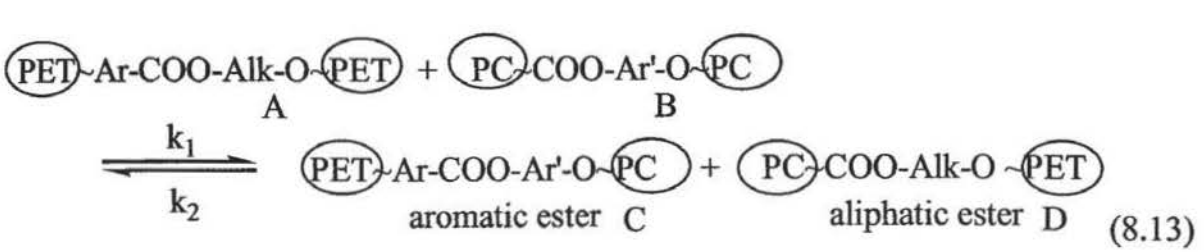

(8.13)

To simplify, A, B, C and D represents the various polymers and copolymers. Transesterification is normally a reversible reaction[43,207], since the ethylene aliphatic carbonate is unstable the reaction will shift further to the right hand side[45,198]. As mentioned earlier, the decomposition products may be CO_2 or cyclic ethylene carbonate (EC)[45,198]. At the start of the reaction the copolymer concentration is much lower than the equilibrium concentration and the reversible reaction can be neglected. Thus

$$-\frac{d[B]}{dt} = k_1[A][B] \tag{8.14}$$

At t = 0 the concentrations of A and B are equal to original blend ratio, $[A_0]$ and $[B_0]$ respectively and at time t,

$$[A] = [A_0] - x \; and \; [B] = [B_0] - x \tag{8.15}$$

Inserting these into (8.14) leads to

$$\frac{dx}{dt} = k_1([A_0] - x)([B_0] - x) \tag{8.16}$$

Integrating gives

$$\frac{1}{[A_0]-[B_0]}(\ln\frac{[A]}{[B]} - \ln\frac{[A_0]}{[B_0]}) = k_1 t \tag{8.17}$$

Plots of $([A_0] - [B_0])^{-1}\ln([A]/[B])$ against t are shown in Fig. 8.22. Obviously the plot is not linear. The initial slope of the curve was taken as the rate constant. These values are listed in table 8.2 and they are close to the values obtained by Godard *et al.*[45]. It can be

seen that the rate constant of the blends with catalyst is greater than that of the blends without added catalyst at the same temperature. The Arrhenius plots of the transesterification reaction are shown in Fig. 8.23. The Activation energy and pre-exponential factor were determined as the slope and intercept of the Arrhenius plot and the values are also listed in table 8.2. It is clear that the activation energies are nearly the same for both blends. This value is close to that of the polycondensation reaction of polyester (about 150 kJ mol^{-1}) [208].

8.3.5 Discussion

It is worth noting that initially in the annealing the crystallisation temperature shifted to lower temperatures and the crystallinity increased in the blends with catalyst. This appears to be at odds with transesterification which should lower the ability to crystallise[6]. It was observed, however, that phase coarsening had occurred and since the original structure was very finely dispersed then crystallisation would be hindered by PC and limited to each fine particles. This results in a higher crystallisation temperature and lower crystallinity. With increasing phase sizes on annealing such hindrances should be decreased and thus the crystallisation temperature shifted to higher temperature and the crystallinity decreased.

It was found that the rate of transesterification was greatly different in samples with different thicknesses, i.e. in the DSC and SEM thick samples and in the optical microscope and FTIR spectroscopic thin sample. The obvious crystallisation and the melting of DSC responses (Fig. 8.3b), and two phase structure (Fig. 8.18d) were

observed for the blends with added catalyst annealed at 523 K for 1h, on the other hand only small crystals were observed in the optical micrographs (Fig. 8.15d) and carbonyl band showed as shoulder in FTIR spectra (Fig.8.20). This can be seen more clearly in the blends without added catalyst. Crystallisation and melting were readily observed in the sample annealing at 523 K for 8 hrs while it took 2 hrs to fully crystallise the sample annealed at 523 K for just 1 h by optical microscopy. This is probably due to a volatile decomposition product, EC, leading to a reversible reaction with ester groups[198]. In thin samples, 20 μm for optical microscopy and less than 5 μm for FTIR, EC can diffuse out of samples more rapidly than with the thick samples, about 800 μm.

8.4 Conclusions

Due to the thermodynamic immiscibility of PET and PC[209] phase separation occurs inevitably in the molten state, but the transesterification also takes place. Both of these factors affect the properties of the blends and the initial microstructure determines which is a dominant factor. With increasing transesterification, the initial immiscible blends become more compatible and eventually miscible blends with one T_g only are produced. The tendency for PET to crystallise is reduced as a result of this process. When random copolymers are formed the blends lose their ability to crystallise completely and no melting is observed.

Transesterification kinetics of PET50/PC50 blends have been studied in this work. It was confirmed that the main reaction was transesterification which was described as a second-order reaction. The activation energy of the transesterification reaction was 170 ± 10 kJ mol^{-1} close to that normally observed for a polycondensation reaction in polyester.

Table 8.1 Assignment of the major absorption bands in the IR spectra of PET and PC at room temperature[203,204]

Assignment	Wavenumber (cm^{-1})	
	PET	PC
Carbonyl C = O stretching	1723	1775
Aromatic skeletal stretching	1504, 1410	1506, 1410
Conformational[205]	1370, 1340	
Ester C(O) – O stretching	1264	1235 - 1165
In plane ring bending	1120, 1018	1015
Out of plane ring deformation	874	832
Coupled vibration of carbonyl and aromatic ring out of plane	727	

Table 8.2 Kinetic rate constants for the transesterification reaction in PET50/PC50 blends using band 1776 cm^{-1} of FTIR spectroscopy

Temperature K	Blends with added catalyst k_1 / min^{-1}	Blends without catalyst k_1 / min^{-1}
503	0.0012	
513	0.0026	0.0018
523	0.0030	0.0025
533	0.022	0.0073
543		0.015
Activation energy / kJ mol^{-1}	170 ± 10	180 ± 10
Pre-exponential factor / s^{-1}	1.96×10^{13}	3.46×10^{13}

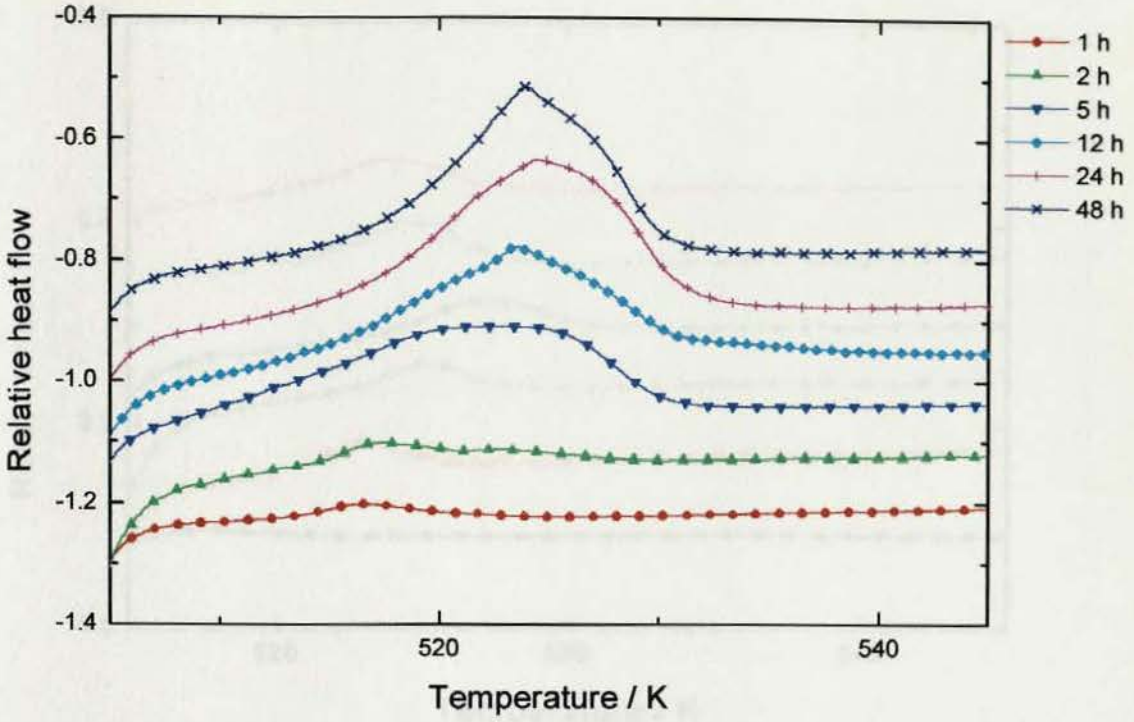

Fig. 8.1a DSC analyses of PET/PC 50/50 blends (prepared with added catalyst) annealed at 503 K for different time and immediately heated to melt at 10 K min^{-1}

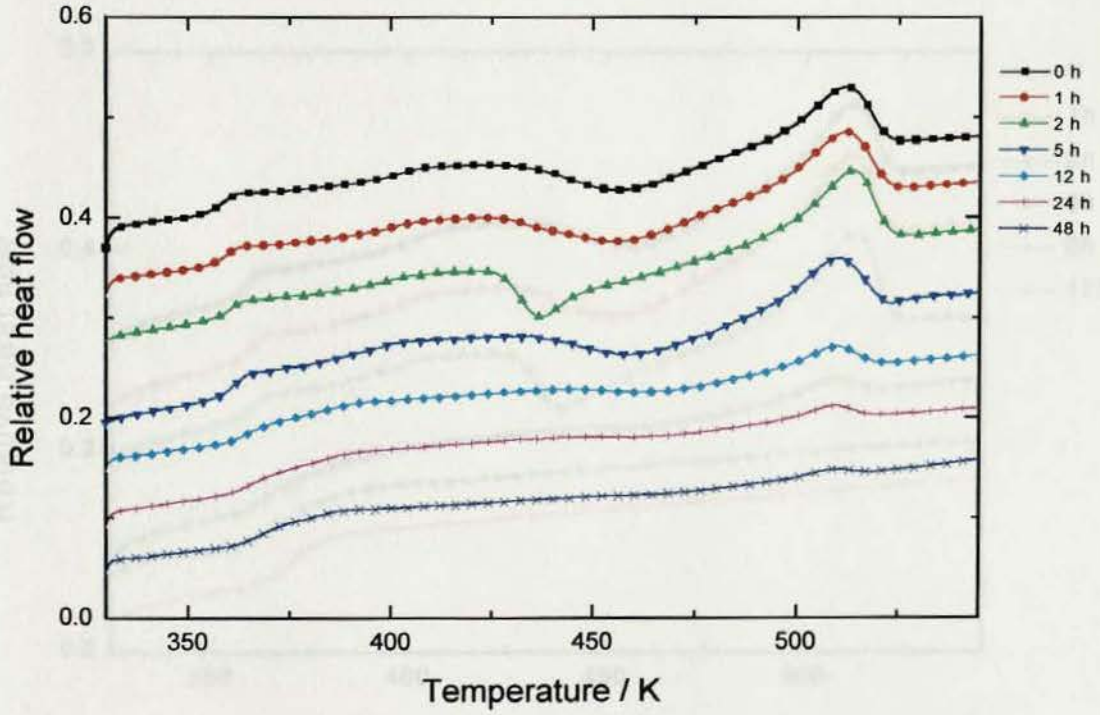

Fig. 8.1b DSC analyses of PET/PC 50/50 blends after Fig. 8.1a at a heating rate of 10 K min^{-1}

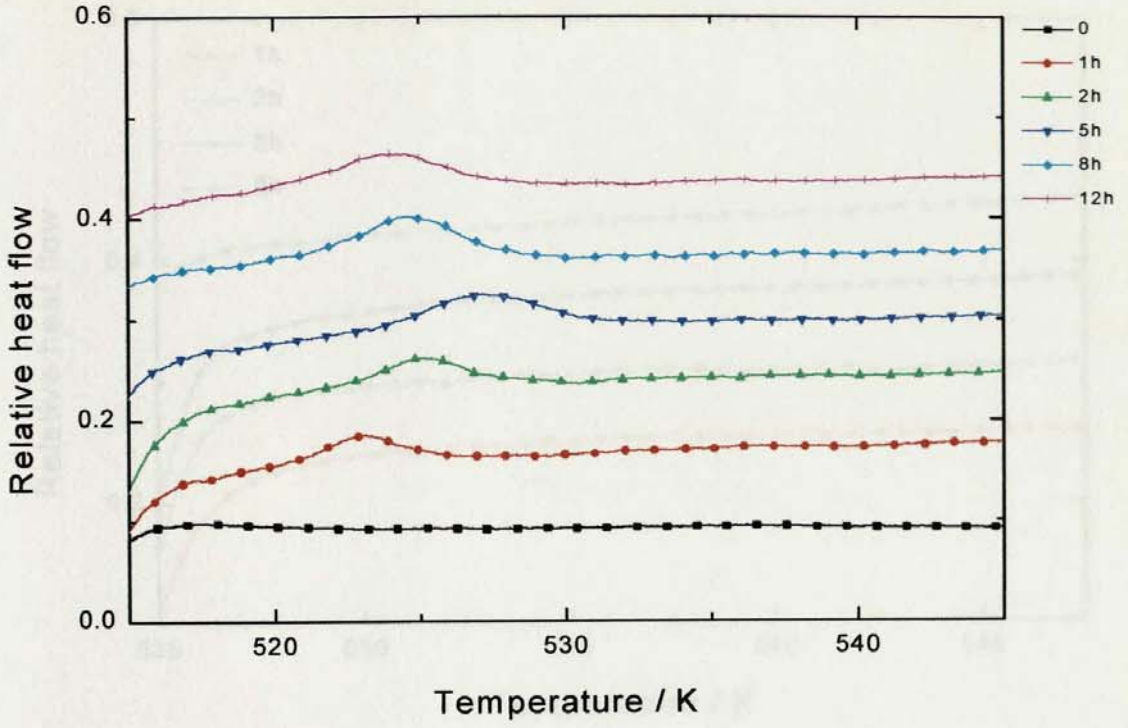

Fig. 8.2a DSC analyses of PET/PC 50/50 blends (prepared with added catalyst) annealed at 513 K for different time and immediately heated to melt at 10 K min^{-1}

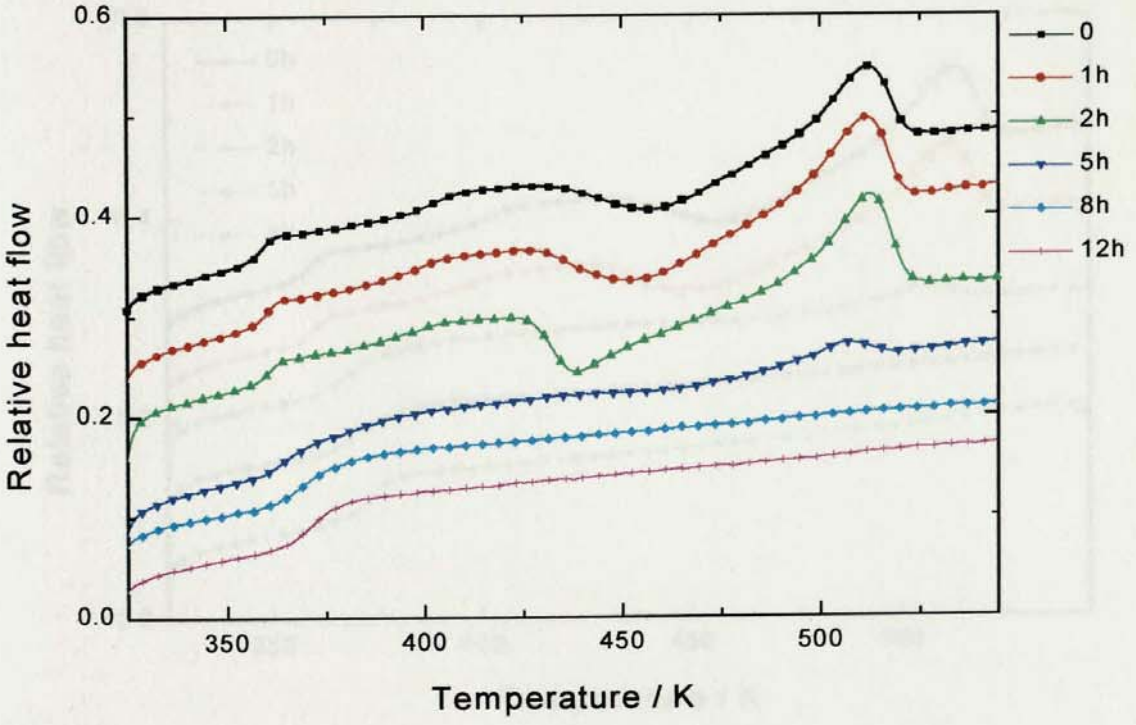

Fig. 8.2b DSC analyses of PET/PC 50/50 blends after Fig. 8.2a, at a heating rate of 10 K min^{-1}

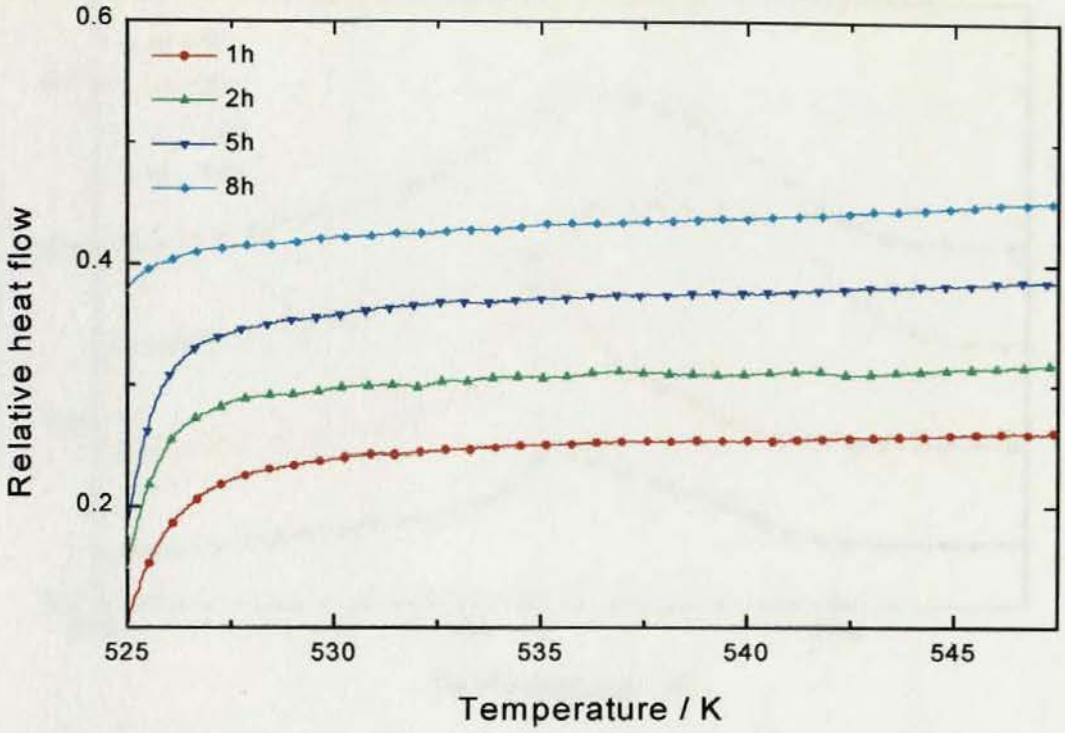

Fig. 8.3a DSC analyses of PET/PC 50/50 blends (prepared with added catalyst) annealed at 523 K for different time and immediately heated to melt at 10 K min^{-1}

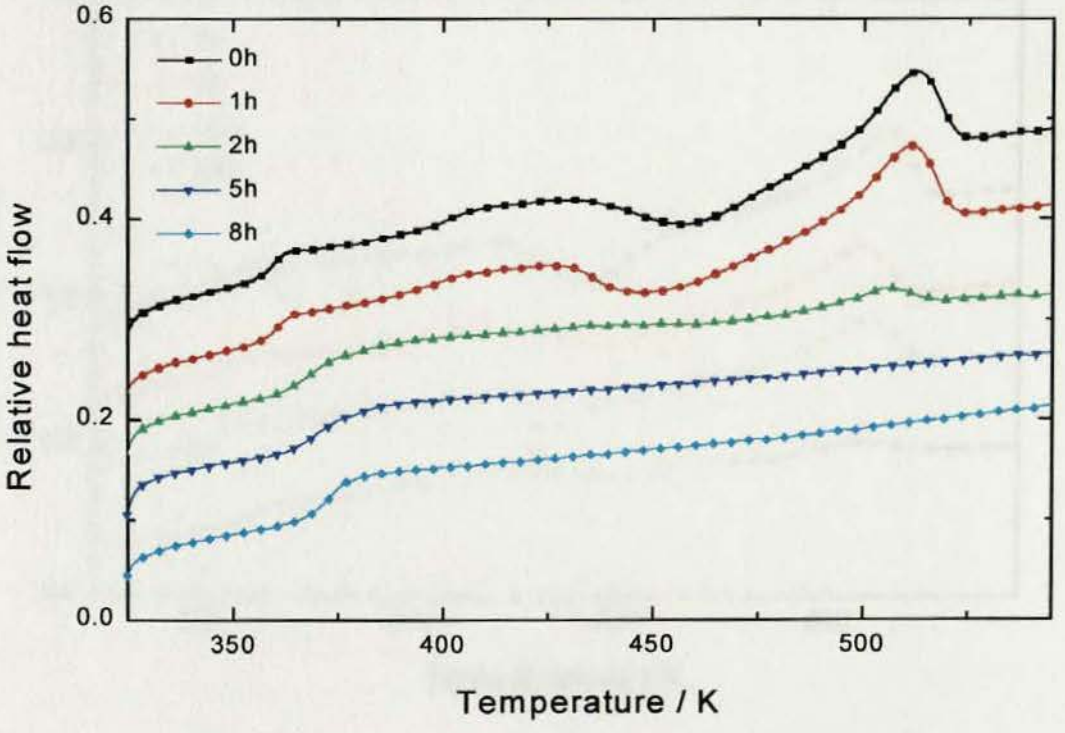

Fig. 8.3b DSC analyses of PET/PC 50/50 blends after Fig. 8.3a, at a heating rate of 10 K min^{-1}

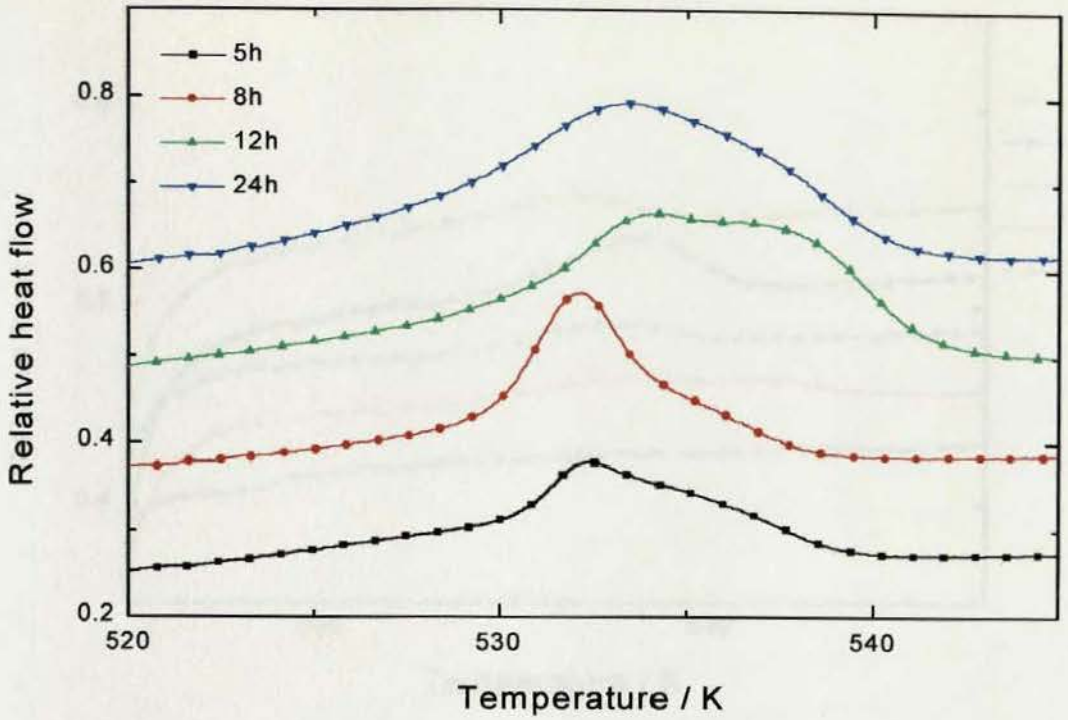

Fig. 8.4a DSC analyses of PET/PC 50/50 blends (prepared without added catalyst) annealed at 513 K for different time and immediately heated to melt at 10 K min^{-1}

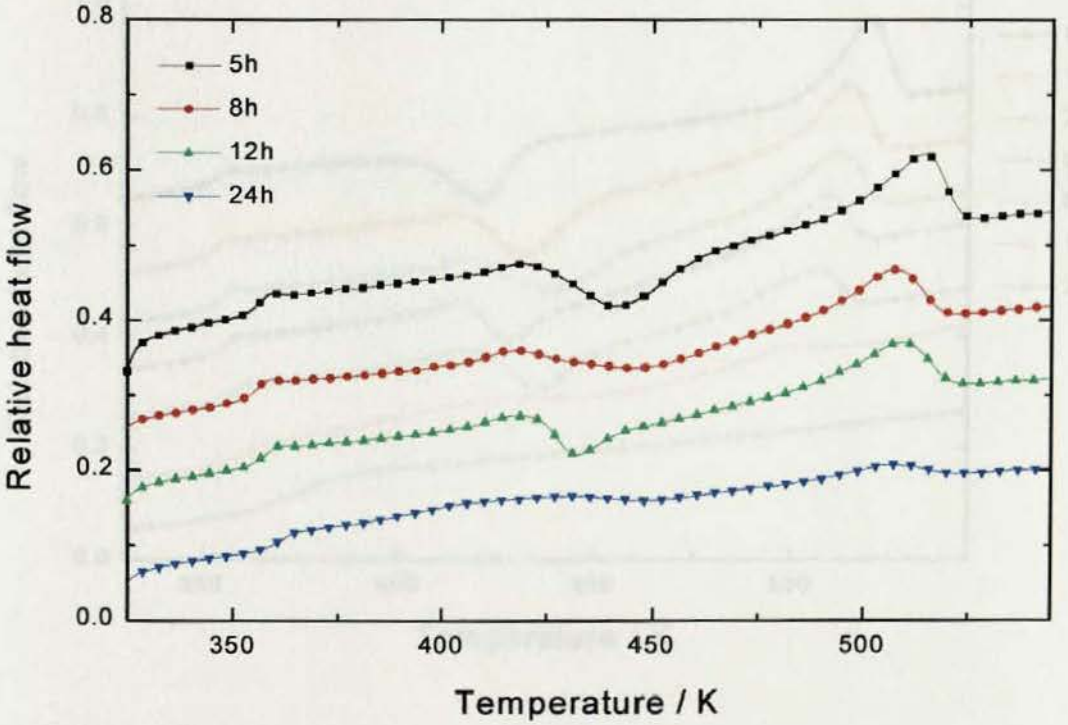

Fig. 8.4b DSC analyses of PET/PC 50/50 blends after Fig. 8.5a, at a heating rate of 10 K min^{-1}

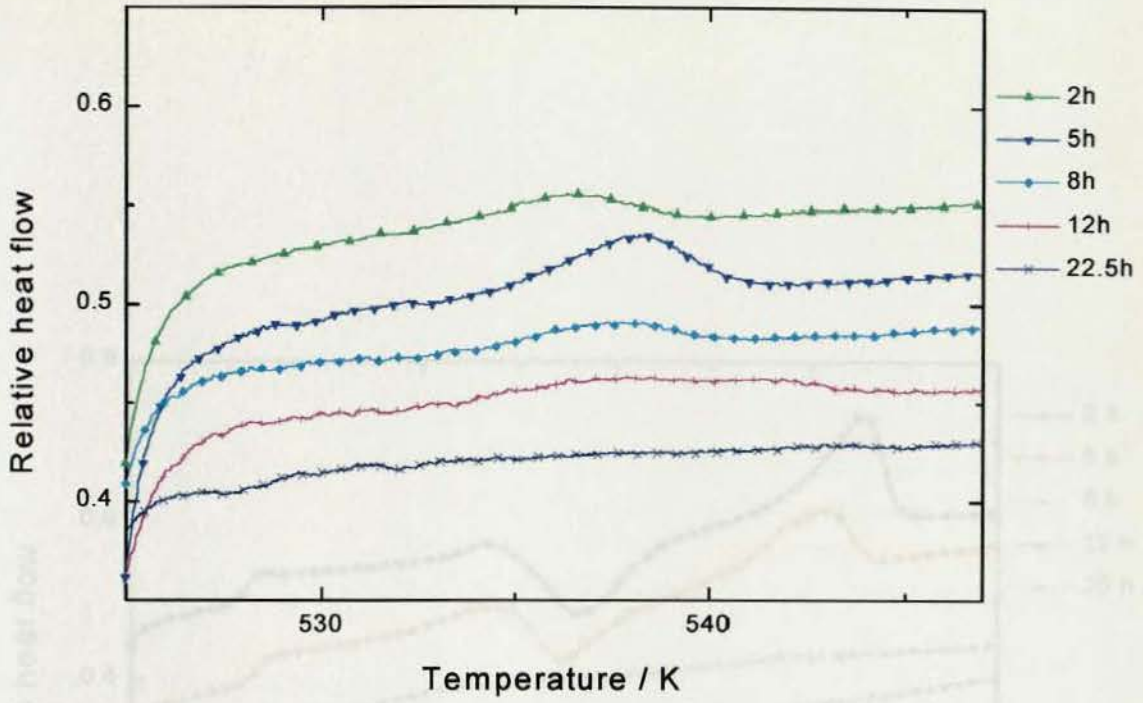

Fig. 8.5a DSC analyses of PET/PC 50/50 blends (prepared without added catalyst) annealed at 523 K for different time and immediately heated to melt at 10 K min^{-1}

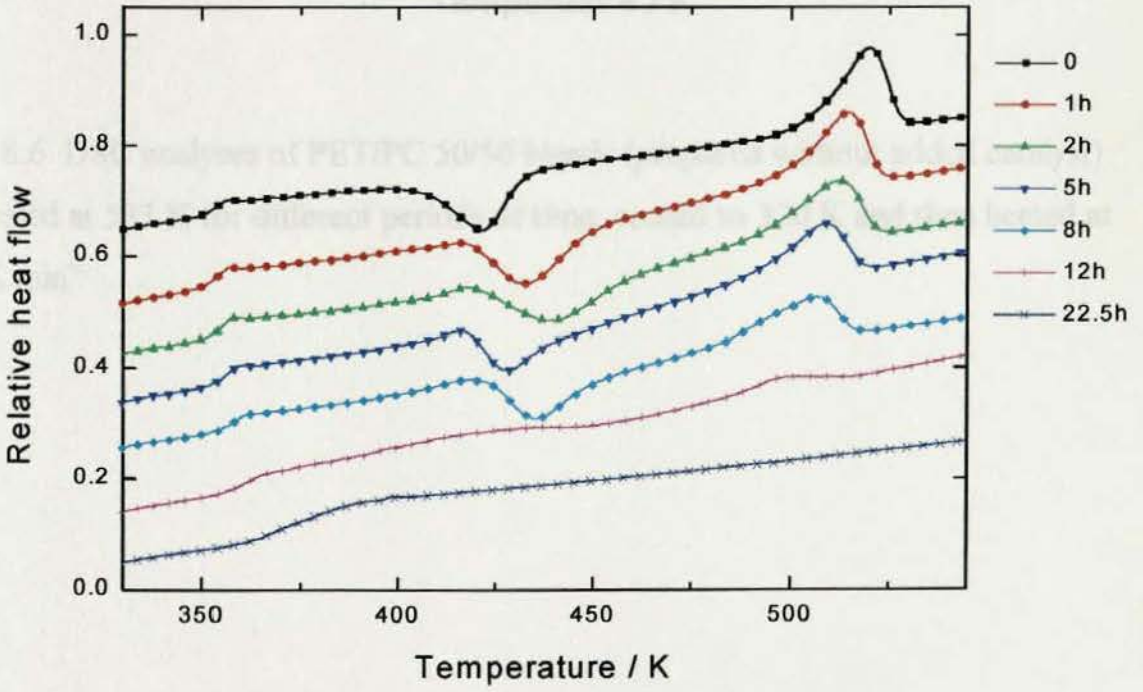

Fig. 8.5b DSC analyses of PET/PC 50/50 blends after Fig. 8.6a, at a heating rate of 10 K min^{-1}

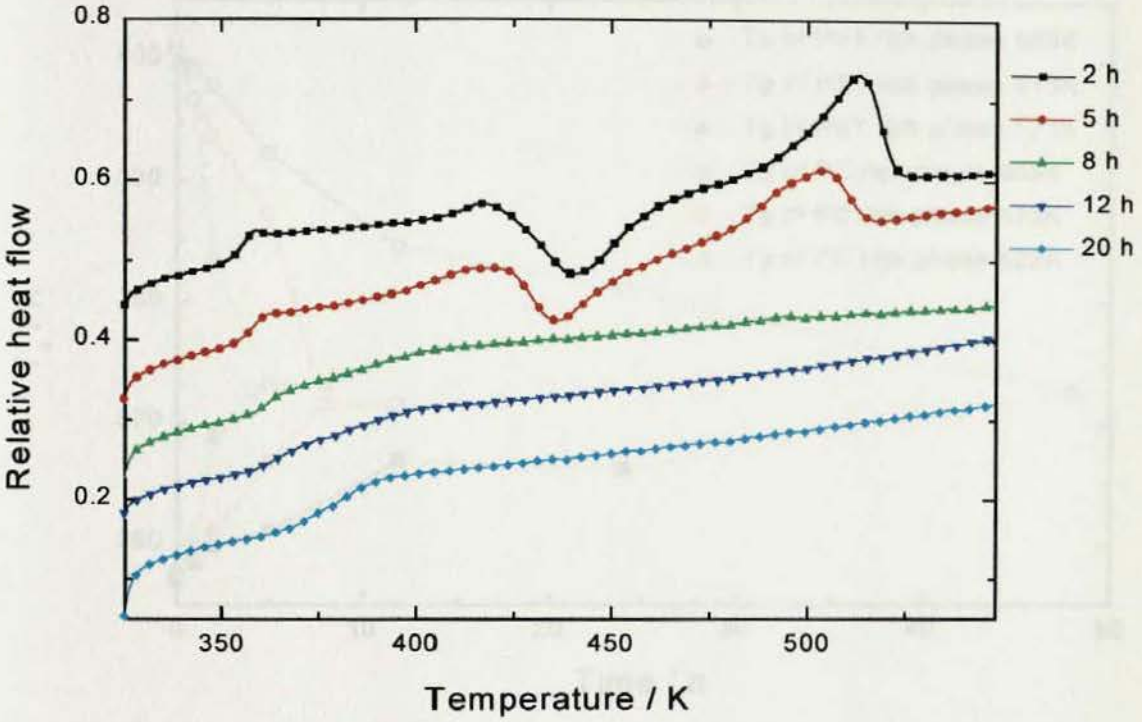

Fig. 8.6 DSC analyses of PET/PC 50/50 blends (prepared without added catalyst) annealed at 533 K for different periods of time, cooled to 320 K and then heated at 10 K min^{-1}

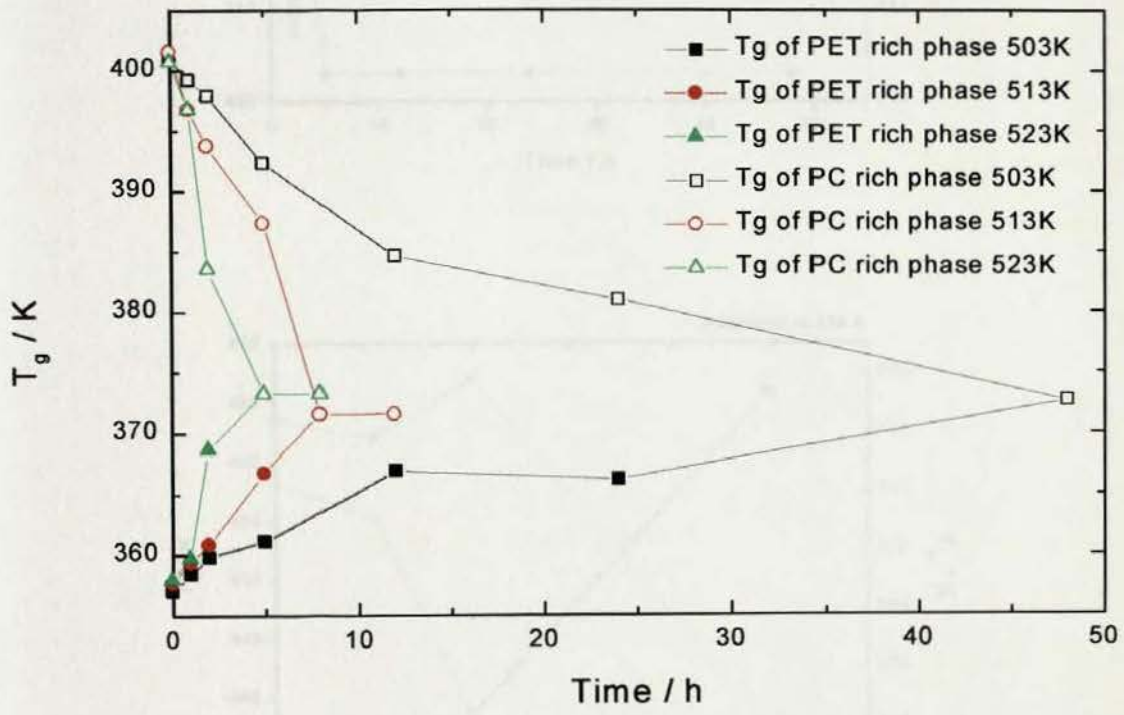

Fig. 8.7a The glass transition temperature of PET/PC 50/50 blends (with catalyst) as a function of annealing temperature and time

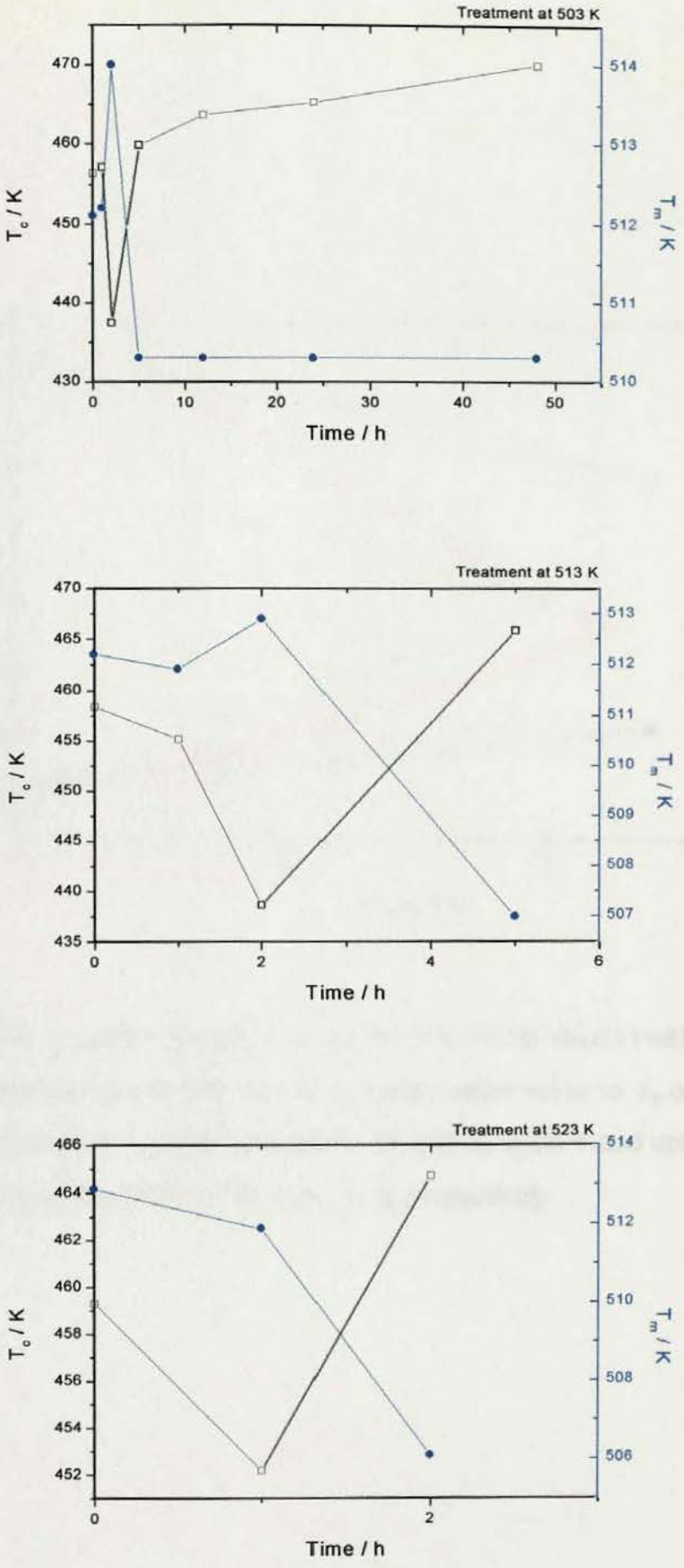

Fig. 8.7b The crystallisation temperature and melting temperature of PET/PC 50/50 blends (with catalyst) as a function of annealing temperature and time

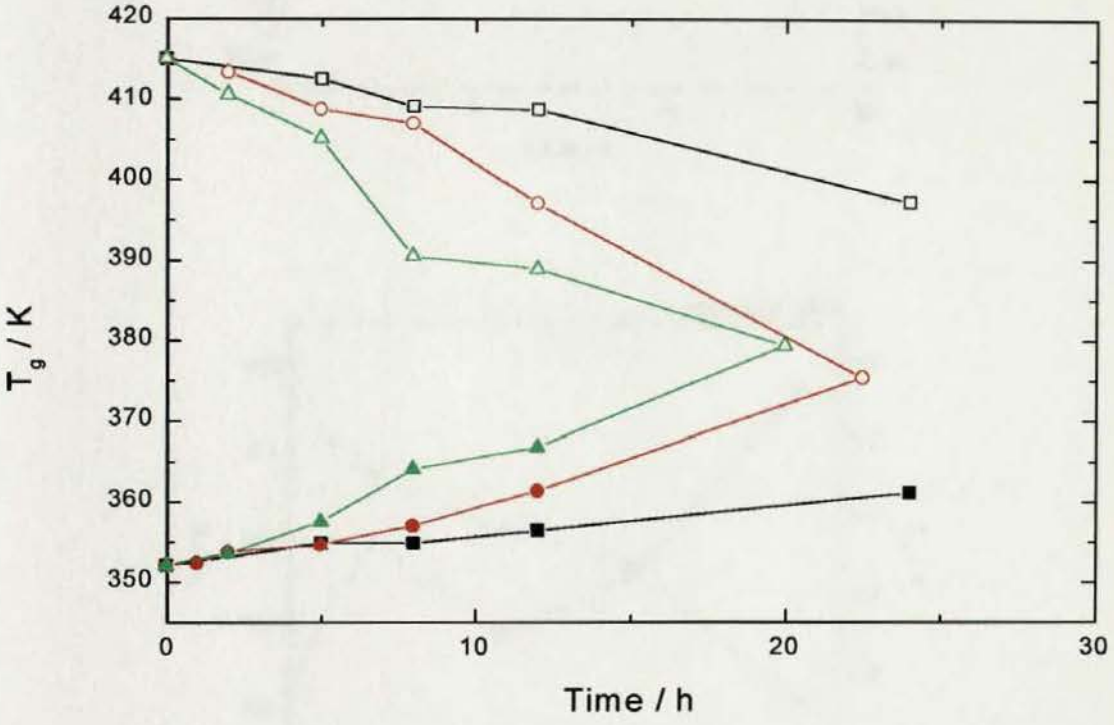

Fig. 8.8a The glass transition temperature of PET/PC 50/50 blends (without catalyst) as a function of annealing temperature and time. Solid scatter refers to T_g of PET rich phase and open scatter to T_g of PC rich phase. Square ■, cycle ● and uptriangle ▲ represent the temperature of 513, 523 and 533 K respectively

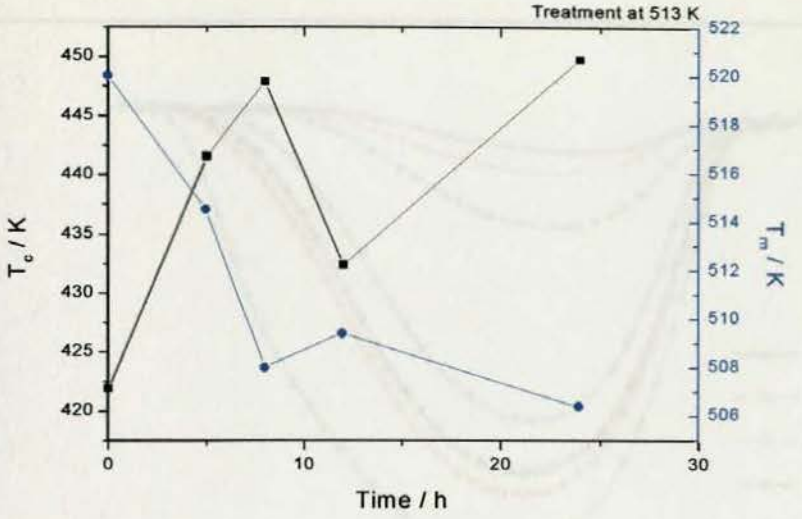

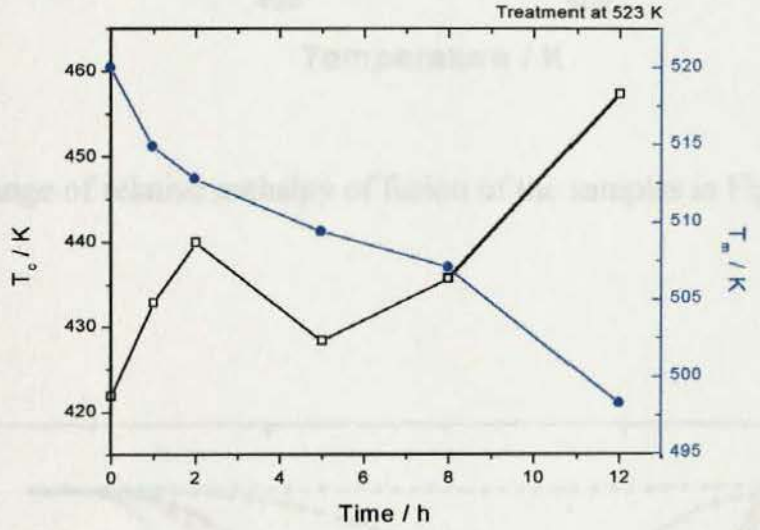

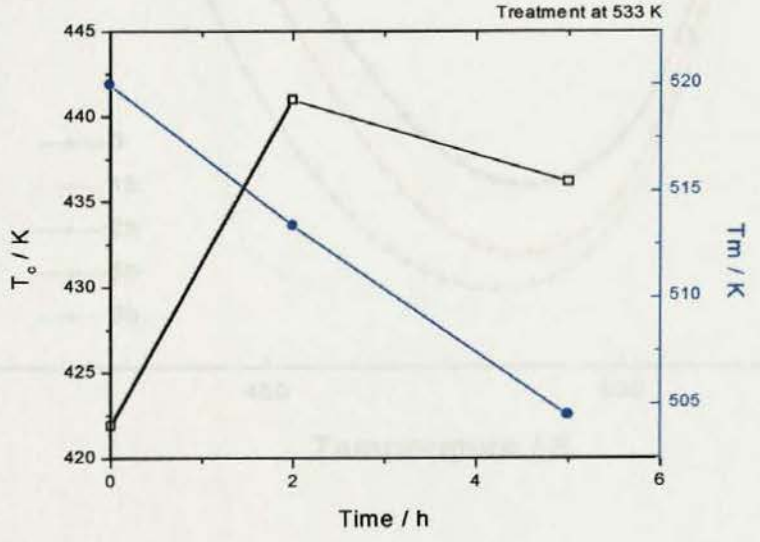

Fig. 8.8b The crystallisation temperature and melting temperature of PET/PC 50/50 blends (without catalyst) as a function of annealing temperature and time

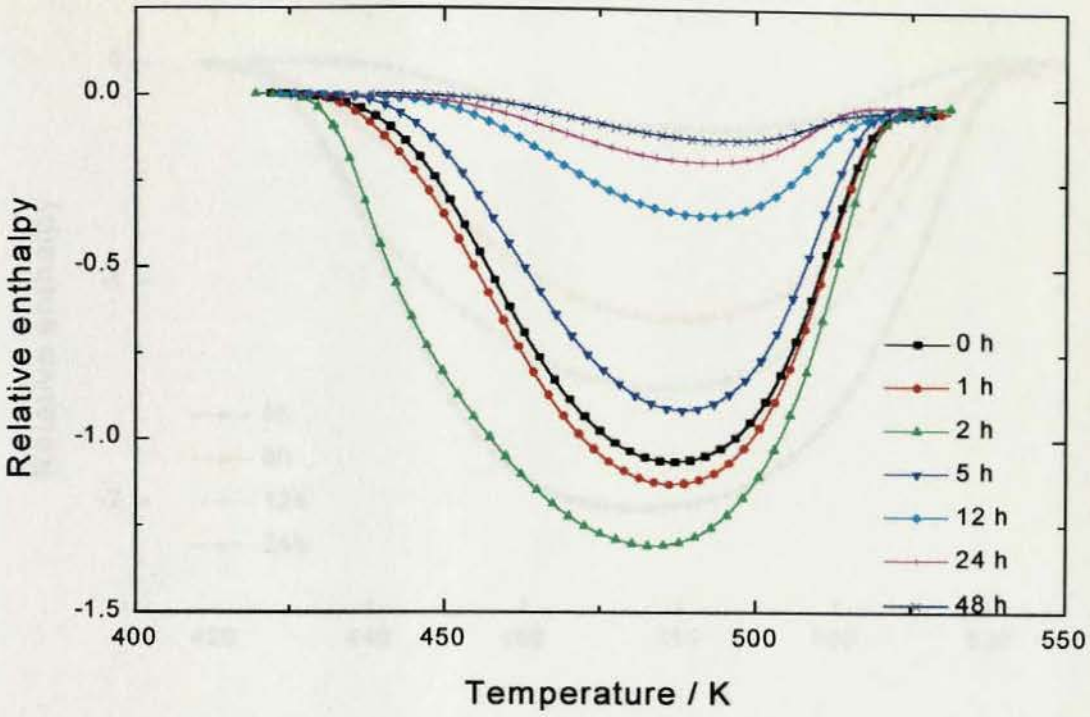

Fig. 8.9a The change of relative enthalpy of fusion of the samples in Fig.8.1b

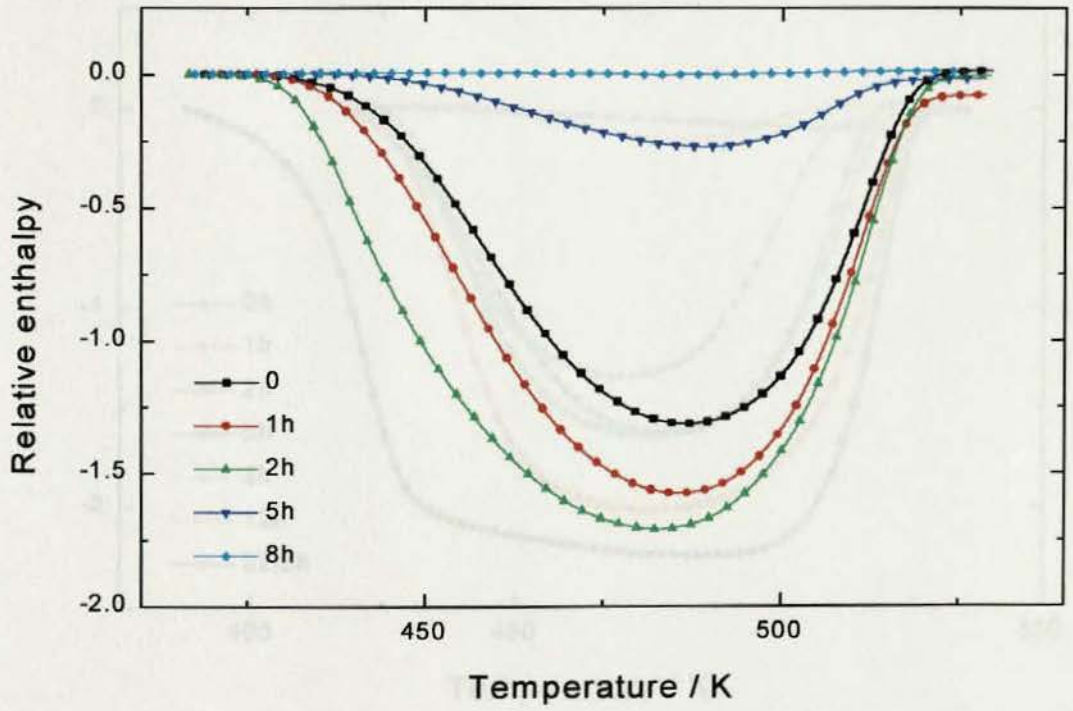

Fig. 8.9b The change of relative enthalpy of fusion of the samples in Fig.8.2b

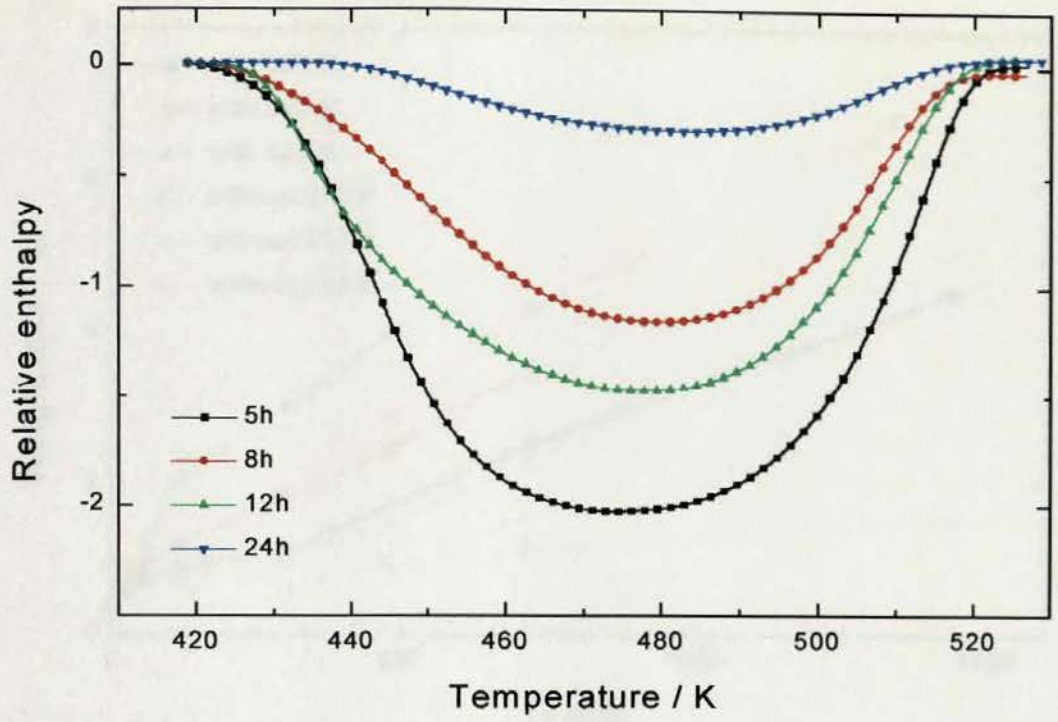

Fig. 8.10a The change of relative enthalpy of fusion of the samples in Fig.8.4b

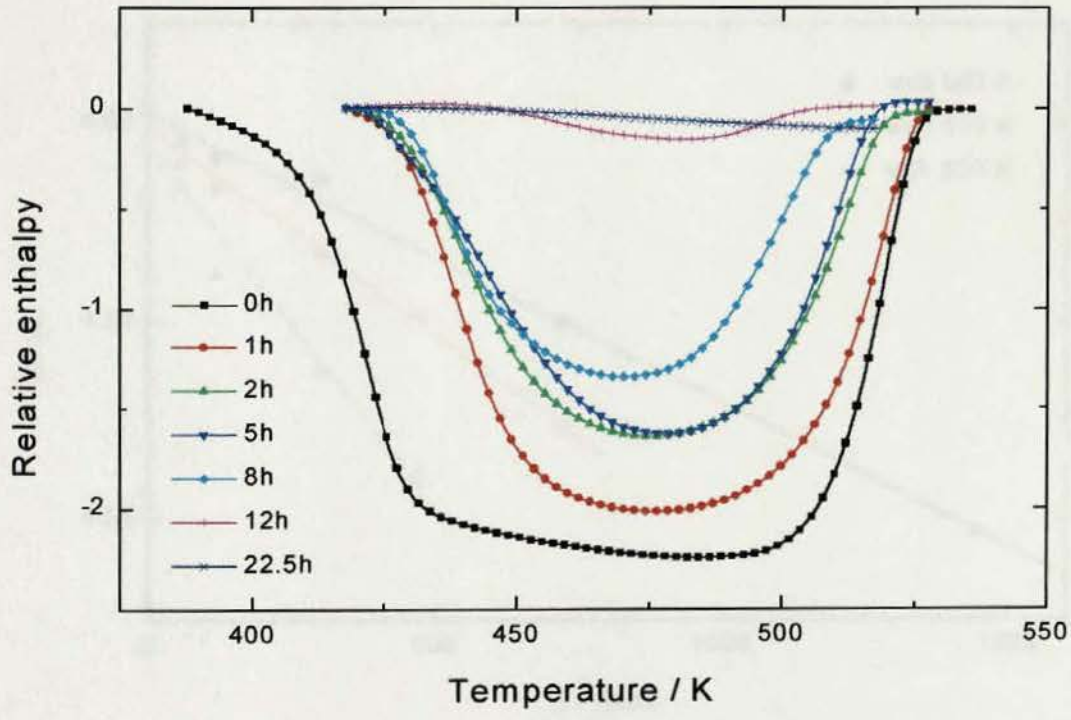

Fig. 8.10b The change of relative enthalpy of fusion of the samples in Fig.8.5b

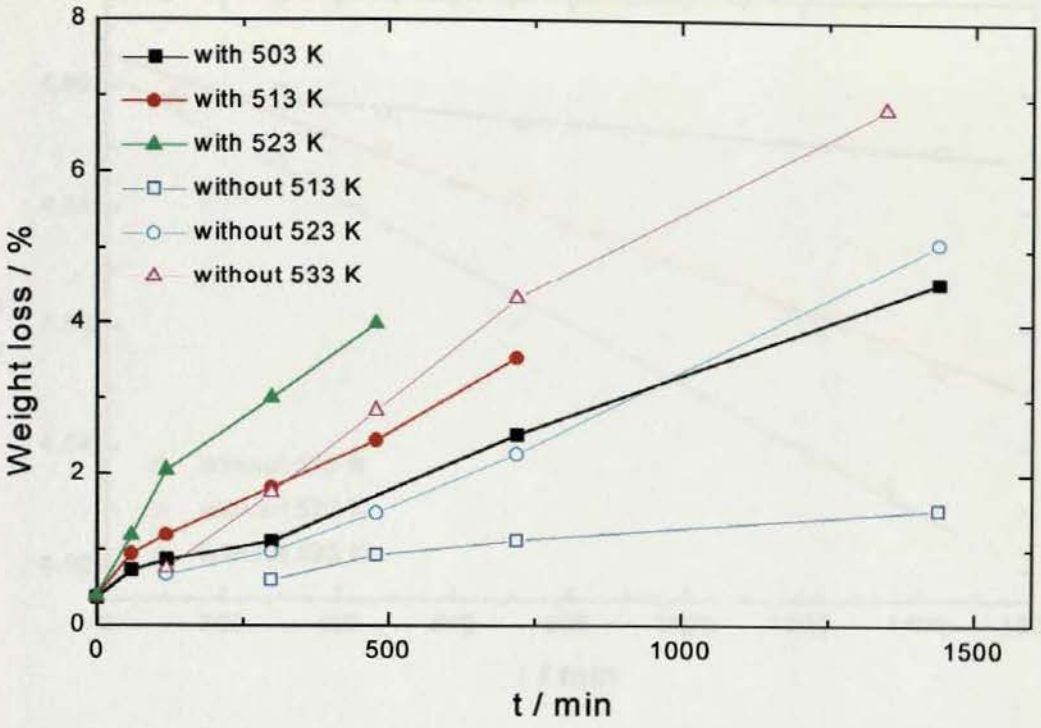

Fig. 8.11 Weight loss of PET/PC 50/50 blends prepared with and without catalyst as a function of thermal treatment time and temperature

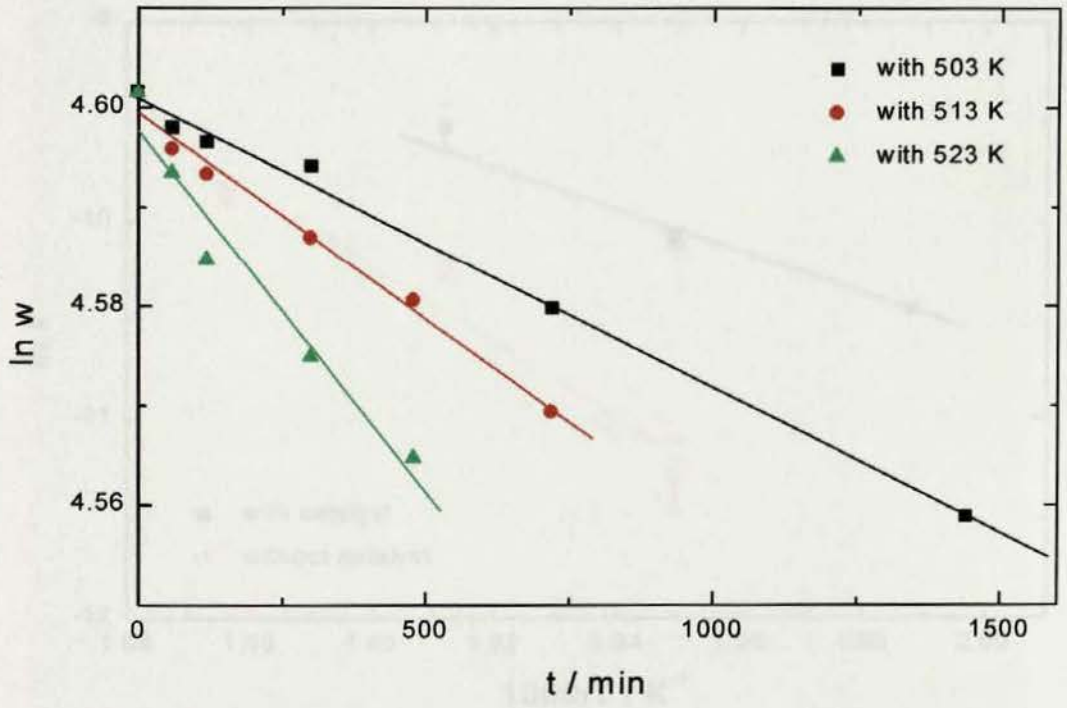

Fig. 8.12a First order rate plot of weight loss with time in the blends with added catalyst

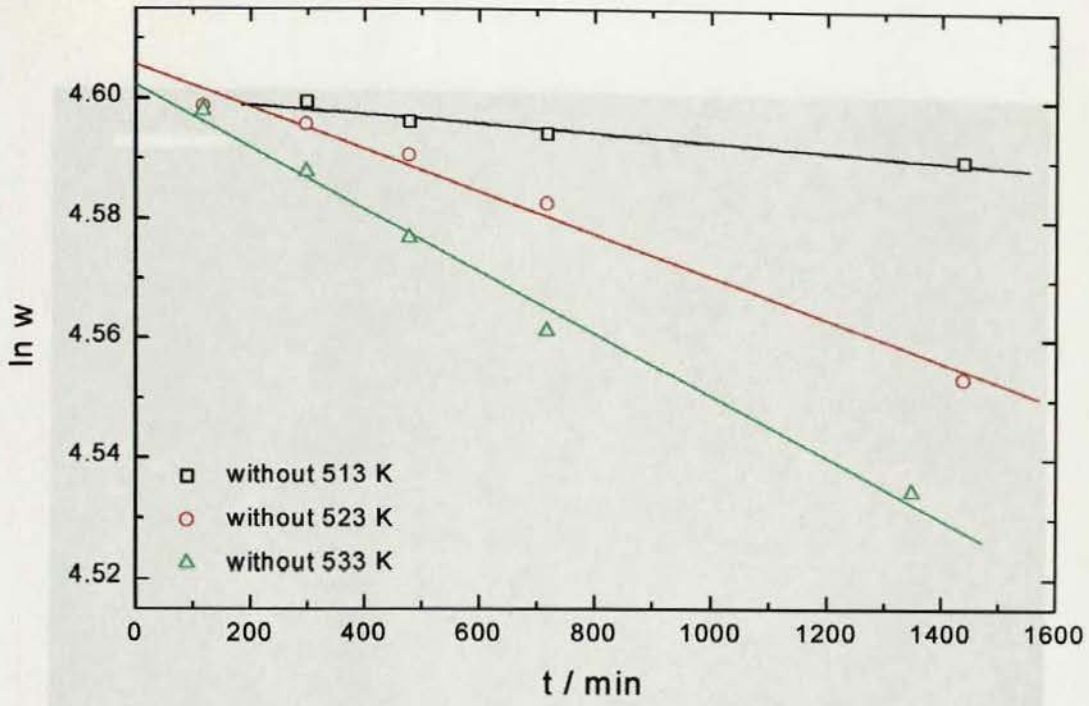

Fig. 8.12b First order rate plot of weight loss with time in the blends without added catalyst

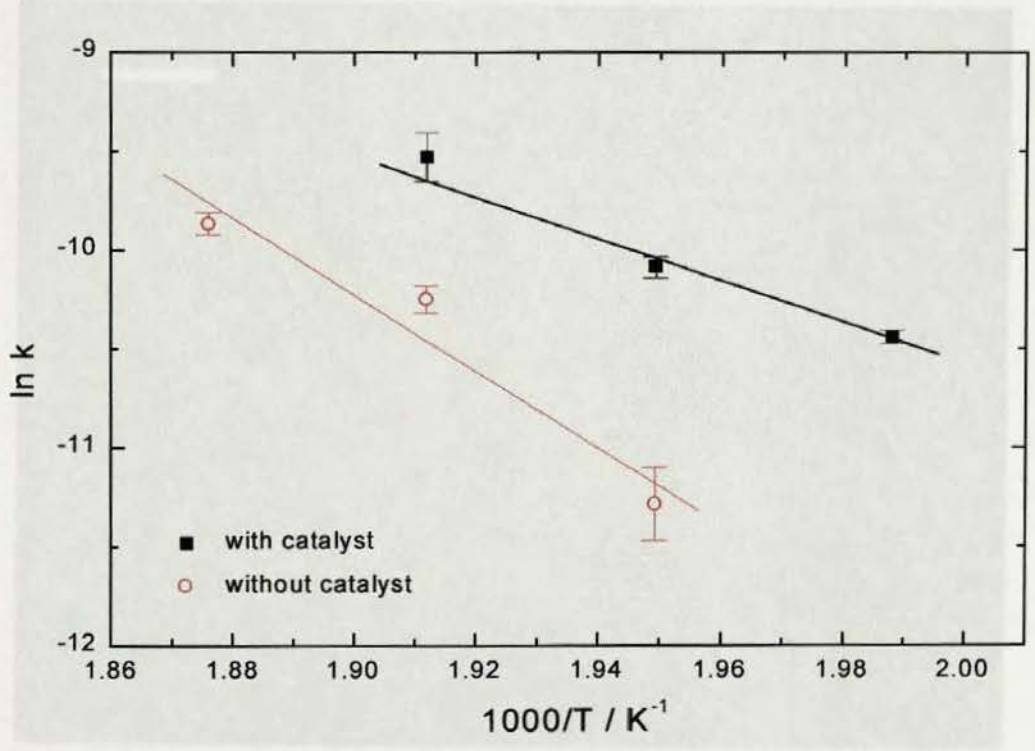

Fig. 8.13 Determination of activation energy of overall decomposition of PET/PC 50/50 blends prepared with and without catalyst

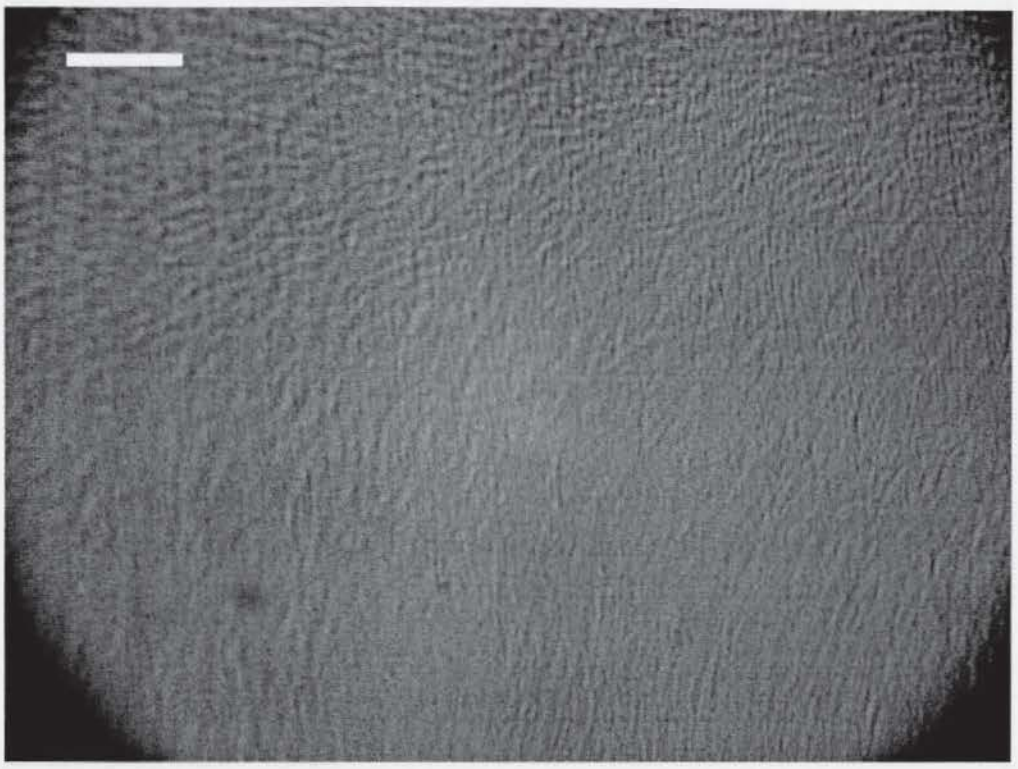

a. 0 min

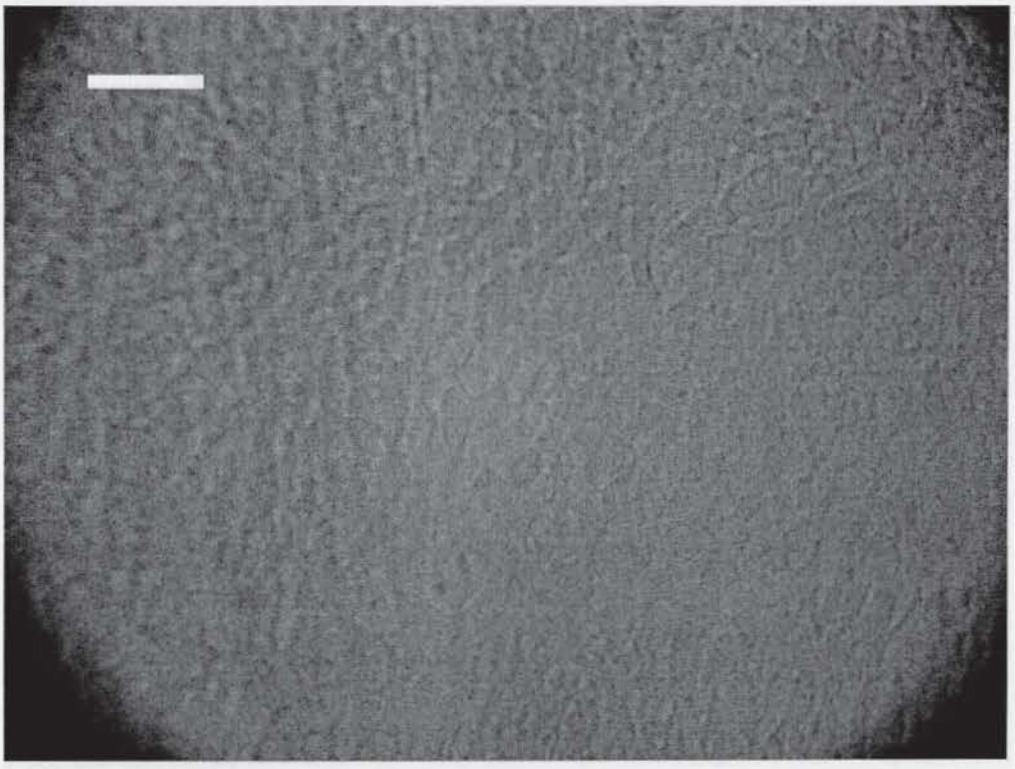

b. 2 min

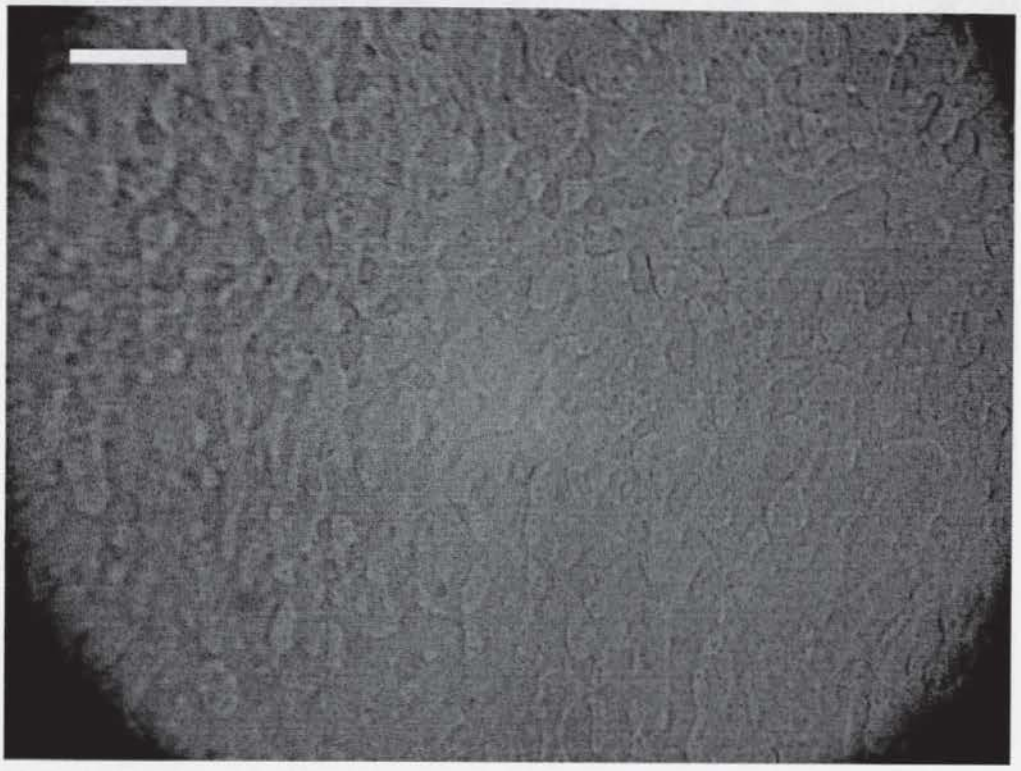

c. 5 min

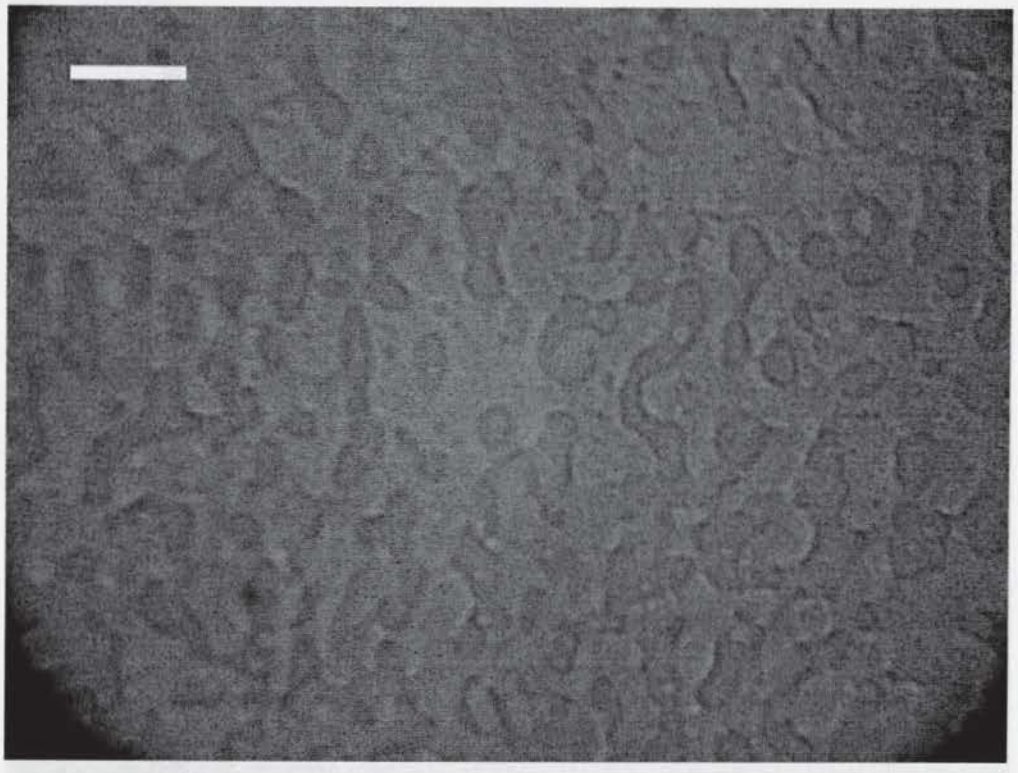

d. 10 min

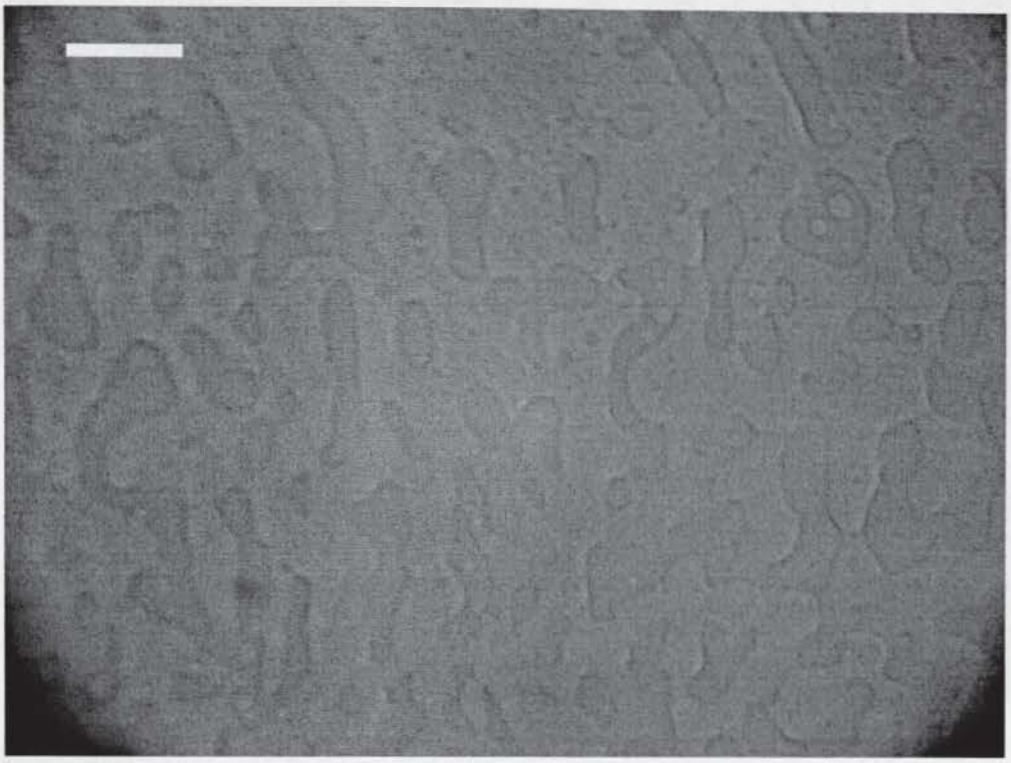

e. 15 min

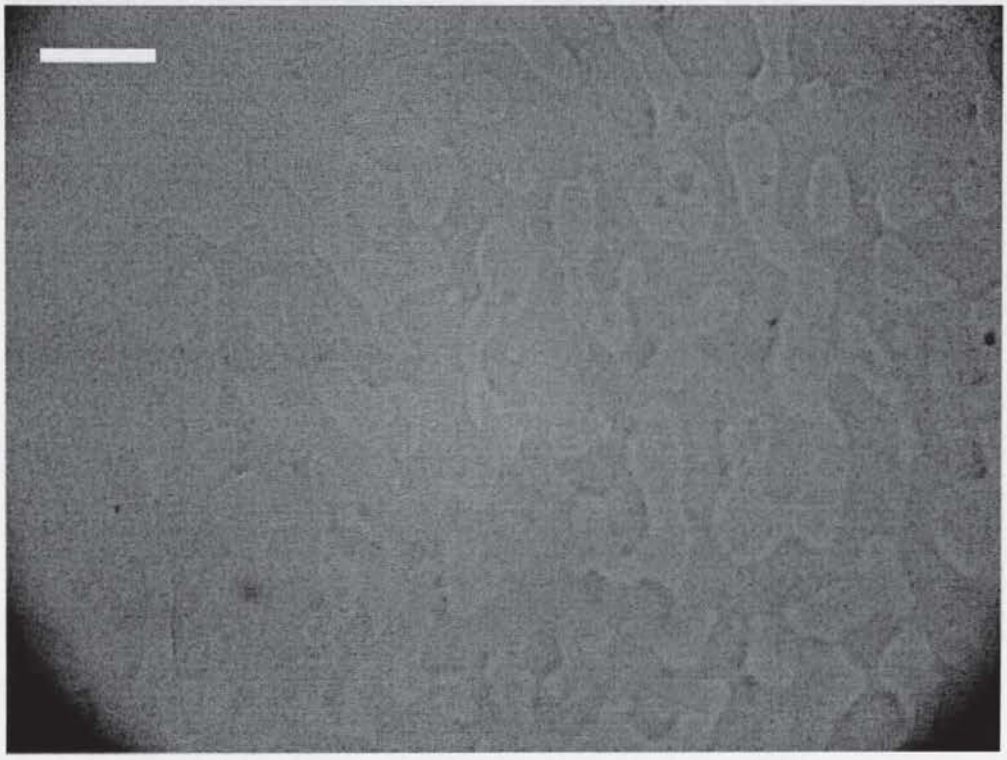

f. 20 min

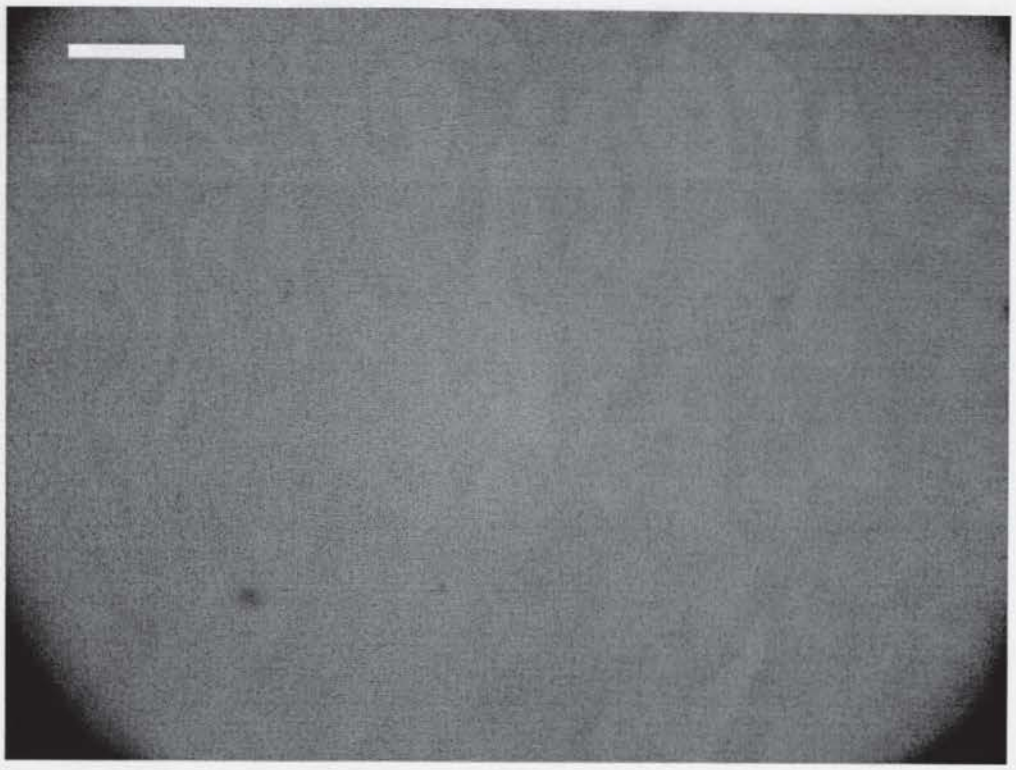

g. 30 min

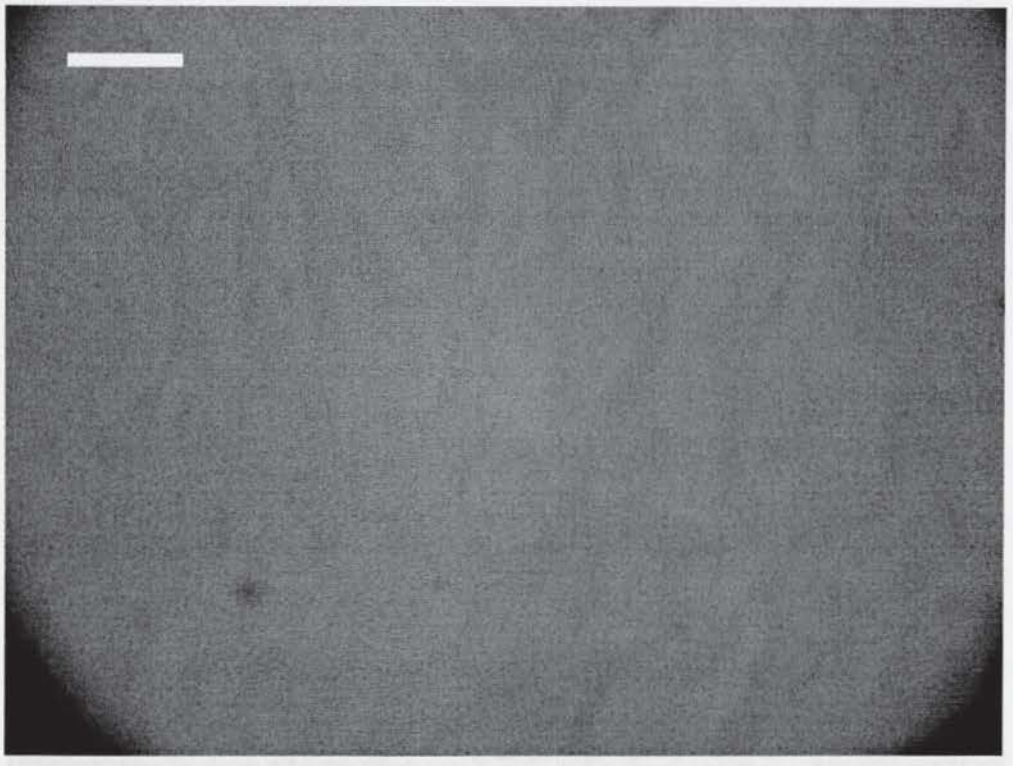

h. 45 min

Fig.8.14 The polarised light micrographs of PET/PC blends prepared with added catalyst heated at 523 K for different time. White bars represent 50 μm

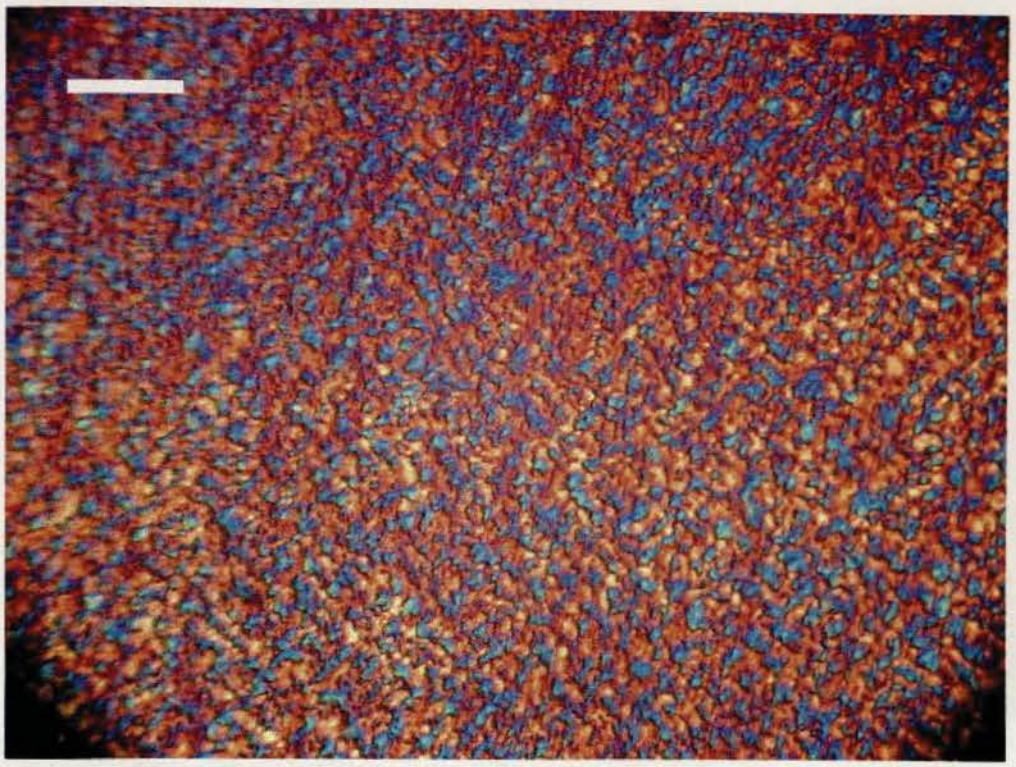

a. 0 min

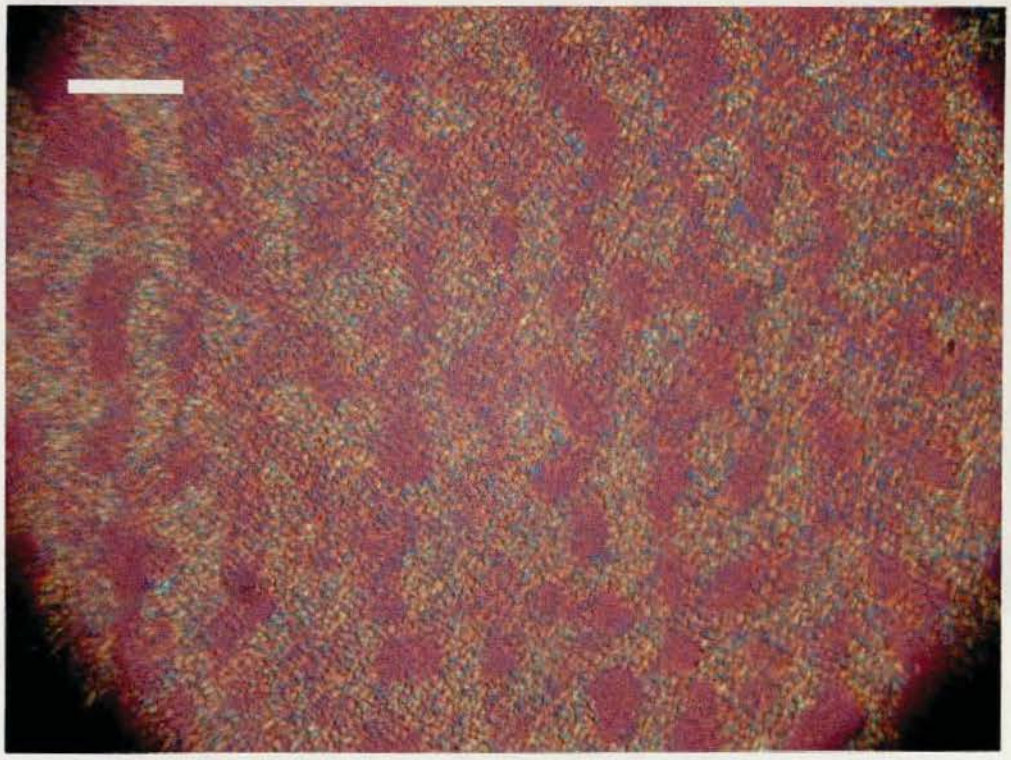

b. 20 min

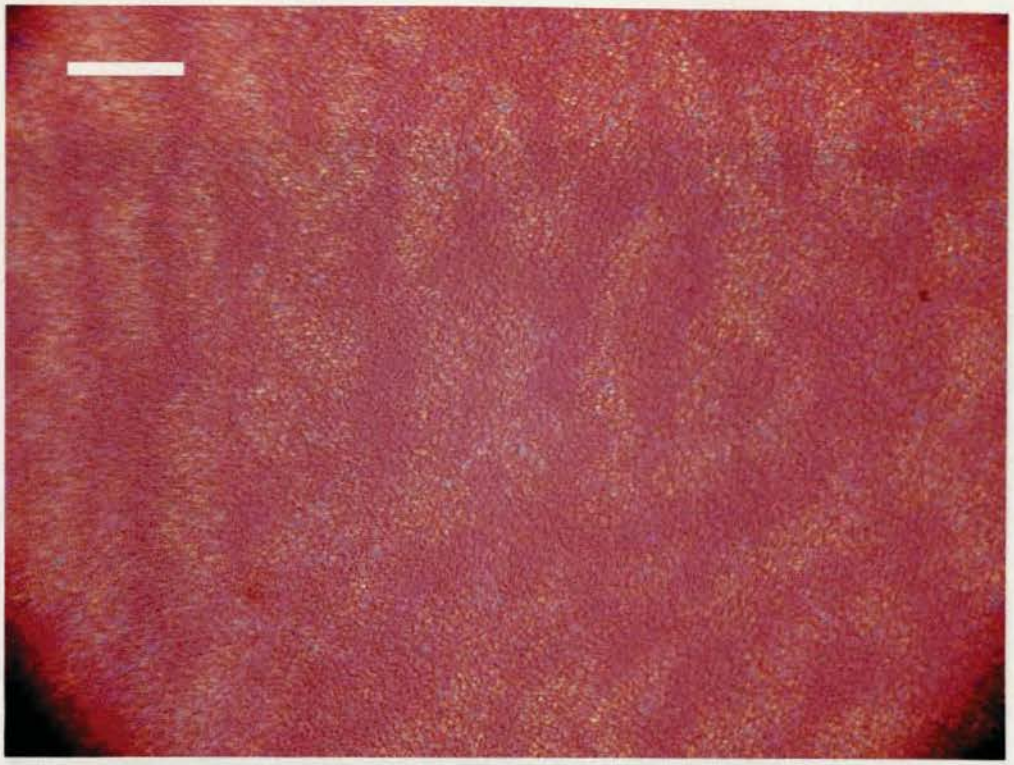

c. 30 min

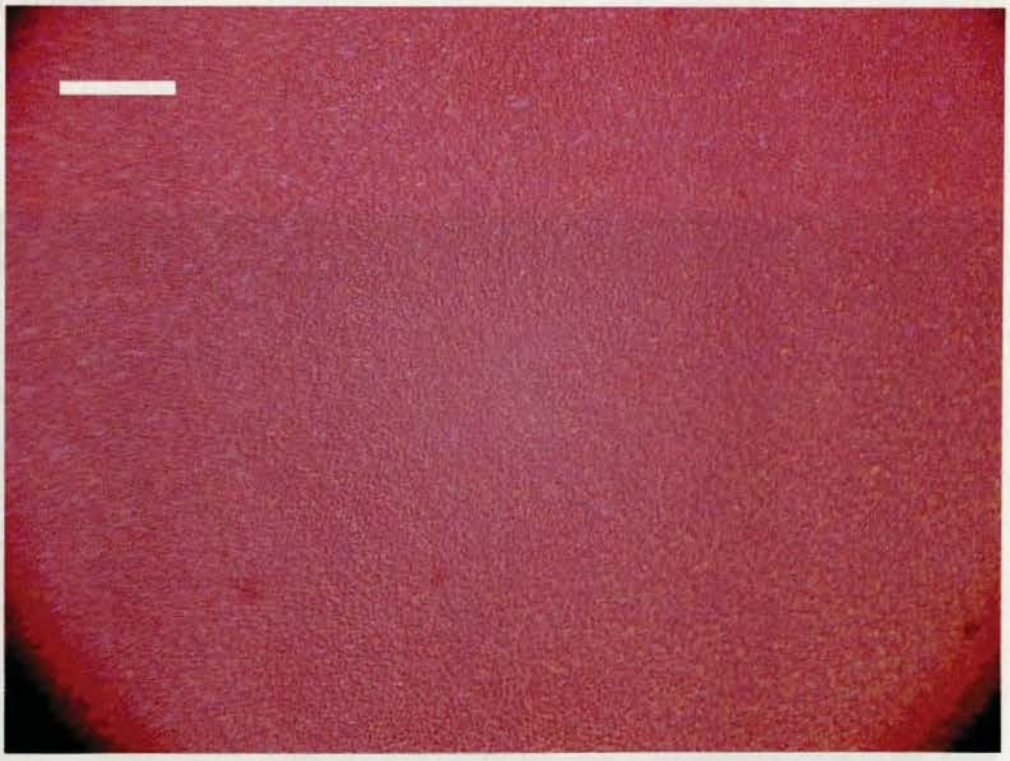

d. 60 min

Fig.8.15 The polarised light micrographs of PET/PC blends preapared with added catalyst annealed at 523 K for different time and then crystallised at 453 K for 20 min. White bars represent 50 μm

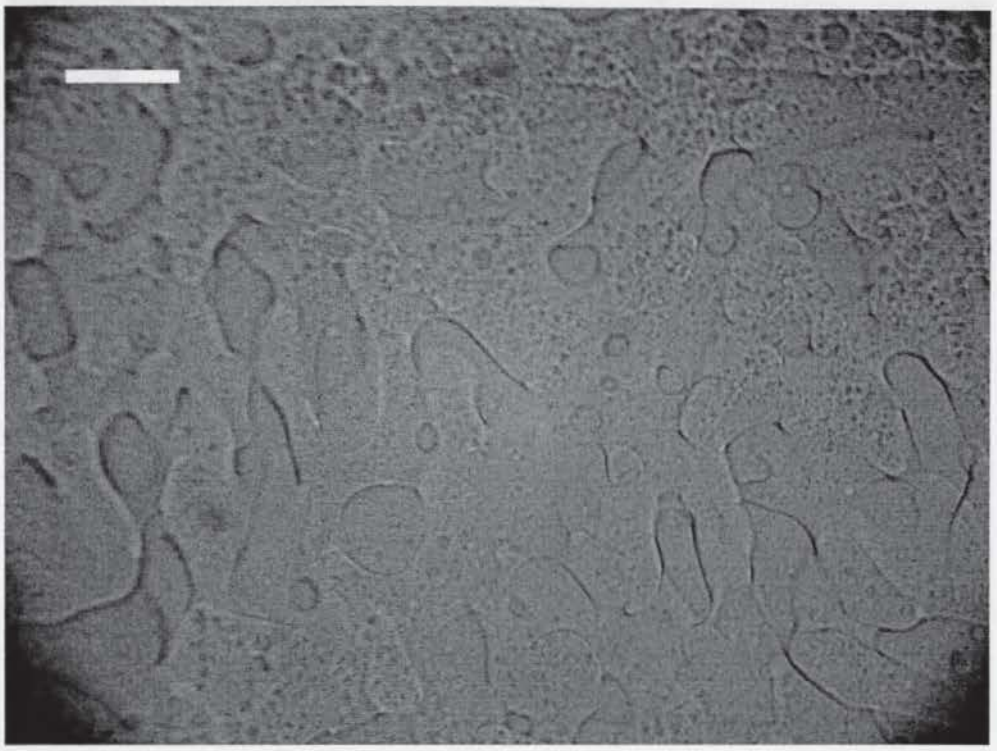

a. 0 min

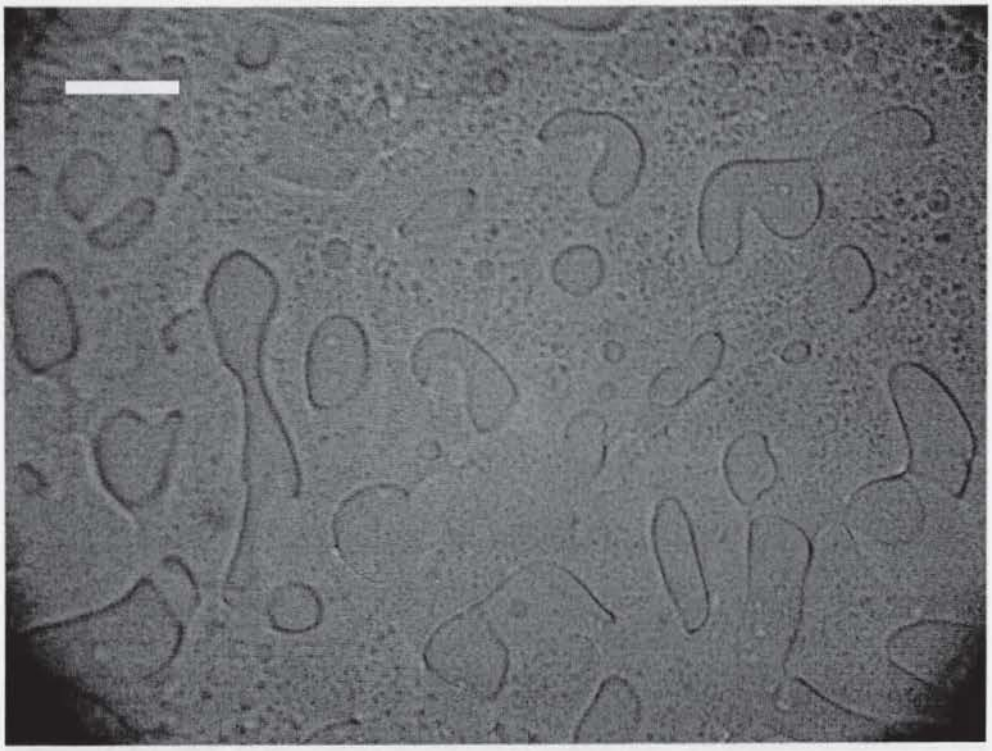

b. 1 min

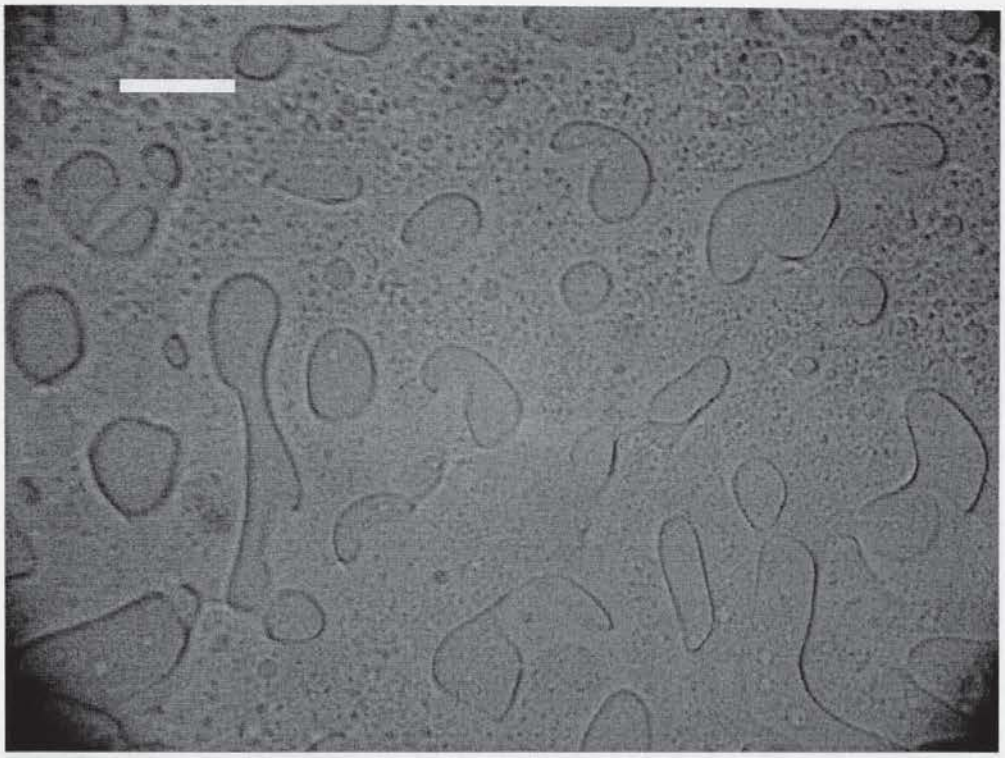

c. 2 min

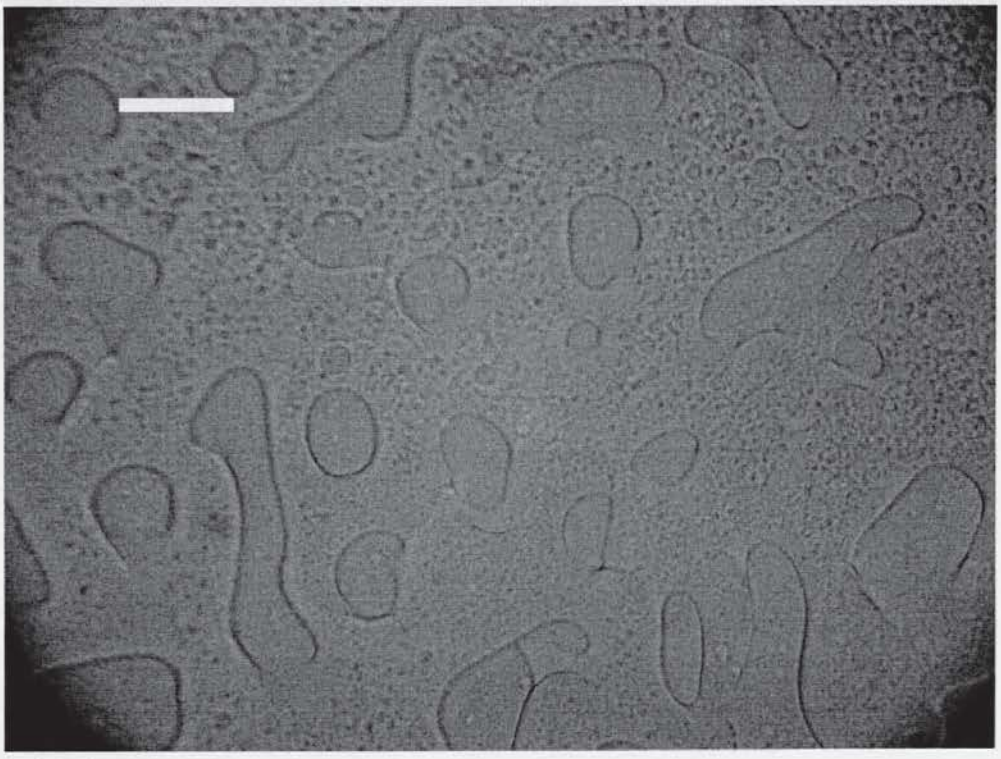

d. 5 min

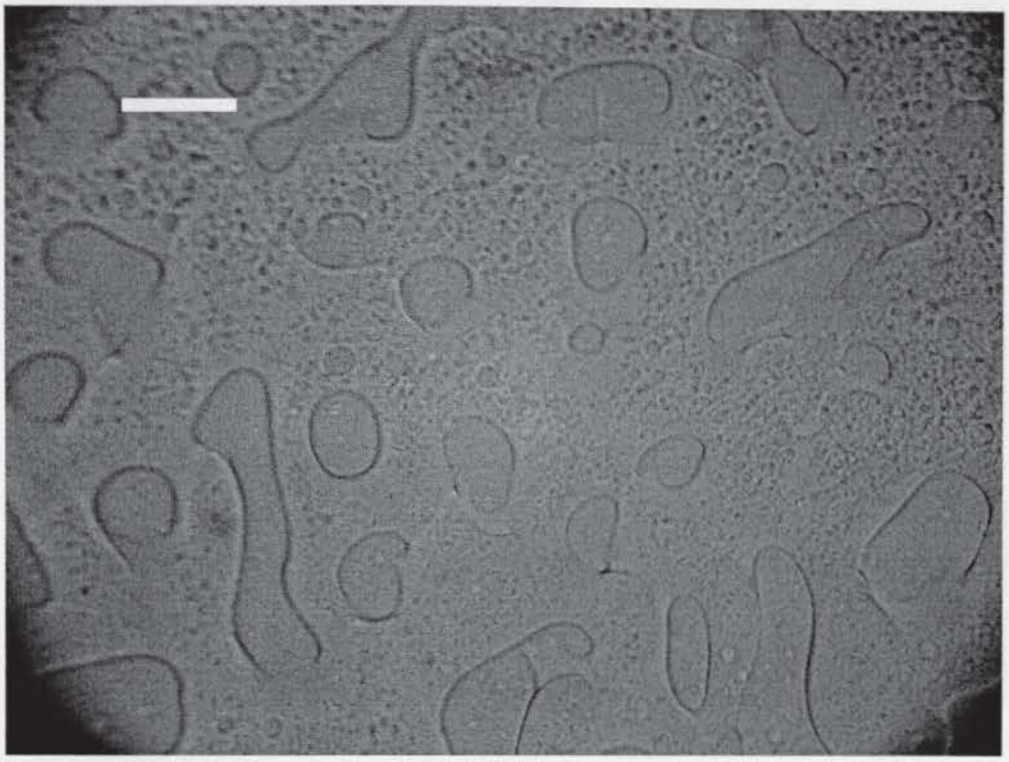

e. 10 min

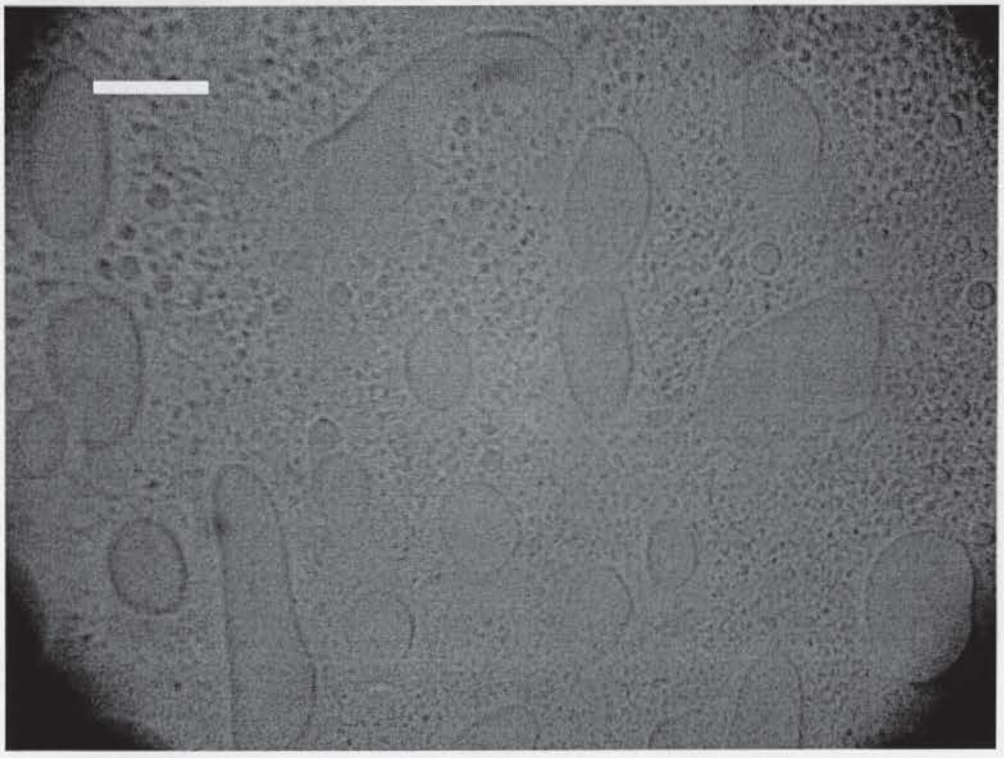

f. 15 min

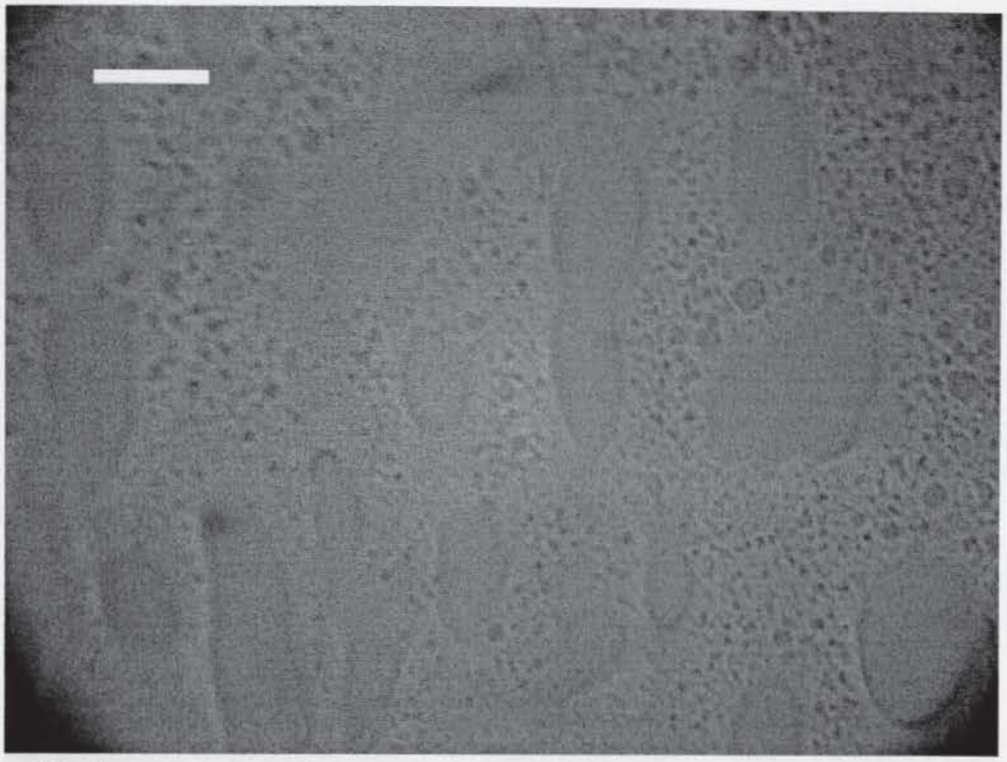

g. 20 min

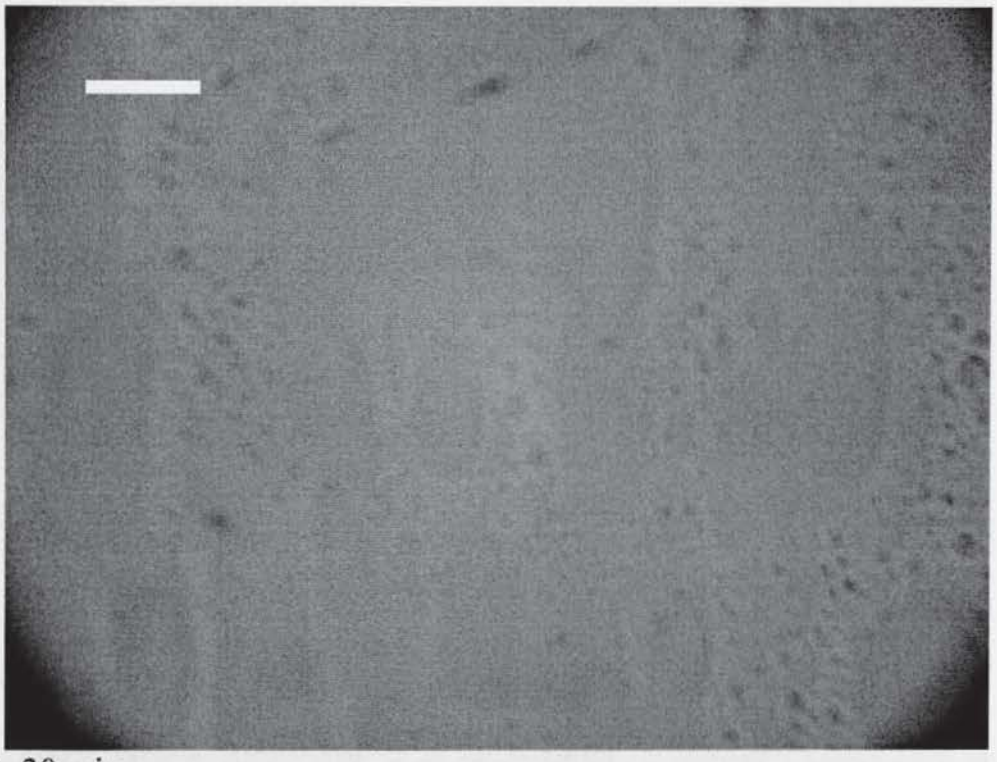

h. 30 min

Fig.8.16 The polarised light micrographs of PET/PC blends prepared without added catalyst heated at 523 K for different time. White bars represent 50 μm

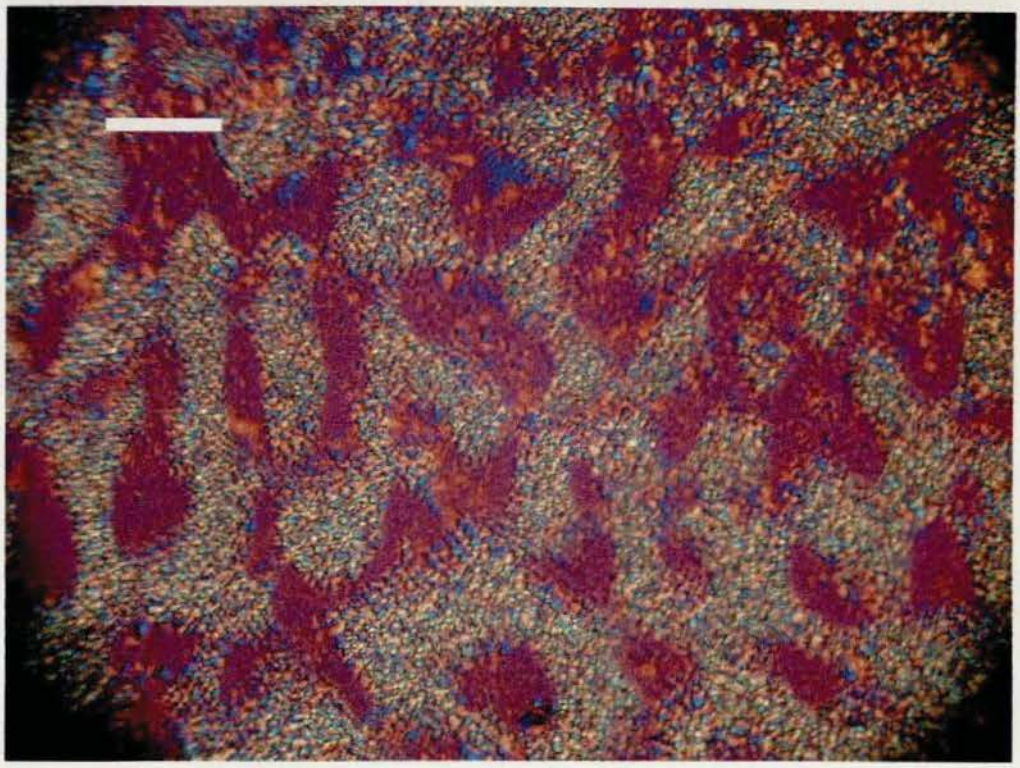

a. Sample crystallised at 453 K for 10 min prior to heating to 523 K

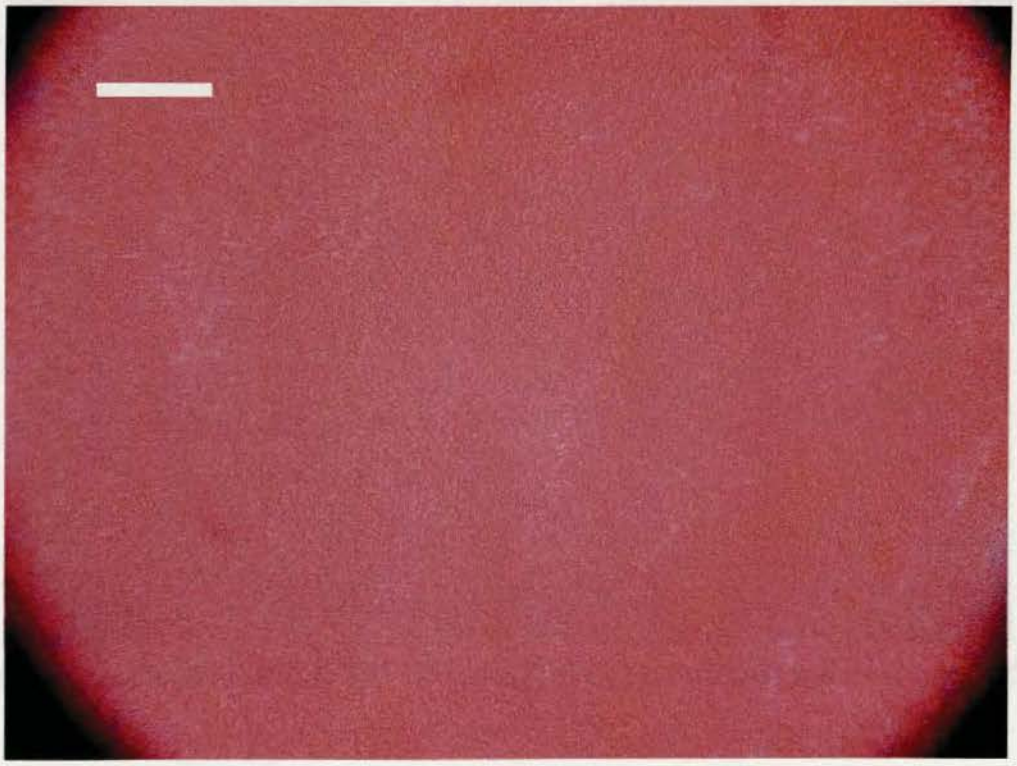

b. Sample crystallised at 453 K for 45 min after 60 min at 523 K

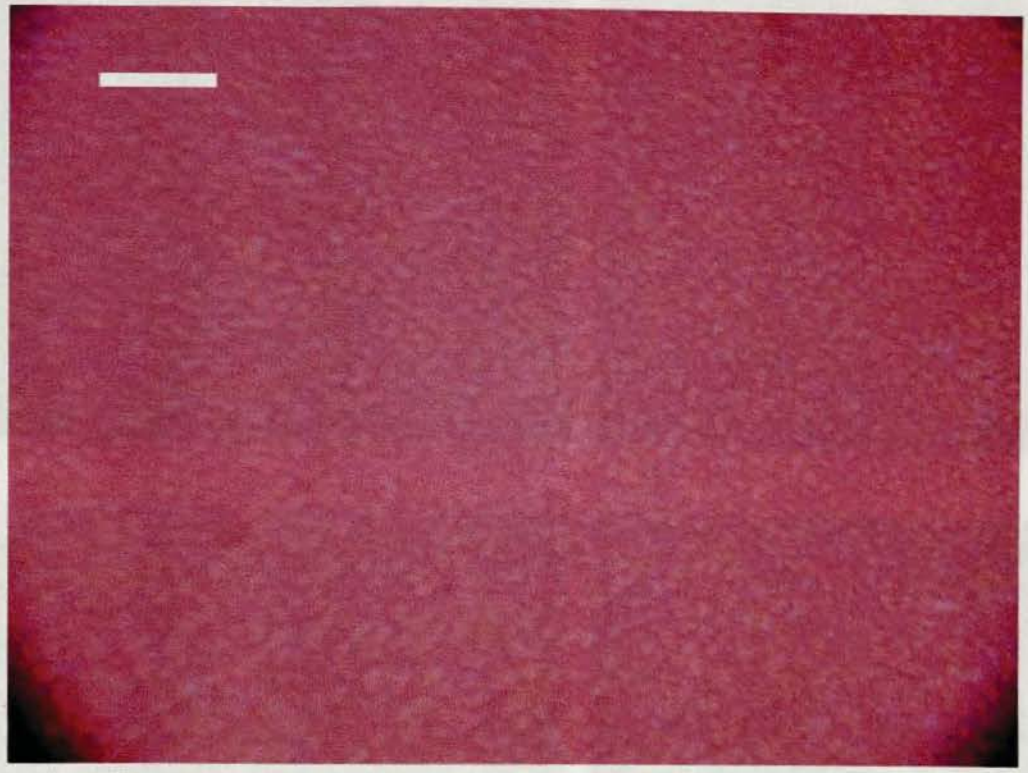

c. Sample crystallised at 453 K for 90 min after 60 min at 523 K

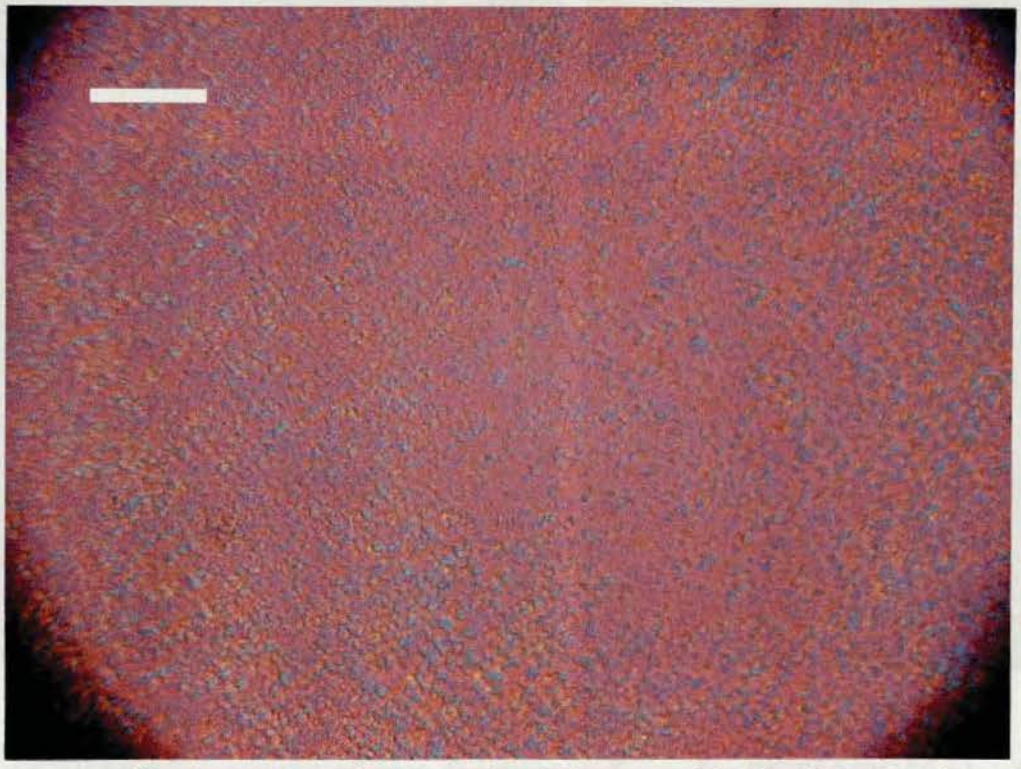

d. Crystallised at 453 K for 120 min (fully crystallised) after 60 min at 523 K

Fig.8.17 The polarised light micrographs of PET/PC blends prepared without added catalyst after annealed at 523 K for 60min. White bars represent 50 μm

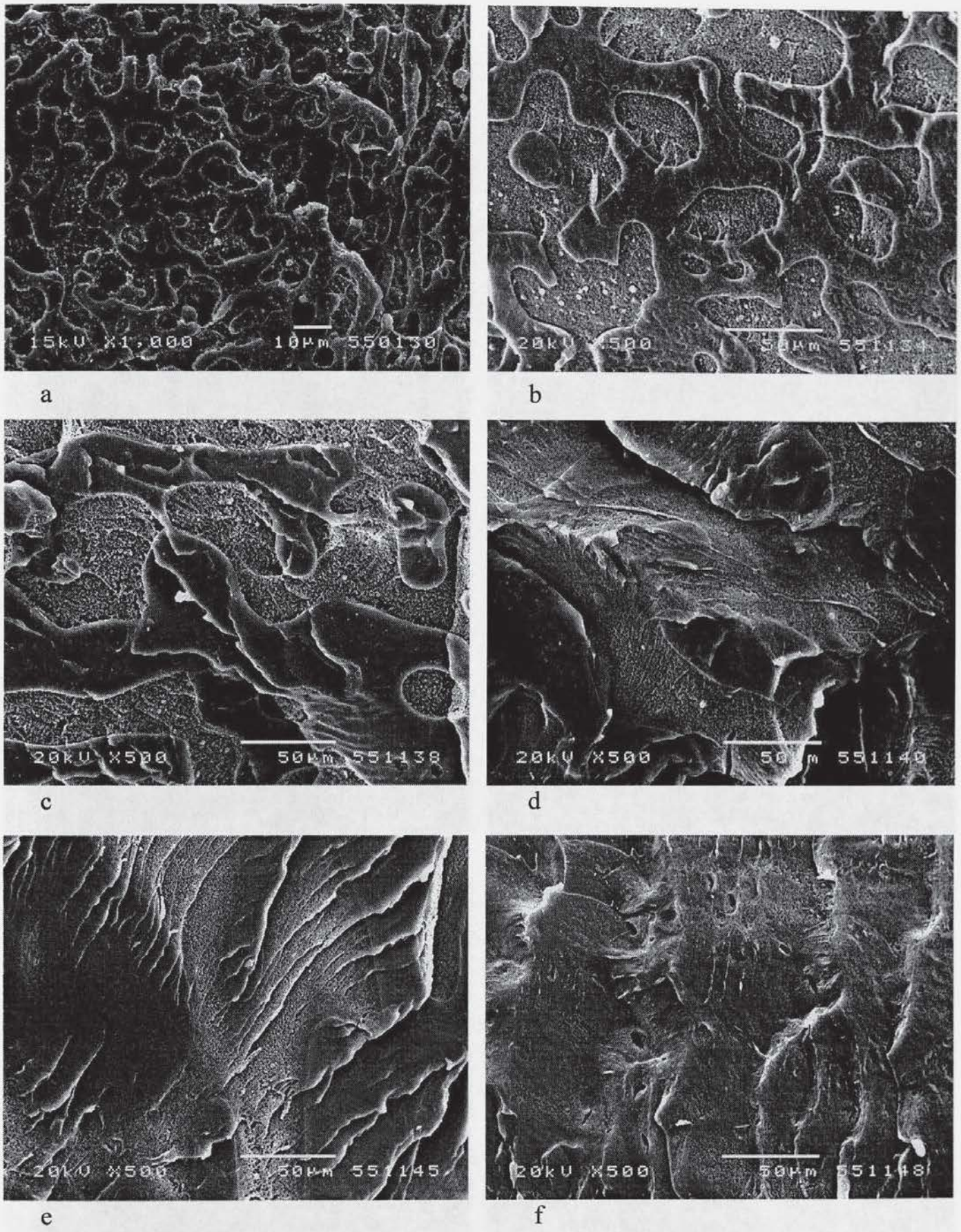

Fig. 8.18 SEM micrographs of cryo-fracture surfaces for PET50/PC50 blend with added catalyst annealed at 523 K for different times: a. 0, b. 15min, c. 30min, d. 60min, e. 120min, and f. 300min.

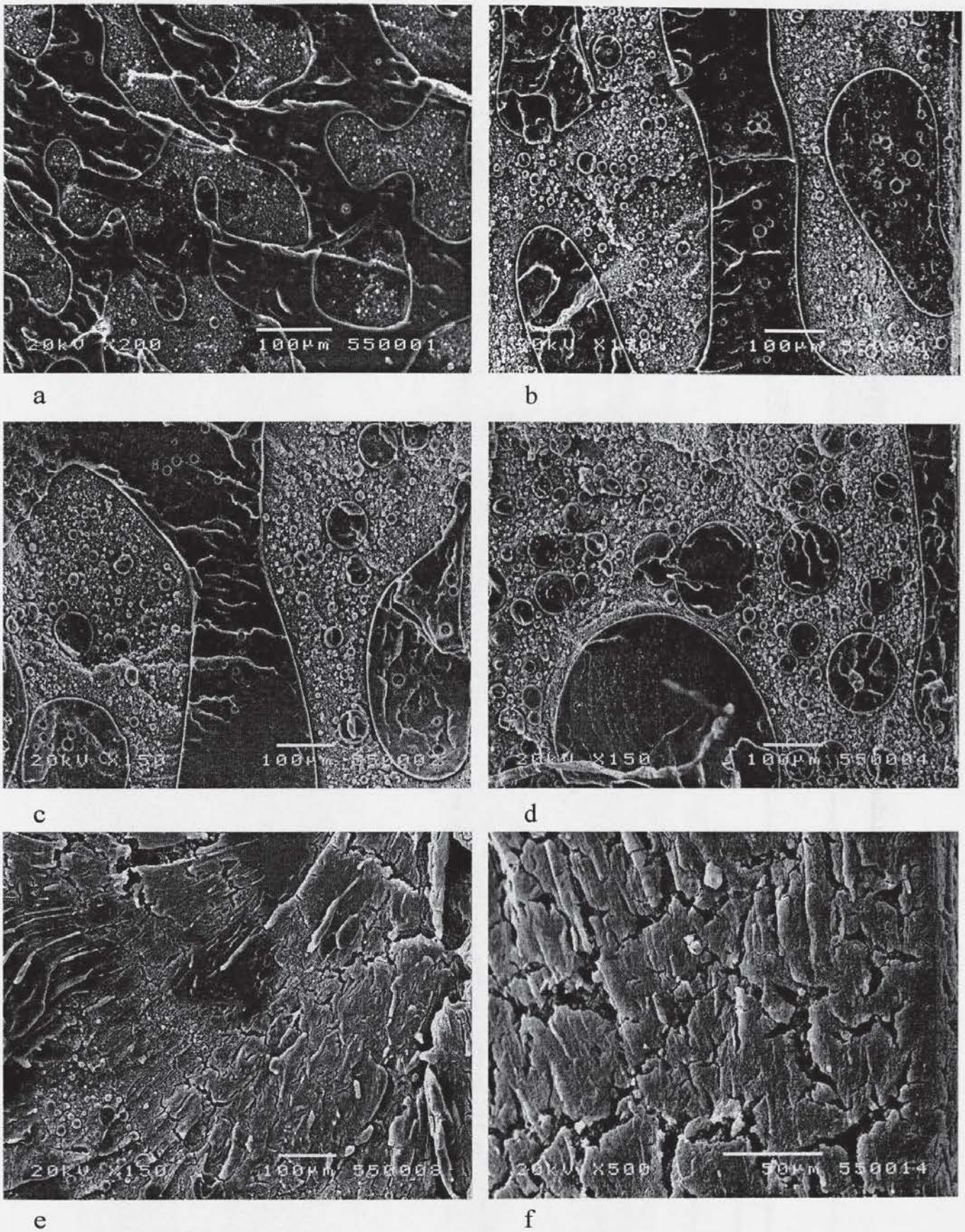

Fig. 8.19 SEM micrographs of cryo-fracture surfaces for PET50/PC50 blend without added catalyst annealed at 523 K for different times: a. 0h, b. 1h, c. 2h, d. 5h, e. 13h, and f. 20h.

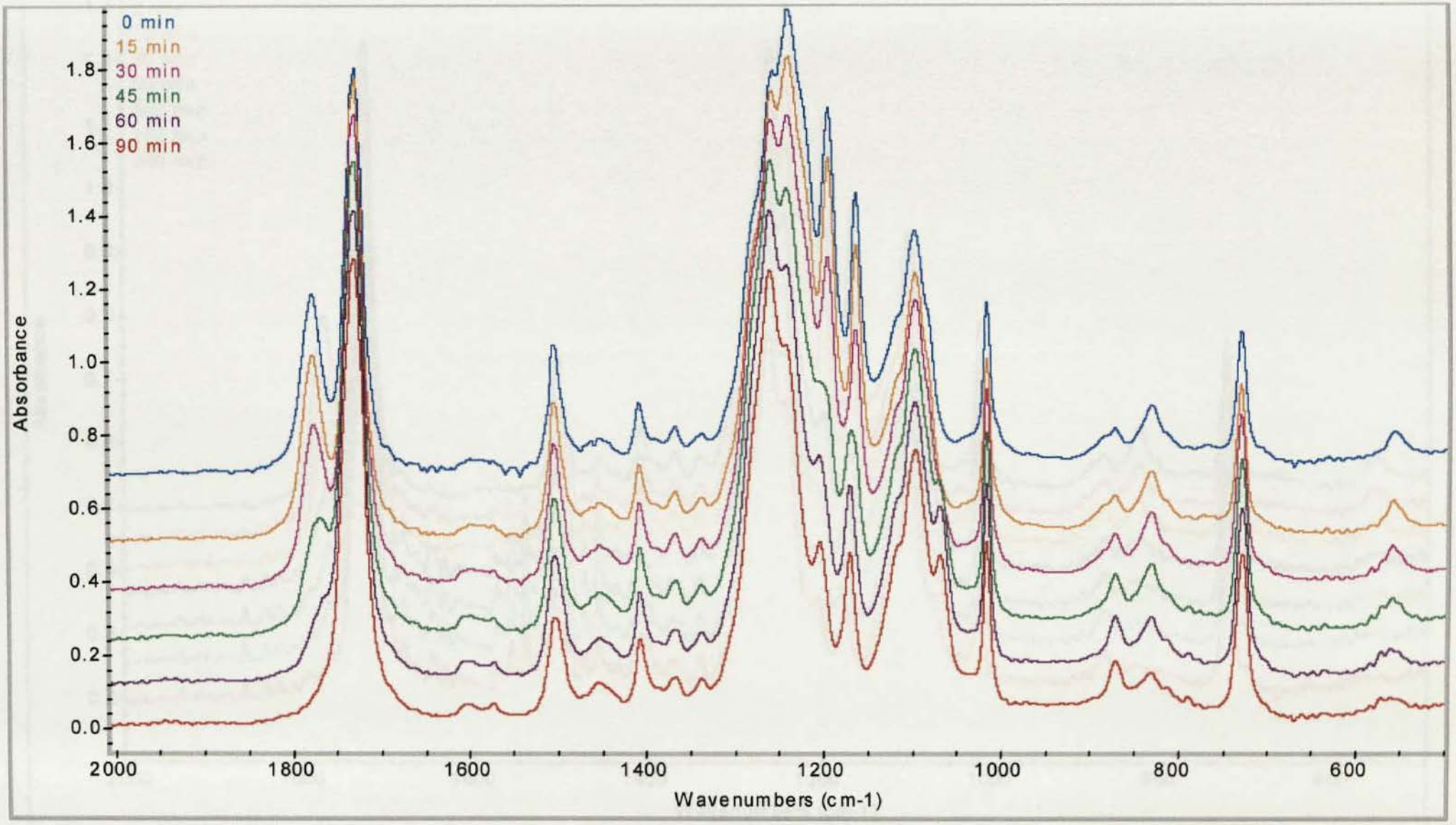

Fig. 8.20 FTIR spectra of blends prepared with added catalyst annealed at 523 K for different time

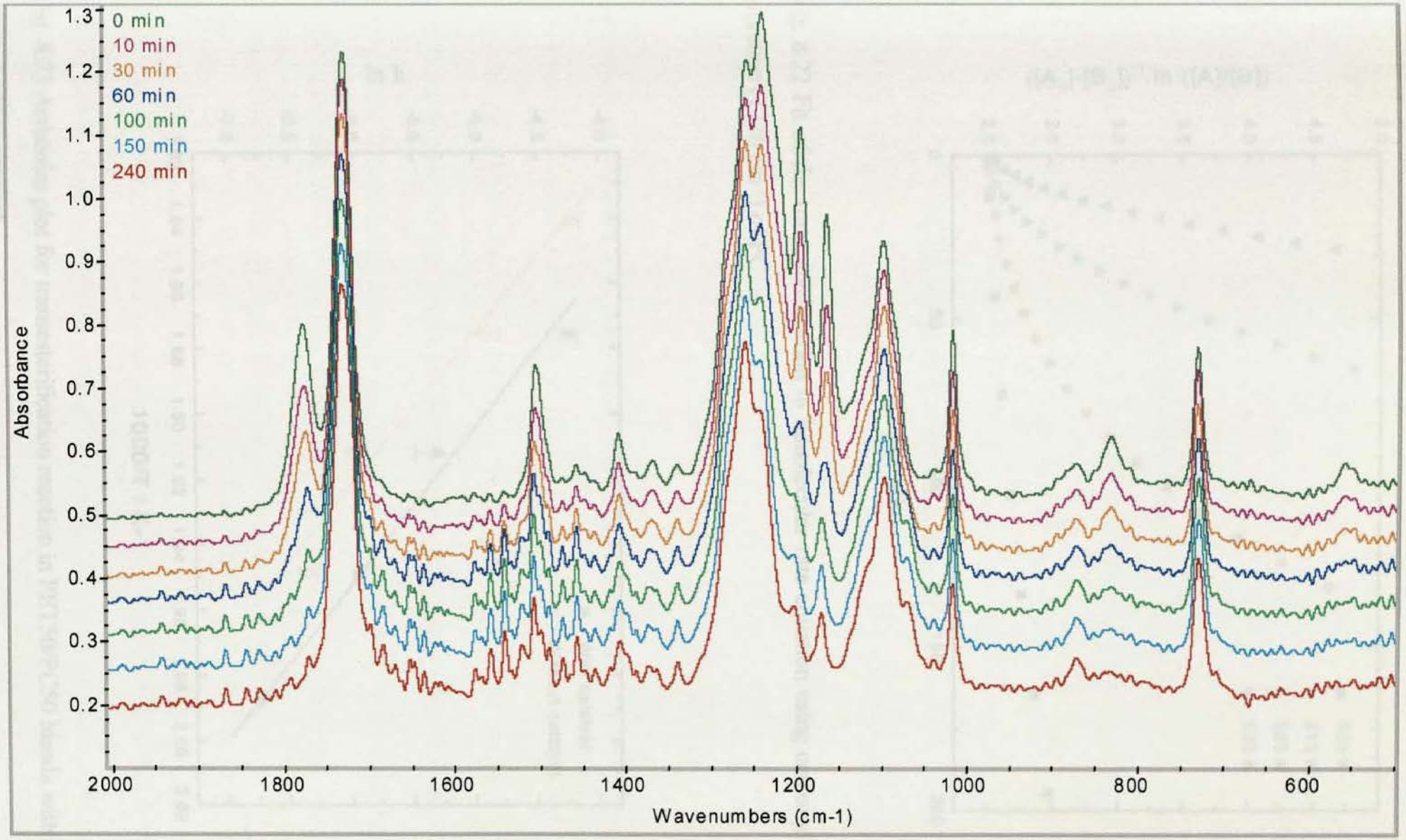

Fig. 8.21 FTIR spectra of blends prepared without added catalyst annealed at 523 K for different time

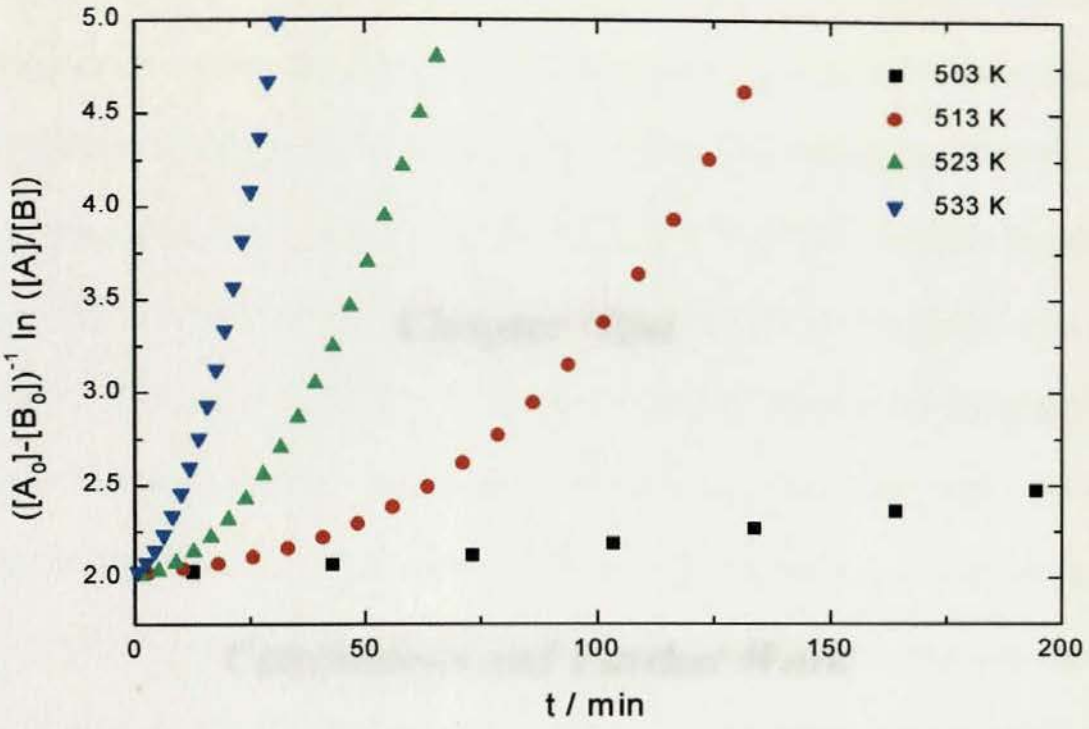

Fig. 8.22 Fit of the transesterification to bimolecular rate equation using carbonyl C=O vibration (1776 cm^{-1}) of PC

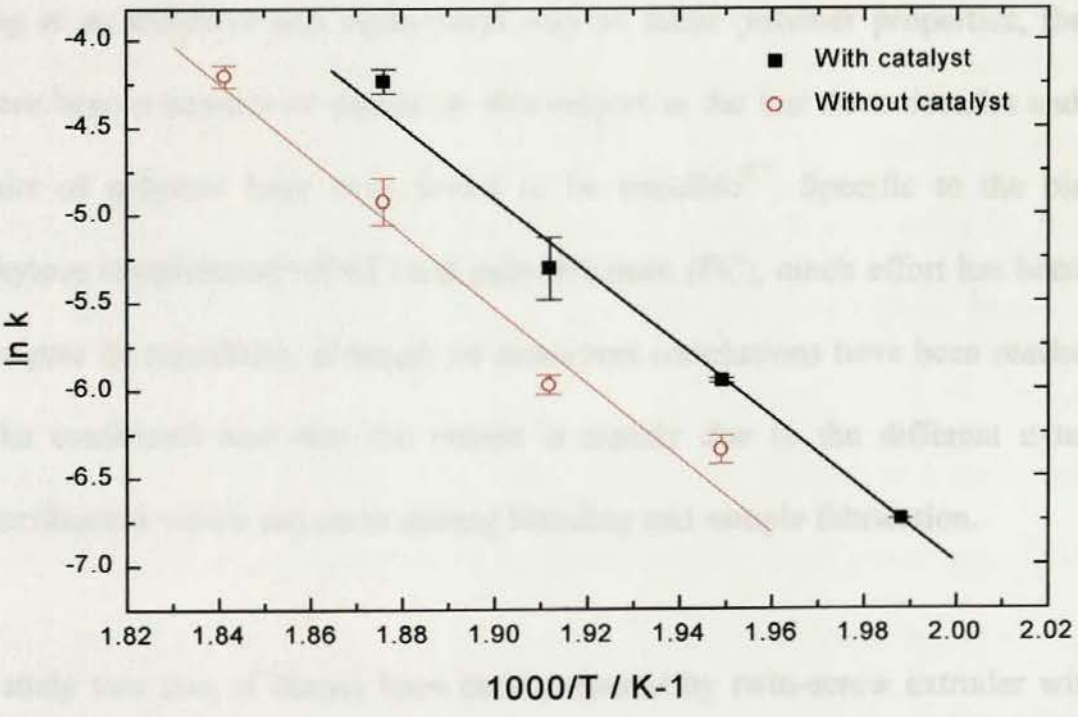

Fig. 8.23 Arrhenius plot for transesterification reaction in PET50/PC50 blends with and without added catalyst

Chapter Nine

Conclusions and Further Work

9.1 Conclusions

Blending is an effective and economical way to tailor polymer properties, therefore there have been a number of studies on this subject in the last three decades and many new pairs of polymer have been found to be miscible[2,7]. Specific to the blend of poly(ethylene terephthalate) (PET) and polycarbonate (PC), much effort has been spent to investigate its miscibility although no consistent conclusions have been reached[34-45]. It can be confirmed now that the reason is mainly due to the different extents of transesterification which can occur during blending and sample fabrication.

In this study two sets of blends have been prepared by twin-screw extruder with and without added transesterification catalyst - Lanthanum acetylacetonate hydrate. By means of DSC and SEM studies, it was found that the blends without added catalyst are

completely immiscible while the blends with added catalyst are partially miscible. The Flory-Huggins interaction parameter of the blends was found to be 0.054 – 0.037 and decreasing with increasing PET concentration[209], clearly indicating that PET/PC blends are not microscopically miscible at any composition. However, when the blends were annealed at high temperature the T_gs shifted towards one another and finally only one T_g was observed. This was consistent with a value calculated from the Fox equation[19] for a compatible system. These observations directly prove that the extent of transesterification determines the final miscibility of the blends. Obviously the nature of the transesterification catalyst is a key factor in determining the rate and extent of reaction. Once the residual catalyst was completely removed from the polycondensation polymers no further exchange reaction was observed[210]. On the other hand, organic Ti catalyst produced a more rapid reaction[44]. Addition of small amounts of the catalyst to the blends would certainly improve the rate of transesterification. It is not unexpected that the blends prepared with added catalyst show partial miscibility while the other blends are immiscible. The kinetics of transesterification in these two blends have been investigated by FTIR spectroscopy and weight loss. The activation energy of transesterification in blends without added catalyst had a similar value to the other blends and these values were close to that of polycondensation reaction in polyester.

Crystallisation and melting behaviours have also been studied and the results are consistent with these conclusions on compatibility. The crystallisation rates of PET in both dynamic and isothermal processes were inhibited by the presence of PC, particularly in the blends with added catalyst. In the blends without added catalyst the retardation was solely due to physical constrain of uncrystallisable PC domains on the

crystallisation of the PET, while in the other blends besides the physical constraint effect (it was much stronger than in blends without added catalyst because of phase domains greatly decreased), limited solubility of PC in the PET was more important since the molecule chains of PC were directly connected to PET chains. The equilibrium melting points of the blends without added catalyst decreased slightly with increasing PC content, however, a greater depression of the equilibrium melting points (about 15K) was observed in the blends with added catalyst.

Multiple melting endotherms are usually observed during melting crystallised PET on thermal analysis. Previously this was explained by either different crystal structures[145,146] or by partially melting and recrystallisation[119]. More recently it was proposed[120,121,153] that it originated from the separated lamellae thickness distributions and recrystallisation on partially melting. From fast heating and stepwise heating in the DSC as well as the study of MTDSC, it was confirmed that multiple melting endotherms are due to a combination of these two factors.

The crystallinity of semi-crystalline polymers measured by DSC is usually measured by using the enthalpy of fusion calculated by integrating the area between a trace and an arbitrarily drawn baseline by analogy to that for low molecular weight materials. This procedure is invalid for polymers in most situations since unlike low molecular weight materials polymers actually melt over a wide temperature range of several decades to a hundred degrees. The enthalpy of fusion is temperature dependent. To avoid this problem the First Law method[104,105] has been applied, in which the residual enthalpy of fusion (at T_l) is measured by subtracting the change of enthalpy on cooling amorphous

material (without crystallisation occurrence) from that of the melting process over the same temperature range. The crystallinity is measured by dividing the enthalpy of fusion of 100% crystalline materials at T_1. Using this method the real crystallinity at any temperature can be measured. The crystallinity of PET measured by this method at T_1 is in good agreement with those by density and WAXD methods.

MTDSC has been successfully applied to the study of the miscibility of the blends from the separated reversing and non-reversing heat flow curves. The results are consistent with the conventional DSC. MTDSC also discloses that the reorganization occurring from above T_c and increasing the modulation period or decreasing modulation temperature improve the reversing process, thus increase the reversing heat capacity and decrease the non-reversing melting.

9.2 Suggestions to Further Work

Quasi-isothermal crystallisation was affected by modulation, however how the modulation parameters affect crystallisation and what the mechanism is are not clear and further investigation is needed. Due to the instability of PET at higher temperature the materials used should be considered in the future work.

Transesterification is an interesting topic. At present only 50/50 blends have been studied the blends in other composition should also be investigated. The catalyst is a key factor to affect the final miscible result and the concentration of the catalyst should also be considered. In kinetic studies, the volatile product is an important aspect to determine the parameters. Thermal gravity analysis (TGA) combining with mass spectra should be used to analyse the exact volatile composition. Nuclear magnetic resonance (NMR) is a powerful tool for analysis of polymer microstructure and can be used in kinetic study.

REFERENCES

1. Manson J. A. and Sperling L. H., *Polymer Blends and Composites*. New York: Plenum, 1976
2. Utracki L. A., *Commercial Polymer Blends*. London: Chapman & Hall, 1998
3. Sperling L. H., *Polymeric Multicomponent Materials: An Introduction*. New York: Wiley, 1997
4. Olabisi O., Robeson L. M. and Shaw M. T., *Polymer - Polymer Miscibility*. New York: Academic, 1979
5. Miles I. S. and Rostami S., *Multicomponent Polymer System*. Harlow: Longman, 1992
6. Porter R. S. and Wang L. H., *Polymer* 1992, **33**.2019
7. Paul D. R. and Newman S., *Polymer Blends, Vol. 1*. Orlando: Academic, 1978
8. Huggins M. L., *J. Chem. Phys.* 1941, **9**.440
9. Flory P. J., *J. Chem. Phys.* 1941, **9**.660
10. Flory P. J., *J. Am. Chem. Soc.* 1965, **87**.1833
11. Flory P. J., Orwell R. A. and Vrij A., *J. Am. Chem. Soc.* 1964, **86**.3507
12. Abe A. and Flory P. J., *J. Am. Chem. Soc.* 1965, **87**.838
13. Orwell R. A. and Flory P. J., *J. Am. Chem. Soc.* 1967, **89**.6814
14. Eichinger B. E. and Flory P. J., *Trans. Faraday Soc.* 1968, **64**.2035
15. Sanchez I. C. and Lacombe R. H., *Macromolecules* 1978, **11**.1145
16. Sanchez I. C., *J. Macromol. Sci. Phys.* 1980, **B17**.565
17. Renuncio J. A. R. and Prausnitz J. M., *Macromolecules* 1976, **9**.898
18. Brandani V., *Macromolecules* 1979, **12**.883
19. Fox T. G., *Bull. Am. Phys. Soc.* 1956, **1**.123
20. Gordon M. and Taylor J. S., *J. Appl. Chem.* 1952, **2**.493
21. Couchman P. R., *Macromolecules* 1978, **11**.1156
22. Scott R. L., *J. Chem. Phys.* 1949, **17**.279
23. Mandelken L., Garrett R. R. and Flory P. J., *J. Am. Chem. Soc.* 1952, **74**.3949
24. Nishi T. and Wang T. T., *Macromolecules* 1975, **8**.909
25. Jonza J. M. and Poter R. S., *Macromolecules* 1986, **19**.1946
26. Utracki L. A., *Polymer Alloys and Blends*. New York: Hanser, 1990

27. Kryszewski M., *Recent Progress in the Studies on the Preparation and Properties of Polymer Blends*. In: Martuscelli E., Palumbo R. and Kryszewski M., editors, *Polymer Blends: Processing, Morphology and Properties*. New York: Plenum, 1980
28. Kressler J., Higashida N., Inoue T., Heckmann W. and Seitz F., *Macromolecules* 1993, **26**.2090
29. Gunther B. and Zachmann H. G., *Polymer* 1983, **24**.1008
30. Whinfield J. R. and Dickson J. T., *Brit. Pat.* 1941, **587,079**
31. Brydson J. A., *Plastics Materials,* 6th ed.. Oxford: Butterworth-Heinemann, 1995
32. Sehanobish K., Pham H. T. and Bosnyak C. P., *Polycarbonates (Overview),* **vol.8 5679**. In: Salamone J. C., editor-in-chief, *Polymeric Materials Encyclopaedia*. New York: CRC Press, 1996
33. Pryde C. A. and Hellman M. Y., *J. Appl. Polym. Sci.* 1980, **25**.2573
34. Nassar T. R., Paul D. R. and Barlow J. W., *J. Appl. Polym. Sci.* 1979, **23**.85
35. Murff S. R., Barlow J. W. and Paul D. R., *J. Appl. Polym. Sci.* 1984, **29**.3231
36. Chen X. Y. and Bireley A. W., *Br. Polym. J.* 1985, **17**.347
37. Hanrahan B. D., Angeli S. R. and Runt J., *Polym. Bull.* 1986, **15**.455
38. Suzuki T., Tanaka H. and Nishi T., *Polymer* 1989, **30**.1287
39. Zheng W. G., Wan Z. H., Qi Z. N. and Wang F. S., *Polym. Int.* 1994, **34**.301
40. Zheng W. G., Qi Z. N. and Wang F. S., *Polym. Int.* 1994, **34**.307
41. Tan Q. and Ma D. Z., *J. Appl. Polym. Sci.* 1993, **48**.747
42. Poter R. S., Jonza J. M., Kimura M., Desper C. R. and George E. R., *Polym. Eng. Sci.* 1989, **29**.55
43. Kotliar A. M., *J. Polym. Sci.: Macromol. Rev.* 1981, **16**.367
44. Pilati F., Marianucci E. and Berti C., *J. Appl. Polym. Sci.* 1985, **30**.1267
45. Godard P., Dekoninck J. M., Devlesaver V. and Devaux J., *J. Polym. Sci.: Polym. Chem.* 1986, **24**.3301; 1986, **24**.3315
46. Reading M., Elliot D. and Hill V.L., *J. Thermal Anal.*1993, **40**.949
47. Gill P. S., Sauerbrunn S. R. and Reading M., *J. Thermal Anal.* 1993, **40**.931
48. Reading M., *Trends in Polym. Sci.* 1993, **8**.248
49. Bailey N.A., *PhD Thesis*, The University of Birmingham, 2000
50. Reading M., Hahn B. and Crowe B. S., *US Patent*, 5,224,775, 1993

51. Sawyer L. C. and Grubb D. T., *Polymer Microscopy*. London: Chapman & Hall, 1987
52. Hobbs S. Y., Dekkers M. E. J. and Watkins V. H., *J. Mater. Sci.* 1988; **23**.1219
53. Haward R. N. and Young R. J., *The Physics of Glass Polymers*, 2nd ed.. London: Chapman & Hall, 1997
54. Fox T. G. and Flory P. J., *J. App. Phys.* 1950, **21**.581
55. Bondi A., *J. Phys. Chem.* 1954, **58**.929
56. Doolittle A. K., *J. App. Phys.* 1951, **22**.1471
57. Doolittle A. K. and Doolittle D. B., *J. App. Phys.* 1957, **28**.901
58. Williams M. L., Landel R. F. and Ferry J. D., *J. Am. Chem. Soc.* 1955, **77**.3701
59. Ferry J. D., *Viscoelastic Properties of Polymers*. New York: Wiley, 1961
60. Blanshard J. M. V. and Lillford P. J., *The Glassy State in Foods*. Nottingham: Nottingham University Press, 1993
61. Gibbs J. H. and DiMarzio E. A., *J. Chem. Phys.* 1958, **28.**373
62. DiMarzio E. A. and Gibbs J. H., *J. Chem. Phys.* 1958, **28.**807
63. Flory P. J., *Proc. R. Soc. London* 1956, **234**.60
64. Cowie J. M. G., *Polymers: Chemistry and Physics of Modern Materials, 2nd ed.*. London: Chapman & Hall, 1991
65. Adam G. and Gibbs J. H., *J. Chem. Phys.* 1965, **43**.139
66. Richardson M. J. and Savill N. G., *Polymer* 1975, **16**.753
67. Reinsh V. E. and Rebenfeld L., *J. Appl. Polym. Sci.* 1996, **59**.1913
68. Murphy B. M., Harward R. N. and White E. F. T., *J. Polym. Sci.: Polym. Phys. Ed.* 1971, **9**.801
69. Fried J. R., *Ph. D. Thesis*, The University of Massachusetts, 1976
70. Wetton R. E., Moore J. D. and Ingram P., *Polymer* 1973, **14**.161
71. Sharma L., *Ph. D. Thesis*, The University of Birmingham, 1998
72. Wunderlich B., *Macromolecular Physics, Vol.2*. New York: Academic, 1976
73. Young R. J. and Lovell P. A., *Introduction to Polymers, 2nd ed.*. London: Chapman & Hall, 1991
74. Hoffman J. D. and Lauritzen J. I., *J. Research NBS, part A* 1961, **65A**.297

75. Hoffman J. D., Davis G. T. and Lauritzen J. I. *The Rate of Crystallization of Linear Polymer with Chain Folding,* **Chap7**. In: Hannay N. B., editor, *Treatise on Solid State Chemistry, Vol.3*. New York: Plenum, 1976

76. Turnbull D. and Fisher J. C., *J. Chem. Phys.* 1949, **17**.71

77. Hoffman J. D., Guttman C. M. and DiMarzio E. A., *Faraday Discuss. Chem. Soc.* 1979, **68**.297

78. Hoffman J. D., *Polymer* 1982, **23**.656; 1983, **24.**3

79. Avrami M., *J. Chem. Phys.* 1939, **7**.1103; 1939, **8**.212; 1939, **9**.177

80. Evans U. R., *Trans. Faraday Soc.* 1945, **41**.365

81. Hay J. N., Sabir M. and Steven R. L. T., *Polymer* 1969, 10.187

82. Banks W. and Sharples A., *Makromol. Chem.* 1963, **59**.233

83. Booth A. and Hay J. N., *Polymer* 1969, **10.**95; 1971, **12.**365

84. Hay J. N and Mills P. J., *Polymer* 1982, **23.**1380

85. Banks W., Gordon M., Roe R.-J and Sharples A., *Polymer* 1963, **4**.61

86. Mandelkern L., Fatou J. G. and Howard C., *J. Phys. Chem.* 1964, **68.**3386.

87. Beech P. R., Booth C., Hillier Z. H. and Pickles C. J., *Euro. Polym. J.* 1972, **8.**799

88. Fann D. M., Huang S. K. and Lee J. Y., *Polym. Eng. Sci.* 1998, **38**.265

89. Runt J. P., *Encyclopedia of Polymer Science and Engineering, Vol.4*. Mark H. F., Bikales N. M., Overberger C. G., Meges G. and Kroschwitz J., editors. New York: Wiley, 1986, p. 482

90. O'Malley J. J., *J. Polym. Sci.: Polym. Phys. Ed.* 1975, **13**.1353

91. Fakirov S., Fischer E. W., Hoffmann R. and Schmidt G. F., *Polymer* 1977, **18**.1121

92. Groeninckx G., Reynaers H., Berghmans H. and Smets G., *J. Polym. Sci.: Polym. Phys. Ed.* 1980, **8.**1311

93. Dawson P. C., Gilbert M. and Maddams W. F., *J. Polym. Sci.: Polym. Phys. Ed.* 1991, **29**.1407

94. Murthy N. S., Khanna Y. P. and Signorelli A. J., *Polym. Eng. Sci.* 1994, **36**.1254

95. Jonas A., Legras R. and Issi J. –P., *Polymer* 1991, **32**.3364

96. Toda T., Yoshida H. and Fukunishi K., *Polymer* 1995, **36**:699

97. Huang J. M., Chu P. P. and Chang F. C., *Polymer* 2000, **41**.1741

98. Hyun J., *Polymer* 2001, **42.**6473

99. Kaisersberger, E. and Mohler, H., *DSC on Polymeric Materials, NETZSCH Annual for Science and Industry, Vol 1*. Wurzburg, 1991.
100. Khanna Y. P. and Kuhn W. P., *J. Polym. Sci.: Polym. Phys. Ed.* 1997, **35**.2219
101. Richardson M. J., *J. Polym. Sci.: Part C* 1972, **38**.251
102. Mathot V. B. F., editor, *Calorimetry and Thermal Analysis of Polymers*. Munich: Hanser, 1994
103. Seguela R., *Polymer* 1993, **34**.1761
104. Hay J. N., *Application of Thermal Analysis of Polymers*. In: Charsley E. L. and Warrington S. B., editors, *Thermal Analysis – Techniques and Application*. Cambridge: Royal Society of Chemistry, 1992
105. Mehmet-Alkan A. A. and Hay J. N., *Polymer* 1992, **33**.3527
106. Mehmet-Alkan A. A. and Hay J. N., *J. Thermal Anal.* 1993, 40.791
107. Gary A. P., *Thermochim. Acta* 1970, **1**.563
108. Blundell D. J., Beckett D. R. and Willcocks P. H., *Polymer* 1981, **22**.704
109. Mathot V. B. F. and Pijpers M. F. J., *J. Thermal Anal.* 1983, **28**.349
110. Mathot V. B. F. and Pijpers M. F. J., *J. Appl. Polym. Sci.* 1990, **39**.979
111. Atkins P. W., *Physical Chemistry, 3rd ed.* Oxford: Oxford University Press, 1986
112. Qiu G., Tang Z.-L., Huang N.-X. and Gerking L., *J. Appl. Polym. Sci.* 1998, **69**.729
113. Quirk R. P. and Alsamarrie M. A. A., *Physical Constants of Polyethylene*. In: Brandrup J. and Immergut E. H., editors, *Polymer Handbook, 3rd ed.* New York: Wiley, 1989
114. Lawton E. L. and Ringwald E. L., *Physical Constants of Poly(oxyethylene-oxyterephthaloyl) (Polyethylene terephthalate)*. In: Brandrup J. and Immergut E. H., editors, *Polymer Handbook, 3rd ed.* New York: Wiley, 1989
115. Mehta A., Gaur U. and Wunderlich B., *J. Polym. Sci.: Polym. Phys. Ed.* 1978, **16**.289
116. *http://funnelweb.utcc.utk.edu/~athas/databank/phenylen/pet/petcalam.html*
117. *http://funnelweb.utcc.utk.edu/~athas/databank/phenylen/pet/petcalcr.html*
118. Bailey N. A., Hay J. N. and Price D. M., *Thermochim. Acta* 2001, **367/368**.425
119. Holdsworth P. J. and Turner-Jones A., *Polymer* 1971, **12**.195

120. Medellin-Rodriguez F. J., Phillips P. J., Lin J. S. and Campos R., *J. Polym. Sci.: Polym. Phys. Ed.* 1997, **35**.1757
121. Zhou C. and Clough S. B., *Polym. Eng. Sci.* 1988, **28**.65
122. Reinsch V. E. and Rebenfeld L., *J. Appl. Polym. Sci.* 1996, **59**.1913
123. Bair H. E., Salovey R. and Huseby T. W., *Polymer* 1967, **8**.9
124. Harrison I. R., *J. Polym. Sci.: Polym. Phys. Ed.* 1973, **11**.991
125. Feng Y., Jin X. and Hay J. N., *Polym. J. (Japan)* 1998, **30**.215
126. Vandermiers C., Moulin J. F., Damman P. and Dosiere M., *Polymer* 2000, **41**.2915
127. Samuels R. J., *J. Polym. Sci.: Polym. Phys. Ed.* 1975, **13**.1417
128. Busfield W. K. and Blade C. S., *Polymer* 1980, **21**.35
129. Wlochowicz A. and Eder M., *Polymer* 1984, **25**.1268
130. Woo E. M. and Fu S. W., *Macromol. Chem. Phys.* 1998, **199**.2041
131. Liu T. and Petermann J., *Polymer* 2001, **42**.6453
132. Wang C., Hsu Y. –C. and Lo C. –F., *Polymer* 2001, **42**.8447
133. Bell J. P. and Murayama T., *J. Polym. Sci.: A-2* 1969, 7.1059
134. Tan S., Su A., Yang X., and Zhou E., *J. Appl. Polym. Sci.* 2000, **77**.993
135. Chung J. S. and Cebe P., *Polymer* 1992, **33**.2312; 1992, **33**.2325
136. Mai K., Mei Z., Xu J. and Zeng H., *J. Appl. Polym. Sci.* 1997, 63.1001
137. Blundell D. J., *Polymer* 1987, **28**.2248
138. Lee Y. and Poter R. S., *Macromolecules* 1987, **20**.1336
139. Lattimer M. P., Hobbs J. K., Hill M. J. and Barham P. J., *Polymer* 1992, **33**.3971
140. Yeh J. T. and Runt J., *J. Polym. Sci.: Polym. Phys. Ed.* 1989, **27**.1543
141. Nichols M. E. and Robertson R. E., *J. Polym. Sci.: Polym. Phys. Ed.* 1992, **30**.755
142. Groeninckx G. and Reynaers H., *J. Polym. Sci.: Polym. Phys. Ed.* 1980, **8**.1325
143. Fontaine F., Ledent J., Groeninckx G. and Reynaers H., *Polymer* 1982, **23**.185
144. Lu X. F. and Hay J. N., *Polymer* 2001, **42**.9423
145. Bell J. P. and Dumbleton J. H., *J. Polym. Sci.: A-2* 1969, **7**.1033
146. Roberts R. C., *Polymer* 1969, **10**.117
147. Sweet G. E. and Bell J. P., *J. Polym. Sci.: A-2* 1972, **10**.1273
148. Alfonso G. C., Pedemonte E. and Ponzetti L., *Polymer* 1979, **20**.104

149. Booth C., Devoy C. J., Dogson D. V. and Hillier I. H, *J. Polym. Sci.: A-2* 1970, **8**.519
150. Lemstra P. J., Kooistra T. and Challa G., *J. Polym. Sci.: A-2* 1972, **10**.823
151. Al Raheil I. A. M., *Polym. Int.* 1994, **35**.189
152. Medellin-Rodriguez F. J., Phillips P. J. and, Lin J. S., *Macromolecules* 1996, **29**.7491
153. Wang Z.-G., Hsiao B. S., Sauer B. B. and Kampert W. G., *Polymer* 1999, **40**.4615
154. Sauer B. B., Kampert W. G., Neal Blanchard E., Threefoot S. A. and Hsiao B. S., *Polymer* 2000, **41**.1099
155. Hoffman J. D. and Weeks J. J., *Res. Nat. Bur. Stand.* 1962, **66A**.13
156. Hoffman J. D. and Miller R. L., *Polymer* 1997, **38**.3151
157. Weeks J. J., *J. Res. Nat. Bur. Std.* 1963, **67A**.441
158. Hoffman J. D., *Soc. Plastics Eng. Tran.* 1964, **4**.315
159. Okazaki I. and Wunderlich B., *Macromolecules* 1997, **30.**1758
160. Hellmuth E. and Wunderlich B., *J. Appl. Phys.* 1965, **36**.3039
161. Kong Y. and Hay J. N., *Polymer* 2002, **43**.1805
162. Wunderlich B., Jin Y. and Boller Y. *Thermochim. Acta* 1994, **238**.277
163. Reading M., Luget A. and Wilson R., *Thermochim. Acta* 1994, **238**.295
164. Schawe J. E. K., *Thermochim. Acta* 1995, **260**.1; 1995, **261**.183; 1997, **304/305**.111
165. Boller Y., Jin Y. and Wunderlich B., *J. Thermal. Anal.* 1992, **42**.307
166. Pyda M., Bolle, A., Grebowicz J., Chuah H., Lebedev B. V. and Wunderlich B., *J. Polym. Sci.: Polym. Phys. Ed.* 1998, 36.2499
167. Marcus S. M. and Blaine R. L., *Thermochim. Acta* 1994, **243**.231
168. Blaine R. L. and Marcus S. M., *J. Thermal. Anal.* 1998, **54**.467
169. Hutchinson J. M. and Montserrat S., *J. Thermal. Anal.* 1996, **47**.103
170. Wunderlich B., Boller A., Okazaki I. and Kreitmeier S., *J. Thermal. Anal.* 1996, **47**.1013
171. Okazaki I. and Wunderlich B., *J. Polym. Sci.: Polym Phys. Ed.* 1996,**34.**2941
172. Simon S. L. and McKenna G. B., *Thermochim. Acta* 2000, **348**.77
173. Assche G. V., Hemelrijck A. V., Rahier H. and Mele B. V., *Thermochim. Acta* 1996, **286**.209; 1997, **304/305**.317

174. Song M., Hammiche A., Pollock H. M., Hourston D. J. and Reading M., *Polymer* 1996, **37**.5661
175. Cheng Y. Y., Brillhart M. V. and Cebe P., *Thermochim. Acta* 1997, **304/305**.369
176. Bailey N. A. and Hay J. N., *J. Thermal Anal.* 1999, **56**.1011
177. Ishikiriyama. K. and Wunderlich B., *J. Polym. Sci.: Polym Phys. Ed.* 1997, **35**.1877
178. Ishikiriyama. K. and Wunderlich B., *Macromolecules* 1997, **30**.4126
179. Schawe J. E. K. and Bergmann E., *Thermochim. Acta* 1997, **304/305**.179
180. Toda A., Tomita C., Hikosaka M. and Saruyama Y., *Polymer* 1997, **38**.2849
181. Cser F., Rasoul F. and Kosior E., *J. Thermal Anal.* 1998, **52**.293
182. Wunderlich B., Boller A., Okazaki I., Ishikiriyama K., Chen W., Pyda M., Pak J., Moon I. and Androsch R., *Thermochim. Acta* 1999, **330**.21
183. Schawe J. E. K. and Winter W., *Thermochim. Acta* 1997, **298**.9; 1999, **330**.85
184. Righetti M. C., *Thermochim. Acta* 1999, **330**.131
185. Chen W., Moon I.-K. and Wunderlich B., *Polymer* 2000, **41**.4119
186. Reading R., *Thermochim. Acta* 1997, **292**.179
187. Jones K. J., Kinshott I., Reading M., Lacey A. A., Nikolopoulos C. and Pollock H. M., *Thermochim. Acta* 1997, **304/305**.187
188. Reading M. and Luyt R., *J. Thermal Anal.* 1998, **54**.535
189. Weyer S., Hensel A. and Schick C., *Thermochim. Acta* 1997, **304/305**.267
190. Lacey A. A., Nikolopoulos C. and Reading M., *J. Thermal Anal.* 1997, **50**.279
191. Wunderlich B., *Thermal Analysis,* New York: Academic, 1990
192. Judovits L., Menczel J. D. and Leray A.-G., *J. Thermal Anal.* 1998, **54**.605
193. Pan R., Cao M. Y. and Wunderlich B., *Heat Capacities of High Polymers Part B: Data Tables for Solid and Liquid.* In: Brandrup J. and Immergut E. H., editors, *Polymer Handbook, 3rd ed.* New York: Wiley, 1989
194. Toda A., Oda T., Hikosaka M. and Saruyama Y., *Polymer* 1997, **38**.231
195. Scherrenberg R., Mathot V. and Hemelrijck A. V., *Thermochim. Acta* 1999, **330**.3
196. Goderis B., Reynaers H., Scharrenberg R., Methot V. B. F. and Koch M. H. J., *Macromolecules* 2001, **34**.1779
197. Fakirov S., *Transreaction in Condensation Polymer.* New York: Wiley, 1999
198. Berti C., Bonora V. and Pilati F., *Makromol. Chem.* 1992, **193**.1665

199. Montaudo G., Puglisi C. and Samperi F., *Macromolecules* 1998, **31**. 650
200. Ignatov V. N., Carraro C., Tartari V., Pippa R., Pilati F., Berti C., Toselli M. and Fiorini M., *Polymer* 1996, **37**. 5883
201. Ignatov V. N., Carraro C., Tartari V., Pippa R., Scapin M., Pilati F., Berti C., Toselli M. and Fiorini M., *Polymer* 1997, **38**. 195; 1997, **38**. 201
202. Fiorini M., Pilati F., Berti C., Toselli M. and Ignatov V., *Polymer* 1997, **38**. 413
203. Hopfe I., Pompe G., and Eichhorn K.-J., *Polymer* 1997, **38**. 2321
204. Holland B. J. and Hay J. N., *Polymer* 2002, **43**. 1835
205. Atkinson J. R., Biddlestone F. and Hay J. N., *Polymer* 2000, **41**. 6965
206. Devaux J., Godard P., Mercier J. P., Touillaux R. and Dereppe J. M., *J. Polym. Sci.: Polym. Phys*. Ed. 1982, **20**.1881
207. Devaux J., Godard P. and Mercier J. P., *J. Polym. Sci.: Polym. Phys*. Ed. 1982, **20**.1901
208. Fettes E. M., editor, *Chemical Reactions of Polymers*. New York: Wiley, 1964
209. Kim W. N. and Burns C. M., *J. Polym. Sci.: Polym. Phys*. Ed. 1990, **28**.1409
210. Wang L. H., Lu M., Yang X. and Porter R. S., *J. Macromol. Sci., Phys.* 1990, **B29**.171

Appendix A

A paper published in Polymer 43 (2002)

Title:

Miscibility and crystallisation behaviour of

poly(ethylene terephthlate)/polycarbonate blends

by

Y. Kong and J. N. Hay

ELSEVIER

Polymer 43 (2002) 1805–1811

polymer

www.elsevier.com/locate/polymer

Miscibility and crystallisation behaviour of poly(ethylene terephthalate)/polycarbonate blends

Y. Kong, J.N. Hay*

Plastic Materials Laboratory, School of Metallurgy and Materials, The University of Birmingham, Edgbaston, Birmingham B15 2TT, UK

Received 11 July 2001; received in revised form 28 August 2001; accepted 2 November 2001

Abstract

Poly(ethylene terephthalate)/polycarbonate blends were produced in a twin-screw extruder with and without added transesterification catalyst, lanthanum acetyl acetonate. The miscibility of the blends was studied from their crystallisation behaviour and variation in glass transition temperature with composition using differential scanning calorimetry, scanning electron microscopy and change in mechanical properties. The blends prepared without the catalyst showed completely immiscible over all compositions, while those prepared in the presence of the catalyst showed some limited miscible. The presence of PC inhibited the crystallisation of PET but this was much greater in the blends prepared in the presence of catalyst suggesting that some reaction had taken place between the two polyesters. The tensile properties showed little differences between the two types of blends.

Keywords: Miscibility; Poly(ethylene terephthalate)/polycarbonate blends; Crystallisation

1. Introduction

Polymer blends are of considerable scientific and industrial interest since blending is an effective way to tailor the properties of polymers. Both poly(ethylene terephthalate) (PET) and bisphenol-A polycarbonate (PC) are important engineering plastics, in particular, PC has high impact strength and its solvent resistance is improved by mixing with PET. Both are polyesters and can react by transesterification in the molten state to form block or random copolymer, which will greatly alter the blend phase behaviour and morphology [1–5]. PET/PC blends have been extensively studied over the past two-decade [6–15]. Some authors [6,7] have found that the blends were miscible in PET content above 60–70 wt% and immiscible below this range. On the other hand, others [8–10] found that the blends were immiscible at all composition range. Others [16,17] have reported that PET/PC blends are partially miscible from 10 to 90% composition. These discrepancies may result from a variety of factors such as the use of solvents in their preparation, ester exchange reactions, molecular weight differences and the analytical techniques used to analyse and define compatibility.

In this paper, two different sets of blends have been prepared with a twin-screw extruder in the presence and absence of a transesterification catalyst, lanthanum acetylacetonate hydrate [15] in order to determine what effect this reaction has in improving the material properties of the PET/PC blends.

2. Experimental

PET was provided by DuPont Co. Ltd as moulding pellets. It has a number average molecular weight of 19.6 kg mol^{-1} and weight average molecular weight of 36.4 kg mol^{-1}. ECP Enichem Polimeri, Italy, supplied the PC. It has a number average molecular weight of about 20 kg mol^{-1}. Lanthanum acetylacetonate hydrate was purchased from Aldrich Chemical Co. Ltd and used as obtained. Pellets of the two polymers were dried at 125 °C for at least 10 h prior to blending in a twin-screw extruder, manufactured by APV, at 100–150 rpm and 50–70% torque. The zone temperatures varied from 295 to 305 °C. The extruded blends were quenched into cold water and pelletised. The catalyst was mechanically dispersed throughout the PC pellets at a concentration of 0.075 wt%.

The blends were dried in a vacuum oven at 100 °C for 12 h and pressed at 280 °C for 2 min at pressure of 7.5 MN m^{-2} on $100 \times 100 \times 0.8$ mm^3 plaque. Amorphous plaques were obtained by quenching into ice/water. Tensile dumbbell specimens were cut directly from the plaques.

* Corresponding author. Tel.: +44-121-414-4544; fax: +44-121-414-5232.

E-mail address: j.n.hay@bham.ac.uk (J.N. Hay).

0032-3861/02/$ - see front matter
PII: S0032-3861(01)00772-8

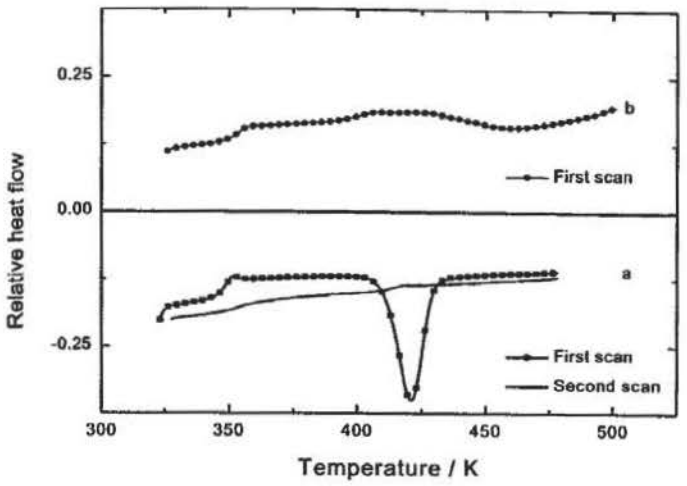

Fig. 1. DSC responses of PET/PC blends at different scans under a heating rate 10 K min^{-1}: (a) PET/PC 70/30 without added catalyst; (b) PET/PC 50/50 added catalyst.

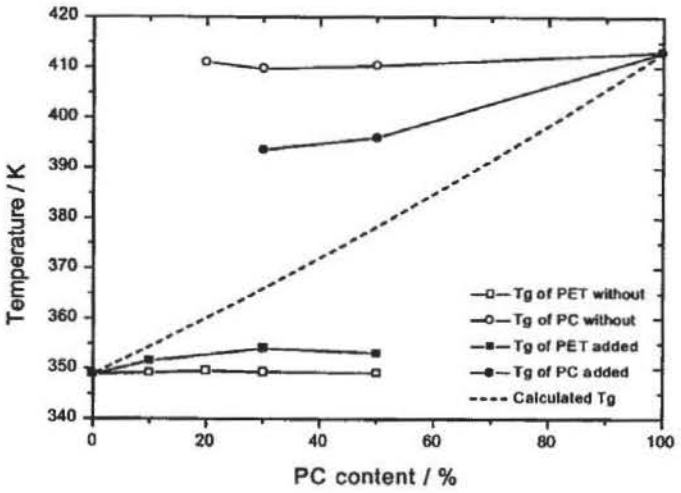

Fig. 2. The effect of PET/PC blend composition on T_gs, dash line is the T_g calculated by Fox equation.

A Perkin–Elmer differential scanning calorimetry, DSC-2, interfaced to a PC was used to measure the thermal properties of the blends. The calorimetry was operated under nitrogen flow of 20 cm^3 min^{-1}. The temperature was calibrated by the mp of ultra-pure materials: stearic acid, indium, tin and lead under different heating rates, corrections being made for thermal lag in the specimens. The glass transition temperature was determined as the midpoint of the step change in specific heat, ΔC_p, at different heating rates and extrapolated to zero heating rate to correct for thermal lag. For the isothermal crystallisation the samples were melted at 550 K for 5 min to erase the previous thermal history and then cooled to predetermined temperature at 160 K min^{-1}. A constant weight of 10.0 ± 0.2 mg was used throughout these measurements.

A scanning electron microscopy (SEM), Joel 5410, was used to examine the extent of phase separation in the blends by examination of their fracture surface. The samples were fractured at liquid nitrogen temperature and etched with diethylene triamine (DETA) for about 1 min at ambient temperature to remove the PC. The specimens were rinsed by distilled water and coated by gold to eliminate surface changing. Silver paint was used to form a conducting pathway between the sample and the mounting block.

Tensile properties were measured on an Instron, model 5566 interfaced to a PC. The crosshead speed was 2 mm min^{-1}. Standard dumbbell-shaped specimens were cut directly from moulded plate. An average of at least five specimens were measured for each determination. The energy to failure at high strain rate (3.5 m s^{-1}) was also investigated using a Zwick impact tester. Dumbbell shaped specimens used were identical to those used in Instron test. An average of at least eight specimens were used. All these tests were carried out at constant temperature of 296 ± 1 K and constant relative humidity of $35 \pm 1\%$.

3. Results and discussion

3.1. Glass transition temperature

Since the glass transition temperature, T_g, depended on the rate at which the glass was formed, a standard quench rate was adopted and corrections were made for thermal lag by linear extrapolation to zero heating rate at constant sample weight. By this method, the T_gs of PET and PC were measured as 349 and 413 K, respectively.

On heating in the DSC, the amorphous blend samples prepared without added catalyst only showed one glass transition at the temperature close to that of PET. This was followed, as can be seen in Fig. 1(a), by an exotherm due to the crystallisation of PET. The size of the exotherm varied with PET composition. No glass transition could be observed in the region of that of PC since it was masked by the crystallisation of PET. However, the second glass transition, close to that of PC, was detected in the second DSC scan of the blend sample once the PET crystallisation was complete. The two T_gs did not vary substantially with blend composition.

However, differences were observed with the blends prepared in the presence of the transesterification catalyst. As can be seen in Fig. 1(b), two T_gs are observed, one close to that of PET which can be attributed to PET-rich phase and the other to that of PC which can be attributed to PC-rich phase, during the first DSC scan above a heating rate of 10 K min^{-1}. The crystallisation of the PET is inhibited and occurs at a much higher temperature, above 425 rather than 400 K. This takes it out of the temperature region of the second glass transition, enabling it to be observed. This is a kinetic effect and at lower heating rates the T_g of PC is hidden by the crystallisation of the PET.

The variation in the T_gs with composition is shown in Fig. 2, where the dash line represents the compositional variation in T_g for a miscible blend system and assuming

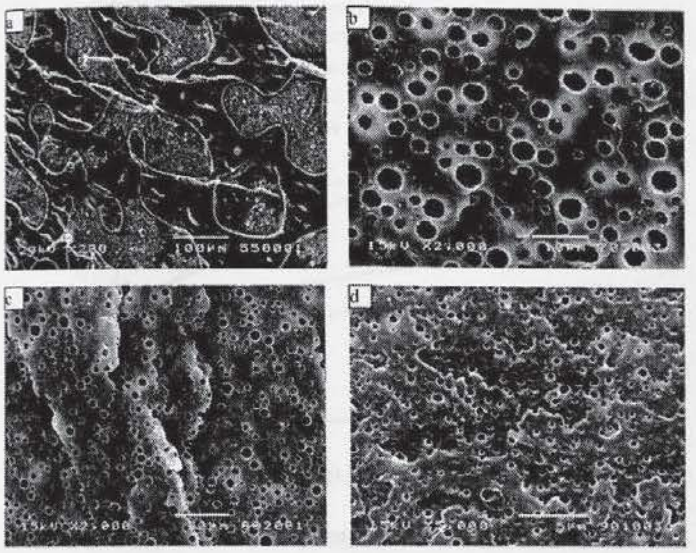

Fig. 3. SEM micrographs of cryo-fracture surface of PET/PC blends prepared without added catalyst etched by DETA for 1 min: (a) PET50/PC50; (b) PET70/P30; (c) PET80/PC20 and (d) PET90/PC10.

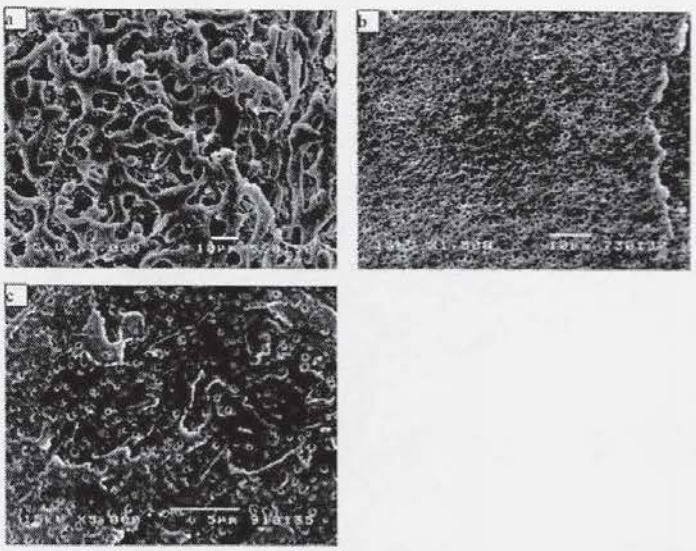

Fig. 4. SEM micrographs of cryo-fracture surface of PET/PC blends in the presence of catalyst etched by DETA for 1 min: (a) PET50/PC50; (b) PET70/P30 and (c) PET90/PC10.

that the Fox equation [18] applies. It can be seen that for the blends without added catalyst, both T_gs are almost independent of composition. For the blends with added catalyst, two T_gs could be observed in the 50/50 and 70/30. The T_g of PET-rich phase is slightly higher than that of 100% PET and increases with PC content increasing while the T_g of PC-rich phase is some what lower than that of PC and also increases with PC content increasing. The values of T_gs suggest that there is only 0.5–0.7% PC in the PET-rich phase for 50/50 and 70/30 blends prepared without added catalyst while there is 8–10% PC in the PET-rich phase for corresponding blends added catalyst. This clearly indicates that the blends prepared without added catalyst is immiscible, on the other hand, these blends prepared in the presence of catalyst shows a partial miscibility. The T_g values also confirm that there is more PET contained in the PC-rich phase rather than PC in the PET-rich phase [11].

3.2. Morphology of the blends

The morphology of the blends was investigated by SEM from the appearance of the fracture surfaces after etching with DETA. DETA has a good selectivity to etch PC without attacking PET [19]. The SEM micrographs of the blends prepared without added catalyst are shown in Fig. 3. All the blends exhibited a binary structure and at 50/50 composition a co-continuous morphology was observed. At lower blend compositions, spherical PC particles were distributed uniformly throughout a continue PET matrix. The etched spherical cavities had sharp boundaries and there was no evidence of an interfacial layer between the PET matrix and PC domains. The PC particles decreased in size from about 3–5 μm in 70/30 to 1–2 μm in 90/10 PET/PC blends.

In the blends prepared with added catalyst it can be seen from Fig. 4 that the 50/50 blend shows a co-continuous morphology and a similar trend with increasing PET composition from 70/30 to 90/10 of small PC particles embedded in a PET matrix. However, the PC particles are significantly smaller than observed previously with the blends prepared without the catalyst. The particle sizes are sub-micron and much more dispersed. It is difficult to accept that 30 and 10% of the sample is present as the dispersed phase. The SEM analysis is in agreement with DSC result that the PET/PC blends prepared without added catalyst being completely immiscible and exhibiting a clear two-phase structure. While the blends prepared in the presence of added catalyst show partially miscibility due to much smaller phases. These demonstrate that two materials appear to be more compatible as a result of the treatment with the transesterification catalyst.

3.3. Crystallisation behaviour of the blends

PET crystallises readily at temperature about 40 K above

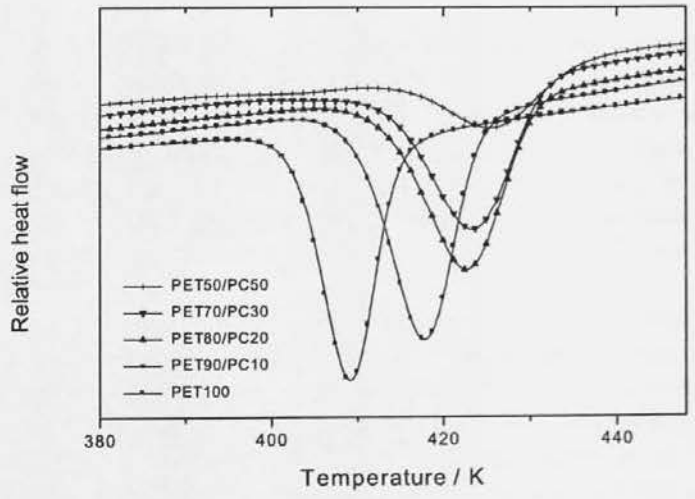

Fig. 5. DSC traces of cold crystallisation of PET and its blends without added catalyst under heating rate 10 K min^{-1}.

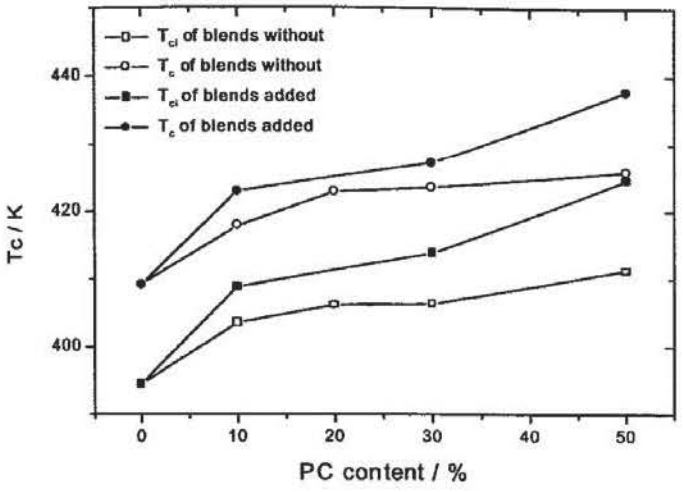

Fig. 6. The crystallisation temperatures of onset and maximum rate point for cold crystallisation of PET and its blends change with composition.

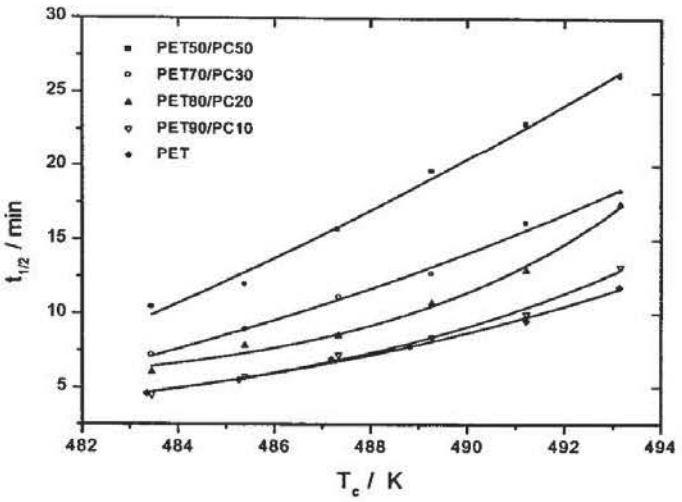

Fig. 8. The half-life, $t_{1/2}$ vs. T_c for PET and its blends without added catalyst.

its T_g, cold crystallisation, or about 60 K below its T_m, hot crystallisation. The cold crystallisation of PET in the blends, without added catalyst, is shown in Fig. 5 as measured by DSC at a heating rate of 10 K min^{-1}. The temperatures of initial onset of crystallisation, T_{ci}, and the temperature of maximum rate of crystallisation, T_c, for the blends are plotted in Fig. 6. These occur at higher temperature than those of PET, and increase with PC content. The corresponding T_{ci} and T_c values for the blends prepared with added catalyst are higher than those without added catalyst. This demonstrated that the PET crystallisation rate is reduced by the presence of PC and the effect is greater in the blends with added catalyst.

Isothermal crystallisation rates were also studied by DSC as a function of temperature in order to understand the nature of this inhibition of the crystallisation of PET by PC. In analysing, the isothermal crystallisation the fractional crystallinity, X_t, developed up to time t was defined to be the ratio of the areas between the heat flow–time curve and baseline of the sample [20,21], i.e.

$$X_t = \frac{\int_0^t \frac{dH}{dt} dt}{\int_0^{t_\infty} \frac{dH}{dt} dt} \quad (1)$$

The degree of crystallinity against time was analysed using the Avrami equation [22–24], i.e.

$$1 - X_t = \exp(-Zt^n) \quad (2)$$

in which X_t is the volume fraction degree of crystallinity, Z is a composite rate constant and n is an Avrami exponent. The equation can also be converted to

$$\log(-\ln(1 - X_t)) = \log Z + n \log t \quad (3)$$

Plots of $\log(-\ln(1 - X_t))$ vs. $\log t$ plots are linear with slope n as is shown in Fig. 7.

The rate constant, Z, was calculated from half-life of the crystallisation, $t_{1/2}$, and the value of n at $t_{1/2}$

$$Z = \frac{\ln 2}{t_{1/2}^n} \quad (4)$$

As can be seen from Fig. 7, there are obvious changes in the slope of each isotherm at about 70% conversion. This is usually interpreted as due to the presence of primary and secondary crystallisation processes. Only the primary process was analysed. The rate parameters obtained from the Avrami equation as a function of crystallisation temperature are listed in Table 1 for PET and both sets of blends.

The n values within experimental error were essentially constant at $\pm$ 0.3 consistent with growth of spherulites from heterogeneous nuclei. For each sample the $t_{1/2}$ increased, and Z decreased, with increasing crystallisation temperature but PET crystallised at a faster rate than the blends at the same crystallisation temperature. PC inhibits the crystallisation of PET. A similar conclusion can be discerned from a plot of the half-life, $\ln(t_{1/2})$ vs. T_c, in Figs. 8 and 9. The effect

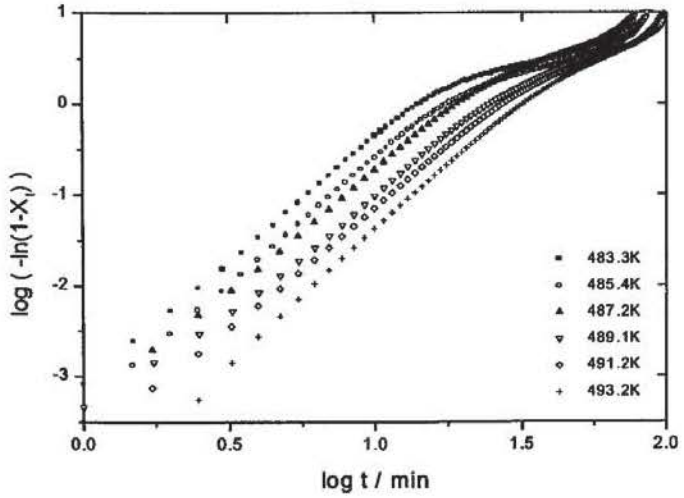

Fig. 7. Avrami analysis for PET isothermal crystallisation.

Table 1
Avrami parameters for PET and its blends molten-crystallisation

Sample	Temperature (K)	$t_{1/2}$ (min)	$n \pm 0.1$	Z ($\times 10^{-4}$ min^{-n})
PET	483.4	4.6	3.0	71.2
	485.3	5.5	3.0	41.7
	487.2	6.9	3.1	17.4
	488.8	7.8	3.0	14.6
	491.2	9.5	3.0	8.11
	493.1	11.8	3.0	4.2
PET/PC 50/50 without catalyst	483.4	10.4	2.7	12.4
	485.4	11.9	2.7	5.2
	487.3	15.8	2.8	3.1
	489.3	19.6	2.8	1.7
	491.2	22.9	2.9	1.5
	493.2	26.1	2.7	1.0
PET/PC 70/30 without catalyst	483.4	7.1	3.1	15.7
	485.4	8.9	3.1	7.9
	487.3	11.1	3.0	5.1
	489.3	12.7	2.9	4.4
	491.2	16.2	2.9	2.2
	493.2	17.9	2.8	2.1
PET/PC 90/10 without catalyst	483.4	4.5	3.1	65.4
	485.4	5.8	3.1	29.8
	487.3	7.2	3.3	10.3
	489.3	8.4	3.1	9.4
	491.2	10.0	3.2	4.4
	493.2	13.2	3.2	1.8
PET/PC 50/50 added catalyst	469.9	9.6	2.9	9.8
	471.8	11.7	3.0	4.3
	473.8	13.4	3.0	2.9
	475.3	15.3	2.9	2.5
	477.6	18.0	2.9	1.6
	479.5	20.2	3.0	0.84
PET/PC 70/30 added catalyst	471.8	12.0	3.0	4.0
	473.8	14.0	3.1	1.9
	475.7	16.0	3.2	0.97
	477.6	19.0	3.1	0.75
	479.5	21.6	3.0	0.65
	481.4	25.0	3.0	0.44
PET/PC 90/10 added catalyst	477.6	13.4	3.0	2.9
	479.5	15.3	3.1	1.5
	481.4	17.7	3.0	1.2
	483.1	21.6	3.0	0.69
	483.3	22.6	3.0	0.60
	485.3	29.8	3.0	0.26
	487.2	34.8	3.0	0.16

is more marked with the blends prepared with added catalyst than those without and indeed the later blends crystallised over a similar temperature range to that of PET but with half-lives which were reduced in proportion to the content of PET in the blend, see Table 1. Thus the 50/50 blends have half-lives which are approximately double those of PET, and similarly with the other blends. The reduction in crystallisation rate in these blends is considered to occur from a physical restriction to the growth by the PC domains.

Very different temperature dependences are observed with the crystallisation half-lives of the blends prepared with added catalyst, see Fig. 9(a), in which they crystallise at much lower temperatures and the displacement to lower crystallisation temperatures is disproportional to the amount of PC present. 10% PC in the blend had a greater effect proportionally than 30 or 50%.

The temperature dependence of the crystallisation half-lives of PET and the 50/50 blends were analysed using the Mandelkern equation [25],

$$\ln(1/t_{1/2}) = A - (4\sigma\sigma_e/R\Delta H_v)\left[T_m^0/T_c\left(T_m^0 - T_c\right)\right] \quad (5)$$

in which A is a constant, σ and σ_e are the surface free energy of substrate and fold surface free energy, respectively, ΔH_v is the heat of fusion of per monomer mole and R is the gas constant. From Fig. 10 it can be seen that the plots of $\ln(1/t_{1/2})$ vs. $T_m^0/(T_m^0 - T_c)T_c$ were approximately linear and parallel indicating that the slopes

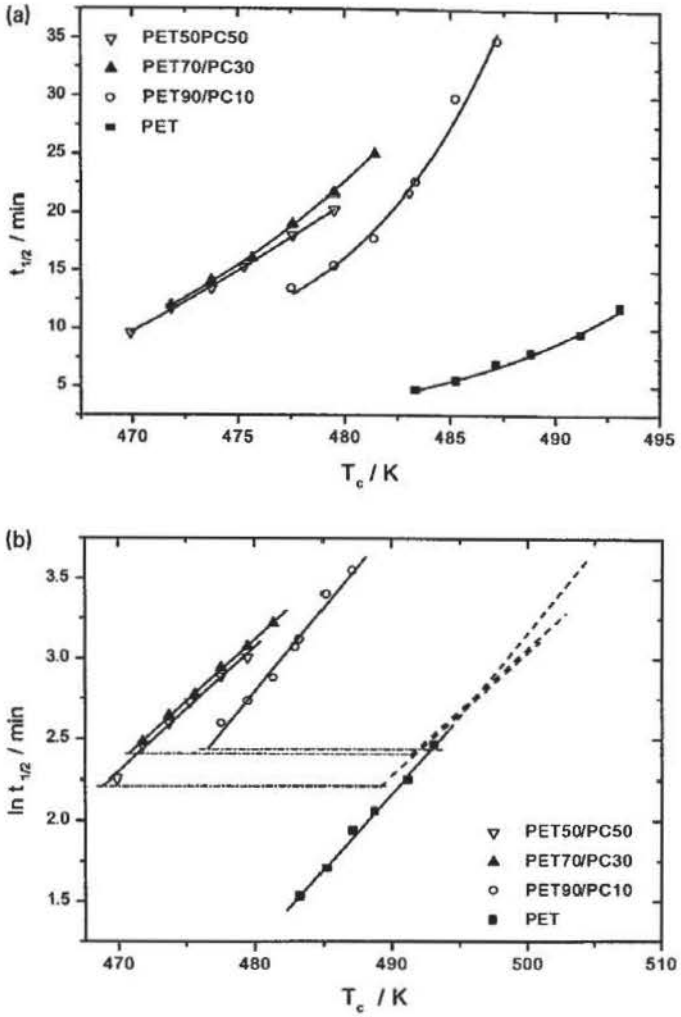

Fig. 9. (a) The half-life, $t_{1/2}$ vs. T_c for PET and its blends added catalyst. (b) $\ln(t_{1/2})$ vs. T_c for PET and its blends added catalyst, the dash lines indicate the shift of each blend.

represent the term $4\sigma\sigma_e/R\Delta H_v$ were similar. Assuming [26] that $\sigma = 0.1\Delta H_v$, the values of σ_e were calculated to be 10.3, 10.0 and 9.0 ± 1.5 kJ mol^{-1} for PET and the two 50/50 blends prepared with and without added catalyst, respectively. Although it can be seen that PC inhibits the crystallisation of PET this cannot be due to the small changes observed in the fold surface free energy, which would be expected if PC were soluble and being rejected during crystallisation.

It is apparent for Eq. (5) that $\ln(t_{1/2})$ is also a function of

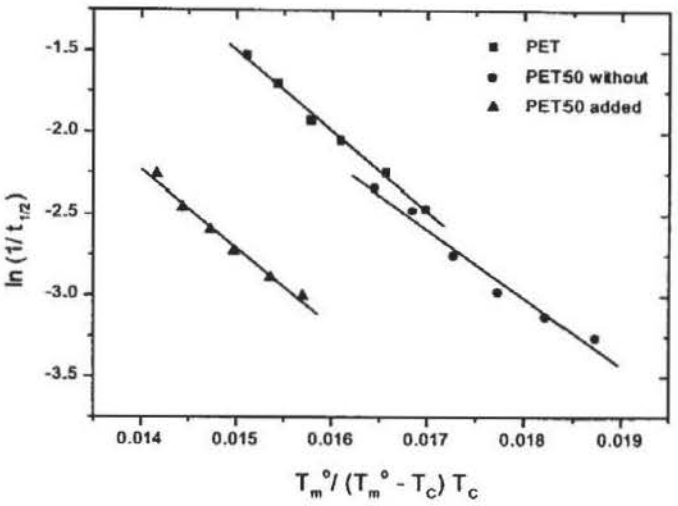

Fig. 10. Temperature dependence of crystallisation rate for PET and 50/50 blends, for PET $T_m^0 = 560$ K, PET/PC 50/50 blend without added catalyst $T_m^0 = 554$ K and PET/PC 50/50 blend in the presence of catalyst $T_m^0 = 546$ K.

the degree of super-cooling, $\Delta T = T_m^0 - T_c$. Plots of $\ln(t_{1/2})$ against T_c, see Fig. 9(b), for each blend could be superimposed onto the PET data by a lateral shift along the temperature axis equivalent to a ΔT value for each blend. These were 15, 19 and 20 K for the 90/10, 70/30 and 50/50 blends added catalyst consistent with a marked lowered of the equilibrium mp in these blends and to the presence of a soluble impurity.

T_m^0 values were measured by the Hoffman and Weeks procedure [27] as 560 and 546 K for PET and the 50/50 blend in the presence of catalyst, respectively. The values do indicate a marked reduction in T_m^0 of the blend from the PET value and so would account for the observed crystallisation behaviour. The behaviour is consistent with partial miscibility of the PC in PET.

3.4. The mechanical properties of the blends

In the tensile tests, all the amorphous blends exhibited ductile failure with a yield point followed by the development of a neck and strain hardening before finally failing. The tensile properties of both sets of blend are listed in Table 2. The elastic modulus increased progressively with PC content in the blends prepared with catalyst and

Table 2
Mechanical properties of PET and PC and their blends

Sample	Young's modulus (GPa)	Ultimate strength (MPa)	Elongation at break (%)	Tensile impact (MJ m^{-2})
PC	1.10 ± 0.01	50.9 ± 3.0	91 ± 16	0.89 ± 0.26
PET50 added	1.39 ± 0.01	46.4 ± 4.8	174 ± 53	0.51 ± 0.13
PET70 added	1.42 ± 0.01	59.4 ± 3.5	389 ± 24	0.33 ± 0.08
PET90 added	1.40 ± 0.02	57.6 ± 3.9	477 ± 32	0.36 ± 0.07
PET50 without	1.18 ± 0.02	45.2 ± 1.5	164 ± 12	0.44 ± 0.09
PET70 without	1.19 ± 0.01	47.1 ± 3.0	288 ± 27	0.36 ± 0.08
PET90 without	1.23 ± 0.02	54.9 ± 4.3	460 ± 37	0.36 ± 0.09
PET	1.29 ± 0.04	52.3 ± 5.2	498 ± 50	0.34 ± 0.04

decreased in the blends without catalyst. The greatest increase in modulus was obtained at 10% composition. The ultimate strength was also greater in these blends although the trend was not so clear. An initial increase was observed with composition followed by a decrease as the co-continuous morphology developed.

In both blend systems the elongation at break decreased gradually with increasing PC content and little differences were observed between the two systems. The tensile impact results changing with PC composition are displayed in Table 2. The tensile impact strength increased limitedly with increasing PC content for both sets of blends with almost identical values at each composition.

4. Conclusions

Blends produced without added catalyst have two T_gs independent of composition and a binary morphology. The blends are completely immiscible over the composition range studied. However, for the blends prepared with added catalyst, two T_gs close to each other are observed over a limited concentration range. Where there are two glass transitions the morphology is of a much more finely divided phase separation and some limited solubility of PC in PET.

The Avrami model was applied to analyse the crystallisation kinetics of PET and both sets of blends where the PET crystallisation is inhibited by the presence PC, particularly for the blends prepared with added catalyst. For blends without added catalyst the main reason is that of PC domains physical constraining the development of the PET crystallisation while for the other blends it is due to the limited soluble PC in PET depression its equilibrium mp.

The tensile and impact properties of the blends are also consistent with this limited solubility.

Acknowledgements

One of the authors, Y.K., acknowledges receipt of a scholarship from ORS Committee during the tenure of this study. Thanks are also due to Mr F. Biddlestone for his technical support.

References

[1] Kotliar AM. J Polym Sci, Macromol Rev 1981;16:367.
[2] Pilati F, Marianucci E, Berti C. J Appl Polym Sci 1985;30:1267.
[3] Godard P, Dekoninck JM, Devlesaver V, Devaux J. J Polym Sci, Polym Chem 1986;24:3301.
[4] Godard P, Dekoninck JM, Devlesaver V, Devaux J. J Polym Sci, Polym Chem 1986;24:3315.
[5] Montaudo G, Puglisi C, Samperi F. Macromolecules 1998;31:650.
[6] Nassar TR, Paul DR, Barlow JW. J Appl Polym Sci 1979;23:85.
[7] Murff SR, Barlow JW, Paul DR. J Appl Polym Sci 1984;29:3231.
[8] Chen XY, Bireley AW. Br Polym J 1985;17:347.
[9] Hanrahan BD, Angeli SR, Runt J. Polym Bull 1986;15:455.
[10] Suzuki T, Tanaka H, Nishi T. Polymer 1989;30:1287.
[11] Zheng WG, Wan ZH, Qi ZN, Wang FS. Polym Int 1994;34:301.
[12] Zheng WG, Qi ZN, Wang FS. Polym Int 1994;34:307.
[13] Tan Q, Ma DZ. J Appl Polym Sci 1993;48:747.
[14] Ignatov VN, Carraro C, Tartari V, Pippa R, Scapin M, Pilati F, Berti C, Toselli M, Fiorini M. Polymer 1997;38:195.
[15] Ignatov VN, Carraro C, Tartari V, Pippa R, Scapin M, Pilati F, Berti C, Toselli M, Fiorini M. Polymer 1997;38:201.
[16] Kim WN, Burn CM. J Polym Sci, Polym Phys 1990;28:1409.
[17] Wang L, Huang Z, Hong T, Porter RS. J Macromol Sci, Phys 1990;B29:155.
[18] Fox TG. Bull Am Phys Soc 1956;1:123.
[19] Hobbs SY, Dekkers MEJ, Watkins VH. J Mater Sci 1988;23:1219.
[20] Booth A, Hay JN. Polymer 1969;10:95.
[21] Hay JN, Mills PJ. Polymer 1982;23:1380.
[22] Avrami M. J Chem Phys 1939;8:212.
[23] Avrami M. J Chem Phys 1939;9:177.
[24] Evans UR. Trans Faraday Soc 1945;41:365.
[25] Mandelkern L, Fatou JG, Howard C. J Phys Chem 1964;68:3386.
[26] Beech PR, Booth C, Hillier ZH, Pickles CJ. Eur Polym J 1972;8:799.
[27] Hoffman JD, Weeks JJ. J Res Natl Bur Stand 1962;66A:13.

Appendix B

A paper published in Polymer 43 (2002)

Title:

The measurement of the crystallinity of polymers by DSC

by

Y. Kong and J. N. Hay

ELSEVIER

Polymer 43 (2002) 3873–3878

polymer

www.elsevier.com/locate/polymer

The measurement of the crystallinity of polymers by DSC

Y. Kong, J.N. Hay*

Plastic Materials Laboratory, The School of Metallurgy and Materials, The University of Birmingham, P.O. Box 363, Edgbaston, Birmingham B15 2TT, UK

Received 25 June 2001; received in revised form 22 January 2002; accepted 5 April 2002

Abstract

The procedures adopted and the inherent assumptions made in the measurement of crystallinity of polymers by differential scanning calorimetry (DSC) are reviewed. The inherent problem in all DSC measurements is concurrent recrystallisation and melting of the polymer sample on heating to the melting point and the variation of the enthalpies of crystallisation and melting, heat capacities and degree of crystallinity with temperature. A First Law procedure is suggested which involves heating the sample between two set temperatures, T_1 and T_2. T_1 is selected by the requirement that the degree of crystallinity of the sample should not change either with temperature or time, and be representative of the sample during its use. T_1 is taken to be ambient or just above the glass transition temperature. T_2 is taken to be just above the observed last trace of crystallinity. Integrating the observed specific heat difference between the sample and the completely amorphous material during these two temperature ranges determined the residual enthalpy of fusion at T_1. Problems are noted in the use of this procedure in that the specific heat of the liquid should not be arbitrarily chosen since this leads to systematic errors in the heat of crystallisation.

The degrees of crystallinity of metallocene polyethylene (m-PE) and polyethylene terephthalate (PET) measured by this procedure have been compared with values measured by density, determined at room temperature.

Keywords: Weight fraction crystallinity; m-Polyethylene; Polyethylene terephthalate

1. Introduction

The degree of crystallinity is the single most important characteristic of a polymer in that it determines mechanical properties, such as yield stress, elastic modulus and impact resistance [1,2]. In particular, amorphous polyethylene terephthalate (PET) is of little commercial value since it has poor mechanical properties, low dimensional stability and high gas permeation rate; on the other hand, crystalline PET has higher strength, good dimensional stability and chemical resistance. It is widely used in the production of fibres and in carbonated beverage containers because of its strength and low gas permeability, especially to carbon dioxide and oxygen.

The degree of crystallinity of a polymer is temperature-dependent [3] and in comparing its effect on material properties it is vital to carry out these measurements at the same temperature, invariably at ambient temperature and not at the melting point.

The various analytical methods used to determine the crystallinity of a polymer namely, wide angle X-ray diffraction (WAXD), density, differential scanning calorimetry (DSC), infrared (IR) and nuclear magnetic resonance (NMR) spectroscopy have been reviewed by Runt [4]. He considered that DSC was 'probably the most widely used technique'. However, despite this, it is probably the most widely misused method [5–11]. The usual procedure in measuring the degree of crystallinity by DSC involves drawing a linear arbitrary baseline from the first onset of melting to the last trace of crystallinity and determines the enthalpy of fusion from the area under this endotherm. The degree of crystallinity is then defined as

$$X_c = \Delta H_f(T_m)/\Delta H_f^o(T_m^o) \quad (1)$$

where X_c is the weight fraction extent of crystallinity, $\Delta H_f(T_m)$ is the enthalpy of fusion measured at the melting point, T_m, and $\Delta H_f^o(T_m^o)$ is the enthalpy of fusion of the totally crystalline polymer measured at the equilibrium melting point, T_m^o. No correction is usually made for the variation in the specific heats with temperature or the differences between the liquid and crystalline values.

Some allowances have also been made for the sample crystallising on heating by separately integrating the exotherm on cold crystallisation and endotherm on melting over appropriate but different temperature regions. The degree of crystallinity is then defined as [8,11]

$$X_c = (\Delta H_f - \Delta H_c)/\Delta H_f^o \quad (2)$$

* Corresponding author. Tel.: +44-121-414-4544; fax: +44-121-414-5232.

E-mail address: j.n.hay@bham.ac.uk (J.N. Hay).

0032-3861/02/$ - see front matter
PII: S0032-3861(02)00235-5

where ΔH_f is the enthalpy of fusion, ΔH_c the enthalpy of crystallisation and ΔH_f^o the heat of fusion of the completely crystalline materials at the equilibrium melting temperature, T_m^o. All are measured at different temperatures and no corrections are made for the change in specific heat. Nevertheless this method has appeared as a recommended method [12]. Both these methods define the degree of crystallinity close to the melting point rather than at room temperature where other analytical measurements are used, and there is little agreement between them. There are several things incorrect with both procedures. The integration baseline, separating exotherms and endotherms, is drawn arbitrarily and does not reflect the specific heats of the partially crystalline material or the liquid and has no physical meaning [13]. Secondly, the range between the end of crystallisation and the beginning of melting is not considered. It is assumed that no melting or recrystallisation occurs on heating. Because of these effects, the degree of crystallinity as measured by DSC conflicted with the values obtained by other methods [14,15]. Conventionally, specific heat differences and the temperature dependencies of the thermodynamic parameters are not considered [16,17]. Finally the enthalpy of fusion of 100% crystalline materials is invariably taken as the value at the equilibrium melting point, T_m^o, rather than in the temperature region of the measurement [3,18,19].

In measuring the degree of crystallinity of Nylon-6, Khanna et al. [20] recommended a method, in which the baseline was drawn between two set temperatures, i.e. one post-T_g and the other above T_m. Although as the authors admitted, the samples post-T_g were a mixture of liquid and solid and the observed specific heat was dependent on the degree of crystallinity. It cannot be taken to represent the specific heat of the liquid line. Despite this a linear baseline between the two observed specific heats was drawn between these set temperatures. This separated the exotherm and endotherm due to recrystallisation and melting and determined the degree of crystallinity from Eq. (2) but overestimates the degree of crystallinity.

Some times ago, Gray [21] and Richardson [13] separately proposed a correct procedure to measure the crystallinity, in which the enthalpy of fusion was measured at the onset of the melting point by subtracting the enthalpy change for the super-cooled liquid from the total enthalpy change over all melting temperature ranges and then the crystallinity was measured at this temperature, i.e.

$$X_c = \Delta H_f(T_{onset})/\Delta H_f^o(T_{onset}). \quad (3)$$

Later this method was called the total enthalpy method [19], however, it has appeared to be ignored by most polymer scientists. Recently, Mathot et al. [22–24] recommended the enthalpy-based crystallinity by using the following relationship, i.e.

$$X_c = \frac{h_a(T_1) - h_x(T_1)}{h_a(T_1) - h_c(T_1)}, \quad (4)$$

where $h_a(T_1)$, $h_c(T_1)$ and $h_x(T_1)$ are the enthalpies of the completely amorphous, crystalline and semicrystalline sample at the temperature T_1, respectively. Obviously, $[h_a(T_1) - h_x(T_1)]$ is the heat of fusion of semicrystalline sample at T_1 and $[h_a(T_1) - h_c(T_1)]$ is the heat of fusion of the 100% crystalline at T_1. Mathot et al. [24] found that the crystallinity measured by this enthalpy procedure was in good agreement with the density procedure although it not necessary the same.

Recently Hay et al. [16,17] also proposed the First Law method. This evaluated the residual enthalpy of the sample at the lower temperature, T_1, which should be room temperature or above but close to the glass transition, and determined the initial degree of crystallinity of the sample prior to heating. The residual enthalpy, ΔH_R, is the algebraic sum of the enthalpies of crystallisation and melting together with the specific heat changes with temperature for the partially crystalline solid, and for the liquid on cooling, as outlined in Fig. 2. This measured the crystallinity of the sample at T_1 closely reflecting the value at room temperature since the crystallinity did not change on heating to the glass transition.

Essentially, the last three methods are equivalent since the enthalpy of fusion is measured at the lower temperature and correction is made for the specific heat changes. In this paper, the degrees of crystallinities of m-PE and PET have been measured using the First Law method and the effect of specific heat baseline corrections evaluated.

2. Experimental

PET was supplied by DuPont Ltd as moulding pellets. It has a number average molecular weight of 19.6 kg mol^{-1} and weight average of 36.4 kg mol^{-1}. The m-PE was purchased from Exxon Chemical Co. France, as the Exact grade 3009. It is a copolymer of ethylene and hexene-1. The number and weight average molecular weights are 40 and 100 kg mol^{-1}, respectively.

PET was dried in a vacuum oven at 100 °C for 12 h and pressed at 280 °C for 2 min at a pressure of 7.5 MN m^{-2} into 100 mm × 100 mm × 0.8 mm plaques. The plaques were quenched in ice water to obtain amorphous sheets. The m-PE was moulded at 160 °C for 5 min under the same pressure. The plaques were then either quenched directly in water or slow-cooled in the hydraulic press to room temperature for 5 h. Discs were cut directly from the plaques for DSC analyses.

A Perkin–Elmer differential scanning calorimetry, DSC-2, interfaced to a PC was used to measure the thermal properties of the moulded samples. The calorimetry operated with a nitrogen flow 20 cm^3 min^{-1}. The temperature of the calorimeter was calibrated from the observed melting points of distilled water and ultra-pure materials—stearic acid, indium, tin and lead—at heating rate of 10, 5 and 2.5 K min^{-1}. Thermal lag corrections were made by extrapolating to zero heating rate. DSC was used adopting the

procedure for measuring heat capacities. Empty aluminium pans, matched in weight to within 0.02 mg, were used for the sample and reference. Initially, the two empty pans were scanned to determine the calorimeter baseline and this was repeated with a sapphire standard sample to calibrate the thermal response of the calorimeter. Finally this was repeated with the polymer disc sample. The same heating rate of 10 K min^{-1} and sample weight of 10.00 ± 0.03 mg was used to obtain comparable results.

Densities were measured on moulded specimens by Archimedes' method: first by weighing in air and then in *n*-heptane at 296 K. An average of at least three determinations on separate specimens, taken from the same sample, were used.

3. DSC analysis

The First Law method is an application of the First Law of Thermodynamics to the crystallisation and melting of a polymer sample on heating in a calorimeter. It involves two separate measurements. The first one determines the overall enthalpy changes on heating a partially crystalline polymer from T_1 to above the melting point, T_2. The second is a virtual experiment of measuring the enthalpy change on cooling the liquid from T_2 to T_1 without crystallisation occurring, see Fig. 1. For a closed system, the difference between these two steps is the enthalpy of fusion of the sample at T_1, i.e.

$$\Delta H_R = \Delta H_{12} + \Delta H_{21} \tag{5}$$

in which

$$\Delta H_{21} = \int_{T_2}^{T_1} C_{p,a}\, dT \tag{6}$$

where ΔH_R is the residual enthalpy of fusion at T_1, ΔH_{12} and ΔH_{21} are the changes in enthalpy on heating and cooling, respectively. $C_{p,a}$ is the specific heat of the amorphous material. ΔH_{12} includes the enthalpy changes due to the change in specific heat of the partially crystalline sample between T_1 and T_2, i.e. $\int C_{p,x}\, dT$, allowing for it to change with degree of crystallinity, crystallisation, annealing and recrystallisation, ΔH_c, as well as partial melting at intermediate temperatures, and final melting ΔH_f. For an initially amorphous sample ΔH_R should be zero. The DSC analysis for partially crystalline sample and the enthalpy changes in these processes are shown diagrammatically in Figs. 1 and 2, respectively.

The amorphous liquid temperature dependence, $C_{p,a}$, can be obtained by several method, i.e. by a linear extrapolation of the specific heat of the liquid measured in the melt; or measured on an amorphous sample above the glass transition temperature prior to the onset of crystallisation or by using reference data. In the first two cases, heat flow measurements in the calorimeter can be used directly instead of the measured specific heat.

The weight fraction degree of crystallinity at T_1, $X_c(T_1)$, is then the ratio of the observed enthalpy of fusion of the sample to that of the completely crystalline material at T_1,

$$X_c(T_1) = \Delta H_f(T_1)/\Delta H_f^o(T_1) = \Delta H_R/\Delta H_f^o(T_1). \tag{7}$$

Normally, the ΔH_f^o is measured at equilibrium melting point T_m^o, and not at T_1; however,

$$d(\Delta H_f^o) = (C_{p,a} - C_{p,c})dT = \Delta C_{p,c}\, dT \tag{8}$$

where $\Delta C_{p,c}$ is the specific heat difference between the completely liquid and crystalline solid, $C_{p,c}$. The enthalpy of fusion of 100% crystalline value at T_1 could be obtained by integrating the above equation form T_1 to T_m^o,

$$\Delta H_f^o(T_1) = \Delta H_f^o(T_m^o) - \int_{T_1}^{T_m^o} \Delta C_{p,c}\, dT. \tag{9}$$

Once $\Delta H_f^o(T_1)$ is obtained, the crystallinity is readily calculated from Eq. (7).

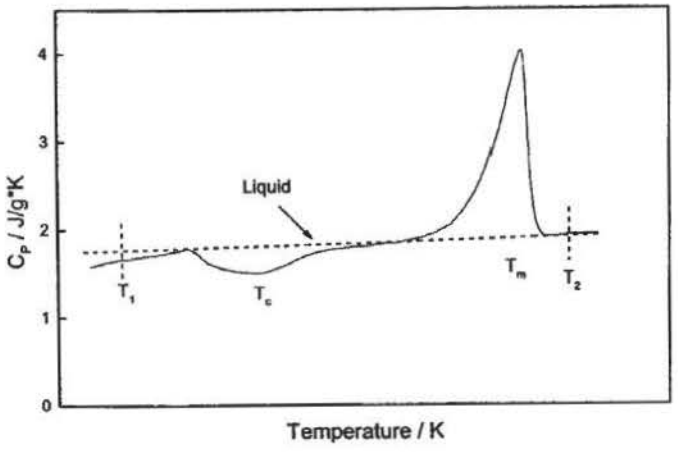

Fig. 1. DSC analysis of a partially crystalline polymer sample showing the presence of recrystallisation and melting.

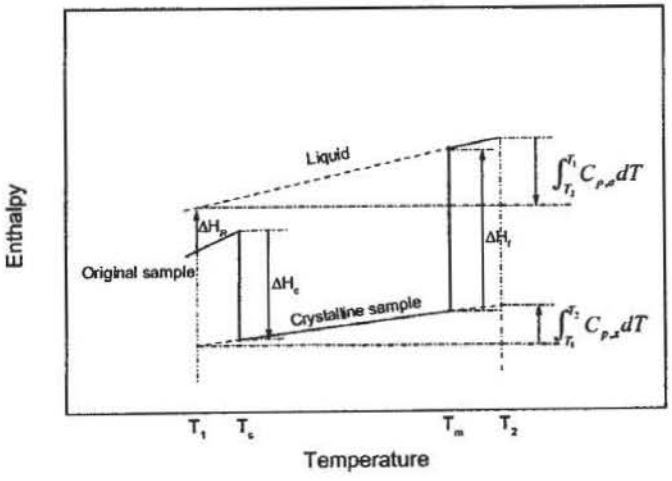

Fig. 2. Schematic of the enthalpy changes on recrystallisation and melting between two set temperatures, T_1 and T_2.

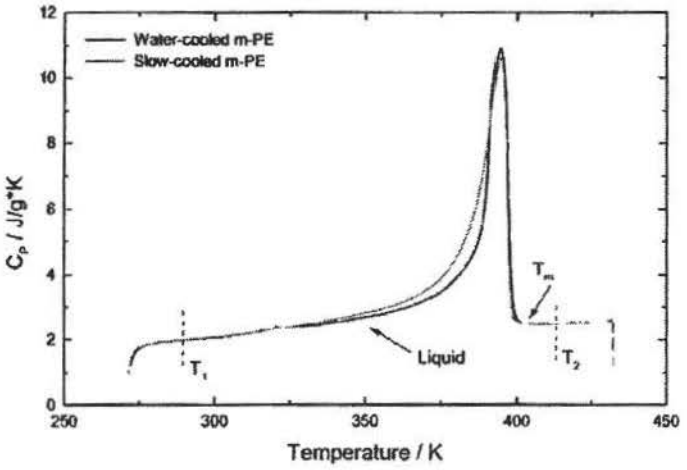

Fig. 3. DSC analyses of m-polyethylene samples along with the amorphous specific heat temperature dependence, extrapolated from the molten state.

4. Results and discussion

4.1. The fractional crystallinity of m-PE

Fig. 3 shows the DSC analyses of water and slow-cooled m-PE samples. m-PE has good thermal stability above T_m and the amorphous specific heat–temperature dependence is well-defined. It is drawn directly onto the DSC thermal response above the melting point and extrapolated to ambient temperature [19,24].

The heat of fusion at 298 K was determined using the First Law method as 116 and 132 J g^{-1} for the water and slow-cooled samples, respectively. The heat of fusion of completely crystalline PE at 298 K was determined [25] to be 243.8 J g^{-1}, which is approximately 17% less than the more commonly used value of 293 J g^{-1} at the equilibrium melting point. The fractional crystallinities of the water and slow-cooled sample were 0.48 ± 0.02 and 0.54 ± 0.02, respectively. These values compared well with the weight fraction crystallinity measured by density at 296 K. They are listed in Table 1. Mathot [24] found that the melting of very low-density polyethylenes could occur as low as −60 °C and the crystallinities were as mush as 40% higher than that at room temperature. In such situation, the degree of crystallinity must be measured at the same temperature, otherwise no comparison can be made with the values determined by other means.

4.2. The fractional crystallinity of PET

PET, amorphous to WAXD and by density measurements, was observed by DSC to have a glass transition at about 353 K, see Fig. 4a and a large exothermic crystallisation at about 410 K. Melting finally occurred above 500 K, although modulated temperature DSC studies indicated that considerable melting and annealing occurred prior to final melting [28]. There were two temperature regions in which only liquid existed—one post-T_g and prior to the onset of crystallisation and the other above T_m. Careful measurement of the heat capacities in these temperature regions indicated that they exhibited different temperature dependencies and the PET was degrading above T_m. As a result, the post-T_g amorphous specific heat–temperature dependence was chosen. The residual enthalpy of fusion determined just above the T_g for these amorphous samples was zero. The determinations were repeated 10 times and the variation in fractional crystallinity was ±0.02, as shown in Table 2. The results are highly reproducible and consistent with WAXD and density results.

Fig. 4b displays the DSC analyses of PET samples crystallised in a vacuum oven at 383 K for different period times. They exhibited less well-defined glass transitions and

Table 1
Fractional crystallinities measured by density and residual enthalpies of fusion

Sample	Density (g cm^{-3})	Residual enthalpy (J g^{-1})	Fractional crystallinity by	
			Density ±0.02	DSC ±0.02
m-PE				
Water-cooled m-PE	0.923	116	0.51	0.48
Slow-cooled m-PE	0.931	132	0.57	0.54
PET				
Amorphous	1.336	0.4	0.01	0.00
110 °C,[a] 1 h	1.350	9.6	0.09	0.10
110 °C,[a] 2 h	1.356	15.5	0.13	0.16
110 °C,[a] 5 h	1.365	19.6	0.19	0.20
125 °C,[a] 18 h	1.375	25.0	0.25	0.26
150 °C,[a] 18 h	1.379	26.4	0.27	0.28
175 °C,[a] 18 h	1.382	30.0	0.29	0.31
200 °C,[a] 18 h	1.392	34.4	0.35	0.36

[a] Crystallinity calculated by density for m-PE, $\rho_a = 0.855$ g cm^{-3}, $\rho_c = 0.999$ g cm^{-3}; Ref. [25]. Crystallinity calculated by density for PET, $\rho_a = 1.335$ g cm^{-3}, $\rho_c = 1.515$ g cm^{-3}; Ref. [26]. Heat of fusion of PE at 298 K: $\Delta H_f^o(298) = 243.8$ J g^{-1}; Ref. [25]. Heat of fusion of PET at 375 K: $\Delta H_f^o(375) = 96.0$ J g^{-1}; Ref. [27]. http://funnelweb.utcc.utk.edu/~athas/databank/phenylen/pet/petcalam.html, http://funnelweb.utcc.utk.edu/~athas/databank/phenylen/pet/petcalcr.html.

with temperature is used as the baseline for integration. Degradation and volatile production from the polymer in the melt or on partially crystalline samples prior to heating negates the use of a specific heat baseline derived from the sample above the melting point or close to the glass transition. Instead the specific heat temperature dependence must be determined separately either from amorphous samples, or from the literature.

By using the First law method, the initial fractional crystallinity of m-PE and PET have been measured and found to be consistent with values determined by density at ambient temperature.

Acknowledgements

Y.K. acknowledges the award of a research scholarship from ORS Committee and the School of Metallurgy and Materials of the University of Birmingham during the tenure of this work. The authors are grateful to Mr M. Razavi-Nouri for measuring the density of m-PE and providing m-PE samples. The authors would also like to express their appreciation to Mr F. Biddlestone for his valuable technical support and assistance.

References

[1] Sperling LH. Introduction to physical polymer science. 2nd ed. New York: Wiley, 1992. p. 198.
[2] Fann DM, Huang SK, Lee JY. Polym Engng Sci 1998;38:265.
[3] Mathot VBF. Thermal characterization of state of matter. In: Mathot VBF, editor. Calorimetry and thermal analysis of polymers. Munich: Hanser, 1994. Chapter 5.
[4] Runt JP. In: Mark HF, Bikales NM, Overberger CG, Meges G, Kroschwitz J, editors. Encyclopedia of polymer science and engineering, vol. 4. New York: Wiley, 1986. p. 482.
[5] O'Malley JJ. J Polym Sci, Polym Phys Ed 1975;13:1353.
[6] Groeninckx G, Reynaers H, Berghmans H, Smets G. J Polym Sci, Polym Phys Ed 1980;8:1311.
[7] Dawson PC, Gilbert M, Maddams WF. J Polym Sci, Polym Phys Ed 1991;29:1407.
[8] Murthy NS, Khanna YP, Signorelli AJ. Polym Engng Sci 1994;36:1254.
[9] Bassett DC, Olley RH, Al Raheil IAM. Polymer 1988;29:1745.
[10] Toda T, Yoshida H, Fukunishi K. Polymer 1995;36:699.
[11] Huang JM, Chu PP, Chang FC. Polymer 2000;41:1741.
[12] Kaisersberger E, Mohler H. DSC on polymeric materials, NETZSCH annual for science and industry, vol. 1. Wurzburg; 1991.
[13] Richardson MJ. J Polym Sci, Part C 1972;38:251.
[14] Fakirov S, Fischer EW, Hoffmann R, Schmidt GF. Polymer 1977;18:1121.
[15] Fontaine F, Ledent J, Groeninckx G, Reynaers H. Polymer 1982;23:185.
[16] Mehmet-Alkan AA, Hay JN. Polymer 1992;33:3527.
[17] Mehmet-Alkan AA, Hay JN. J Therm Anal 1993;40:791.
[18] Seguela R. Polymer 1993;34:1761.
[19] Blundell DJ, Beckett DR, Willcocks PH. Polymer 1981;22:704.
[20] Khanna YP, Kuhn WP. J Polym Sci, Polym Phys Ed 1997;35:2219.
[21] Gary AP. Thermochim Acta 1970;1:563.
[22] Mathot VBF, Pijpers MFJ. J Therm Anal 1983;28:349.
[23] Mathot VBF, Pijpers MFJ. Thermochim Acta 1989;151:241.
[24] Mathot VBF, Pijpers MFJ. J Appl Polym Sci 1990;39:979.
[25] Quirk RP, Alsamarrie MAA. Physical constants of polyethylene. In: Brandrup J, Immergut EH, editors. Polymer handbook, 3rd ed. New York: Wiley, 1989. p. V/19.
[26] Lawton EL, Ringwald EL. Physical constants of poly(oxyethylene-oxyterephthaloyl) (polyethylene terephthalate). In: Brandrup J, Immergut EH, editors. Polymer handbook, 3rd ed. New York: Wiley, 1989. p. V/101.
[27] Mehta A, Gaur U, Wunderlich B. J Polym Sci, Polym Phys Ed 1978;16:289.
[28] Bailey NA, Hay JN, Price DM. Thermochim Acta 2001;367–8:425.
[29] Holdsworth PJ, Turner-Jones A. Polymer 1971;12:195.
[30] Zhou C, Clough SB. Polym Engng Sci 1988;28:65.